2013

Production History Matching and Forecasting of Shale Assets Using Pattern Recognition

Soodabeh Esmaili
West Virginia University

Production History Matching and Forecasting of Shale Assets

Using Pattern Recognition

Soodabeh Esmaili

Dissertation submitted to the
College of Engineering and Mineral Resources
at West Virginia University
in partial fulfillment of the requirements
for the degree of

Doctor of Philosophy
in
Petroleum and Natural Gas Engineering

Approved by

Shahab D. Mohaghegh, Ph.D., Chair
Samuel Ameri, M.S., P.E., Department Chair
Khashayar Aminian, Ph.D.
Timothy Carr, Ph.D.
Grant Bromhal, Ph.D.
Thomas Snow, M.S., P.E.

Department of Petroleum and Natural Gas Engineering

Morgantown, West Virginia
2013

Keywords: Shale Gas, AI-based Modeling, Pattern Recognition, Data-driven Modeling

ABSTRACT

Production History Matching and Forecasting of Shale Assets Using Pattern Recognition

Soodabeh Esmaili

Generating long-term development plans and reservoir management of shale assets has continued apace. In this study, a novel method that integrates traditional reservoir engineering with pattern recognition capabilities of artificial intelligence and data mining is applied in order to accurately and efficiently model fluid flow in shale reservoirs. The methodology is efficient due to its relatively short development time and is accurate as a result of high quality history matches it achieves for individual wells in a multi-well asset.

The technique that is named Artificial Intelligence (AI) Based Reservoir Modeling is a formalized and comprehensive, full-field empirical reservoir model. It integrates all aspects of shale reservoir development from well location and configuration to reservoir characteristics and to completion and hydraulic fracturing. This approach not only has a much faster turnaround time compared to the numerical simulation techniques, but also models the production from the field with good accuracy, incorporating all the available data. This integrated framework enables reservoir engineers to compare and contrast multiple scenarios and propose field development strategies.

AI-based Modeling is applied to a Marcellus Shale asset that includes 135 horizontal wells from 43 pads with different landing targets. The full field AI-based Shale model is used for predicting the future well/reservoir performance, forecasting the behavior of new wells/pads and to assist in planning field development strategies. Furthermore, this study takes advantage of applying advanced pattern recognition tools in order to investigate the impact of design and native parameters on gas production as well as optimizing the completion and stimulation parameters for newly planned wells.

*This dissertation is dedicated to **my family***

For their unconditional love, unwavering support

and endless encouragement

ACKNOWLEDGEMENT

Over the past three years I have received support and encouragement from a great number of individuals. My sincere appreciation and special thanks goes to my advisor, Professor **Shahab D. Mohaghegh**, who has been a dedicated mentor, a knowledgeable advisor and a great friend. Without his guidance and support, this journey wouldn't be possible.

I would also like to thank Professor **Sam Ameri**, the department chair, for his blessings during this long process; he's always been there for me. I would like to offer my appreciation to my committee members: Professor **Timothy Carr**, Mr. **Thomas Snow**, Professor **Kashy Aminian** and Dr. **Grant Bromhal**; many thanks for your interest in my work, supportive inputs and thought-provoking suggestions.

I also would express my gratitude to my fellows in PEARL (Petroleum Engineering and Analytics Research Lab) team for their assistance over the past three years as I moved from an idea to a completed study. I am also grateful for my classmates in Petroleum and Natural Gas Engineering Department of WVU and my friends in all over the world for their friendship, positive inspirational messages and encouragements. My sincere appreciation is extended to my best friend, Amirmasoud Kalantari, who was always with me during the project; thank you for countless hours listening to me talk about my research and for your supportive and priceless assistance.

I also want to thank the ISI for providing the software packages. I would like to thank Range Resources and RPSEA for providing the information and financial assistance to allow me to do this work.

I want to acknowledge the help and support that I received during these years from Ms. Beverly Matheny, Dr. Melanie Cook, Dr. Constinia Charbonnette and Dr.Grace Atebe.

Finally, my deepest gratefulness goes to each and every member in my family for their unflagging love and unconditional support throughout my life and my studies. Although they are thousands miles away and I missed them in every single moment in past three years, my own success is a reflection of the love and support they have given me throughout these years.

Above all, utmost appreciation to the Almighty God for the divine intervention in this academic endeavor; I would not have come this far without his blessing.

NOMENCLATURE

D= Production Decline Rate (1/time)

q= Production Rate (MCF/time)

q_{DL}= Dimensionless Rate - $\frac{1}{q_{DL}} = \frac{k_f\sqrt{A_{cw}}[m(p_i)-m(p_{wf})]}{1422 q_g T}$

t_{DAc}= Dimensionless time- $t_{DAc} = \frac{0.00633 k_f t}{(\emptyset \mu c_t)_{f+m} A_{cw}}$

k_f= Bulk fracture permeability of dual porosity models, md

A_{cw}= Well-face cross sectional area to flow, ft^2

T= Temperature, °F

b= Hyperbolic Constant (Dimensionless)

t=Time

ω= Dimensionless Storativity ratio

λ= Dimensionless interporosity parameter

D_∞=Decline Constant at infinite time (1/time)

n=Time exponent

τ= Chacteristics Number of Periods (Dimensionless)

P_{pwf}=Pseudo flowing bottomhole pressure (Psi)

P_{pi}= Pseudo reservoir pressure (Psi)

t_a= Pseudo time

t_{ca}=Material balance time

μ_g= Gas Viscosity (cp)

c_t=Total Compressibility (1/Psi)

Z=Gas deviation factor (Dimensionless)

S_g=Gas Saturation (Dimensionless)

h=Thickness (ft.)

Table of Contents

List of Figures

List of Tables

1. CHAPTER I

INTRODUCTION

1.1 Overview of Unconventional Resources

Unconventional development of energy resource plays, including coal beds, tight sands and shales has been a growing source of natural gas development in the United States. Since 1998 unconventional natural gas production has increased nearly 65%. This growth has resulted in unconventional production becoming an increasingly larger portion of total natural gas production in the United States, increasing from 23% in 2010 to 49% of total dry gas production in 2035 (Figure 1.1) [U.S. EIA, 2012].

The term "Unconventional Reservoirs" addresses those types of reservoirs that cannot be produced at economic flow rates or that do not produce economic volumes of oil and gas without assistance from massive stimulation treatments or special recovery processes and technologies [Naik, 2005]. Shale gas is one out of several types of unconventional gas resources. Tight gas and coalbed methane are two other sources of developed unconventional gas resources, both with the property of the gas being stored in tight formations. However, shale is far tighter and less permeable than these two categories of unconventional gas resources [Knudsen, 2010].

Shale is one the most common sedimentary rocks in the world and is primarily composed of clay and fragments of other minerals such as quartz and calcite. Shale can be the source, reservoir and the seal for natural gas. Shale formations normally have low permeability (limited ability for gas or fluids to flow easily through the shale formation) and normally require stimulation techniques such as fracturing to economically produce shale gas. Shale gas is natural gas that is attached to, or adsorbed onto, organic matter or it is contained in thin, porous silt or sand beds interbedded in the shale [Alberta Energy, 2009].

Besides the natural complexities of shale formations and existing difficulties in extracting gas, shale is going to be one of the key sources in meeting U.S. energy demands. United States has a wide distribution of highly organic shales containing vast resources of natural gas (Figure 1.2). Already, the fledgling Barnett Shale play in Texas produces 6% of all natural gas produced in United States. Several factors such as advanced horizontal drilling and hydraulic fracturing have come together in recent years to make shale gas production economically viable. Analysts have estimated that by 2011 most new reserves growth (50% to 60% or approximately 3 BCF/day) will come from unconventional shale gas reservoirs.

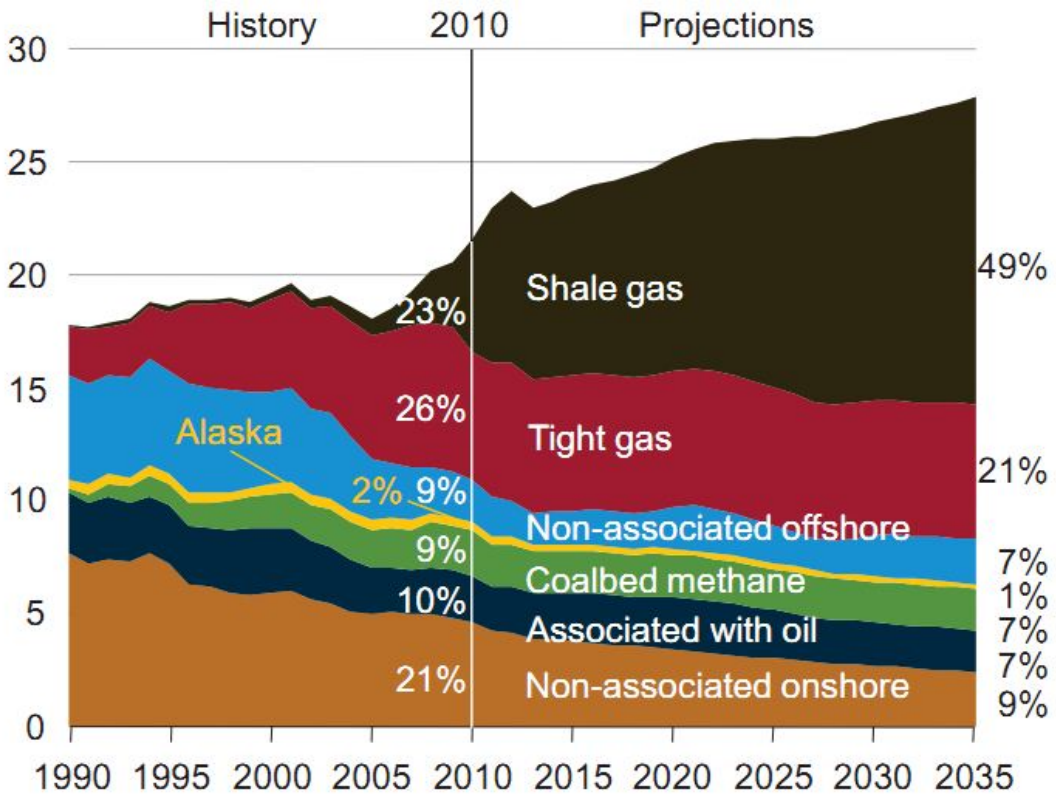

Figure 1.1: United States Natural Gas Production from Different Sources, 1990-2035-[U.S. EIA, 2012]

The total recoverable gas resources in four new shale plays (the Haynesville, Fayetteville, Marcellus and Woodford) may be over 550 TCF. Total annual production volumes of 3 to 4 TCF may be sustainable for decades. This potential for production in the known onshore shale basins, coupled with other unconventional gas plays, is predicted to contribute significantly to the U.S's domestic energy outlook [U.S. DOE, 2009].

The variety of rock types observed in organic-rich shale implies the presence of a range of different types of "Shale Gas" reservoirs. Each reservoir may have distinct geochemical and geological characteristics that may require equally unique methods of drilling, completion, production and resource and reserve evaluation [Cramer, 2008].

However, in all cases a thorough understanding of the fundamental geochemical and geological attributes of shale is essential for resource assessment, development and environmental stewardship. Four properties are important characteristics in each shale play : 1)maturity of the organic matter, 2)type of gas generated and stored in the reservoir, 3) TOC content of the strata; and 4) permeability of the reservoir. Shales can be classified based on maturity as thermogenic and biogenic. Thermogenic gas is generated from cracking

of organic matter or the secondary cracking of oil and biogenic gas (such as in the Antrim shale gas field), which is generated from microbes in area of fresh water recharge. Thermogenic gas is associated with mature organic matter that has been subjected to the relatively high temperature and pressure in order to generate hydrocarbons, while biogenic gas can be associated with either mature or immature organic matter [Rokosh et al., 2008].

Organic maturity is often expressed in terms of vitrinite reflectance ($\%R_0$) and the value above 1% R_0 indicates the organic matter is sufficiently mature to generate gas and could be an effective source rock.

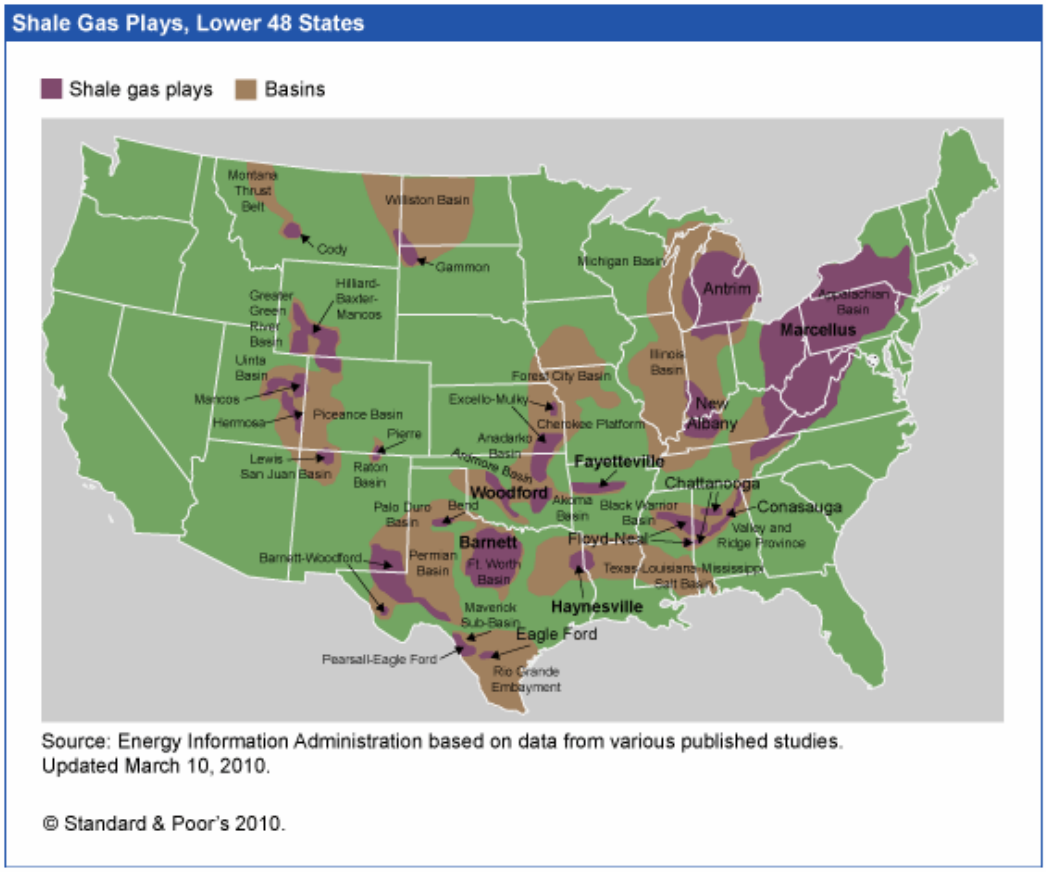

Figure 1.2: Shale Gas Plays Distribution in United States-EIA, 2010

Total organic carbon (TOC) is a fundamental attribute of gas shale and is a measure of present-day organic richness. The TOC content, together with the thickness of organic shale and organic maturity, is a key attribute that aids in determining the economic viability of a shale play [Rokosh et al., 2008]. A TOC of 1.0wt.% is widely regarded as the minimum value for defining a potential source rock [Peters et al., 1993].

Shale in particular exhibits permeability lower than Coal Bed Methane (CBM) and tight gas and, because of this, forms the source and seal for many conventional oil and gas pool. Permeability of the shale matrix is the most important parameter influencing sustainable shale gas production. To sustain yearly production, gas must diffuse from the low-permeability matrix to induced or natural fractures. Generally, higher matrix permeability results in a higher rate of diffusion to fractures and a higher rate of flow to the wellbore and consequently greater recovery of hydrocarbons and larger drainage area. Additionally, microfractures within shale matrix may be important for economic production; however these microfractures are not easily determined in situ in a reservoir [Rokosh et al., 2008].

Shale gas reservoirs generally recover less gas (from <5% to 20%) relative to conventional gas reservoirs, although the naturally well-fractured Antrim Shale may have a recovery factor as high as 50%-60% [Speight, 2013]. To increase the recovery factor, innovation in drilling and completion technology is paramount in low-permeability shale reservoirs. In recent years, improvements in the use of horizontal drilling combined with multi-stage fracturing have resulted in some shale gas formations becoming some of the most attractive natural gas resources in United States.

1.1.1 Marcellus Shale Play

The Marcellus is the most expansive shale play in the U.S. extending on a northeast-southwest trend from west central New York into Pennsylvania, Maryland, Ohio, Virginia and West Virginia, and covering an area of 95,000 square miles (Figure 1.3) [U.S. DOE, 2010]. The Marcellus Shale with an average thickness in the range of 50 to 100 ft., thins to the north, the west, and the south, and pinches out in eastern Ohio, western West Virginia, and southwestern Virginia. The Marcellus reaches subsurface depth over 9,000 ft. along the preserved basin axis; it outcrops to the east and north and subcrops to the west and south. The estimated production depth between 4,000 to 8,500 feet, together with an average gas content of 60 scf/ton, result in a gas-in-place estimate up to 1,500 tcf [USGC, 1993; USDOE, 2009].

A renewed interest in the Marcellus Shale was initiated in 2003 when Range Resources-Appalachia, LLC drilled the first “new” Marcellus well in recent years and began experimenting with techniques used in the Barnett [Arthur et al., 2008]. Since 2005 Marcellus Shale development has increased in Pennsylvania and the Appalachian Basin.

Current development practices in the Marcellus Shale involve the drilling of both horizontal and vertical wells. Regardless of the preferred well orientation, Marcellus Shale well completions require formation stimulation, typically in the form of hydraulic fracturing to produce economic volumes of natural gas.

Further, based on development in other gas shales, it is likely that horizontal well drilling will become the preferred method of drilling for gas development from the Marcellus Shale [Arthur et al., 2008].

1.2 Problem Description

Understanding reservoir properties like lithology, porosity, organic carbon, water saturation and mechanical properties of the rock, which include stresses, beforehand and planning completions based on that knowledge is the key to production optimization. Therefore, the final objective is to increase our ability to integrate proprietary laboratory and petrophysical measurements with geochemical, geological,

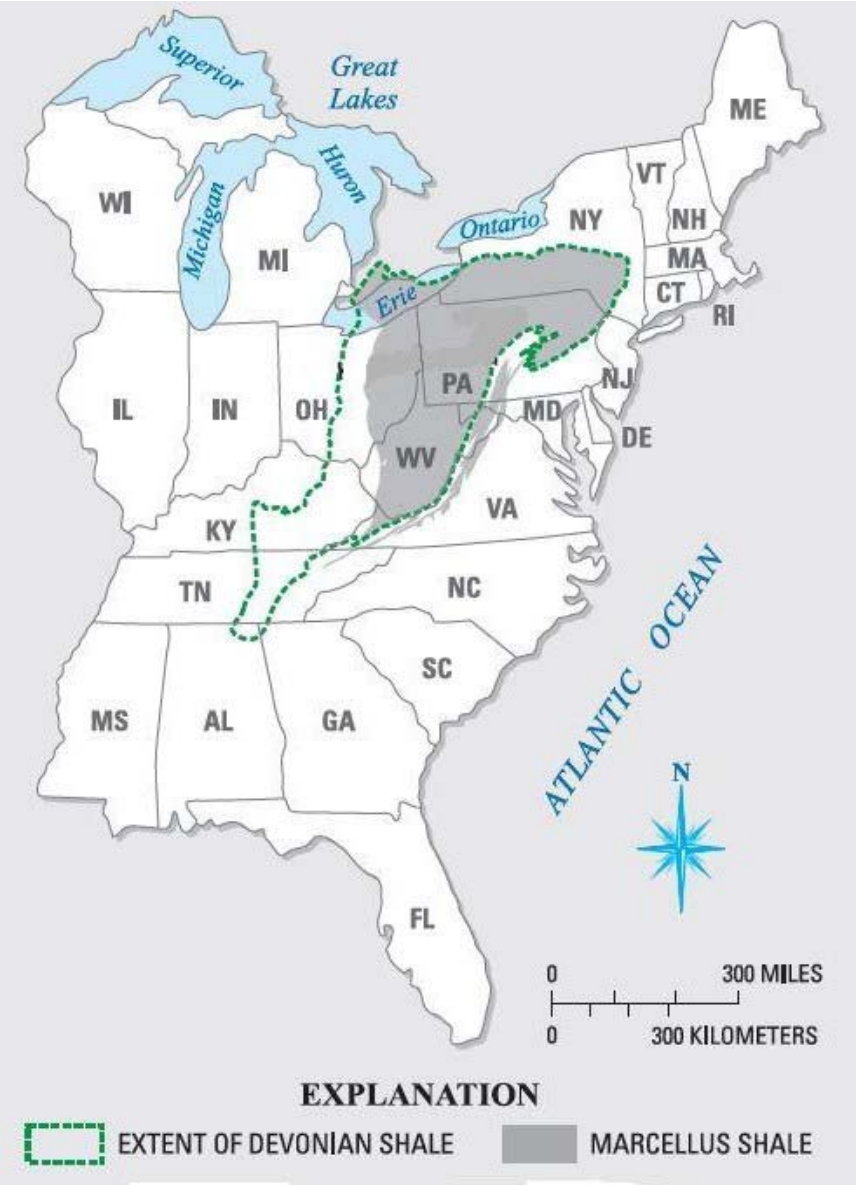

Figure 1.3: Distribution of the Marcellus Shale Formation- [Source: Taylorgeoservices-Marcellus Shale Services]

petrologic, and geomechanical knowledge, to develop a more solid understanding of shale plays and to provide better assessments, predictions, and models. There are still many problems to be solved and many challenges to overcome. These challenges make unconventional gas an exciting technical area.

Simulation and rate-transient analysis better represent the actual physics involved in reservoir dynamics, but early applications face steep problems. In the case of rate-transient analysis, formulations were not initially available to handle the physical geometry of the completions. Simulation is more flexible, but there is significant uncertainty as to the nature of the resulting completion, production mechanisms and how to model these [Strickland et al., 2011]. Studies have shown that Darcy flow and instantaneous capillary equilibrium applied in simulators for conventional reservoirs are inadequate for reliable simulation of shale gas reservoirs [Andrade et al., 2010]. With the complex nature of shale gas reservoirs, many capabilities necessary to accurately simulate these reservoirs are lacking which allows us to question how representative are these simulation models [Arogundae et al., 2012].

Civan et al. (2011) [Civan et al., 2011] presented some conditions of the design parameters that should be considered to build a proper shale gas simulator. They emphasized non-instantaneous dynamic distribution of fluids and transport of fluids in interconnected nano-pores as two defining features that make modeling of these reservoirs different from the conventional systems. They proposed a quad-porosity approach accounting for a complicated reservoir pore structure that includes pores in the organic matter, inorganic matter; natural and hydraulic fractures with heterogeneous wettability, and different relative permeability and capillary pressure functions.

More importantly though, there are several shortcomings in these detailed approaches. Firstly, detailed grid-based numerical techniques usually are resource intensive and time consuming. Furthermore, the best-of-practice approach can very well be an optimal collection of algorithms available for conventional reservoirs [Biswas, 2011].

Many difficulties on shale gas modeling caused engineers to rely heavily on the simplest, most accessible tool: such as using a reduced physics models [Wilson et al., 2012] or using the simplest production data analysis approach (e.g Decline Curve analysis) by knowing the fact that tools of traditional production data analysis have not been sufficient to identify the flow behavior in the shale system.

Numerical models capable of modeling the most important features of tight gas and gas shales are undergoing further development to include better representations of the basic physics controlling gas flow as the industry learns more [Lee et al., 2010]. The basic principles of physics and thermodynamics

controlling fluid flow in porous media are the basis in today's commercial models, but still there are many questions that need to be answered in order to make sure that we have a full understanding of the physics controlling fluid flow in shale media.

From what it has been discussed above, an effective and robust technology is needed to overcome these difficulties and give us a tool to perform full-field modeling and history matching of a shale formation.

1.3 Objectives

The objectives of this research are:

- To develop a realistic and versatile shale gas pattern recognition based reservoir simulation model by integrating and incorporating all hard data (field measurements)
- To investigate the short-term and long-term impact of parameters on production from shale
- To analyze the well behavior to offer the findings as lesson learned workflow

1.4 Organization of This Dissertation

The study is divided into seven chapters. The outline and organization of this dissertation are as follows:
Chapter I present an overview of shale gas reservoirs. The research problem and the dissertation objectives are discussed.
Chapter II presents an inclusive literature review. The existing approaches on shale gas assessments are reviewed.
Chapter III presents an overview of Artificial Intelligence and Neural Network. The architecture and algorithm used in this dissertation will be shown.
Chapter IV describes the methodology and workflow that is used in this study.
Chapter V describes the development of Spatio-temporal database and the taken steps in preparation of the data for modeling.
Chapter VI discusses the history matching workflow and the results. In this chapter the results of the wells with poor history match will be discussed.
Chapter VII presents the steps in validating the AI-based shale model. In this chapter, the forecasting and prediction capability of the model will be showed.
Chapter VIII presents the comprehensive sensitivity analysis results, optimization study and generated type curves.
Chapter IX offers conclusionary remarks and recommendations for future work.

2. CHAPTER II

LITERATURE REVIEW

2.1 Introduction

Production from shale assets has become one of the most significant sources of US domestic energy today. Consequently, research related to unconventional reservoirs has increased significantly in order to better understand the inherent complexities of their behavior. Analytical, numerical and statistical analyses have been applied to large multi-variable data set from shale assets with different degrees of success. A vibrant and fast-growing literature exists related to various aspects of gas shale, including operational (e.g., drilling, completion, and production) and technological challenges. The latter mainly involves difficulties in formation evaluation/characterization, in modeling macro- and micro-scales of gas flow and transport, and in developing reliable reservoir simulators.

In this chapter, a review of literature will be conducted in four sections. The first section discusses the analytical methods of shale gas assessment with focus on Decline Curve and Rate Transient Analysis. In the second section, the numerical analysis methods of shale gas will be reviewed. The third section discusses the data-driven or statistical analysis approaches. In the fourth section of this chapter, the works related to sensitivity analysis in shale will be reviewed.

2.2 Analytical Approaches to Shale Assessments

For almost every oil and gas producer well, there has always been some sort of analysis done on the production data. The origin of all these analyses is the diffusivity equation which is a combination of continuity equation, flux equation (Darcy's Law) and an equation of state. Production analyses for shales have been developed over the last 50 years based on models for the production of gas from coal beds and applied initially to low pressure fractured reservoirs [Walton, 2012]. With rapid demand for production from shale the need for development of a reliable, fast and cost efficient model is proceeding apace. Accordingly, decline curve and rate transient analysis has attracted much attention.

2.2.1 Decline Curve Analysis

The "Arps" decline curve relations is one of the primary and most widely used tools to estimate the oil and gas reserves. These analyses are based on empirical equations related to production rate with time and is derived by the definition of the "loss ratio" and "derivative of the loss ratio" as follows:

$$Loss - Ratio \qquad \frac{1}{D} \equiv -\frac{q}{dq/dt} \ldots\ldots\ldots\ldots\ldots\ldots\ldots\ldots\ldots\ldots\ldots\ldots\ldots\ldots\ldots\ldots\ldots\ldots (1)$$

$$Derivative\ of\ the\ Loss - Ratio \qquad b \equiv \frac{d}{dt}\left[\frac{1}{D}\right] \equiv -\frac{d}{dt}\left[\frac{q}{dq/dt}\right] \ldots\ldots\ldots\ldots\ldots\ldots\ldots (2)$$

Depending on the decline rate parameter, Arps differentiated decline into three different types as Exponential Decline (b=0), Hyperbolic Decline (0<b<1) and Harmonic Decline (b=1) [Arps, 1944]. The Arps decline rate equations are based on observations of the conventional reservoirs and are only applicable for the boundary dominated flow, but the work done by Fetkovich (1980) provided some more theoretical bases to the Arps decline equations by developing type curves for early transient flow. However, they did not discuss the possibility of the value of the b-parameter for greater than one.

For unconventional reservoir, the common practice is to use hyperbolic rate decline relation and it has been shown that the value of b-parameter could exceed one. Many attempts have been made in order to apply the decline curve equations in shale reservoir properly. In 2008 Ilk *et al.* introduced the "power-law loss ratio" rate decline model to estimate gas reserves in tight gas reservoirs. Their model is based on different functional form for the D-parameter as Equation 3 which shows the loss ratio can be approximated by a decaying power law function with a constant behavior at large times (i.e. the D_∞ - constant).

$$D = D_\infty + D_1 t^{-(1-n)} \ldots\ldots\ldots\ldots\ldots\ldots\ldots\ldots\ldots\ldots\ldots\ldots\ldots\ldots\ldots\ldots\ldots\ldots\ldots\ldots (3)$$

The model has been applied on different synthetic and actual cases and it showed much more flexibility to match transient, transition and boundary dominated flow. The work by Valko (2009) presented another new decline curve model called the "Stretched Exponential Decline Model (SEPD)". In this new model, a new set of parameters; n (is the exponent and it is equal to b-parameter in Arps relations), τ (is the characteristic number of periods) and q_i (is the initial production rate) were defined and can be used in order to estimate the rate in each time step as equation 4:

$$q = q_i \exp\left[-(\frac{t}{\tau})^n\right] \ldots\ldots\ldots\ldots\ldots\ldots\ldots\ldots\ldots\ldots\ldots\ldots\ldots\ldots\ldots\ldots\ldots\ldots\ldots\ldots (4)$$

In the Arps formulation, by increasing values of b-parameter, the rate of depletion becomes slower and very large EUR will result. In contrast, the SEPD model has a bounded nature, i.e. as depletion gets slower, n assumes smaller values. Similar to work done by Valko, Boulis *et al.* (2009) proposed several

functional forms for the b-parameter in order to evaluate the b-parameter as a monotonically decreasing function of time. Based on their study, b-parameter can be characterized as the following models:

- $b(t) = b$ $\quad constant\ (Arps\ hyperbolic\ rate - decline\ realtion)$
- $b(t) = b_0 \exp[-b_1 t]$ $\quad exponential\ function$
- $b(t) = b_0 t^{-b_1}$ $\quad power - law\ function$
- $b(t) = 1/(b_0 + b_1 t)$ $\quad rational\ function$

They also derived the corresponding rate-decline relation for each b-parameter model and solved the differential equation related with each b-parameter model. The models were applied to different numerical and actual cases and they investigated that the performance of the models can vary under different conditions. As conclusion of their work, using the constant b-parameter for the data that do not exhibit boundary-dominated flow significantly over-estimates the reserve. The reserve estimated by using the exponential function is conservative because this model cannot represent the transient flow regime. They have also observed that the computed b-parameter trend exhibits a power-law behavior in some cases and for those cases, the matches are outstanding and the reserves are reliable. Moreover, the rational function for the b-parameter is the most flexible model that can properly represent early time as well as middle and late time behavior of production data. Under these observations, they suggested the use of all the b-parameter models in conjunction to yield better resolution and to decrease the uncertainty in reserves estimates.

Despite improvements in applying Decline Curve Analysis (DCA) in shale, prediction of future decline by using deterministic DCA is far from actual future production trend and thus the single deterministic value of reserves is not close to the true reserves [Cheng et al., 2010]. Unlike these deterministic estimates, probabilistic approaches provide a range of estimates for reserve and thus attempt to bracket the true value. The work done by Cheng *et al*. (2010) offered a modified bootstrap algorithm employed to preserve data structure. In this method, each pair of rate-time is matched by using conventional decline curve and residuals from the fitted model and observed data is constructed. Then different bootstrap realizations will be generated by incorporating the random samples from residuals into fitted model. They also were able to improve the coverage rate of confidence level and to estimate more accurate reserves. They applied their method to 100 oil and gas wells and showed that by using this probabilistic approach, much wider confidence level and more reliable p-50 values can be obtained.

On the other hand, instead of generating synthetic data sets, Can *et al.* (2012) used large data sets comprising many wells to obtain parameter distributions from well groups exhibiting similar decline behavior.

In this study, the existing wells were grouped based on their productivity index in order to obtain common stretched exponential decline model (SPED) parameters for similar wells. They used a group's common n and τ parameters to generate the model response for an individual well, and the well's specific production parameter q_0 and they came up with the probabilistic criteria of P index (P10-P50-P90) for each individual group. The capability of the model for production forecasting was validated by three actual unconventional field data sets (both oil and gas) and also simulation cases.

2.2.2 Rate Transient Analysis

The other analytical methods for shale gas reservoir that have proved practical, reliable and inexpensive, is rate transient analysis which is being used to evaluate the shale gas production in order to extract hydraulic fracture and reservoir properties. The analysis usually includes flow regime determination and solving the diffusivity equations for different type of flow behavior. It has been observed that most the shale wells behavior is controlled by transient linear flow (transient matrix drainage into fractures) and it is the only flow regime in these wells that could last for years. Therefore most of the literature is devoted to solving equations for transient linear flow however, there are some papers that have concentrated on the existence of other flow regimes.

In the work done by Bello (2008 & 2009), all possible flow regimes in shale gas have been introduced although he developed the equations for transient flow regimes. Based on his definition, five flow regimes can be identified (Figure 2.1). Region 1 is due to transient flow only in the fractures. Region 2 is bilinear flow and occurs when matrix drainage begins simultaneously with the transient flow in fractures. Region 3 is the response for homogenous reservoir. Region 4 is dominated by transient matrix drainage and is the flow regime that lasts several years. Region 5 is the boundary dominated transient response.

Using the massive multi-stage hydraulic fracture treatment in order to create or enhance complex networks of fractures connected to the well is a common practice in shale wells. As a result, production analysis of these types of wells in terms of estimating the fracture properties, extension of stimulated reservoir volume (SRV), and the amount of gas became very important.

Anderson *et al.* (2010) proposed an analysis method and model that accounts for multiple transverse fractures in a horizontal well. The presented methodology is basically using three particular plots (as

following) to provide the reliable identification of dominant flow regimes exhibited in the data as well as estimates of bulk reservoir properties, apparent skin and hydrocarbon pore volume:

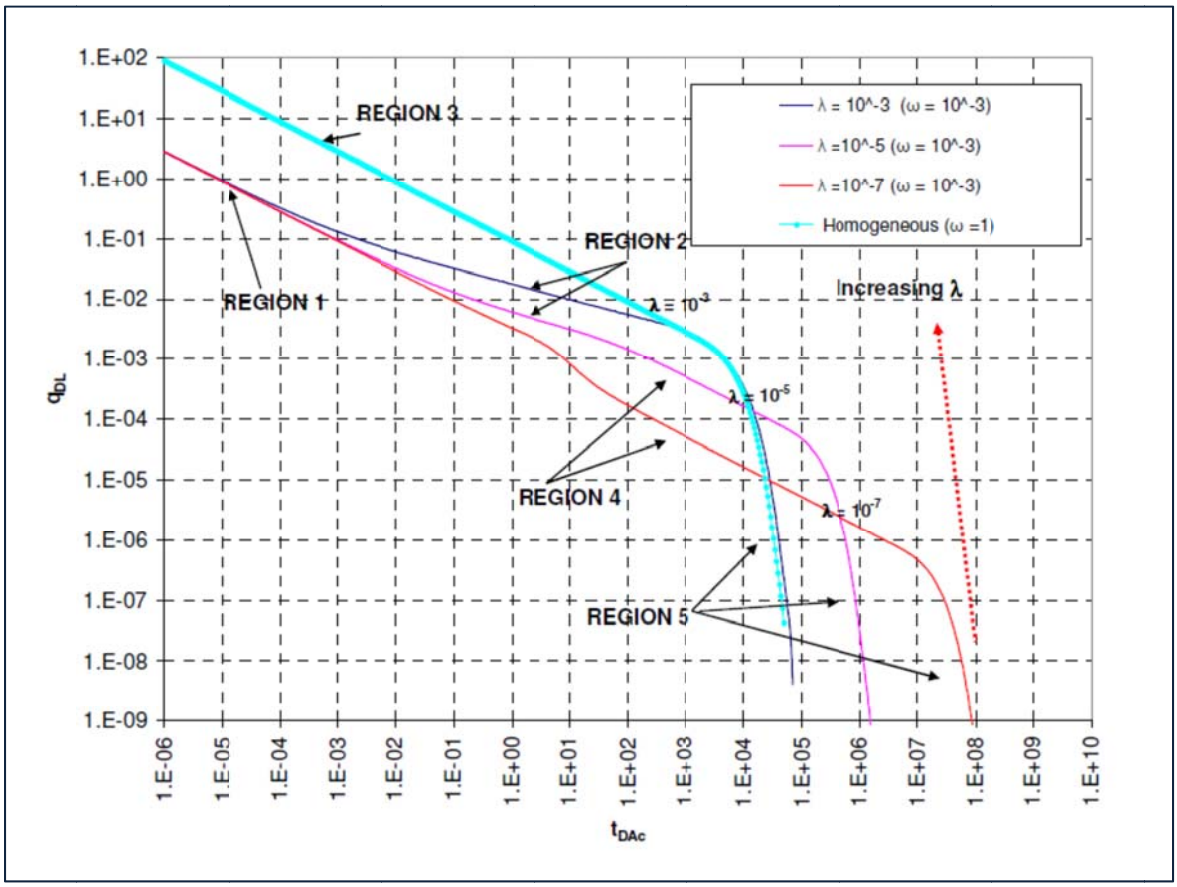

Figure 2.1: Illustration of the five flow regions. λ, ω are interporosity and storativity respectively

- Log-Log Plot: $\frac{q}{P_{pi}-P_{pwf}}$ and $\left[\frac{d}{dlnt_a}\left(\frac{P_{pi}-P_{pwf}}{q}\right)\right]^{-1}$ versus Pseudo time OR $\left[\frac{d}{dlnt_{ca}}\left(\frac{P_{pi}-P_{pwf}}{q}\right)\right]^{-1}$ versus material balance time
- Square-Root Time Plot: $\frac{P_{pi}-P_{pwf}}{q}$ versus $\sqrt{t}$
- Flowing Material Balance Plot: $\frac{q}{P_{pi}-P_{pwf}}$ versus $\frac{2qt_{ca}P_i}{(\mu_g c_t Z)_i (P_{pi}-P_{pwf})}$

Anderson *et al.* (2010) took advantage of using derivative rate function that is not affected by skin impact for flow regime identification. By knowing the flow regime, either square-root time and/or flowing material balance plot can be used to estimate the matrix permeability, fracture spacing, stimulated reservoir width, apparent skin and hydrocarbon pore volume. The procedure is also including the production forecasting based on the depletion of SRV and contribution of flow from unstimulated

surrounding matrix. The proposed methodology was applied on different case studies and the above-mentioned properties were estimated. However, in some cases the calculated values are far from the reality which might be because of assumptions made in developing the models such as having bi-wing fractures in each stage. On the other hand, as mentioned earlier, the transient linear flow (Region 4 in Figure 2.1, half-slope line in log-log plot) is the dominant flow regime in shale gas well and in some cases, it might be the only observed flow behavior. Therefore, estimating some of the essential parameters such as stimulated reservoir volume, hydrocarbon pore volume and consequently production forecasting would be impossible due to lack of boundary dominated flow regime exhibited in data.

In order to overcome this problem, Nobakht *et al.* (2010) proposed a simplified forecasting method which is only based on the transient linear flow. The method is simple as it relies on a plot of inverse rate versus square root time. It is rigorous in that it is based on the theory of linear flow and combines the transient linear flow period with hyperbolic decline during the boundary dominated flow. The workflow includes the estimation for the end of linear flow by using the slope of the straight line in root-time square plot under the assumption of constant flowing pressure which is a representative of transient linear flow. The transient linear flow is directly followed by boundary-dominated flow which can be represented by traditional hyperbolic decline. By applying the hyperbolic decline curve on time periods after end of transient linear flow, the rate can be forecasted. The method was validated by comparing its results against numerically simulated results and it was found that for all practical purpose reliable forecast can be obtained from this method however, it needs to be modified in different aspects.

The equations used in work done by Nobakht *et al.* (2010) are based on liquid flow theory. To account for gas flow, pressure should be replaced by pseudo-pressure and time should be substituted by pseudo-time or material balance time to account for the change of gas properties. Using the pressure and time by itself will cause an overestimation in fracture half-length and matrix permeability and should be corrected before using in a reservoir model in forecasting. Nobakht *et al.* (2012) analytically derived a correction factor for the slope of the square root of time plot for constant flowing pressure case. In their analytical model, every required gas property was calculated using average pressure in the region of influence. The average pressure in the region of influence depends on initial pressure, flowing pressure and gas properties as following:

$$\frac{\bar{\bar{P}}}{\bar{Z}^{**}} = \frac{P_i}{Z_i^{**}}\left[1 - 0.220\,\frac{\left(Z\mu_g c_t\right)_i (P_{pi} - P_{pwf})}{S_{gi}P_i}\,\frac{\sqrt{\bar{\mu}_g \bar{c}_t}}{(\mu_g c_t)_i}\right] \qquad (5)$$

In order to simplify the problem, the authors made some assumption such as having ideal gas and constant gas viscosity and they came up with a correction factor which is a function of average pressure and initial pressure (Equation 6):

$$f_{CP} = \sqrt{\frac{\bar{P}}{P_i}} \dots \dots \dots (6)$$

The fracture half-length calculated from the slope of square-root time plot can be multiplied by given correction factor to improve the linear flow analysis. The method was applied to a different simulation and an actual multi-fractured horizontal well in different shale plays. It showed that by using the correction factor, a good agreement between the simulation result and this analytical approach can be achieved.

In practice, tight gas and shale gas wells are produced under high drawdown to maximize production. Therefore the assumption of having constant flowing pressure is not far from the reality. However, production under constant rate is very common too. Nobakht *et al.* (2012) also developed an analytical model for analyzing transient linear flow data for a constant-gas rate production constraint. In contrast with the case of production under constant flowing pressure, the pseudo-time does not have a linear relationship with time and it should be taken into account in fracture half-length calculation based on square-root time plot. Meanwhile, the square-root time plot in this case should be based on the $(\frac{P_{pi}-P_{pwf}}{q})$ in order to account for gas. The pseudo-time as it has shown in equation 7, is a function of gas properties in average pressure in the region of influence.

$$t_a = (\mu_g c_t)_i \int_0^t \frac{dt}{\bar{\mu}_g \bar{c}_t} \dots \dots \dots (7)$$

Similar to the boundary condition of constant flowing pressure, the authors simplified the problem for calculating the average pressure, although the process is still iterative and it involves finding the average pressure, pseudo time and fracture half-length. The developed analytical model was validated using a number of numerically simulated cases with high accuracy.

As explained earlier, the presence of skin changes the shape of data points when plotted on log-log scales and this can have a huge effect on the interpretation particularly in flow regime determination [Nobakht et al., 2012]. For example a well with purely transient linear flow and with skin in a reservoir, which is infinite acting, may appear alike and be interpreted as finite acting reservoir simply because of the skin

effect. Nobakht *et al.* (2012) presented an easy method to analyze the production data from shale gas well with significant skin, which is based on square-root time plot. They introduced the new terms of modified normalized pressure and normalized rate as follows:

$$P_{pm} = \frac{P_{pi} - P_{pwf}}{q} - b' \quad \dots (8)$$

$$q_m = \frac{1}{P_{pm}} \quad \dots (9)$$

In which b' is the intercept of normalized pressure plot versus square-root of time. After calculating the modified normalized pressure and rate, these data will be used for the purpose of diagnosing flow regimes.

A fundamental problem with the application for conventional rate transient analysis to ultra-low permeability reservoirs is that current methods were derived with assumption for viscous laminar flow (i.e., flow that can be described with Darcy's law). Shale reservoirs have recently been observed to contain a wide distribution of pore sizes, including nanopores associated with organic matter [Clarkson et al., 2012]. Clarkson *et al.* (2012) developed a simple approach to model transport at various scales for shale gas reservoir by using the dynamic slippage concept and accordingly they modified the rate transient analysis techniques. The model incorporates the dynamic gas-slippage factor into transport equation and solves it numerically. The result of this new model was checked by the result of a model (the fracture porosity was set equal to the estimated meso-macroporosity of the shale and dynamic-slippage effects were accounted for by use of a table of transmissibility multipliers as a function of pressure) comes from commercial simulator and it showed an acceptable consistency.

Moreover, in this work they modified the definition of pseudo-pressure and pseudo-time to account for apparent gas-permeability change caused by slippage effects and desorption compressibility as equations 10 and 11 show:

$$m^*(P_i) - m^*(P_{wf}) = 2\int_{P_{wf}}^{P_i} \frac{1}{K_g(P)\mu_g Z} pdp \quad \dots (10)$$

$$t_a^* = (\mu_g c_t^*)_i \int_0^t \frac{dt}{\overline{\overline{K_g \mu_g c_t^*}}} \quad \dots (11)$$

Several high permeability and low permeability simulation runs were defined and the effect of slippage and desorption were investigated. The analysis showed that the effect of non-Darcy flow becomes more significant as the permeability (effective pore size) decreases because of the effects of slippage and diffusion, although the correction for desorption may still be in significant error if flowing pressure is below Langmuir pressure. The new model was also applied on an actual multi-fractured horizontal well and the authors concluded that there are more potentially important factors rather than multi-mechanism flow that may cause the variation of apparent gas-permeability with pressure during shale gas production. As instance the stress-dependent porosity and permeability may cause a considerable change in fracture conductivity and should be incorporated into transport equations. The authors incorporated the nonstatic porosity and permeability changes into the definition of pseudo-time and pseudo-pressure. This clearly showed that failure to account for these variables, non-Darcy flow and desorption effects during rate transient analysis can lead to significant errors in derived hydraulic fracture and reservoir properties.

2.3 Numerical Approaches to Shale Assessments

Numerical modeling of shale gas reservoir carries a very specific problem due to its distinct properties such as multiple gas-storage mechanisms, complex interaction between natural fractures and induced (hydraulic) fractures, and inherent heterogeneity associated with rock properties. Since most of the shale gas reservoirs are naturally fractured, the dual porosity models fit the best for modeling of fluid flow in this type of reservoir. Dual porosity approaches were introduced as dual porosity models in early 1960s by Warren and Root (1963).

In dual porosity modeling, fractures are idealized as parallel fluid conductive conduits separating sugar cube matrix blocks. Fluids cannot move between the matrix blocks without first entering the fractures. Fluids can only move in the fractures and matrix blocks act as source terms feeding the fractures [Ghods, 2012]. Figure 2.2 shows the idealization of fractured rock into dual porosity system.

The application of dual porosity models for shale gas was introduced by Carlson and Mercer (1991). They coupled Fick's laws for diffusion within the matrix and desorption in their transient radial reservoir model for shale gas. Modifications included the use of the pressure-squared forms valid for gas at low pressures to linearize the diffusivity equation. They provided a Laplace space equation for the gas cumulative production from their model and used it to history match a sample well.

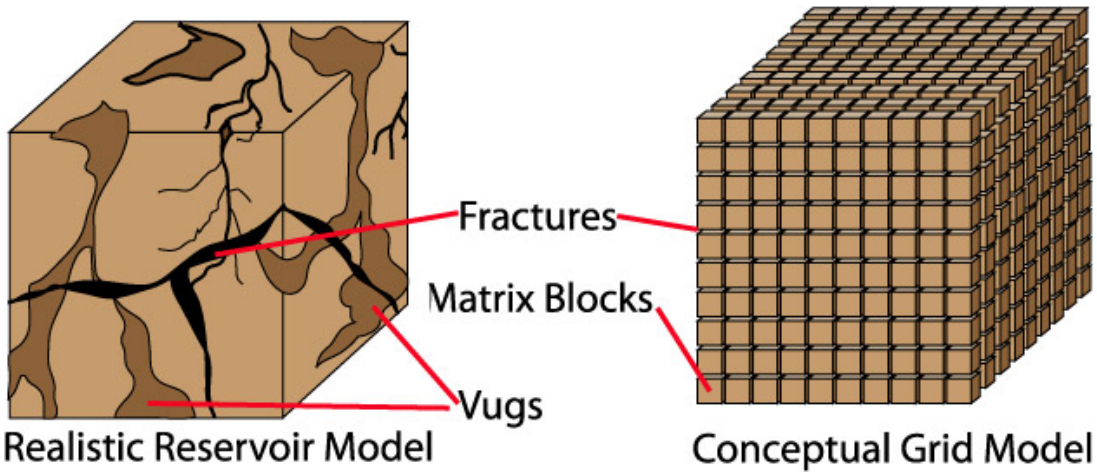

Figure 2.2: Realistic versus Conceptual Model for Dual Porosity Systems

Eventually, dual porosity methods have been widely accepted and became the industry standard for modeling shale gas. Because of the significant contribution of hydraulic fractures and also their interaction with natural fractures in shale gas well performance, it is very important to properly model the hydraulic fractures. Modeling the hydraulic fractures by using commercial reservoir simulators is usually done by generating the local grid refinement and inclusion of high conductivity to those fine grids to represent the hydraulic fractures. Several authors have used this technique (Kalantari *et al.* (2010), Li *et al.* (2011), Osholake *et al.* (2011)) to numerically model a shale reservoir. The work done by Chaudhri (2012) is one of the most recent studies in this regard. In this work, he used a set of logarithmically spaced Local Grid Refinements (LGRs) to model fractures and surrounding propped rocks. The smallest gird size is 1 inch to model induced fractures and the largest gird size is 150 ft. to model the matrix blocks. Three permeability values representative the matrix permeability, stimulated rock volume permeability and fracture permeability were used. The values of this permeability are used as uncertainty variables during production history matching and forecasting. Although explicitly modeling the hydraulic fractures by utilizing logarithmic local grid refinements is widely used in simulation of hydraulic fractures, it makes simulations painfully slow. Consequently most of the works which have used this method for the history matching and forecasting purpose, are only limited to a single well or a single pad because of the large number of grid blocks in the model and the complexity of the flow behavior.

Alternatively, the widespread application of microseismic mapping in defining the extension of Stimulated Reservoir Volume (SRV) has improved the simulation techniques of shale gas in terms of time and complexities. Based on the definition given by Mayerhofer *et al.* (2008) microseismic events are mainly created as a result of shear slippages around the hydraulic fractures. The mechanisms include

shear slippages induced by altered stresses near the tip of fractures as well as shear slippages related to leakoff- induced pore pressure changes. In shale reservoirs diffusivity related pore pressure changes cannot move very far from the actual fracture planes unless natural fractures in alternate directions are open and hydraulically enhanced as a network structure thus serving as a conduit for fluid movement. This means that a large event cloud structure must be approximately equivalent to the actual fracture network size. Thus the microseismic even cloud structure observed by microseismic fracture mapping provides a means to estimate the SRV in very tight reservoirs and become a key part in shale gas modeling workflows and case studies such as the one presented by Du *et al.* (2009).

Du *et al.* (2009) presented an integration workflow that incorporates all essential information in shale gas such as seismic attributes, logs, core analysis, hydraulic fracturing data, microseismic maps, etc. Here in this workflow, a microseismic event envelope is not only used to estimate 3D enhanced stimulated volume, but is also applied to modify and recalculate the natural fracture geometries and attributes. It means that after generating the discrete fracture network (DFN) based on FMI interpreted fracture data, the microseismic event will be displayed over the DFN network in order to capture the best alignment between natural fractures and hydraulic fractures and thus, the DFN properties can be modified. This approach is proved to be very effective in achieving good results for matching production histories however; it is quite labor-intensive particularly in the case of a huge number of wells.

Conversely, the Volumetric Fracture Modeling Approach (VFMA) is very suitable for multi-well or full-field simulation where other fracture modeling may not work [Harikesavanallur et al., 2010]. In VFMA, the stimulated volume is modeled using different zones of influence around each stage of the frac job. Each zone is created by digitizing over the event locations and selecting the horizontal and vertical extent. This methodology provides flexibility in capturing any irregular 3D shape of fracture with microseismic even pattern. In this approach, Harikesavanallur *et al.* (2010) defined three distinct zones as propped frac, crushed zone and unstimulated zone to match the production of water flowback. The simulation run commenced with the propped frac and crushed zone being initially filled with water and then several realizations with varying proportions of propped frac and crushed zone were created to determine the optimum reservoir properties and extent of each zone that provides an acceptable match to the water flow back. The simulation result by using VFMA was compared to having the planar fractures with constant width and variable half-length (used as matching parameter with the other reservoir properties). The comparison of pressure distribution in the reservoir shows that although both approaches provided a match to the historical production data, only the VFMA matches the evidence from microseismic regarding the extent of the induced fracture network and pressure drop. Moreover, the small cells

representing the fractures in planar approach force short time steps due to the throughput constraints resulting in longer simulation run times.

Conventional hydraulic fracture models, developed to simulate bi-wing planar fractures, are adequate for non-fractured formations or where high stress anisotropy favors planar fracture propagation. However, these planar models are inadequate for simulating complex fracture geometry in shale gas. With the recent introduction of complex fracture propagation models, the ability to model hydraulic fracture growth in complex geologic environments typical of many unconventional reservoirs is now possible [Cipolla et al., 2011]. A newly developed algorithm for automated gridding of complex hydraulic fractures in numerical reservoir simulation models was presented by Cipola *et al.* (2011) that allow the efficient application of the "complex hydraulic fracture modeling to reservoir simulation" and includes the integration of seismic and geological data with complex hydraulic fracture models, microseismic measurements and reservoir simulation. In this workflow, well-scale measurements such as logs, core and drill cuttings is used in order to characterize rock mechanical properties, stress variations, and distribution and orientation of natural fractures (building the DFN). The addition of microseismic monitoring provides a key measurement to contain the DFN and geomechanical model, while also providing information that can be used to correlate hydraulic fracture growth with larger scale seismic characterization.

In the workflow presented by Cipola *et al.* (2011), the hydraulic fractures are not modeled by simply defining bi-wing planar instead they used two different approaches to model the complex fracture network; Wiremesh simply approximates the complex fracture network using an orthogonal set of fractures and Unconventional Fracture Model (UFM) which honors the natural fracture characteristics (i.e. DFN and mechanical properties). Two automated gridding algorithms have been developed for orthogonal hydraulic fractures that can be used in conjunction with classical reservoir simulation software and for un-structured complex fractures. These automated gridding algorithms were used to generate a reservoir simulation grid. This workflow was successfully tested on a horizontal well in Barnett Shale and it has gone through the history matching process by using both complex hydraulic fracture models. By introducing the new fracture modeling and automated reservoir simulation grid generation and accommodating all the technical components (seismic, geology, geomechanics, microseismic…) in a common software platform, it is now possible to efficiently apply the seismic to simulation workflow for unconventional reservoirs in well-scale.

Recent researches reveal that matrix blocks in dual porosity systems can be treated as a dual porosity media which are composed of sub-matrices with nano-Darcy permeability (organic and non-organic materials) and micro-fractures with milli- to micro-Darcy permeability (Figure 2.3). By using this

hypothesis, Dehghanpour *et al.* (2011) developed a triple porosity model for the inner shale reservoir. They assumed that viscous Darcy flow is dominant in macro- and micro-fracture networks and diffusion and desorption mechanisms occur in sub-matrices and extended the existing transient and pseudo steady state dual porosity formulations to account for the third medium. The governing equation is gas continuity under the assumption that global flow toward the wellbore is only through the large fractures and those micro and macro fractures are acting as a source. The equations (pressure functions) were solved by using Laplace transformation for both transient and pseudo-steady-state conditions. The study also includes the sensitivity analysis of the effect of porosity and permeability of each continuum on pressure transient behavior of a shale reservoir which showed that the existence of micro fractures in the shale formations can significantly delay the wellbore pressure drop. In other words, the micro fractures feed the macro fracture network and support the pressure medium.

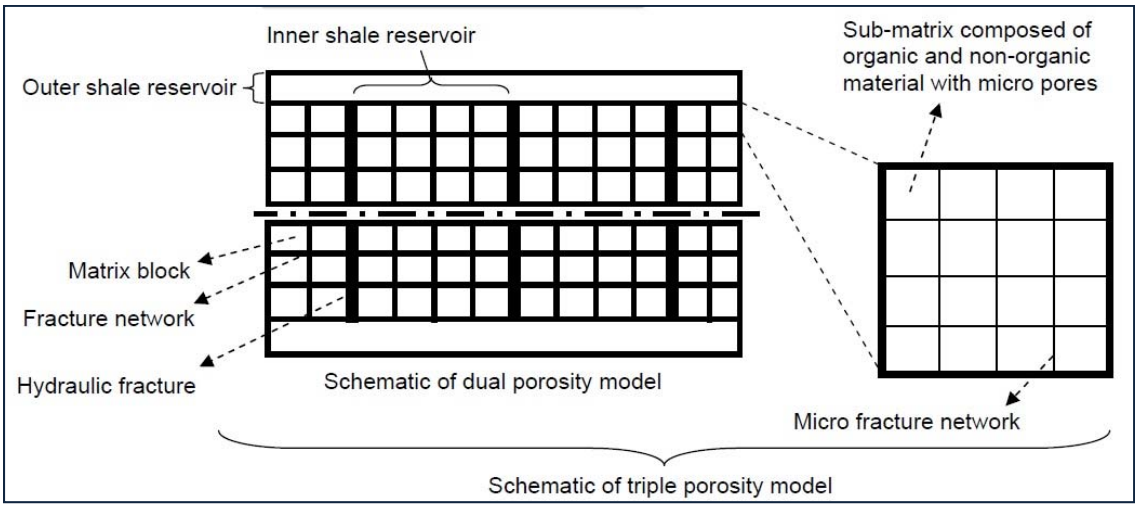

Figure 2.3: Schematic illustration of Triple Porosity Model-SPE 149501

Furthermore, coupling the triple porosity model with linear flow in hydraulic fractures creates the quad-porosity model which was presented by Hudson *et al.* (2012). In this definition, at a micro-scale system, shales are characterized by four micro systems: gas-bearing organic pores, water-wet inorganic pores, healed natural fractures and induced fractures from stimulation operations. Two models were considered in this study: a lumped-parameter based approach utilizing exponential functions as the transfer functions and a differential model derived from the conservation equation. The lumped-parameter approach is also considered as a "tank" approach by which various regions or systems of certain characteristics interact with each other by exchange of mass (based on material balance). The visualization of each lumped system as a tank draining into other tank systems and including internal mechanisms is given in Figure 2.4. The solid tanks represent the four different porosity systems. The dashed tanks represent internal

physical phenomena that may occur within each respective system. The valves represent the connectivity between each system. The differential model was derived in mathematical form of a continuum treatment of the various characteristic systems interacting with each other. A commercial simulator was used to solve the resulting differential equations of the model. The comparison of these two models showed that a four porosity system in series (gas flows through the organic porosity, inorganic porosity, natural fractures, and hydraulic fracture in that order) can be represented adequately as a dual-porosity case, thus suggesting that quad-porosity systems can be modeled as dual-porosity systems to achieve nearly identical results. This may also be due to the fractures not containing any gas initially.

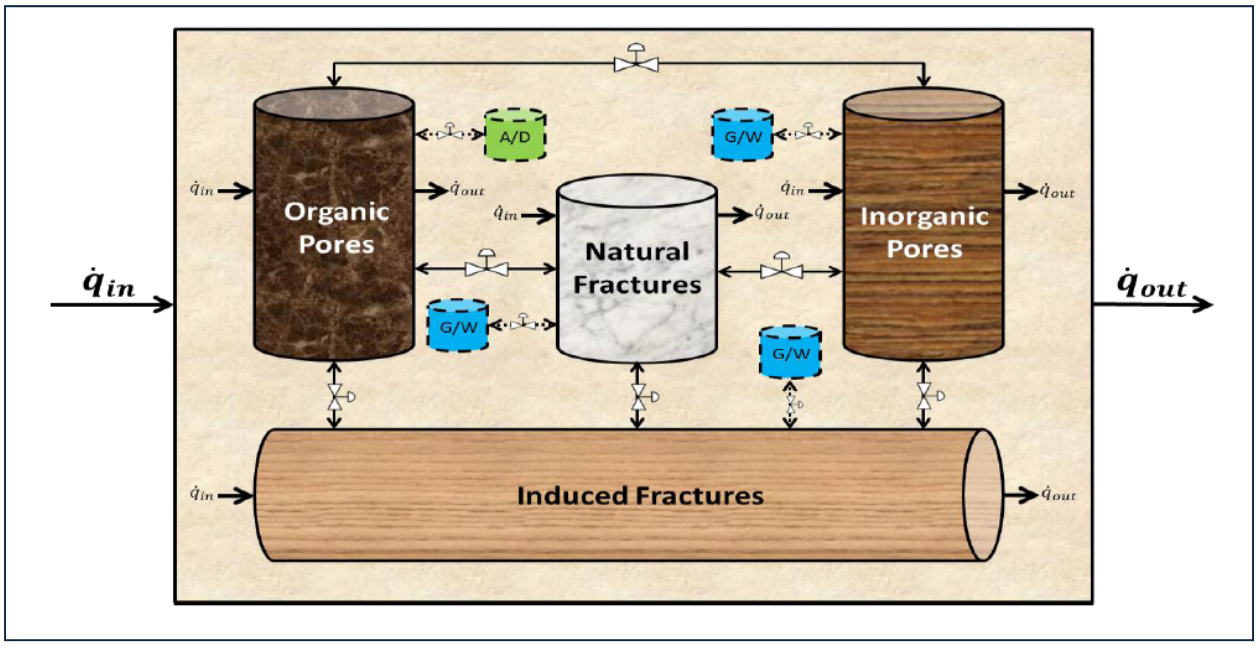

Figure 2.4: Tank representation of the quad-porosity reservoir model-SPE 153535

In the realm of numerical approaches to shale gas modeling, several attempts have been made in order to optimize the computational time by simplifying the problems. One approach is making the proxy models, which represent the physics associated with full-order simulation models, more computationally efficient. These proxy models are usually used for optimization purposes since they avoid hundreds of flow simulation realizations. Wilson *et al.* (2012) presented a general workflow for applying optimization to the development of shale gas reservoirs. The workflow is started with a detailed full-physics simulation model, which includes highly-resolved fracture networks, dual-porosity, dual permeability regions, and gas desorption and then a much simpler and faster reduced physics surrogate model is developed. The reduced physic model with single porosity system, without desorption or grid refinement but with tuned values for permeability and porosity in the stimulated zone could provide results in close agreement with

full-physics model. In this model, instead of explicitly modeling fractures, each fracture is represented through an additional perforation along the wellbore in the stimulated zone. The reduced physics model was then tuned by using the gas production of the full-physics model and used for field development optimization. The generalized pattern search algorithm (GPS) was applied in the optimization process to determine the optimal locations, lengths, and number of fracture stages for a prescribed number of horizontal wells.

2.4 Data-Driven Approaches to Shale Assessment

A counterpart of numerical and analytical models is the data-driven approach that seeks causes reflected in the data. Data-driven modeling is based on the analysis of all the data characterizing the system under study. A model can then be defined on the basis of connections between the system state variables (input, internal and output variables) with no or only a limited number of assumptions about the "physical" behavior of the system. Data-driven modeling has been developed with contributions from artificial intelligence, data mining, machine learning, and pattern recognition. These models can complement or replace the "knowledge-driven" models describing behavior of physical systems [Solomatine et al., 2008].

Data-driven modeling has broad applicability to the real world; in fact they have already been successfully applied in many industries such as medicine, marketing, risk management, sales forecasting, etc. Using this approach for shale gas assessment is not an exception specifically when analytical and numerical modeling of "full-field" shale assets is either impractical or leaves much to be desired [Mohaghegh 2013]. Data-driven models have been applied in shale reservoir assessment for different purposes; such as history matching and forecasting, building the proxy models, sensitivity analysis, estimating the hydraulic fractures properties.

In 2009, Mohaghegh introduced a new reservoir modeling technique known as Top-Down Intelligent Reservoir Modeling (TDIRM) as an alternative or a complement to traditional reservoir simulation and modeling which is based on the integration of classic reservoir engineering with artificial intelligence and data mining techniques. Top-Down full field subsurface modeling approaches the reservoir simulation and modeling from the opposite angle by attempting to build a realization of the reservoir starting with well production behavior (history). The production history is augmented by core, log, well test and seismic data in order to increase the accuracy and fine tune the Top-Down model. The model is then calibrated (history matched) using the most recent wells as blind dataset. This technique was applied on different conventional oil and gas reservoirs with a different production history and a degree of

complexities to predict the production performance of the field/wells, best infill location, remaining reserve estimation, etc.[Khazeni (2010), Mohaghegh (2009), Mohaghegh (2010), Kalalntari-dahaghi (2010)].

Upon achievement of good results in conventional reservoirs, the TDIRM was applied on several shale reservoirs. Kalantari *et al.* (2009) used this technique to reassess the potential of New Albany Shale. This study has been done on 55 vertical wells with limited production history(6-9 years out of the 20 years production history was available to the author) and well logs. By using the NFFLOW/FracGen and defining several set of natural fractures, the authors performed history matching to generate a complete production profile for each well. This generated synthetic production profile was then used to perform decline curve and type curve analysis which is a part of TDIRM workflow. Upon completion of these steps, the discrete, intelligent, and predictive models were developed for reservoir (production) attributes such as the first 3, 6, 9 month and 1, 3, 5, 10 years of cumulative production, decline curve information (D_i, Q_i, b) , EUR, Fracture Half-length, matrix and total porosity and permeability, initial gas in place and well recovery factor. These sets of discrete models were then integrated using fuzzy pattern recognition in order to achieve a cohesive model of the reservoir as a whole. The model was used as a guideline to estimate the remaining reserve in the field and to propose the best spots for infill drilling (6 wells) which can be profitable (economic analysis showed that the NPV for 5 years of these wells is positive). In this work, the TDIRM was also validated by removing 10% of the wells and the 1-year cumulative production of these wells was successfully predicted.

Another example of the TDIRM is the study that was done by Grujic *et al.* (2010) who applied the technique on Lower Huron shale in Eastern Kentucky. He followed the same workflow as Kalantari by starting with the history matching of 77 vertical wells by using NFFLOW/FracGen to acquire natural fracture network properties, fracture permeability and fracture aperture. This information along with extracted properties from Decline curve and Type curve analysis was incorporated into the Spatio-temporal database which includes the log properties and completion data (total mass of injected proppant, propped intervals and amount of injected fluid). As a final step of TDIRM's workflow, the history matching of monthly gas rate by using this database was then performed and was used for forecasting purposes. The high applicability of this approach to shale gas was demonstrated in these two studies where the developed TDIRM was able to successfully identify the most prolific zones for future development, estimating the remaining reserves, and also performance of existing and newly drilled wells.

In the context of data-driven modeling of shale, Shelley *et al.* (2010) has also applied the approach to evaluate the production potential of hydraulically fractured horizontal completions by better understanding the complex interaction between non-homogenous formations and hydraulically fracture horizontal completion. The key steps in this study are data quantification and integration, data visualization and QC, Artificial Neural Network (ANN) modeling, engineering validation and finally opportunity identification and quantification. The workflow was followed for a database including the production of 28 horizontal hydraulically fractured wells in Bakken, and some other information such as mud log (due to lack of reservoir properties, the mud log was used as an indicator of permeability), completion types, frac type, fluid and proppant volume, etc. The ANN model developed from this database was feed-forward type and it predicted the best-month oil cumulative production for the wells. The sensitivity analysis performed on this model determined the significance of a single parameter or combinations of parameter on a desired outcome such as number of completions, total treatment volume and conductive proppant.

Confidence in decision making by using the data-driven model is obtained when information derived from these models is supported with information derived from discrete modeling (reservoir simulation). Therefore, the data-driven model for Bakken shale was validated by comparing it against the reservoir simulation results. The ANN was then used for several horizontal wells in Bakken shale to provide the guidance on how to complete/frac those wells. In all cases, the predicted production by ANN was in a good consistency with actual production, meaning the proposed completion and fracturing methods indicated by ANN was correctly estimated.

Furthermore, the ANN model was used to improve hydraulic fracture understanding and facilitate decision making pertaining to the completion and stimulation of horizontal Bakken wells in Traux and Wildrose [Shelley et al., 2011]. These wells have been completed and fractured by different methods and in different treatment stages. The ANN model estimated a best calendar month of cumulative oil production for each well and it showed that all of the Traux wells evaluated are producing in a manner consistent with the data-driven model however; this is not the case in the Wildrose area. A 3-D frac simulator was used to evaluate the hydraulic fracture geometry created for these wells and it has been proved that the frac development is happening out of zone because of scarcity of effective barrier in this area on top of pay zones. In addition, the analysis indicated that frac staging methodology along with the number of frac treatments can significantly affect in-zone frac length. Based on this observation, creating two fractures per plug & perf frac stage versus one fracture for a ball drop frac sleeves stage may increase the production by 80%.

Recently, Shelley *et al.* (2012) developed a data-driven model for 55 horizontal wells in Eagle Ford (completed in oil and gas window) in order to derive the best practices for the completion of hydraulically fractured horizontal wells. In this study, the workflow presented by the same author (2010) was followed and ANN model was trained and validated in order to predict the first 30 days of equivalent oil, oil and gas. The data indicates that gas production is strongly influenced by depth, while oil production is related to higher molecular weight gas observed during lateral drilling. Performed sensitivity analysis on data-driven model also showed that the stimulation method for those wells in gas window should be different from those in oil window. While the number of fracture treatment and proppant conductivity would be effective to increase oil, the gas wells in the gas window respond to large stimulation volume.

As mentioned earlier, the data-driven models can also be used as a complement to traditional reservoir simulation, where the simulation results are used to train the ANN. In these cases, where performing traditional modeling is cost and time prohibitive, the ANN can be used as a "proxy". Several studies have been done for various types of proxy model, the scope of which lie beyond the bounds of this dissertation. As an example, however, a recent work done by Siripatrachai *et al.* (2012) will be presented here. In this work, two ANNs are developed. The first one called "Gas Production Prediction ANN" can instantly predict the production profile of a hydraulically fractured horizontal well completed in shale gas reservoir. The second ANN called "Equivalency ANN" is developed to establish equivalent hydraulic fracture representations between transverse hydraulic fracture and crushed zone representations. A feed forward Backpropagation neural network was used for both models with different hidden layers and neurons in each layer. A numerical reservoir simulator was used to generate a production profile from reservoir properties and design characteristics for the first network and establish equivalency for the second network. The output of the first neural network is the gas rate at different time intervals while the output for the second ANN is the specific characteristics of crushed zone (major axis length, minor axis length, permeability and fracture spacing for crushed zone). Both models were validated by several blind datasets and it showed that the generated networks can predict gas rates within ±10% and ±15% respectively.

2.5 Sensitivity Analysis in Shale Reservoirs

Sensitivity analysis is the study of how the uncertainty in the output of a mathematical model or system (numerical or otherwise) can be apportioned to different sources of uncertainty in its inputs [Wikipedia]. The sensitivity analysis in shale is usually preformed to evaluate the influence of input parameters on productivity of wells/fields and it can be done based on numerical simulation models or data-driven

models (statistical analysis). A vibrant and fast-growing literature exists related to sensitivity analysis in shale based on mentioned methods and in this section some of those methods will be addressed.

As discussed earlier, reservoir simulation is the preferred method to predict and evaluate well performance in shale reservoir. However, in many of presented models, some important features of shale reservoirs have largely been neglected. Cipolla *et al.* (2009) has performed a series of reservoir simulations using reservoir properties typical for Barnett shale to evaluate the likely impact of gas desorption and stress dependent fracture permeability. The reservoir has been modeled by using the dual permeability method to represent all network fractures in both un-stimulated volumes and also by locally refining the grid in the stimulated volumes using a logarithmically spaced grid design.

This study showed that the desorbed gas contribution is relatively small within the first 5 years of production and thus not likely to materially impact production economics. Moreover, the impact of desorption increases when the network fracture spacing is smaller, with most of the additional gas produced later in the well life. On the other hand, the study reveals that stress dependent fracture conductivity reduces ultimate gas production as drawdown in the fracture network continues to increase throughout the well life and network fractures "close". Nevertheless because of the relatively high Young's modulus of the Barnett shale, the impact of stress-dependent network-fracture conductivity does not appear to be significant, mostly affecting the mid to late life production behavior and could reduce gas recovery.

The impacts of gas desorption and stress-dependent fracture conductivity were also evaluated by the same author (Cipola *et al., 2010*) for typical Marcellus Shale reservoir properties. The impact of desorbed gas production in Marcellus was similar to that of the Barnett and is probably a minor component in the economic development of the Marcellus. In contrast to the Barnett, the lower Young's modulus of the Marcellus could mean that stress dependent network-fracture conductivity will play a significant role in the well performance and could substantially reduce initial production rates and ultimate gas recovery.

In other work done by Kalantari *et al.* (2009) sensitivity analysis has been performed by using NFFlow/FracGen in order to history match several vertical wells (without hydraulic fractures) in New Albany Shale. In this study, sensitivity analysis was done with the purpose of scrutinizing the influence of initial reservoir pressure, matrix porosity, matrix permeability, net pay thickness, natural fracture length, fracture density and aperture reduction factor on flow behavior. This study showed that the key parameters on production behavior are initial reservoir pressure, aperture reduction factor, fracture length and density.

On the other hand, some sensitivity analyses have been conducted to show the importance of hydraulic fracture design in shale. One sensitivity analysis worth noting, Cheng (2012), investigates the impacts of the number of perforation clusters and cluster spacing. From a reservoir engineering standpoint, it is desirable to create more fractures with shorter spacing, but in this study, Cheng showed that the number of clusters does not necessarily improve well production performance. By using the numerical dual porosity model, she has defined different cases for different number of fractures and cluster spacing for a horizontal well (same lateral length in all cases) to investigate the impacts of these two parameters on production performance of the well. Based on her findings, decreasing the cluster spacing so as to increase the total number of fractures may significantly reduce gas production when the cluster spacing is reduced to an inadequately small size where the width of fractures is strongly inhibited because of the mechanical interaction.

As shown by Cheng (2012), increasing the number of clusters does not necessarily improve well production performance and a very particular attention needs to be paid to the effectiveness of hydraulic fracturing treatments. In the study presented by Osholake *et al.* (2011) the impact of some other factors such as multi-phase flow, proppant crushing, proppant digenesis, capillary pressure and reservoir permeability on ultimate gas recovery was investigated. By using a numerical reservoir simulation model, the impact of each post hydraulic fracture parameter when it is modeled individually and when the combination of several parameters are modeled was studied. Based on this study, using the expensive proppant or bigger proppant does not necessary imply a significant increase in the ultimate gas recovery. By incorporating each individual parameter into a simulation model it has been found that proppant digenesis effect when compared to other effects has the most significant impact on production regardless of the conductivity of the hydraulic fracture created. On the other hand, when all the post hydraulic fracture effects were simulated, the drop in production by adding proppant crushing to the multiphase flow and single phase effect is more significant than any other introduction of a post hydraulic fracture effect.

As mentioned earlier, the sensitivity analysis can be done by using statistical methods which are basically data oriented analysis. The impact of individual variables on the production outcome is often difficult to interpret with any degree of confidence when traditional linear regression methods are used, because of the impacts of missing data, erroneous data, non-linear data, and subtle interrelationships among variables. Lafollette *et al.* (2012) have done a comprehensive study on more than 15,000 producing Barnett wells by using the booted tree models, which have the capability of overcoming the difficulties inherent in more traditional methods. The study used this technique plus Geographical Information System pattern recognition to aid in interpretation of production result trends and to demonstrate the

effect of completion and hydraulic fractures. The relative importance of true vertical depth, Y path, total fracturing fluid volume, injection rate, perforation length and 20/40 mesh proppant on maximum gas rate was studied and it showed that total fracturing fluid volume is the most important predictor of maximum gas rate. The larger jobs are statistically shown to yield better gas rate. Besides, the higher injection rate and higher quantities of 20/40 mesh sand showed improved productivity but with less degree of influence.

The discussed workflow was also applied on more than 3500 wells in Bakken Light Tight Oil play by the same author [LaFollette et al., 2013]. In this study, LaFollette *et al.* investigated the impacts of well location, well architecture (azimuth, well dip angle and completed lateral length), completion and stimulation on production results by using multivariate statistical modeling in conjunction with geographic information systems pattern recognition. Three different production proxies such as first 12 month of oil production, barrels oil per completed length of lateral and barrels oil per lbm proppant were used as indicators of well productivity, efficiency of completed well length and efficiency of fracturing proppant use respectively. Similar to the previous study, the multiple regression analysis was used to identify the significant target variables and then boosted tree models were applied on each of three target production proxies to rank the relative importance of key variables as well as their interactions. Well location, a proxy for reservoir quality in unconventional reservoirs, is one of the most important variables for prediction of all well production and efficiency metrics modeled in the study. On the other hand, completed lateral length presented challenges as the longer laterals are less efficient in terms of barrels of oil per completed laterals. Furthermore, proppant concentration, coarse mesh proppant use and treatment size are significant in enough of the individual models to indicate that proppant conductivity should not be ignored in these reservoirs.

In recent work done by Bartuska *et al.* (2012), the information of five wells in Marcellus was used to evaluate the effect of different completion parameters (such as different landing target, different trajectories, different stages and cluster spacing) on the first 30 days of initial production. The completion diagnostics such as proppant and fluid tracers was integrated with production, stimulation and geologic data to provide useful information as to the effectiveness of the completion design. In this study, different chemical tracer was pumped in each stage in order to give an estimation of the fracture network's ability to deliver frac fluid to the wellbore as well as investigating any effects wellbore trajectory might have on fluid loading recovery. The chemical tracer returns showed that load fluid recovery per stage varies by location in the target zone. The highest recoveries of load fluid were from the heel stages while more fluid recoveries from toe stages have been observed in those wells with toe-down trajectory. Moreover, spectral gamma ray logs were used to optimize near-wellbore proppant placement and to identify unstimulated

sections of lateral. The longer wellbore and more clusters per stage are allowed for more uniform near-wellbore proppant coverage and significant improvements in production.

2.6 Summary

In this chapter the most recent available approaches to shale reservoir assessments was presented. As discussed, the analytical solutions are very well-known and popular due to their simplicity and ease of use. Despite the development of interesting achievements in Decline Curve Analysis (DCA) in shale, the lack of sensitivity to major physical phenomena associated with shale makes the use of DCA impractical. Rate transient analysis, on the other hand, represents the actual physics involved in shale but they typically cannot capture the very long transient behavior in matrix blocks exhibited by shale reservoirs particularly in early stages of well/reservoir life. In comparison, numerical reservoir simulators are good tools for in-depth numerical analysis that cannot be handled satisfactorily with analytical tools. Although the numerical methods are more rigorous and robust in capturing the physical properties of shale, the computational demand of such method is much necessary. Using grid refinements and/or unconventional fracture networks for representing the hydraulic fractures and complex fracture networks is not only time consuming for simulation (even impractical once the modeling goes beyond a single pad), but also unsuitable for history matching purposes.

When compared to other techniques, data-driven modeling may provide an alternative solution when analytical and numerical modeling of full-field shale reservoirs is impractical. This study proposes a novel method that integrates traditional reservoir engineering with pattern recognition capabilities of artificial intelligence and data mining in order to accurately and efficiently model fluid flow in shale reservoirs in full-field scale. This approach not only has a much faster turnaround time compared to the numerical simulation techniques, but also models the production from the entire asset (and not just a single well, like most numerical simulation studies) with good accuracy, incorporating all the available data. This integrated framework enables reservoir engineers to compare and contrast multiple scenarios and propose field development strategies.

3. CHAPTER III

BACKGROUND

The scope of this chapter is to provide a brief introduction to the Artificial Neural Network and Pattern Recognition sections and to present the architecture of used neural networks in this dissertation.

3.1 Artificial Neural Network Overview

An Artificial Neural Network (ANN) is a mathematical model inspired by biological neural networks. Neural Networks are designed to process information in a similar, but simplified, manner as the human brain. Resemblances to the human brain include [Popa, 2004]:

- Knowledge acquired through a learning process
- Local processing in artificial neurons (known as nodes or processing elements)
- Storage of experimental knowledge available for future use in interneuron connections (synaptic weights)
- Massive parallel processing implemented by profuse connection pattern.

Neural networks present some additional fundamental features providing them with the capability of solving a variety of complex scientific and engineering problems. These features include adaptability, massive parallelism, high connectivity and ability to perform pattern recognition (pattern recognition is the study of how machine can observe the environment, learn to distinguish patterns of interest from their background and make sound and reasonable decisions about categories of the patterns [Basu et al., 2010]), detect trends, and solve highly non-linear problems through deriving meaning from complicated or imprecise data.

A neural network consists of an interconnected group of artificial neurons and it processes information using the connectionist approach to computation [Wikipedia]. The main characteristics of ANN are that they have the ability to learn complex nonlinear input-output relationships, use sequential procedure and adapt themselves to the data. Being essentially non-linear regression models, the ANN perform an input-output mapping using a set of interconnected simple processing nodes or neurons. Each neuron takes in inputs either externally or from other neurons and passes it through an activation or transfer functions such as a logistic or sigmoid curve. Data enter the network through the input units arranged in what is called an input layer (Figure 3.1). These data are then fed forward through successive layers including the

hidden layer in the middle to emerge from the output layer on the right. The inputs can be any combination of variables that are thought to be important for predicting the output [Solomatine et al., 2008].

In a typical neural network data processing procedure, the data is divided into three separate sets:

- Training- set of examples used for learning to fit parameters (weights) of the classifier.
- Testing (or Calibration) - set of examples used to tune the parameters of a classifier, such as choosing the number of hidden layers using in a neural network.
- Production (Or Verification) - set of examples (not previously seen by the neural network to ensure its integrity and robustness) used only to assess the performance or generalization of a fully specified classifier.

The hidden layer is the essential component that allows the neural network to learn the relationships in the data. Training an ANN is the process of determining the optimal weights for the problem of interest. Once the network is trained, the connecting weights between neurons are established and it is said the network has "learned".

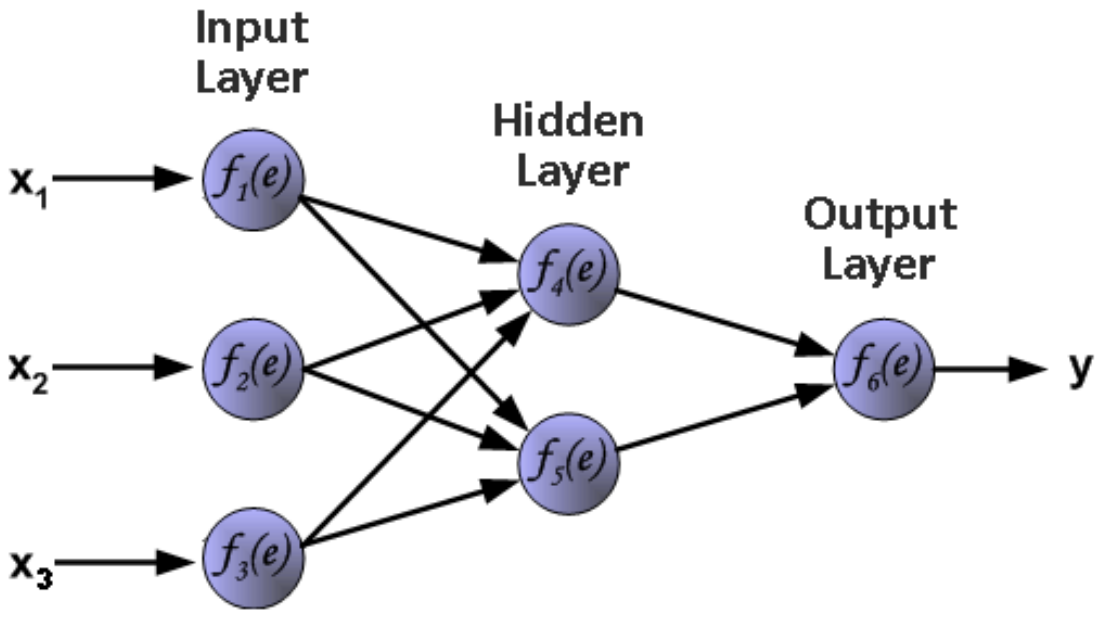

Figure 3.1: Schematic of Simple Neural Network (Source: Bernacki et al.)

Activation or transfer functions are the most important part of an ANN which transforms input signals to output signals. There are too many transfer functions available for different systems but the most common

are the logistic sigmoid, the hyperbolic tangent, the Gaussian and the linear transfer function. In general, linear neurons require very small learning rates in order to train properly. Gaussian transfer functions are employed in radial basis function networks often used to perform function approximation [Priddy et al., 2005]. For petroleum engineering problem it has been observed that the hyperbolic tangent and logistic sigmoid transfer functions work best, and since in this study these functions are being utilized the training process of ANNs, these two functions will be explained in more detail.

3.1.1 Sigmoid Transfer Function

The non-linear curved S-shape function, called the sigmoid function is the most common type of transfer function used to construct the neural networks. It is mathematically well behaved, differentiable and strictly increasing function [Chakraborty, 2010]. A sigmoidal transfer function can be written in the form of:

$$f(y) = \frac{1}{1 + e^{-\alpha y}} \quad \ldots \ldots \ldots \quad (12)$$

The sigmoid function is achieved using exponential equation and it gives the scaled outputs in the range between 0 and 1. By varying shape parameter, α, different shapes of the function can be obtained which adjust the abruptness of the function. The sigmoid function has another useful characteristic; its derivative is easily expressed in terms of its output as follows;

$$f'(y) = f(y)(1 - f(y) \quad \ldots \ldots \ldots \quad (13)$$

3.1.2 Hyperbolic Tangent Transfer Function

Similar to sigmoid function, hyperbolic tangent function is a nonlinear transfer function frequently used in the training of ANNs. The difference between hyperbolic tangent and sigmoid function is that the output from hyperbolic tangent function is in the ranges of -1 and 1 and it is also differentiable anywhere. Because of this greater numeric range the hyperbolic tangent function is often used in place of the sigmoid function [Siripatracai, 2011]. Hyperbolic tangent function is expressed in the form of:

$$f(y) = \frac{e^{y} - e^{-y}}{e^{y} + e^{-y}} \quad \ldots \ldots \ldots \quad (14)$$

3.2 Training the Neural Network

As mentioned earlier, training a neural network is the process of feeding it, teaching patterns and letting it changes its weights according to some learning rules. The objective of training an ANN is to determine the optimal weights of connections between neurons that yield satisfactory network performance i.e. low error. The learning process of an ANN can be categorized into three different types [Neuro AI Webpage]:

- ***Supervised Learning***-or *associate learning* in which the network is trained by providing it with input and matching output patterns. These input-output pairs can be provided by an external teacher or by the system which contains the neural network (self-supervised).
- ***Unsupervised Learning***- or *self-organization* in which an output unit is trained to respond to clusters of patterns within the input. In this paradigm the system is supposed to discover statistically salient features of the input population. Unlike the supervised learning paradigm, there is no priori set of categories into which the patterns are to be classified; rather the system must develop its own representation of the input stimuli.
- ***Reinforcement Learning***- this type of learning may be considered as an intermediate form of the above two types of learning. Here the learning machine does some action on the environment and gets a feedback response from that environment. The learning system grades its action good (rewarding) or bad (punishable) based on the environmental response and accordingly adjusts its parameters. Generally, parameter adjustment is continued until an equilibrium state occurs, following which there will be no more changes in its parameters. The self-organizing neural learning may be categorized under this type of learning.

Apart from the learning process, having proper network architecture is an important factor in building an ANN. Different factors such as number of hidden layers, number of neurons in each layer, connection between layers (fully or partially connected) affect the network architecture and can be changed by the designer. In addition, the number of training sets and functional links are influential to the training and performance of the network. Since training an ANN is an experiential process, a good starting point for training a network is proposed by Neuroshell (1998) as following:

$$Number\ of\ Hidden\ Neurons = \frac{N_{input} + N_{output}}{2} + \sqrt{N_{set}}$$

Where N_{input} is the number of inputs, N_{output} is the number of outputs, and N_{set} is the number of training sets. Using this formula as starting point for the training of the network, network architecture is

adjusted accordingly as training continues. Increasing number of hidden layers as well as number of neurons increases the complexity of the network. This allows the network to handle more complicated problems [Siripatrachai, 2011]. To successfully train the network, functional links are frequently added to input and/or output layers. Functional inputs and outputs are added to the network to provide additional relationships between original inputs and outputs. Functional links can be product, quotient, and eigenvalue of parameters where eigenvalue is an alternative way to represent parameters in matrix form with a single number. As an important remark, adding functional links created from outputs in the input layer is strictly prohibited. The mentioned training process is a general guideline and depending on the complexity of the problem, more neurons, hidden layers, and functional links may be required.

As the training of the network continues, one may encounter overlearning which is one of the most common problems in training of ANN. Overlearning or memorization, occurs when the network starts to memorize the given data set instead of generalizing. The result from memorized network initially appears to be in good agreement with the actual outputs. However, when the network is tested with the new data sets, the network does not produce the proper results for new data sets. Having a complex network and longer training for a simple problem may result in the network's overlearning. On the other hand, underlearning may occur from a lack of training due to too short of a training period or the architecture of the network is not sophisticated enough to handle the complexity of the problem. An underlearned network usually results in a poor performance. To obtain a generalized network, the data sets are randomly divided into 3 parts: 1) Training sets, 2) Validation sets, and 3) Testing sets. Both validation sets and testing sets are excluded from training. During training, error in validation sets is monitored. As the training continues, validation and training error should decrease. At some point, the validation error typically begins to increase. This is an indication that the network has started to memorize the relationships between inputs and outputs of the training sets. As stated earlier, a memorized network could lead to a false impression or misleading that the network is properly trained. When overlearning occurs, the training must be stopped.

Another challenge in training the artificial neural network is finding the global optimal solution. As the training continues, network errors decrease and approaches global optimal solution. It is important to avoid the local minima which are not the solution to the problem, and make ensure that the network's global optimal solution is reached [Siripatrachai, 2011].

3.3 Feed Forward Backpropagation Network

The number of types of ANNs and their uses is very high. Since the first neural model by McCulloch and Pits (1943), hundreds of different models considered as ANNs have been developed. The differences between them might be the functions, the accepted values, the topology, or the learning algorithms, for example.

For the purpose of this study, only an ANN using the Backpropagation algorithm for learning the appropriate weights will be presented since it is one of the most common models used in ANNs and many others are based on this model.

The Feed Forward Backpropagation network is a network in which the artificial neurons are organized in layers, send their signals “forward”, and then the errors are propagated backwards. The network receives inputs by neurons in the input layer, and the output of the network is given by the neurons on an output layer. There may be one or more intermediate hidden layer. The Backpropagation algorithm uses supervised learning, which means that the inputs and outputs is provided into the network and then the error which is the difference between actual and expected results, is calculated. The idea of the Backpropagation algorithm is to reduce the error, until the ANN learns the training data. The training usually begins with random weights, and the goal is to adjust them so that error will be minimal [Gershenson].

The weights associated with each interneuron connection affect the information so that the network can control the flow of information. The processing units in the hidden and output layers are characterized by the following activation function which is a sigmoid function [Hykin, 1994]:

$$f(y) = \frac{1}{1 + e^{-\alpha(\sum Wi * yi)}} \ldots\ldots\ldots\ldots\ldots\ldots\ldots\ldots\ldots\ldots (15)$$

The graphical representation of this function can be seen in Figure 3.2.

To illustrate this process, the three layer neural network with two inputs and one output, shown in Figure 3.1, is used [Bernacki et al.]. Each neuron is composed of two units. The first unit adds products of weights coefficients and input signals. The second unit realizes a nonlinear function, called neuron activation function. Signal “e” is adder output signal, and y = f(e) is the output signal of nonlinear element. Signal y is also the output signal of neuron (Figure 3.3).

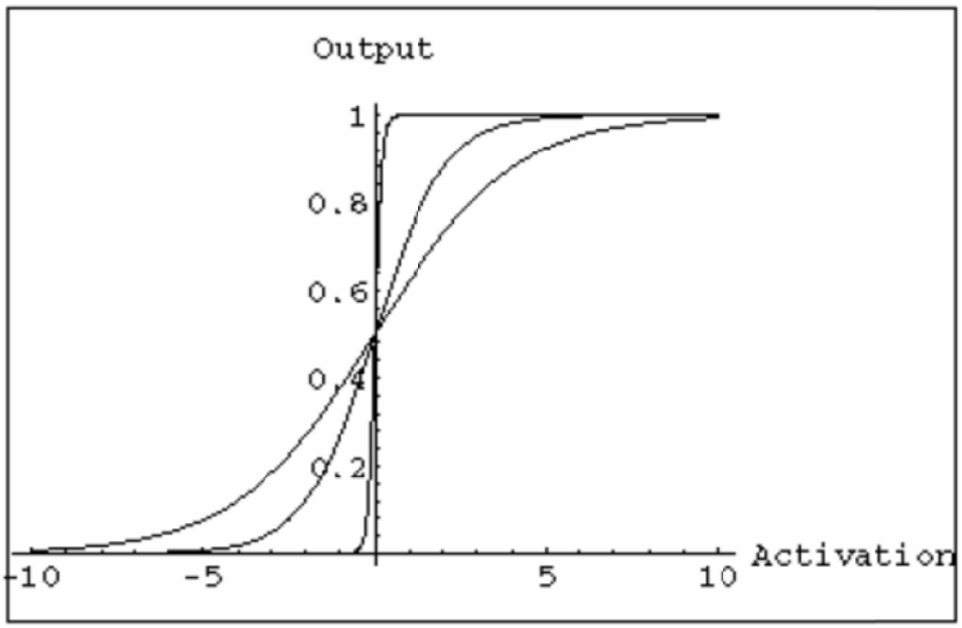

Figure 3.2: Activation Function for Back Propagation Networks

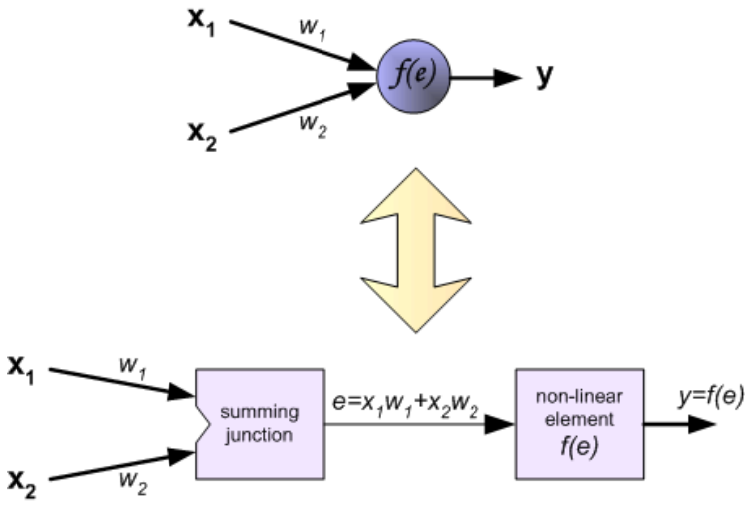

Figure 3.3: Each neuron is composed of two units. First unit adds products of weight coefficients and input signals. The second unit realizes nonlinear (activation) function. [Bernacki et al.]

In this particular case, the training data set consists of input signals (x_1 and x_2) assigned with the corresponding target (desired output) z. The network training is an iterative process in which, weight coefficients of nodes in each iteration, are modified using new data from training data set. Each teaching step starts with forcing both signals from the training set. After this stage, the output signals values for each neuron in each network layer can be determined.

Figure 3.4, illustrates how the signal is propagating through the network. Symbol $w_{(xm)n}$ represents weights of connections between network input x_m and neuron *n* in input layer. Symbols y_n represents output signal of neuron *n*.

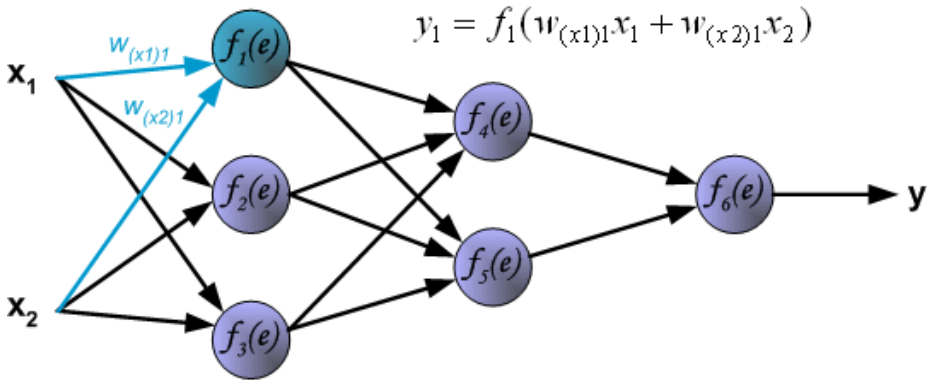

Figure 3.4: Propagation of signals through the input layer [Bernacki et al.]

In next step, the signal will be propagated through the hidden layer and output layer. Symbol w_{mn} represents weights of connections between outputs of neuron *m* and input of neuron *n* in the next layer. (Figure 3.5and Figure 3.6)

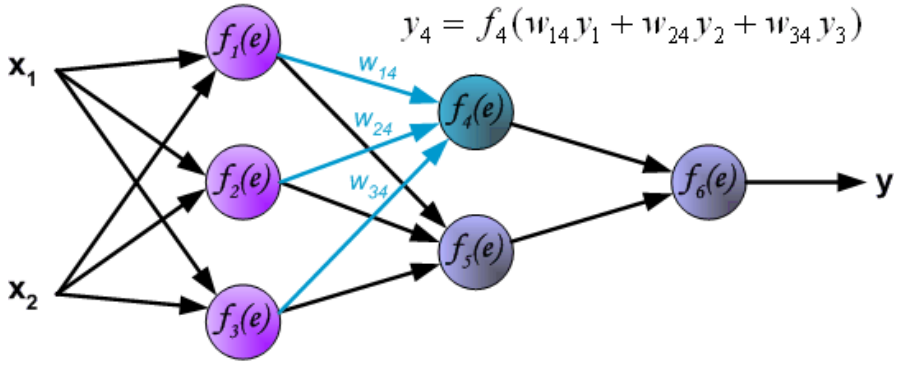

Figure 3.5: Propagation of signals through the hidden layer [Bernacki et al.]

In the next algorithm step, the output signal of network y is compared with the desired output value (the target), which is found in training data set. The difference is called error signal δ of output layer neuron. It is impossible to compute error signal for internal neurons directly. In Backpropagation method, the error signal δ (computed in single teaching step) is propagated back to all neurons, which output signals were input for discussed neuron.

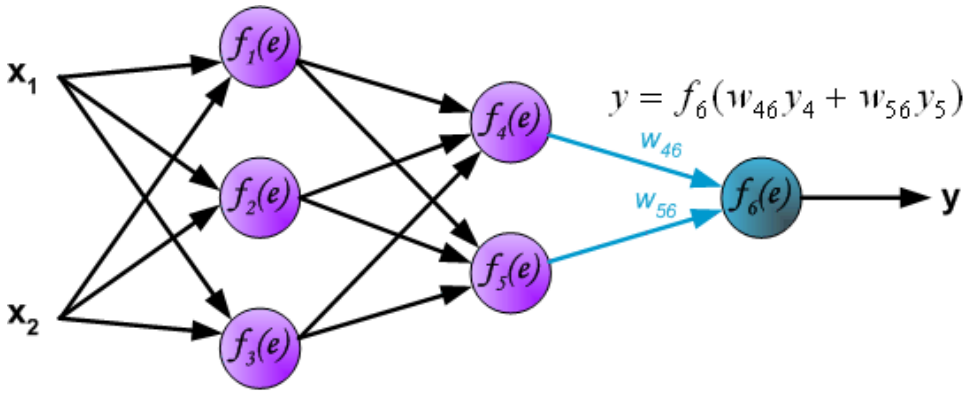

Figure 3.6: Propagation of signals through the output layer [Bernacki et al.]

The weights' coefficients w_{mn} used to propagate errors backward, are equal to those weights' coefficients used during computing output value. Only the direction of data flow is changed (signals are propagated from output to inputs one after the other). This technique is used for all network layers. If propagated errors came from few neurons, they are added (Figure 3.7).

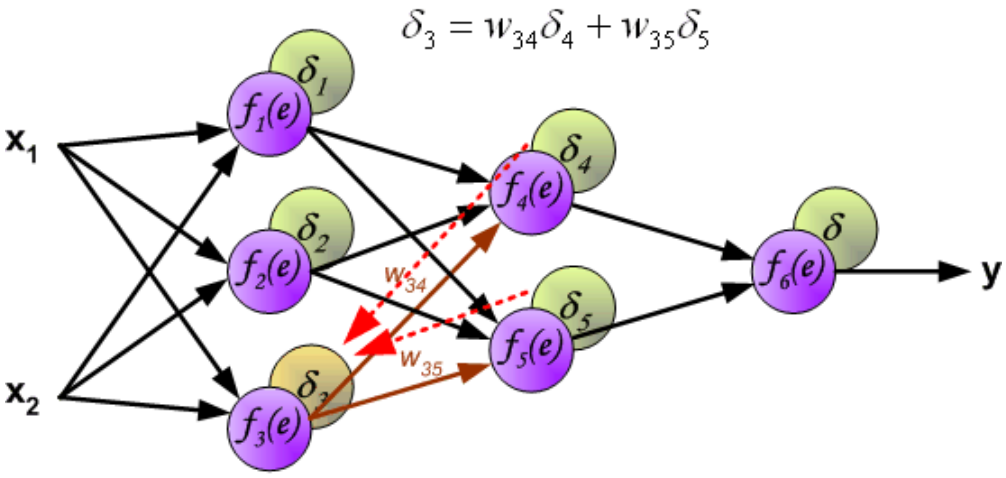

Figure 3.7: Error Back Propagation from Hidden Layer to Input Layer [Bernacki et al.]

When the error signal for each neuron is computed, the weights coefficients of each neuron input node may be modified (Figure 3.8). In formulas given in Figure 3.8, $df(e)/de$ represents derivative of neuron activation function (which weights are modified). Coefficient η affects network teaching speed. There are a few techniques to select this parameter. For example, when a method starts teaching with small parameter value during the teaching process, that parameter increases when the teaching is advanced and then increased again in the final stage.

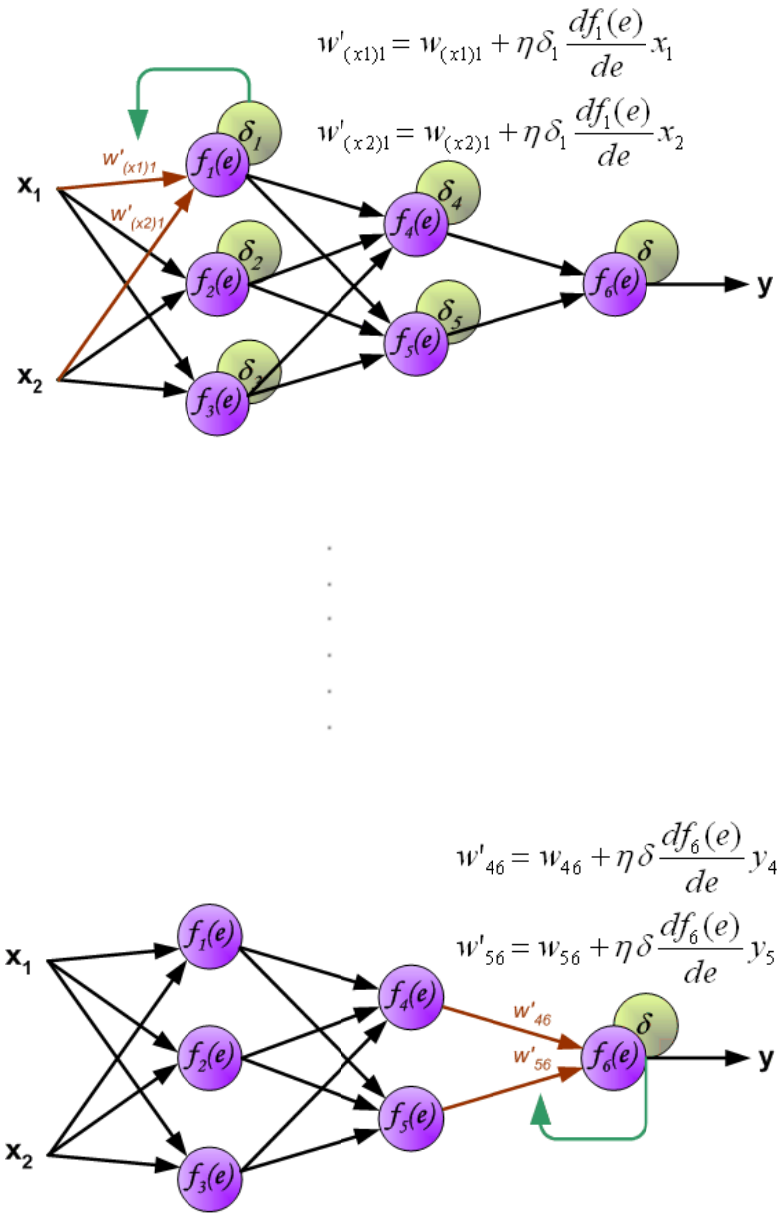

Figure 3.8: When the error signal for each neuron is computed, the weights coefficients of each neuron input node maybe modified. [Bernacki et al.]

Backpropagation has some problems associated with it [Robert Gordon Uni.]. Perhaps the best known is having several local minima as it was explained in previous section. This occurs because the algorithm always changes the weights in such a way as to cause error to fall but the error might have to rise as part of a more general fall as shown in Figure 3.9. If this is the case, the algorithm will get stuck (because it cannot go uphill) and the error will not decrease further. There are several solutions for this problem. One is very simple; reset the weights to different random number and try training again. Another solution is to add "momentum" to the weight changes. This means that weight change in this iteration depends not just on the current error, but also on previous changes. For example: (constant is <1)

$$W^{+} = W + current\ change + (Change\ on\ previous\ iteration * constant)$$

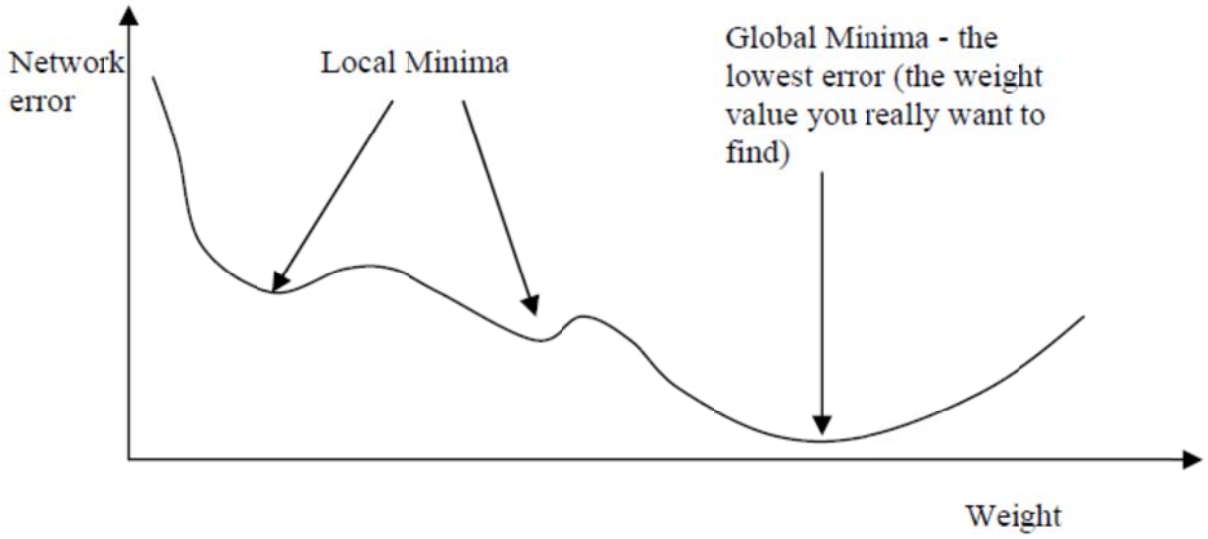

Figure 3.9: Local and Global Minima in Backpropagation Algorithm-[Robert Gordon Uni.]

There are other known problems with Backpropagation algorithm as well. These tend to manifest themselves as the network gets larger but many can be overcome by reinitializing the weights to different starting values. It is also worth noting that many variations on the standard Backpropagation algorithm have been developed over the years to overcome such problems [Robert Gordon Uni.].

3.4 Architecture of Neural Network in this Dissertation

The neural networks have been used in this dissertation to develop different data driven models for different purposes by using the IDEA^{TM} software package. The feed-forward Backpropagation networks applied for this dissertation utilize three layers comprising input, output and single hidden layer even though the number of nodes in hidden layer is governed by the total number of inputs required to

successfully represent a specific pattern. The parameters associated with the learning algorithm of Backpropagation are learning rate, momentum parameter and weights decay. The learning rate is the most important parameter. It scales the magnitude of weights adjustments and, thus, can dramatically affect the rate of learning. Momentum can improve performance by adding inertia to the trajectory of the weights during learning. This has an averaging and smoothing effect. Finally, weight decay has the effect of controlling the growth of weights and results in the learning rule preferring smaller weights. The default values of these parameters in IDEA^{TM} are used for all developed neural network models since they are based on many years of experience in working with different neural network models (Figure 3.10).

As shown in Figure 3.10, the "Vanilla" and "Enhance" type of Backpropagation methods are used in this dissertation. The "Vanilla" network only uses the "Learning Rate" which is an indication of how fast you want the network to learn the information presented. This is usually a moderate to low number (between 0 and 1).

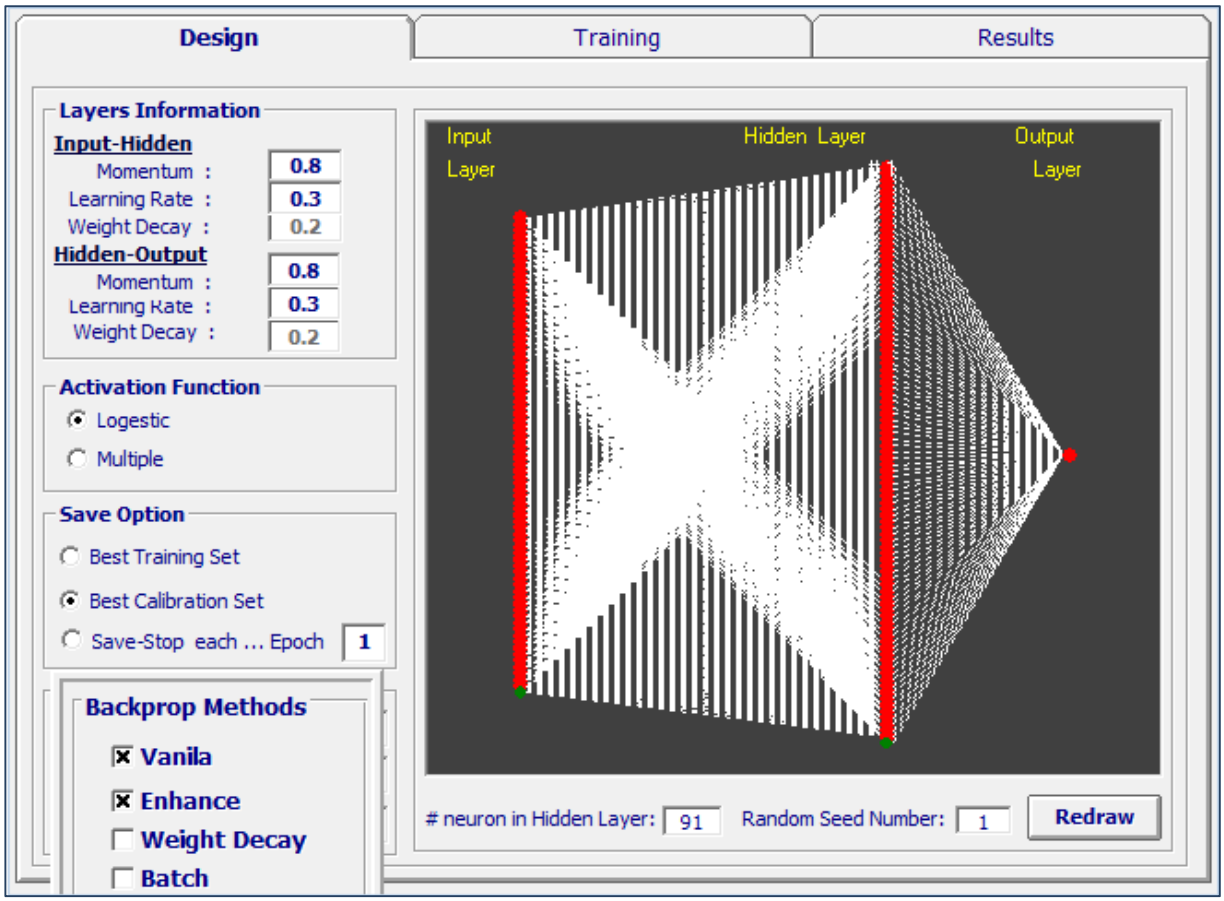

Figure 3.10: Architecture of Neural Network –Backpropagation Design Parameters

A large learning rate may cause the network to miss global minimum in the search space and could cause problem convergence during training. A small learning rate value may prolong the learning process and slow it down to a crawl. "Vanilla" networks do not need any other parameters to be assigned other than

learning rate. The “Enhance” networks need the learning rate as well as Momentum. Momentum is an extra push to the learning process that serves two purposes. First, it may accelerate the learning process, and second, it has the potential to kick the solution out of the local minima, that usually exists in the search space and causes the solutions to converge pre-maturely.

IDEA^{TM} provides different activation functions such as Logistic (Sigmoid), Gaussian and tangent Hyperbolic and Gaussian Complement but for the purpose of this dissertation the activation or transfer function of Sigmoid or Logistic is used.

4. CHAPTER IV

4.1 Methodology and Workflow for AI-Based Shale Modeling

The goal of the study is to develop an artificial intelligent based reservoir model which is capable of accurately and efficiently modeling fluid flow in shale reservoirs. The technique consists of different key steps such as Spatio-temporal database development, history matching process by training several neural networks, model validation by using blind data sets and sensitivity analysis. These steps are outlined and detailed in the following chapters. In this chapter the general workflow and methodology will be explained briefly.

The workflow showed in Figure 4.1 presents the methodology workflow. As shown in this figure, an AI-based model approaches the reservoir simulation and modeling from an opposite angle by attempting to build a realization of the reservoir starting with well production history. The production history is augmented with core, log, hydraulic fractures, and completion data in order to increase the accuracy and fine tune the AI-based model. The model is then trained and history matched while simultaneously developing several neural networks. This model is calibrated using the production history of the most recent wells as blind dataset. The final history matched and calibrated model is used to strategize the field development in order to improve the hydrocarbon recovery.

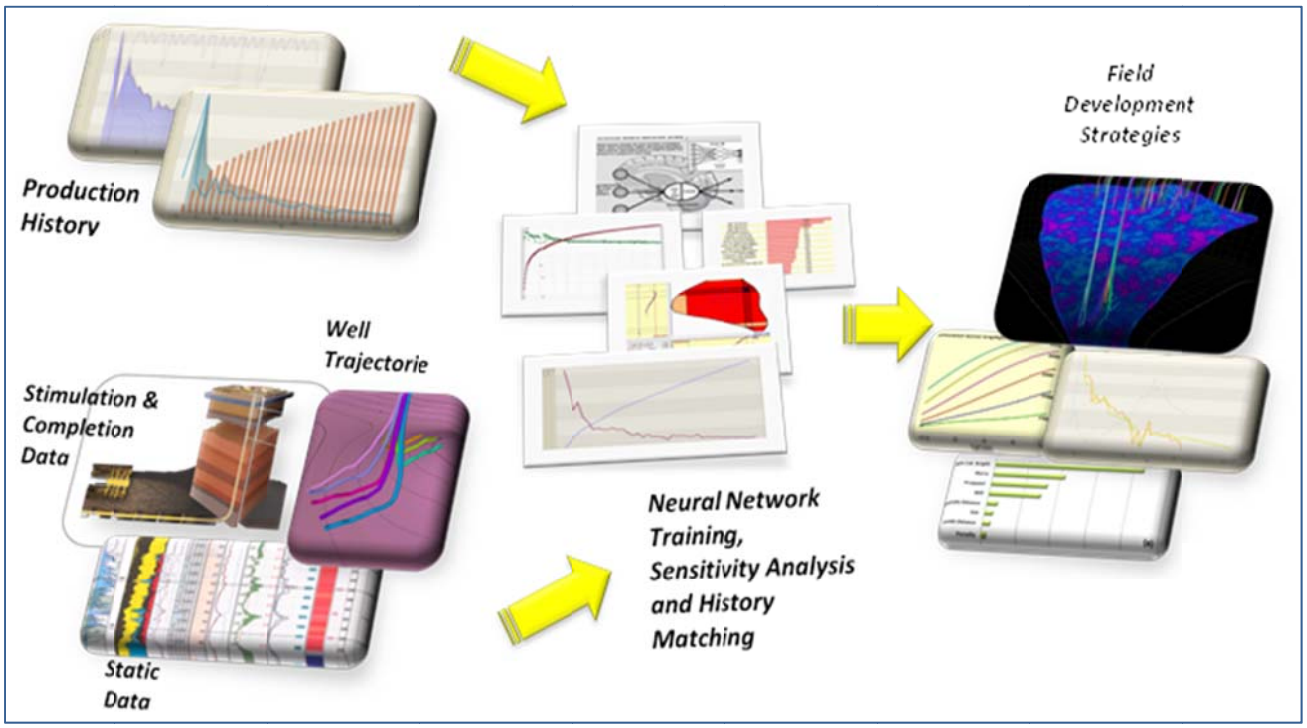

Figure 4.1: General Workflow in Developing the Artificial Intelligent (AI) Based Reservoir Model

The first and most important step in development of the AI-based reservoir model is preparing a representative Spatio-temporal database. The extent at which this Spatio-temporal database actually represents the fluid flow behavior of the reservoir that is being modeled, determines the potential degree of success in developing a successful model. This database is an integration of static information such as reservoir characteristics, geomechanical properties, completion and stimulation data and also dynamic information such as rich gas production, wellhead pressure and water production.

The developed Spatio-temporal database in the previous step is the main source of information for building and history matching the AI-based reservoir model. History matching process in this study has gone through a process of inclusion and exclusion of certain parameters based on their impact on model behavior. As it has shown in Figure 4.2, during the history matching process, the impact of adding offset wells, different flow regimes, distances between the laterals and different well types were studied.

Besides, a propriety algorithm (dubbed Fuzzy Pattern Recognition (Bezdek et al. 1992)) was also used to identify the influence of each individual parameter as well as the impact of their combination (Key Performance Indicator)

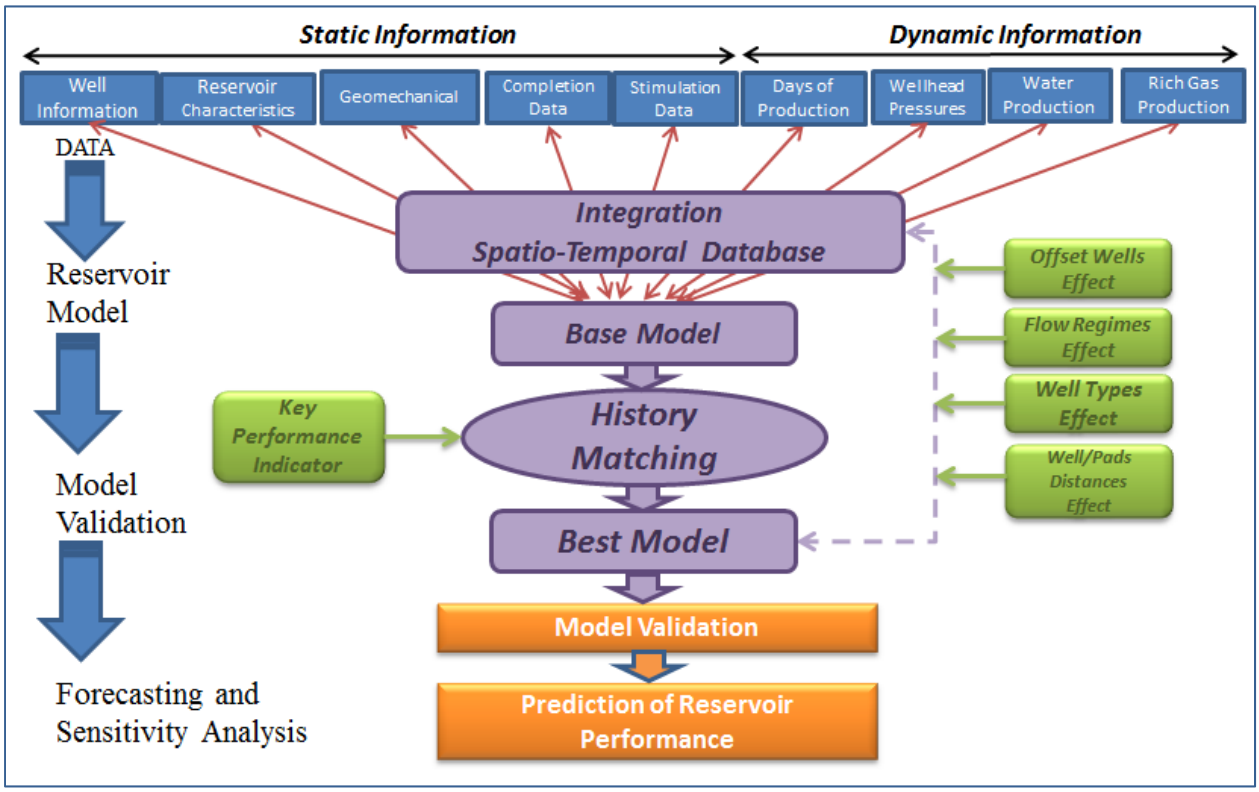

Figure 4.2: Detailed Workflow in Development of AI-based Shale Reservoir Model

Upon achieving the best history matched model, three scenarios were defined in order to validate the capability of model for forecasting the future reservoir performance as well as the prediction of new wells/pads behavior.

Similar to any other reservoir simulation model, the trained, history matched and validated AI-based shale reservoir model is deployed in predictive mode to be used for performing sensitivity analysis and decision making purposes.

The sensitivity analysis was performed in two steps. The first step is evaluating the impact of different parameters by using the best validated history matched model. In this scenario, those parameters that were involved in the best history matched model were increased by 30 percent and the impact of this increase on production behavior of different well types was studied.

In the second scenario of sensitivity analysis, more parameters were selected (mostly those that did not show the clear behavior in the first scenario and those that were not included in best history matched model). Additionally, two data-driven models were developed to represent the early time production indicator (the best 3 months) and the late time production indicator (the best 24 months). The behaviors of these two models as function of different parameters were studied.

The optimization study also was performed by three different methodologies known as "Well Quality Analysis", "Fuzzy Trend Analysis" and "Key Performance Indicator" in order to examine the optimum well location, deviation type, the minimum distance between the laterals, the best practices of completion and stimulation.

4.2 Overview of IMAGINE^{TM} Software Package for AI-Based Modeling

In order to perform the AI-based modeling, the software package of IMAGINE^{TM} developed by Intelligent Solution Inc. (ISI), was used. The process of development an AI-based model starts with importing data including the well-based data and production rate data. The well-based data by itself consists of two sets of attributes knows as reservoir attributes such as well coordinates, porosity, completion data, stimulation data and well attributes that changes with time such as days of production, water production, etc.

Once all the data is imported, the static modeling can be performed. The first step toward static modeling is to define the reservoir boundary and modify the grid sizes. By using the geostatsitcal models (Kriging, Invers Distance Weighting, Nearest Point) the reservoir properties can be populated based on the given

values at well locations. Reservoir delineation comes after populating grid blocks with geostatistics and determines effective drainage area of each well in the unit. The last step in static modeling shows volumetric and geostatic results in numeric data tables. In this step the missing data for wells will be filled by using the values from geostatistics distribution maps.

The next and final step in IMAGINE^{TM} is AI-based modeling which allows the user to do the history matching and to create predictive models. By using the "Build and History Match" module, the predictive models for time-variant attributes (here is the rich gas production rate) will be created. The inputs and outputs of the main well, the offset well status (number of offset well, type of offset well in terms of injection or production, the inputs for offset well) and the start and end date for history matching and prediction should be specified in this step. Once creating the predictive model, the training of neural networks for the model starts which the architecture and algorithm was previously explained.

"Deploy Time-Based Model" module in the AI-based modeling step allows the user to deploy developed time-based models for different operational cases as well as in the presence of new wells. By using the cascading process in this step, the model output values in previous time-steps are feed-backed as input for current time-steps.

IMGAINE^{TM} also offers the other modules such as well modeling (generating the type curves, decline curves,…) and field design (for pattern recognition and detecting the under performer wells) which were not used in this study. The detailed capabilities of this software and other packages can be found on ISI's website.

5. CHAPTER V

SPATIO-TEMPORAL DATABASED DEVELOPMENT

The first and the most important step in the development of an AI-based reservoir model is to prepare a representative Spatio-temporal database. The extent at which this spatio-temporal database actually represents the fluid flow behavior of the reservoir that is being modeled, determines the potential degree of success in developing a successful model. The nature and class of the AI-based shale reservoir model is determined by the source of this database. The term spatio-temporal defines the essence of this database and is inspired from the physics that controls this phenomenon [Mohaghegh, 2011]. An extensive data mining and analysis process should be conducted at this step to fully understand the data that is housed in this database. The data compilation, quality control and preprocessing are the most important and time consuming steps in developing an AI-based reservoir Model.

This study focused on part of Marcellus Shale including 135 wells with multiple pads, different landing targets, diverse reservoir properties and completely different completion and stimulation information (Figure 5.1). In order to create the spatio-temporal database the given information should be processed and prepared to be used. This process for each category of given information is described in following sections.

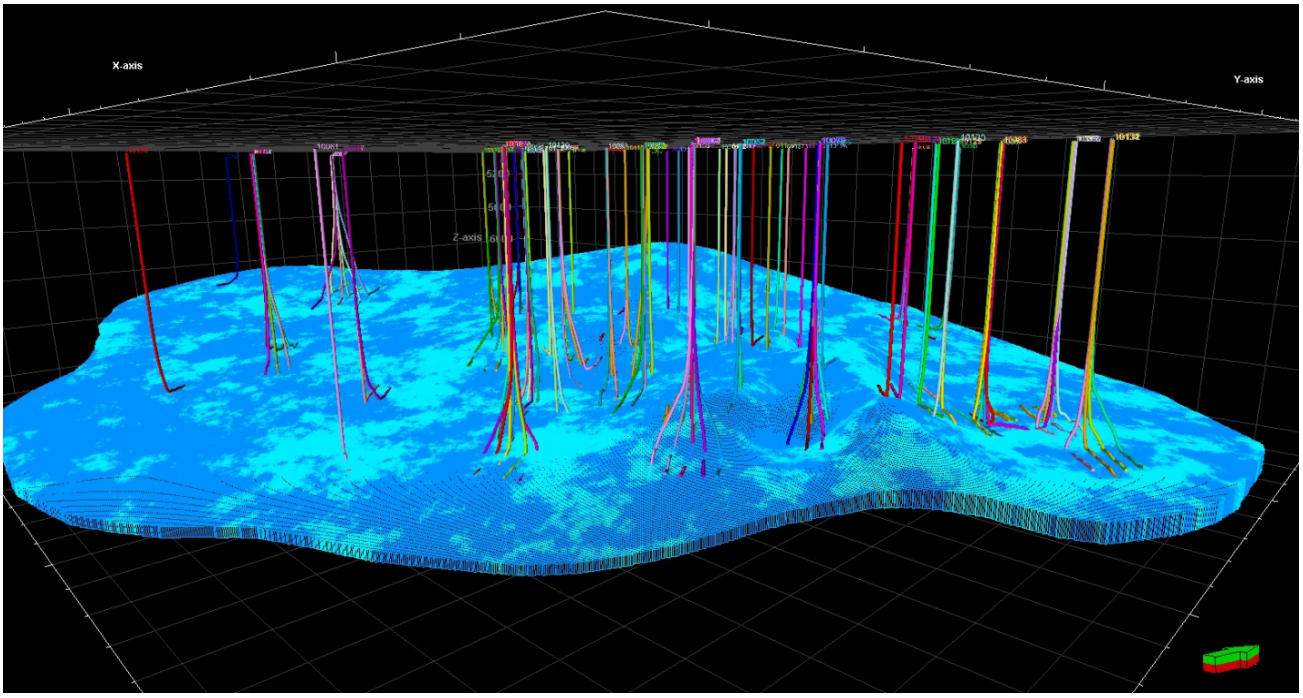

Figure 5.1: The Area of Study- The map shows the distribution of Bulk Modulus in Lower Marcellus.

5.1 Reservoir Characteristics

Marcellus Shale in the area of Pennsylvania consists of two prolific layers as Upper Marcellus (UM) and Lower Marcellus (LM) which are separated by a thin bed limestone layer known as Purcell. Based on the well deviation and completion strategy, one or both layers may be exposed to the production. Reservoir characteristics of each layer including matrix porosity, matrix permeability, pay thickness, net to gross (NTG), initial water saturation and total organic content (TOC) of each well was given by the operator. In order to have a consistent value for each of these properties in well locations, it was assumed that the properties inherited from the completed zone. For instance, if the well is landed and completed in Upper Marcellus, the reservoir properties of this layer should be taken into account. Based on this assumption, five different well configurations (Figure 5.2) were defined and the reservoir characteristics were estimated.

- **Model 1**- these types of wells were landed and completed in Purcell. Because of its low thickness and brittleness, the fracture propagation usually occurs to the upper and lower layers, therefore it was assumed that both UM and LM are contributing into production. The total thickness of UM and LM and the weighted average (Equations 16 and 17) for the rest of the properties were used in these wells.

$$Average\ Property\ (\emptyset, K, TOC) = \frac{(Property\ of\ UM * h_{UM}) + (Property\ of\ LM * h_{LM})}{Total\ Thickness} \dots\dots\dots\dots (16)$$

$$Average\ of\ Water\ Saturation = \frac{(S_W\ in\ UM * h_{UM} * \emptyset_{UM}) + (S_W in\ LM * h_{LM} * \emptyset_{LM})}{(h_{UM} * \emptyset_{UM}) + (h_{LM} * \emptyset_{LM})} \dots\dots\dots\dots\dots (17)$$

- **Model 2**- these types of wells were landed and completed in UM, therefore this is the only layer contributing into production of these wells and the reservoir characteristics of this layer was considered.
- **Model 3**- these well types are very similar to model 2 but they have landed and completed in LM, so the reservoir characteristics of this layer were only taken into account.
- **Model 4**- these wells, as shown in Figure 5.2, have down-dip trajectories and have been completed in all three layers although the number of stages completed in each layer is different. As a result, the number of stages should be a factor in estimating the average properties. For these wells, the average of reservoir characteristics based on Equation 18 and total thickness of UM and LM was considered.

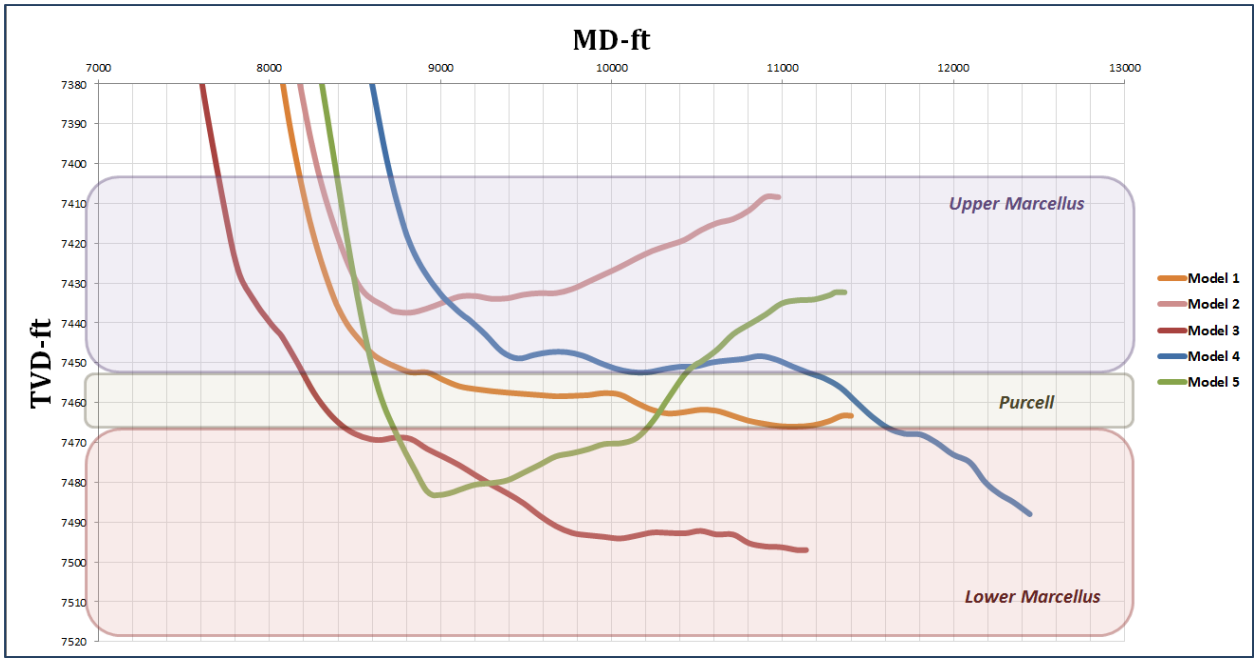

Figure 5.2: Different Well Configurations in Spatio-Temporal Database

$$Avearage\ Property = \frac{\left[\left((No.of\ stages\ completed\ in\ UM + \frac{No.of\ Stages\ completed\ in\ Purcell}{2}) * Property\ of\ UM * h_{UM}\right) + \left((No.of\ stages\ complted\ in\ LM + \frac{No.of\ Stages\ completed\ in\ Purcell}{2}) * Property\ of\ LM * h_{LM}\right)\right]}{\left((No.of\ Stages\ completed\ in\ UM * h_{UM}) + (No.of\ Stages\ Completed\ in\ LM * h_{LM})\right)} \quad \ldots (18)$$

- **Model 5**- these wells have an up-dip deviation and have also been completed in all three layers therefore the same equation as model 4 was used to estimate the reservoir characteristics.

5.2 Geomechanical Properties

The interpreted geomechanical logs including shear modulus, bulk modulus, minimum horizontal stress, poisson's ratio, and young's modulus information for 30 vertical wells in the area were provided by the operator. On the other hand, the conventional logs such as GR, bulk density and sonic for these 30 wells and 50 more vertical wells were also available. In order to incorporate the geomechanical properties in database, a workflow for generating the synthetic geomechanical logs from conventional logs by using the neural network was prepared (Figure 5.3).

As shown in Figure 5.3, the synthetic geomechanical logs were generated for 50 wells by developing several data-driven models. The data-driven models were validated using wells with actual geomechanical logs that have been removed from the database to serve as blind validation wells. After model validation, the geomechanical information of 80 vertical wells was used in order to generate the distribution maps for all 135 horizontal wells in the area of study for both Upper Marcellus and Lower Marcellus.

Figure 5.4 shows the distribution of Minimum Horizontal Stress in Lower Marcellus by using the information of 30 well and 80 wells. (The details of this workflow can be found in SPE 163690)

The aforementioned five geomechanical properties for each well in each layer of UM and LM was then extracted from distribution maps and the same method as explained in section 5.1 was applied to estimate the average properties for each well.

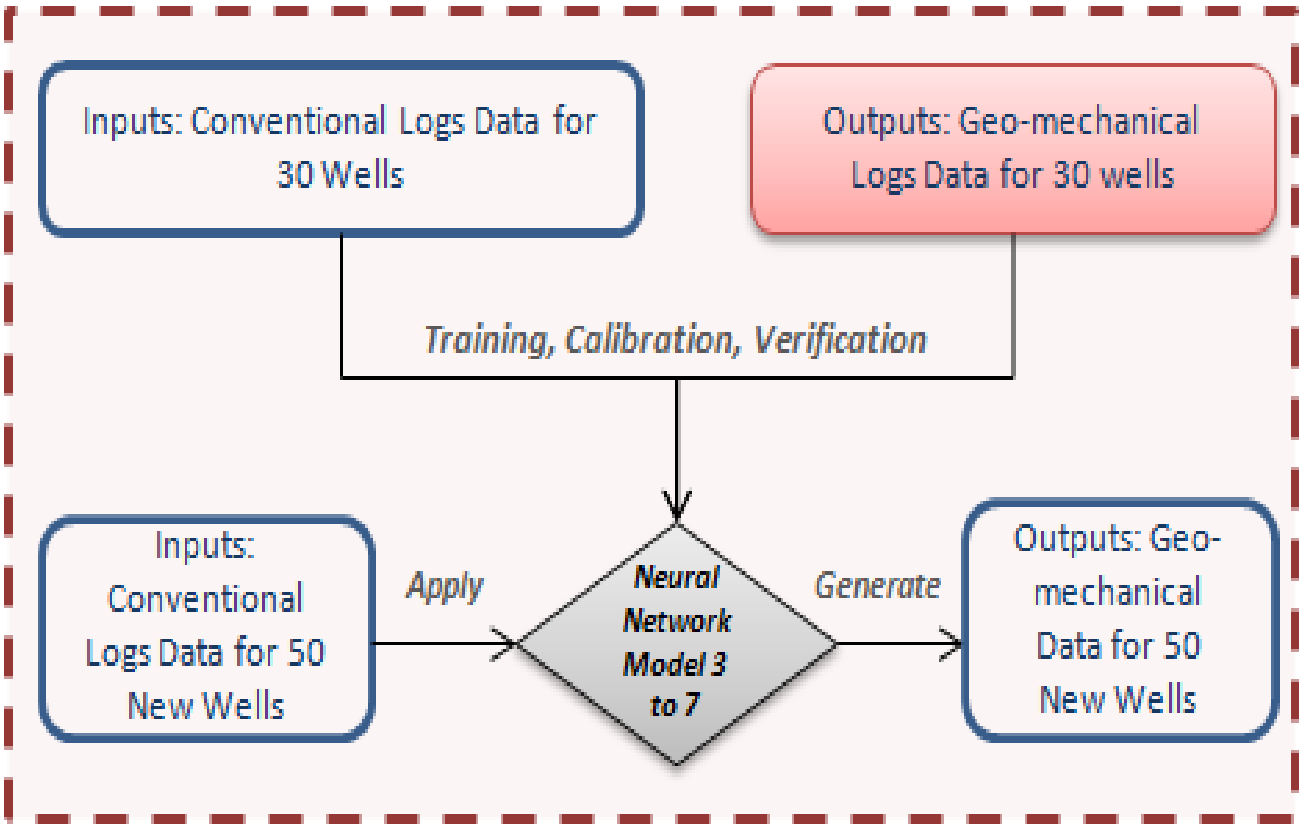

Figure 5.3: Flow Chart for Generating the Synthetic Geomechanical Logs by Using Conventional Logs

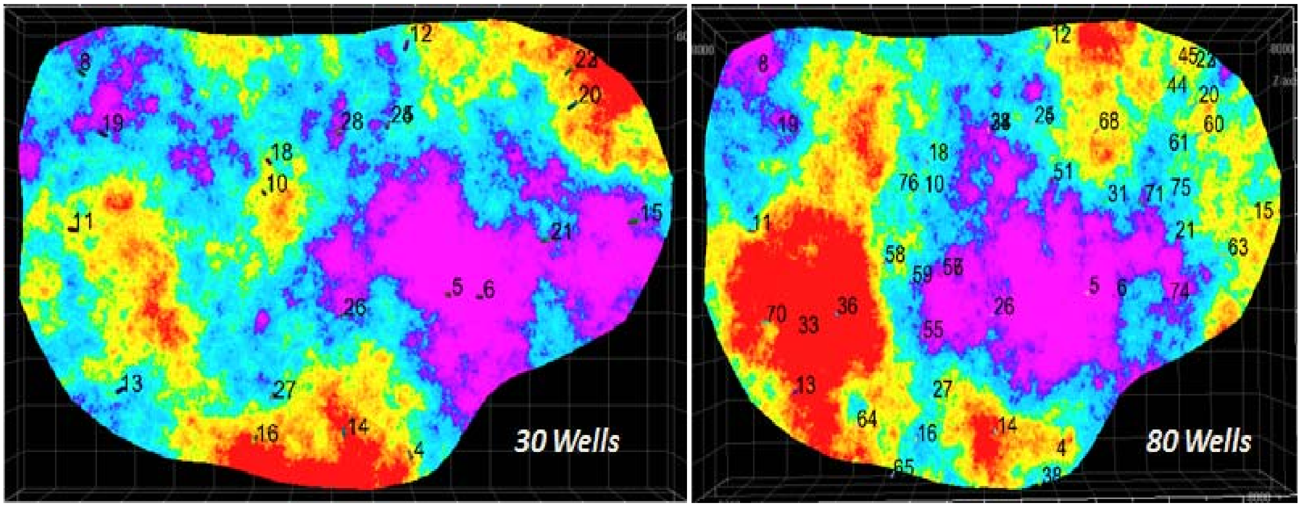

Figure 5.4: Min Horizontal Stress Distribution in Lower Marcellus

5.3 Completion and Stimulation Data

The completion data of the wells include some information regarding the shot density, perforated/stimulated lateral length, number of stages and etc. which was imported into the database. The stimulation data, on the other hand, was provided in stage base by operator which comprises complete information about the amount of injected clean water, rate of injection, injection pressure, amount of injected slurry and etc. Since the production is available on a per well basis, the volumes of fluid and proppant for multiple hydraulic fracture stages performed on the same well were summed while the rates and pressures for these cases were averaged.

5.4 Production History

The production history of the wells contains the dry gas rate, condensate rate, water rate, casing pressure and tubing pressure in daily format. The maximum and minimum length of production history is about five years and one and half years respectively. Because of scattered condensate rates and also low condensate to gas ratio (maximum is about 16 STB/MMCF), this data was combined with the dry gas (Equation 19) and the rate of rich gas was estimated for the wells.

$$GE_{Cond} = 133{,}800 \, \frac{\gamma_o}{M_o} \, \frac{SCF}{STB} \quad \ldots\ldots\ldots\ldots\ldots\ldots\ldots\ldots \quad (19)$$ [1]

[1] William D.McCain, Ir (1990), "The Properties of Petroleum Fluids", Page 195.

Where $\gamma_o = \frac{141.5}{Condensate\ API + 131.5}$ (known as condensate specific gravity) and $M_o = \frac{44.43\,\gamma_o}{1.008 - \gamma_o}$ (known as condensate molar density). The API degree of condensate was reported by operator as 58.8 at reservoir temperature. In order to remove the associated noises with daily production rates, the monthly basis of this information was used in database. The corresponding monthly wellhead pressure and water rate was also prepared. It has to be noted that, as a common practice in Marcellus, the production is happening from casing in the first couple of months of production and then it is switched through tubing and in calculating the average wellhead pressure, this was taken into account.

The initial spatio-temporal database after the aforementioned calculations has six main groups as well information, reservoir characteristics, geomechanical properties, completion data, stimulation data and production and operational constraints. Table 5-1 shows the list of data that was initially incorporated into spatio-temporal database.

Table 5-1: List of Initial Parameters in Spatio-Temporal database

Group1- Well Information	Easting	***Group 5- Stimulation Data***	Avg. Inj. Pressure(psi)
	Northing		Avg. ISIP
	MD (ft)		Avg. Breakdown Pressure
	BTU Area*		Avg. Maximum Pressure
	Deviation Type (Down-Dip, Straight, Up-Dip)		Avg. Injection Rate(bbl/min)
Group 2- Reservoir Characteristics	Matrix Porosity		Avg. Max Rate
	Matrix Permeability (mD)		Avg. Breakdown Rate
	Net Thickness (ft)		Fluid Vol.(bbl)
	Water Saturation (%)		Slurry Vol.(bbl)
	TOC (%)		Clean Water Vol.(bbl)
	Avg. Langmuir Vol. (scf/ton)		Max Proppant Concentration(lb/gal)
	Avg. Langmuir Pressure (psi)		Proppant per Stage(lb)
Group 3- Geomechanical Properties	Bulk Modulus		Total Proppant Inj.(lb)
	Shear Modulus		Avg. Fracture Gradient
	Young's Modulus	***Group 6- Production and Operational Constraints***	Monthly Rich Gas (MCF/month)
	Poisson's Ratio		Average Monthly Wellhead Pressure (Psi)
	Min Horizontal Stress		Monthly Water (bbl/Month)
Group 4- Completion Data	Stimulated Lateral Length(ft)		No. of Days of Production
	Shot Density (shots/ft)		No. of Months of Production
	Total Clusters		
	Total No of Stages	*The area is divided into 4 BTU sections of Dry, Low, Medium and Wet based on the condensate content of gas.	
	Cluster Spacing		

6. CHAPTER VI

HISTORY MATCHING OF AI-BASED SHALE RESERVOIR MODEL

In conventional numerical reservoir simulation the base geological model will be modified to match production history, while AI-based reservoir modeling starts with the static model and tries to honor it and leaving it unmodified during the history matching process. Instead, the uncertainties associated with this static model is analyzed and quantified at a later stage in the development.

The model development and history matching in AI-based shale reservoir models are performed simultaneously during the training process. The spatio-temporal database developed in the previous step is the main source of information for building and history matching the AI-based reservoir model. History matching process in this study has gone through a process of inclusion and exclusion of certain parameters based on their impact on model behavior. Figure 6.1 shows the evolution process of developing the AI-based reservoir model from the base model to the best history matched model (with optimum number of inputs).

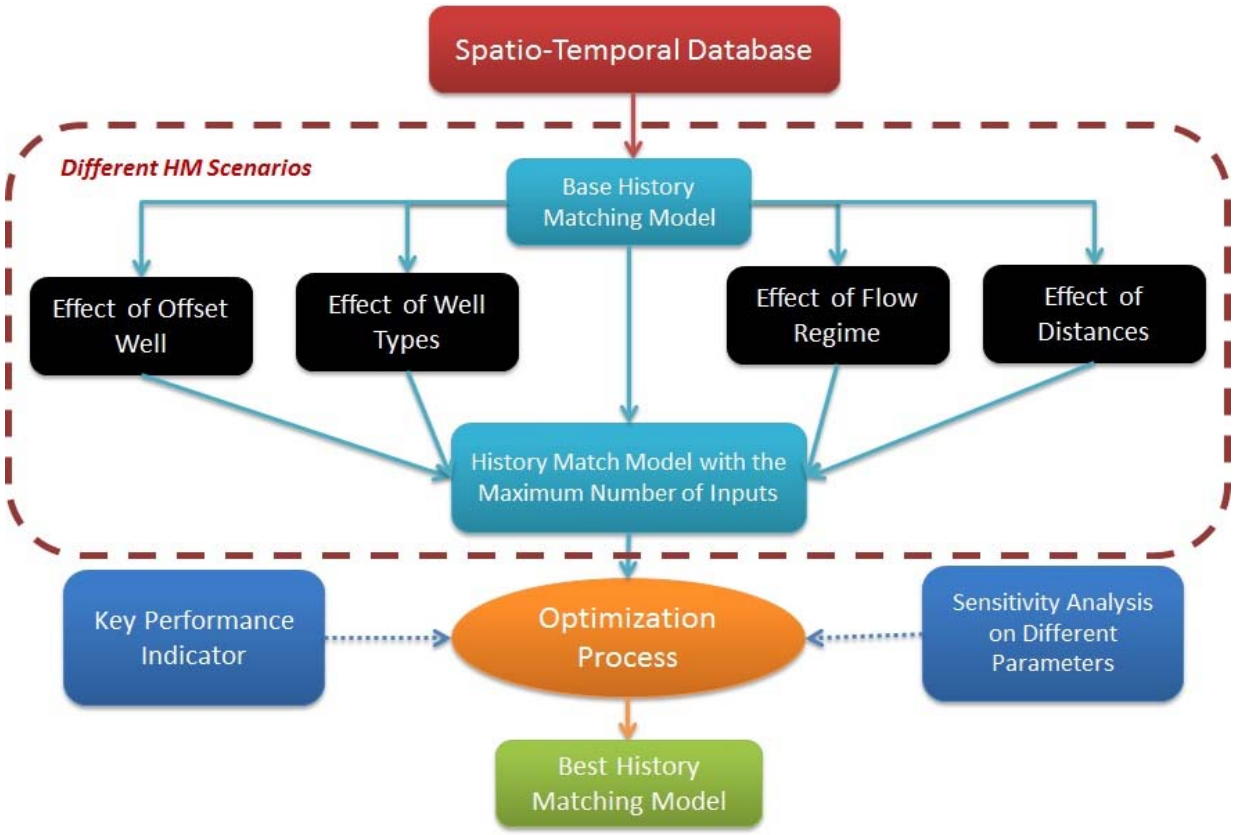

Figure 6.1: History Matching Workflow

6.1 Base Model

As shown in Figure 6.1, the base model was built by incorporating all available data which was listed in Table 5-1. The production of water and other operational constraints data in one time step behind the current time (i.e. at (t-1)) was also imported in the base model. The rich gas production at (t-1) and (t-2) was incorporated as inputs of the base model and at the end, the model included 47 parameters.

As explained before, a feed-forward Backpropagation neural network with 79 neurons in the hidden layer was used to develop the base model. In the development process, 80 percent of data was used for neural network training and 20 percent for calibration and verification (10 percent each). Figure 6.2 shows the cross plot of neural network training, calibration and verification. In this figure the x-axis is the predicted monthly gas rate by neural network while the y-axis is the actual gas production rate.

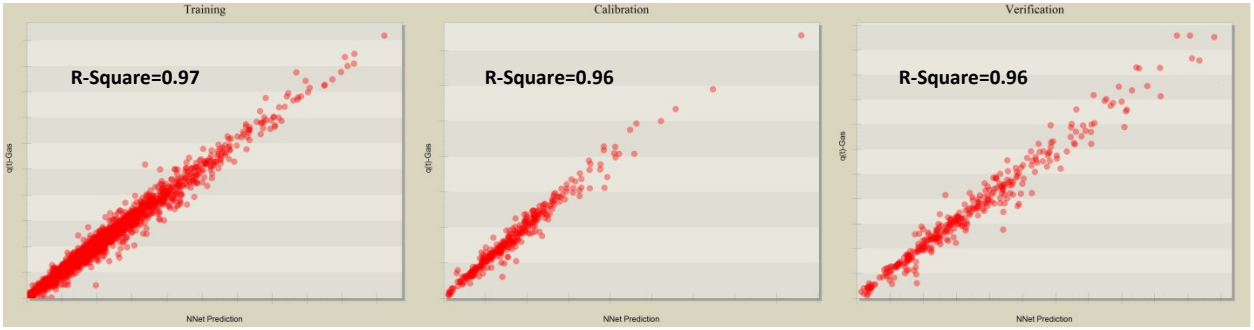

Figure 6.2: Training, Calibration and Verification Cross Plots for Base Model

After completing the neural network training process, the model has gone through the sequential updating in which the model output values in the previous time-step was feed-backed as input for current time-steps in order to have a continuous gas rate profile. Figure 6.3 and Figure 6.4 show the history matching result for two wells (a good sample: left plot; a poor sample: right plot) and the entire field. In these plots, the orange dots represent the actual monthly rate while the green solid line shows the AI-based model results. Furthermore the orange shadow illustrates the actual cumulative production and the green one corresponds to cumulative production output by the AI-based model.

As shown in Figure 6.4, the AI-based model has underestimated the actual gas rate after 2011(identified by a red circle) when more wells come to the production and it may cause a problem in forecasting since this part will be fed as start point for the forecasting. Although the history matching result for the entire field looks acceptable, the result for each individual well needs to be improved especially over the last months of production as illustrated in Figure 6.3 (right graph).

Figure 6.3: The History Matching Results for Two Wells in Base Model- Left Plot is the Sample of Good HM and Right Plot is the Sample of Poor HM.

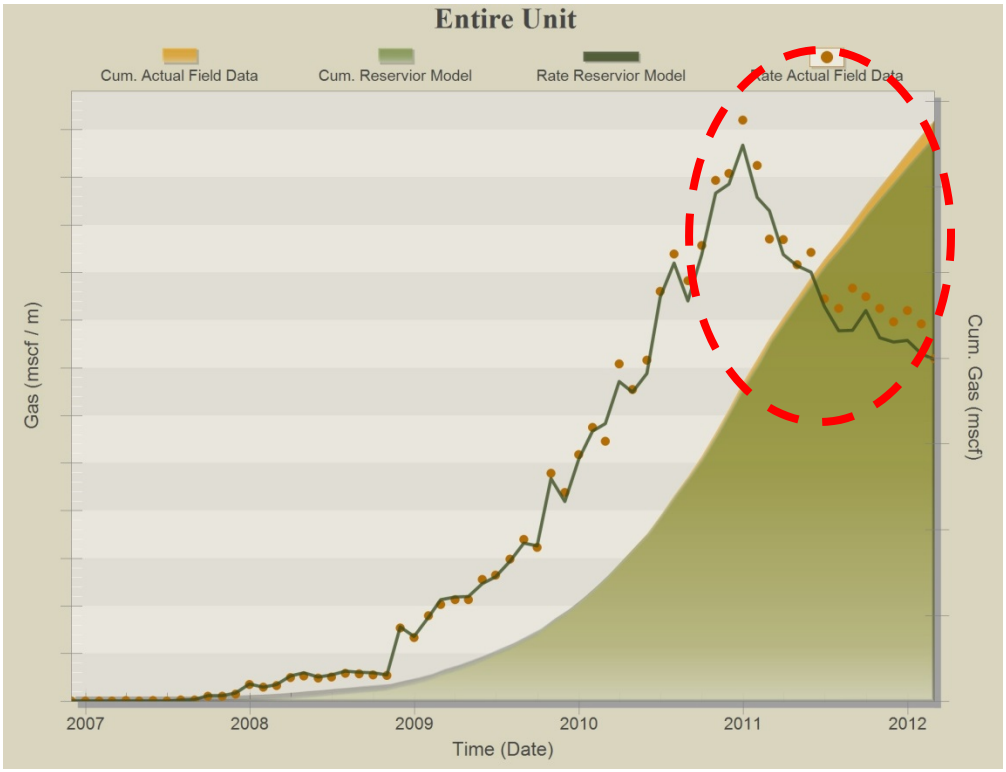

Figure 6.4: The History Matching Result for Entire Field- Base Model

6.2 Effect of Offset Wells

The production history of Marcellus wells in this area shows that interference of the wells located on the same pad or nearby pads cannot be ignored. Figure 6.5 shows the production history of two wells that are located 1500 ft. away. Well # 10036 came to the production in June 2009 while well #10040 was

completed and came to production in May 2010. As it has shown in this figure, during the fracturing of Well # 10040, the water is pushed into existing well (here Well#10036) and it makes some abnormality (usually decrease) in gas production. This process is known as "Frac Hit" and it usually happens in Marcellus.

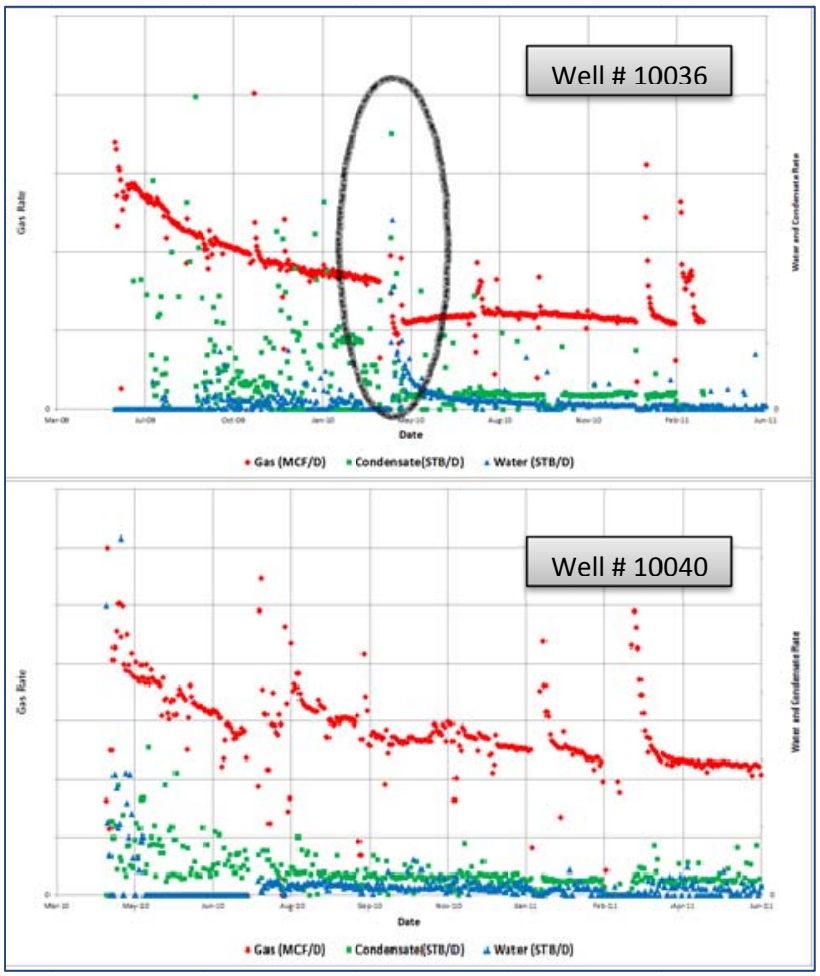

Figure 6.5: Process of Frac Hit in Two Wells 1500 ft. away

In order to quantify the impacts of offset well and taking any well interference effects into account, all aforementioned properties for one closest offset well were included in the modeling and a model with 93 inputs was obtained.

The same as the base model, the feed-forward Backpropagation neural network with 99 neurons in the hidden layer was used and data was randomly partitioned as training (80 percent), calibration (10 percent), and verification (10 percent). Figure 6.6 shows the cross plots of training, calibration and verification for this model. In this figure the x-axis is the predicted monthly gas rate by neural network while the y-axis is the actual gas production rate.

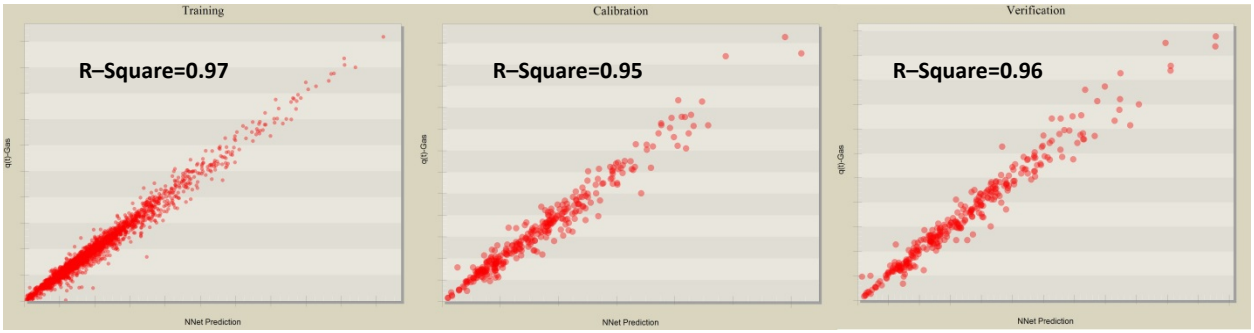

Figure 6.6: Training, Calibration and Verification Cross Plots for Effect of Offset Well Model

Figure 6.7 shows the history matching result of Well # 10036 in base case (Left Plot) and when the effect of one offset well was added to the model (Right Plot). As shown in this figure, after adding the effect of offset well, the AI-based model was able to capture all the fluctuations in this well much better than the base model and the history matching result was improved.

Figure 6.8 represents the history matching result of the entire field in this model. Compared to the base model, the effect of the offset well could fix the issue of underestimating over the tail of field production; however, adding this effect caused some issues at the beginning of field production (identified by the red circle). This might be due to the fact that the effect of the offset well does not show itself at the beginning of production when each well is producing from its own drainage area. Moreover, at early time, most of the wells are located in a single pad and they have been drilled with longer distance. Figure 6.9 illustrates that not only adding the impact of offset well doesn't improve the result, but also makes the result much worse. In order to overcome this problem, a parameter should be defined which identifies the different well configuration.

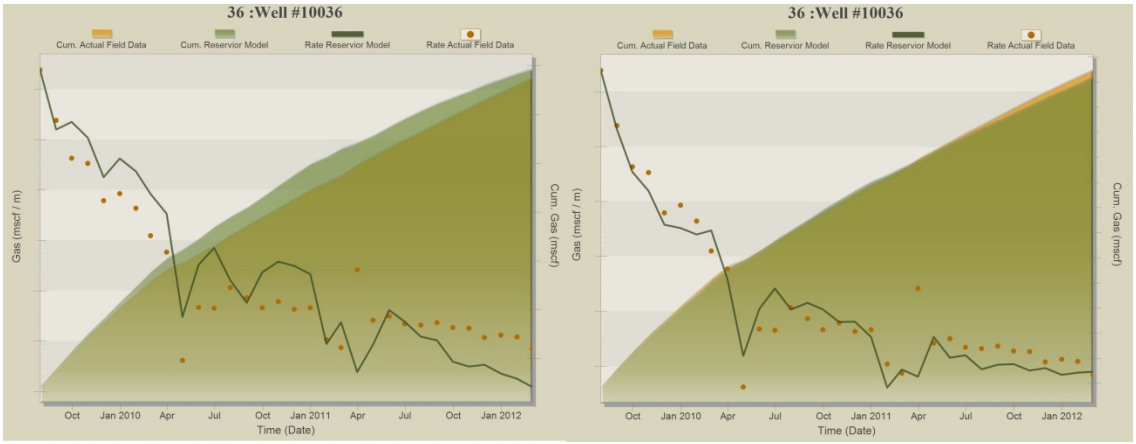

Figure 6.7: History Matching Results for Well # 10036 in Base Model (Left Plot) and Offset Well Model (Right Plot)

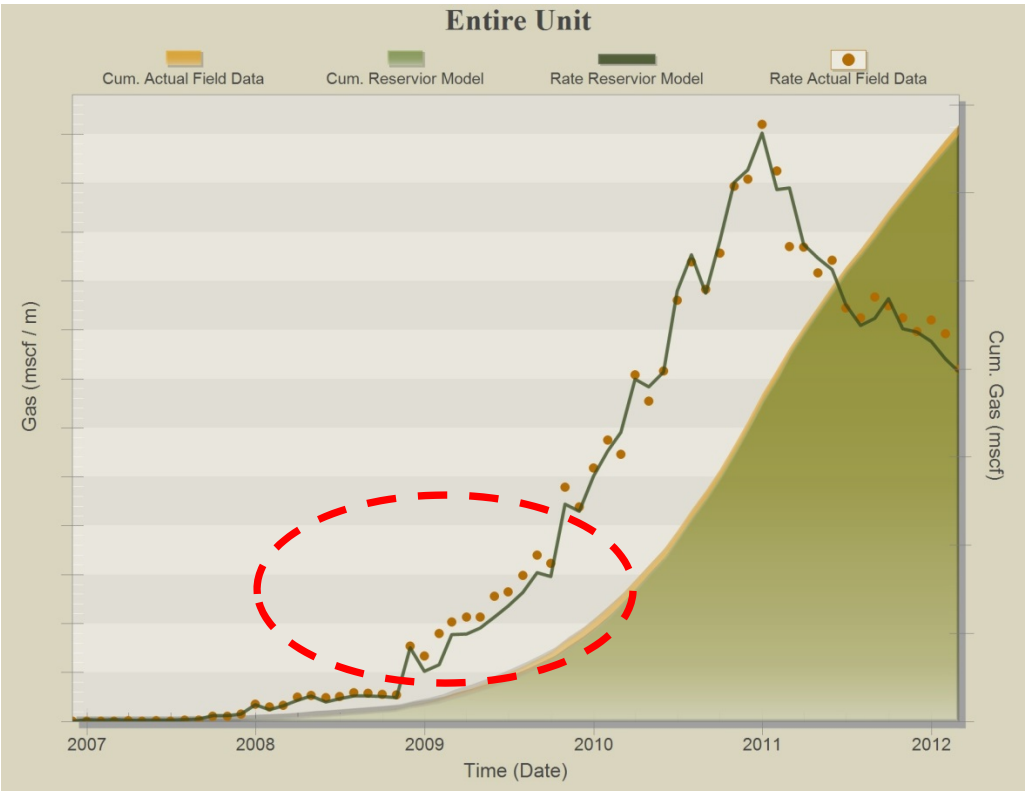

Figure 6.8: The History Matching Result for Entire Field- Effect of Offset Well Model

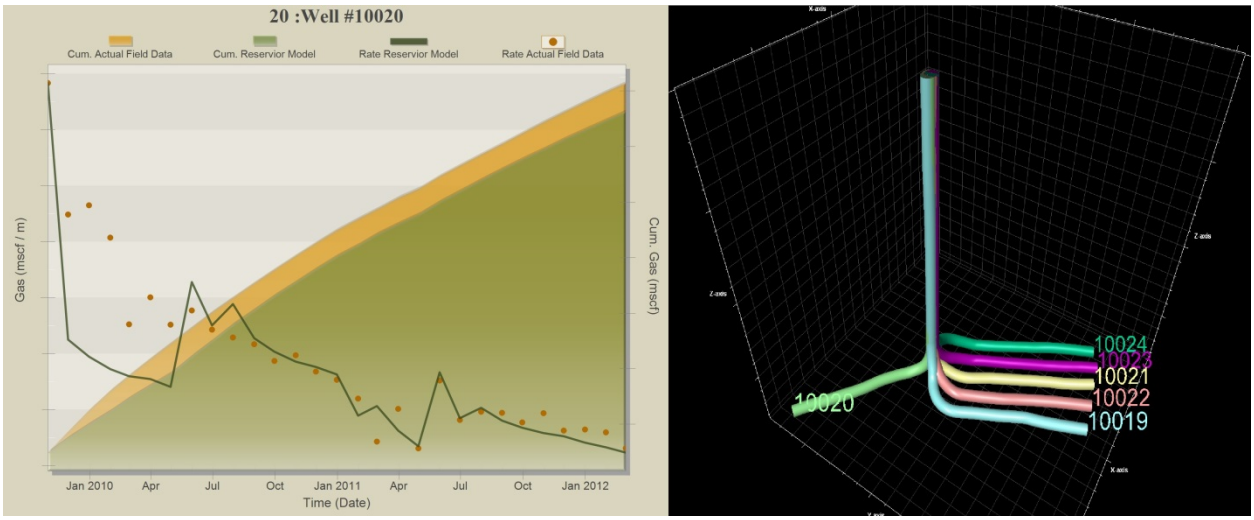

Figure 6.9: The History Matching Result of Well # 10020 after adding the Effect of Offset Well- The Right Plot Shows that This Well is not sharing the drainage area.

6.3 Effect of Well Types

Drilling multiple wells from a pad is a common practice in the Marcellus Shale. Usually three main types of laterals can be defined (Figure 6.10):

- ***Type one Lateral***: This type of lateral has no neighboring laterals and does not share drainage area. It does not experience any "Frac Hits" from wells in the same pad and its reach will be as far as its hydraulic fractures.
- ***Type two Lateral***: The second type of lateral has only one neighboring lateral and therefore it shares part of the drainage area and "Frac Hits" are possible from laterals in the same pad.
- ***Type three Lateral***: The last type is bounded by two neighboring laterals; thus, the drainage area will be shared and "Frac Hits" are possible from both sides in the same pad.

Based on this definition, a new parameter was added to the database as "Type" of the well by assigning a value of 1 to 3 in order to incorporate such information.

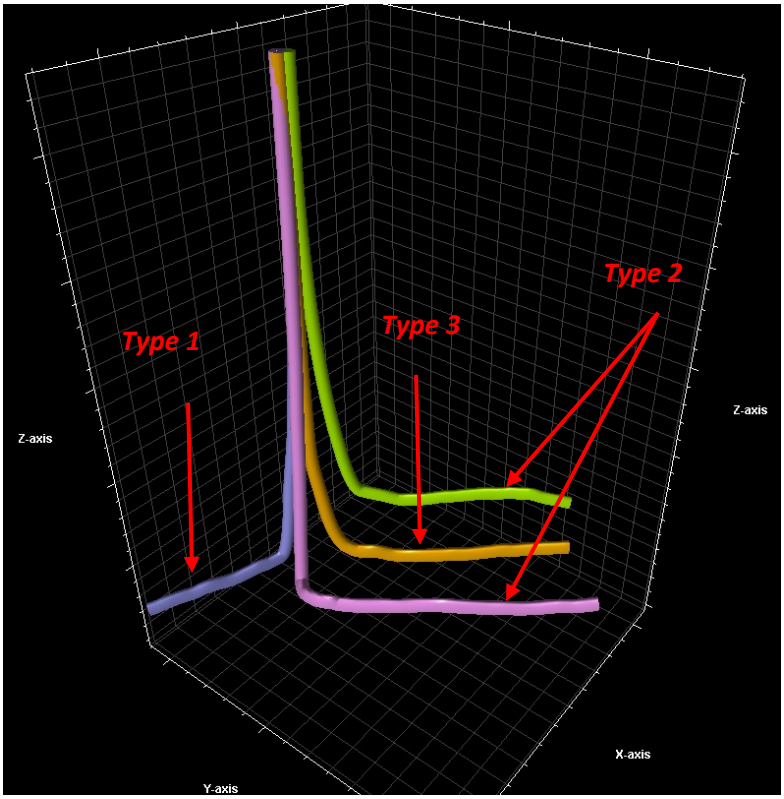

Figure 6.10: Different Well Types Definition in Dataset

Similar to the previous models, the feed-forward Backpropagation neural network with 80 neurons in the hidden layer was used and the data was randomly partitioned to training (80 percent), calibration, and verification (10 percent each). Figure 6.11 shows the cross plots of training, calibration, and verification. Figure 6.12 and Figure 6.13 shows the result of two wells and the entire field after adding the well type parameter to the model respectively.

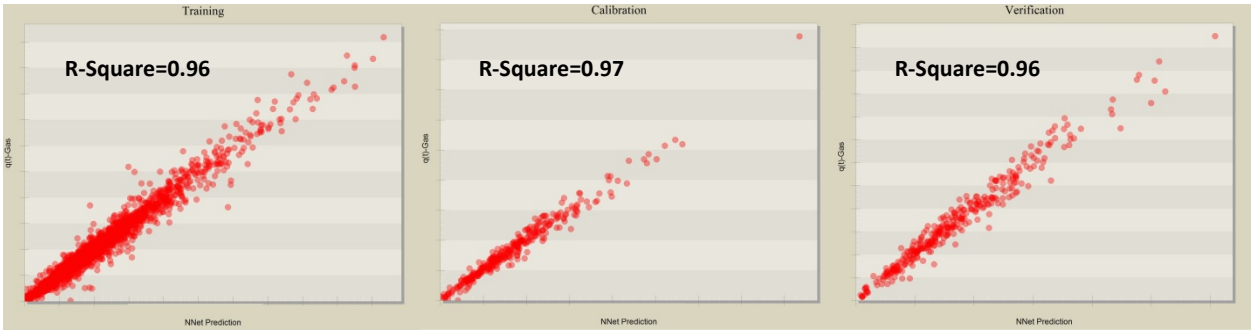

Figure 6.11: Training, Calibration and Verification Cross Plots for Effect of Well Type Model

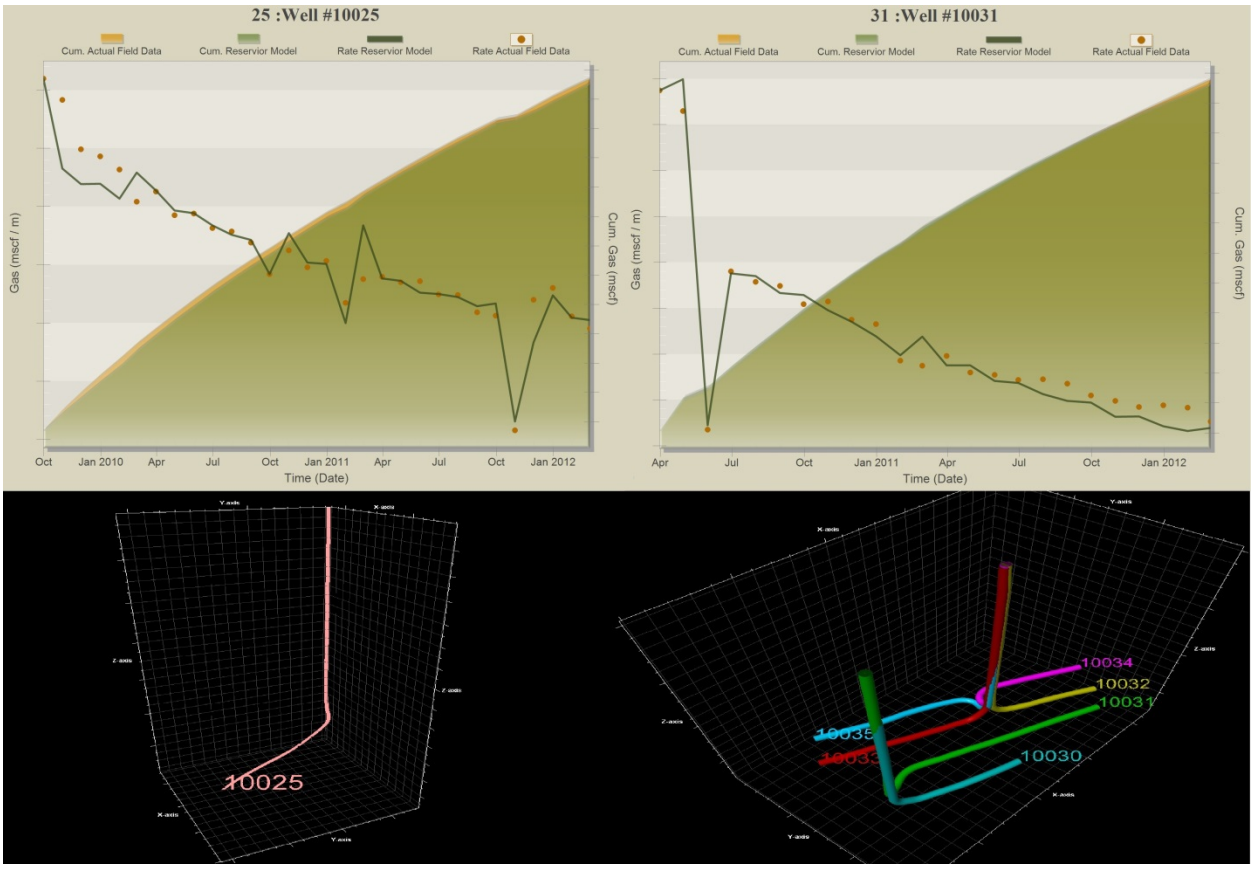

Figure 6.12: History Matching Results for Well # 10025 (Located on a single pad- type 1) and Well # 10031 (Located in a multi-well pad- type 3)

As shown in Figure 6.13, the AI-based model cannot capture the actual rich gas at the end of production (the same problem as Base Model). It has to be noted that the effect of each parameter is investigated individually on the model behavior and the combination of these parameters may have the different impact. For example as explained earlier, adding the offset well to the model has a reverse impact on type

1 wells. Having well type in database may solve this issue for these well. The result of a model by using all parameters will be discussed later in this chapter.

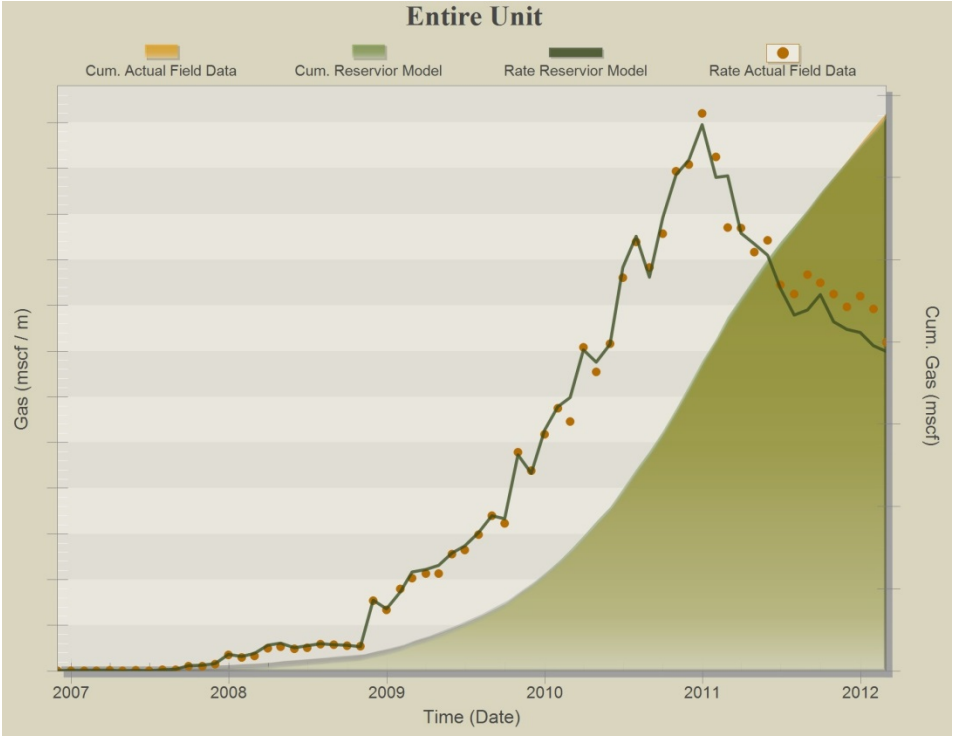

Figure 6.13: The History Matching Result for Entire Field- Effect of Well Types Model

6.4 Effect of Flow Regimes

The details of rate transient analysis were discussed in chapter 2 and, as mentioned earlier, one application of this approach is flow regime determination. By looking at the gas rate of the wells, two distinct behaviors can be observed. The RTA module of Fekete Harmony Software package was used to determine the flow regime for each well. The initial information such as PVT properties, well configuration, temperature profile, completion strings, production history (gas rate, casing and tubing pressure) and etc. was imported to estimate the corresponding bottomhole flowing pressure.

The deterministic superposition time method of unconventional gas was then used in order to generate the square root time plot and essential type curves, which are used for flow regime determination. The square root time plot is a plot of normalized pressure (Equation 20) versus linear superposition time (Equation 21) on a Cartesian graph which is the best representative of variable gas properties as a function of pressure.

$$Normalized\ Pressure = \frac{P_{pi} - P_{pwf}}{q} \ldots \ldots \ldots \ldots \ldots \ldots \ldots \ldots \ldots \ldots \ldots \ldots \ldots \ldots \ldots \ldots \ldots \ldots \ldots \ldots \ldots \ldots \ldots \ldots (20)$$

$$Linear\ Superposition\ Time = \sum_{j-1}^{n} \frac{q_j - q_{j-1}}{q_n} \sqrt{t - t_{j-1}} \ldots \ldots \ldots \ldots \ldots \ldots \ldots \ldots \ldots \ldots \ldots \ldots \ldots \ldots \ldots \ldots (21)$$

In which P_{pi} and P_{pwf} are pseudo pressure for initial reservoir pressure and flowing bottomhole pressure respectively. It should be noted that for unconventional reservoirs, the superposition function should be based on $\sqrt{t}$, because the flow is predominantly linear. As shown in Figure 6.14 the linear flow regime (which is a dominant flow in shale gas wells) results in a straight line in square root time plot. As clearly illustrated in this figure, at the beginning of production history of the well, there are points which are diverting from straight line and they might represent the bi-linear flow, radial flow in fractures and/or initial clean up. Since it is nearly impossible to distinguish between these effects, the behavior was simply identified as "skin effect".

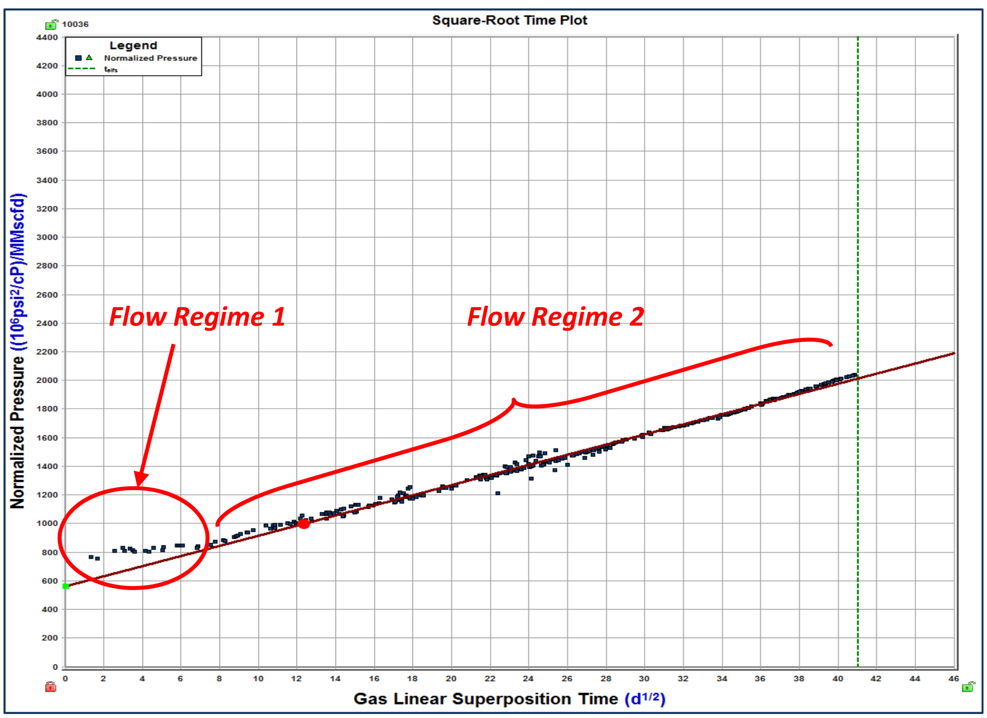

Figure 6.14: Square-root time plot for Well # 10036

The presence of skin effect, as explained by Nobakht et al. (2012), changes the shape of Log-Log plots (type curves), therefore using the Log-Log plots for flow regime determination can be impractical here because the "Skin Effect" is observed in all the wells. On the other hand, the derivative plots are not usually affected by the skin and they can be used to check the validity of results from square-root time plots. Figure 6.15 shows the normalized gas rate and its derivative versus linear superposition time for the

well # 10036. As shown in this figure, the half slope line (as an indication of transient linear flow regime) can obviously be observed. These analyses were performed for all wells. Two flow regimes were identified and then used as a dynamic input in database.

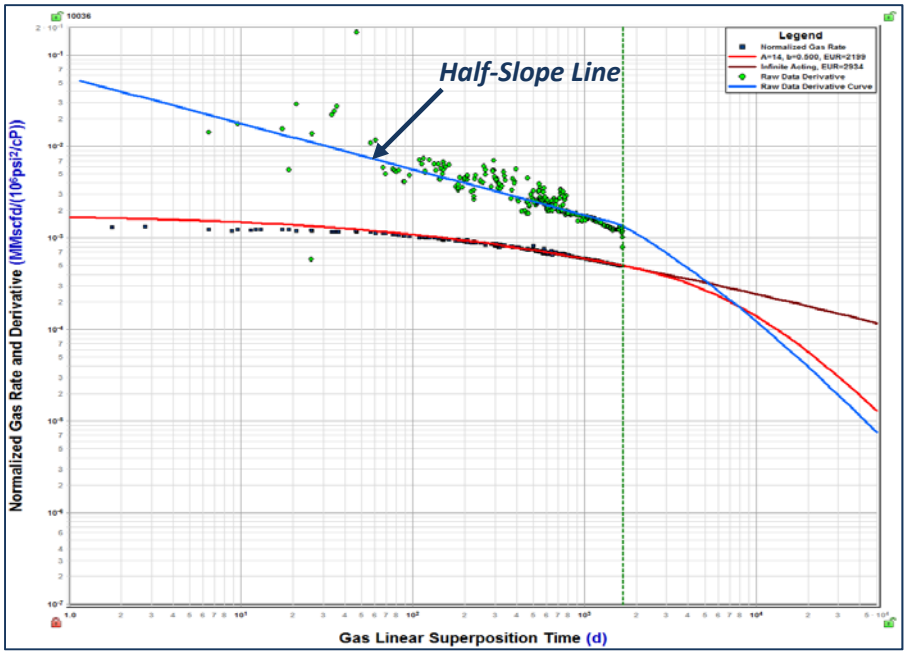

Figure 6.15: Normalized Gas Rate and Derivative Plot for Well # 10036

In addition, as discussed by Cheng (2012), the damages caused by injected water can be different in cases of having delay in bringing the well to production at the beginning. This can have an impact on the duration of the first flow regime (skin effect) in wells because in this case, the capillary forces suck the water into the matrix and water saturation dissipates farther into it during the shut in and it may cause more damages. This can be observed as more and longer fluctuations in gas rates when the well comes to the production. Moreover, Holditch (1979) has stated that delay caused more damages because injected water may reduce the formation permeability in the invaded zone due to clay swelling, scaling and fines migration.

Therefore another parameter as the days between completion and start-up production was also added to the database and a model with 50 inputs was created. Similarly, a feed-forward Backpropagation neural network with 81 neurons in the hidden layer was trained by using 80 percent of the data, and the rest was used as calibration and verification. Figure 6.16 shows the cross plots of training, calibration and verification for this model.

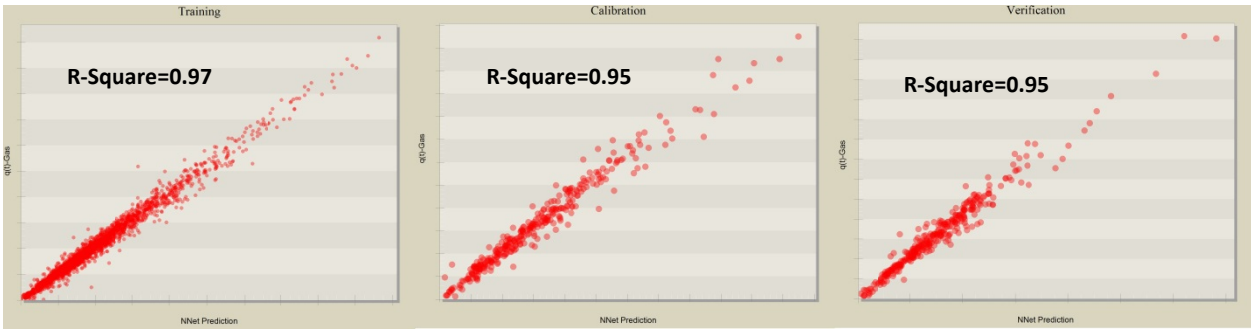

Figure 6.16: Training, Calibration and Verification Cross Plots for Effect of Flow Regime Model

Figure 6.17 shows the history matching result of Well # 10050 in both base model and the model with effect of flow regime.

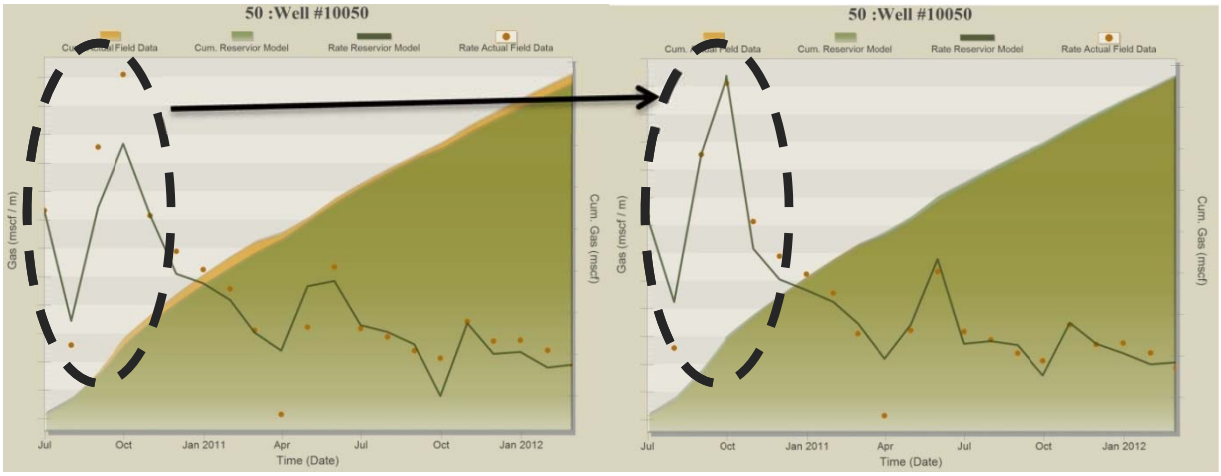

Figure 6.17: History matching result of Well #10050 in Base Model (Left Plot) and Flow Regime Model (Right Plot)

Figure 6.18: The History Matching Result for Entire Field- Effect of Flow Regime Model

As expected, introducing a different flow regime helps the AI-based model to capture the transition between first and second flow regime (for this well the first 4 month identified as flow regime 1).The flow regime identification, however, could not improve the history matching results over the last months of production (Figure 6.18).

6.5 Effect of Distances

Due to different drilling policies, the distances between the wells and the pads varies along the area of study and consequently the interference between wells could be different. In order to consider the impact of relative location of the wells, two distances were defined and fed to the neural network for training:

- Distance between the laterals in the same pad-Inside Distance
- Distance to the closest lateral of a nearby pad-Outside Distance

Figure 6.19 shows the inside and outside distance between two laterals and two pads.

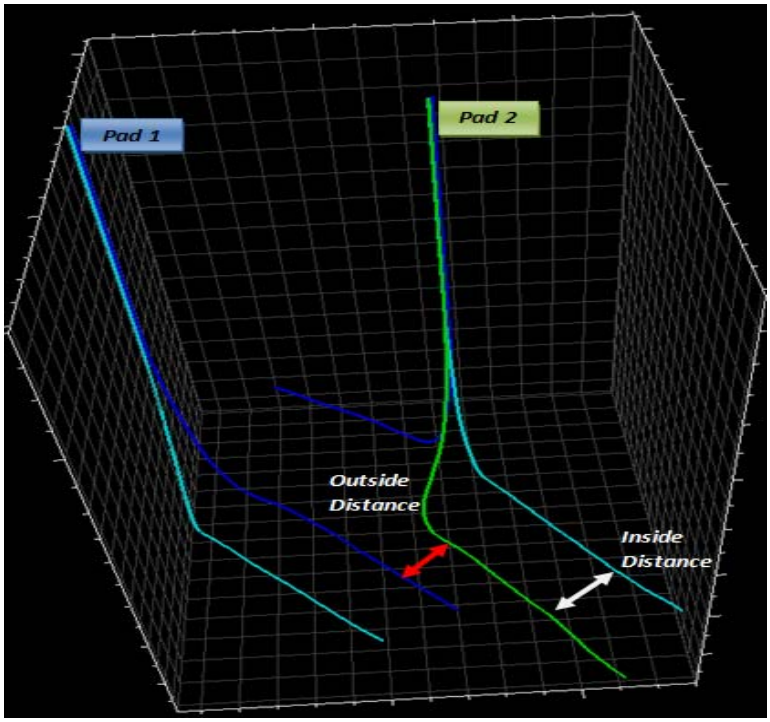

Figure 6.19: Inside and Closest Outside Distances

After estimating the inside and outside distance for each well, a feed-forward Backpropagation neural network with 80 neurons in the hidden layer and 49 input parameters was trained. The data was randomly partitioned into training (80 percent), calibration (10 percent) and verification (10 percent). Figure 6.20 shows the cross plot for each of these partitions.

Figure 6.21 and Figure 6.22 represent the history matching result for two wells (a good sample: left plot; a poor sample- right plot) and the entire field respectively. As shown in figure 6.22, the AI-based model was not able to fully capture the gas rate production over the last months of production.

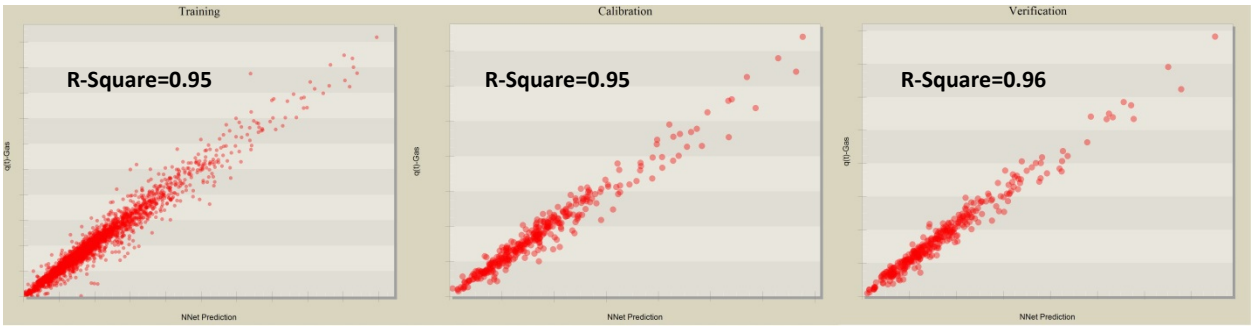

Figure 6.20: Training, Calibration and Verification Cross Plots for Effect of Distances Model

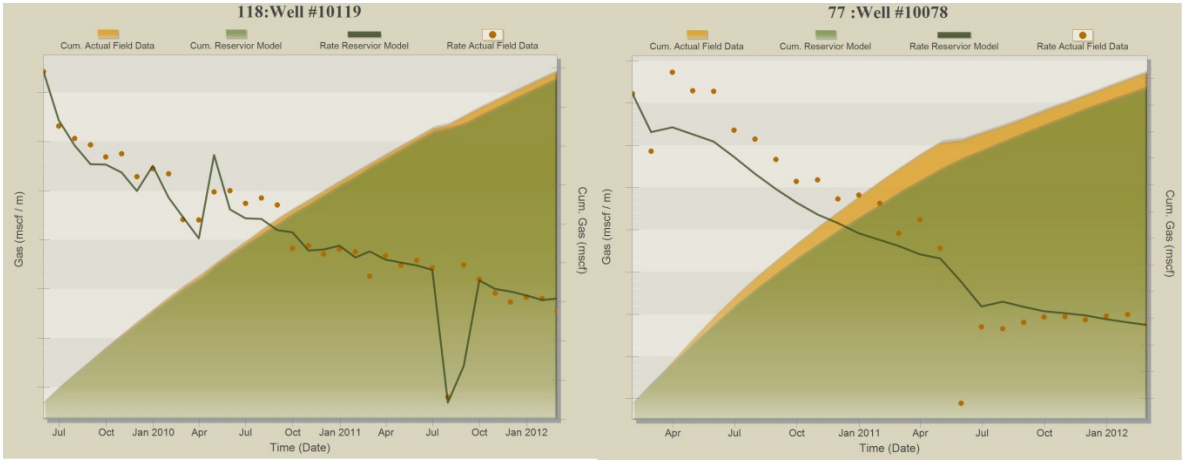

Figure 6.21: The History Matching Results for Two Wells in effect of Distances Model- Left Plot is the Sample of Good HM and Right Plot is the Sample of Poor HM.

Figure 6.22: The History Matching Result for Entire Field- Effect of Distances Model

6.6 History Matching Model with Maximum Number of Inputs

As mentioned earlier, the individual impact of each introduced parameter may not improve the history matching results of the wells and entire field but the combination of these parameters could be helpful to achieve good results. Therefore, a history matching model with a maximum possible number of inputs was defined which includes 105 parameters. By using the feed-forward Backpropagation neural network including 106 neurons in the hidden layer, the data was randomly partitioned into training, calibration and verification. The cross plots of each partition has shown in Figure 6.23.

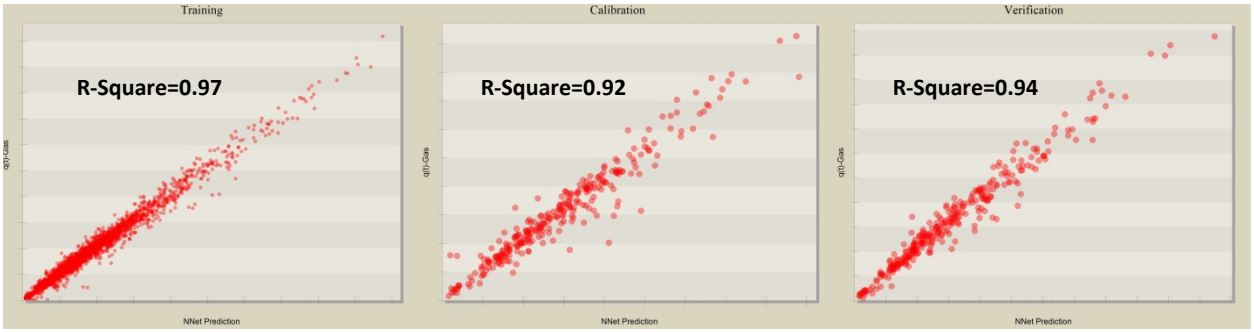

Figure 6.23: Training, Calibration and Verification Cross Plots for History Matching Model with Maximum Number of Inputs

The history matching results for each individual well show significant improvement in this model and consequently, the history match of the entire field became better (Figure 6.24).

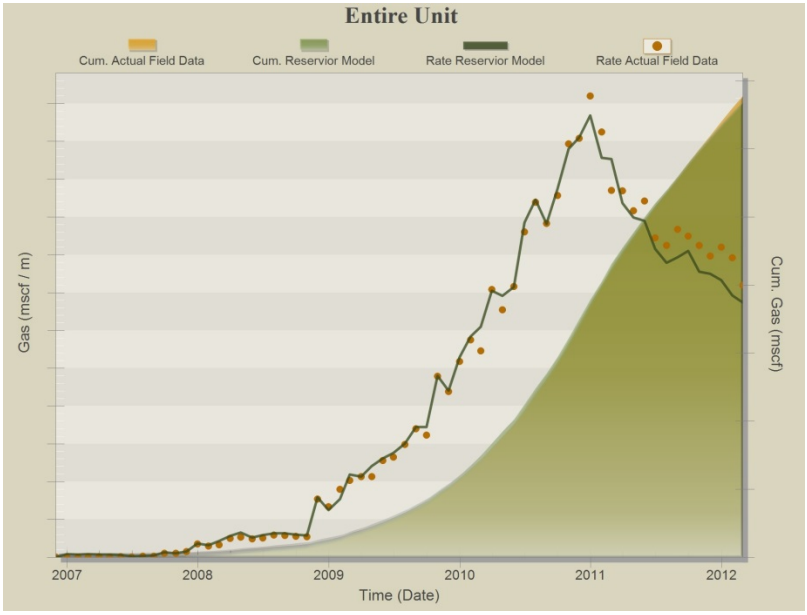

Figure 6.24: The History Matching Result for Entire Field- History Matching Model with Maximum Number of Inputs

6.7 Key Performance Indicator (KPI)

The history matching process, as shown in Figure 6.1, is a process of exclusion and inclusion of different parameters as it explained to improve the results of history matching for every single well. In previous sections it was tried to improve the results by adding some new features and finally a model with 105 inputs was achieved. This may not be very practical, however, especially when it is compared to the conventional history matching process that usually involves less parameter. Therefore it was tried to minimize the number of parameters resulting not only the same result but also better history matching.

In order to do this during the history matching process, a propriety algorithm is used to identify the influence of the combination of parameters. During Fuzzy Pattern Recognition, a curve is generated from the existing data. The slope of the curve determines the degree of influence of a parameter on the production indicator (the output: the target of the correlation). Therefore, the parameter with the largest slope is identified as the parameter with the highest influence on the output. In order to simplify the analysis of the order of influence of parameters, the slopes are normalized, giving the parameter with the highest slope a value of 100.

The KPI is a very useful step in choosing the input parameters for the history matching process since it identifies the contribution of parameters to the output of the system.

Figure 6.25 and Figure 6.26 shows the KPI result for the top 30 parameters in the model with maximum number of inputs before and after developing the AI-based model respectively. In the other words, the KPI ranking of parameters after developing the AI-based model represents the influence of each parameter during the training- the higher ranking, the higher influence.

6.8 Best History Matched Model

Although the history matching results by using the maximum combination of parameters is extremely useful, one may reasonably argue that dealing with large number of inputs is not a correct and effective way for modeling through neural network training, calibration and verification process.

Accordingly, the history-matching process was performed with a minimum combination of parameters that should be used to achieve an acceptable history match results for individual wells and for the entire field (The total number of inputs was decreased from 105 to 36). The following factors were taken into account for reducing the number of inputs in order to achieve the best history matching results:

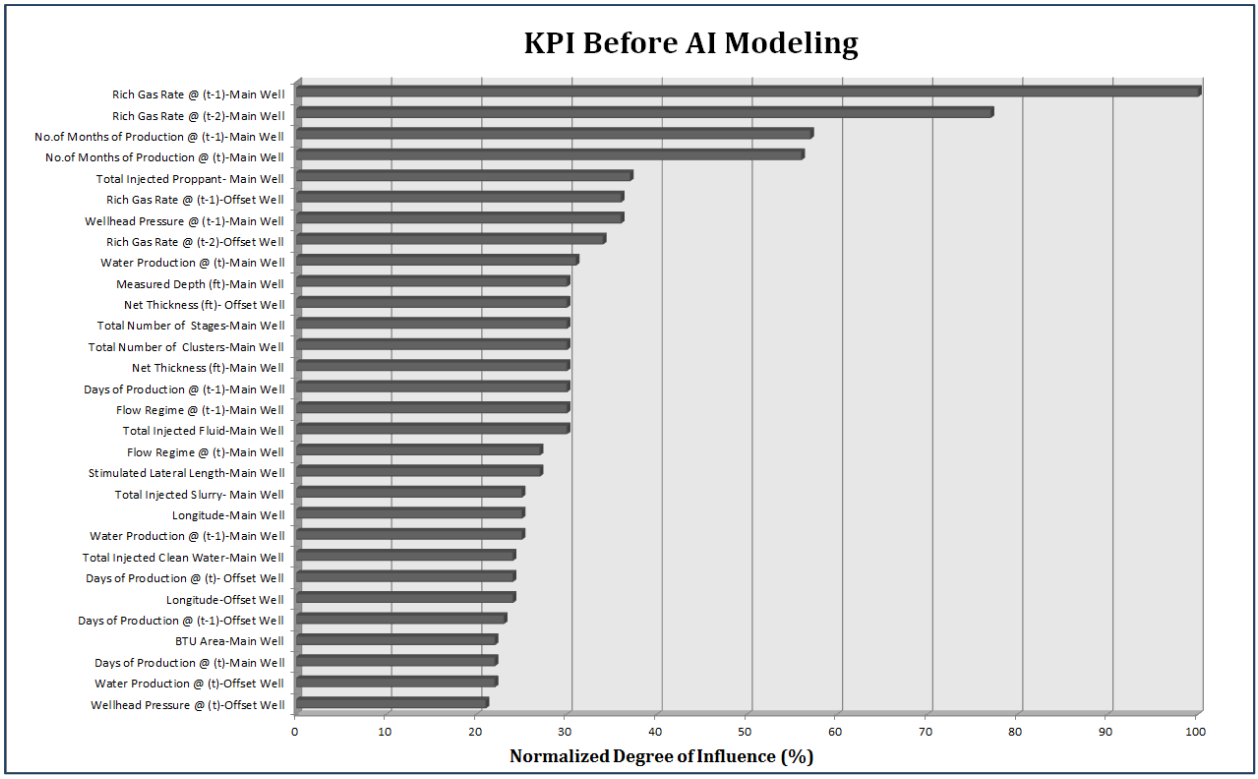

Figure 6.25: KPI Results *Before* AI-Modeling- Based on the history matching model with maximum number of inputs

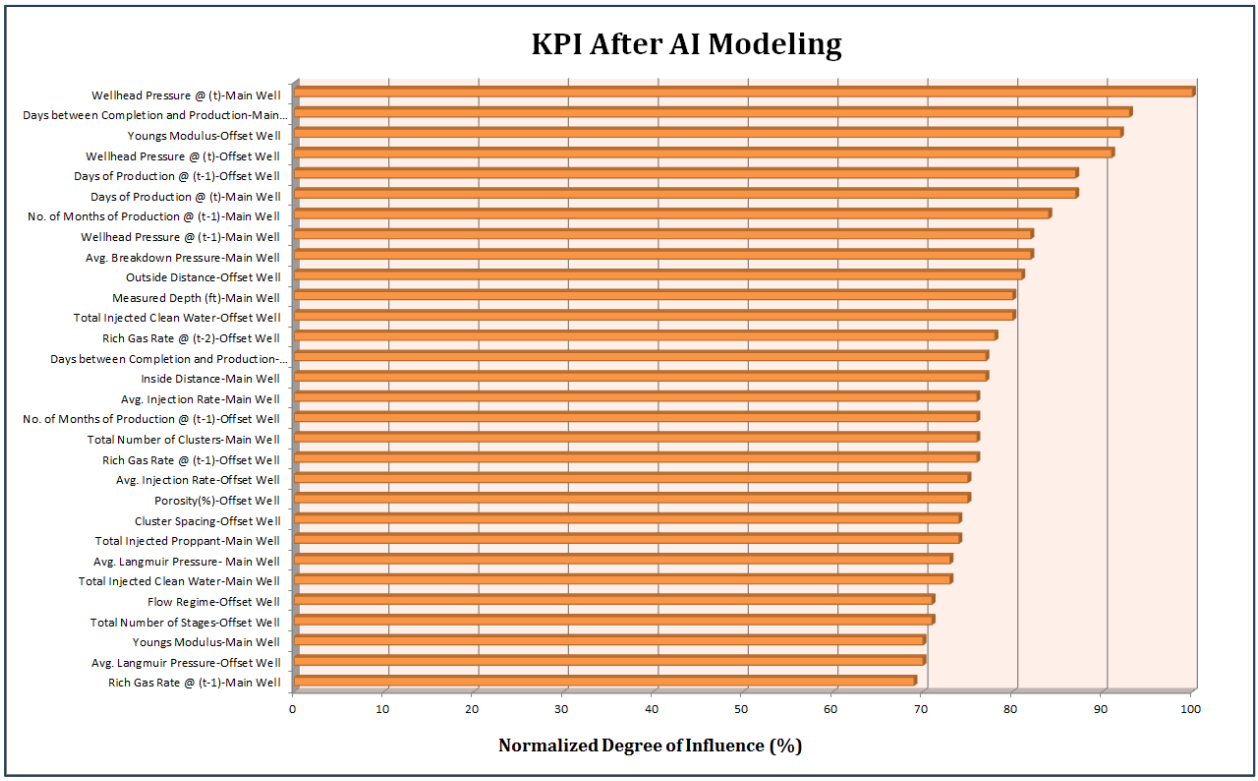

Figure 6.26: KPI Results *After* AI-Modeling- Based on the history matching model with maximum number of inputs

1- There are some parameters in the database that are dependent on other parameters. For example, matrix porosity and permeability are between those parameters that a linear relationship can describe their dependency. Injected clean water, injected slurry and injected fluid are other good examples which one can be representative of the rest. Therefore, one parameter was kept in the database in order to avoid the redundancy.
2- Some of the wells in the database have some properties which are almost the same for all of those wells. For instance, cluster spacing for the 90% of the wells is about 100 ft. As a result, these features were removed from the database because they did not provide additional information to explain different well's behavior.
3- The Key Performance Indicator (KPI) process was performed to rank the most influential input parameters. In this process, not only the impact of each parameter, but also the combined influence of different inputs on monthly gas production can be identified. A propriety algorithm was used to identify the influence of the combination of parameters. The effect of each parameter on the system's behavior was amplified or dampened (in a non-linear fashion) by the presence of other parameters in the system. Based on the result of KPI, some parameters such as Average Injection Pressure, Langmuir Volume, Langmuir Pressure and etc. with less influence on gas production, were removed.
4- Using the dynamic properties (except gas rate) at a time step behind (@ t-1) helps the network to predict the behavior of gas production at current time step. Though, if these parameters do not represent the behavior properly, they might confuse the network. As a result these parameters cause an inverse impact on the results. During the history matching process, in order to achieve the best history match result, it was found that using some of the dynamic parameters at (t-1) has a negative effect on production; therefore, in the best history matched model, they were not used.
5- There are still some debates about the existence of initial water saturation in Marcellus Shale. The initial or connate water saturations in high quality gas shale such as Marcellus is very low because of the excessive drying of shale at high temperatures and pressures during gas generation and migration as well as burial history and capillary hysteresis [Wang 2010]. Therefore, the initial water saturation was not involved in achieving the best history matched model; furthermore, this parameter didn't show such a high impact in KPI.
6- The given data for water production of each well shows some abnormality which might be due to incorrect reporting or inappropriate measurements. This information was also removed from the optimizing the number of parameters.

The best history matched model with the optimum number of inputs includes 36 parameters and a feed-forward Backpropagation neural network with 71 neurons in the hidden layer was used for training, calibration and verification. Figure 6.27 shows the cross plots of each partition for the best history matched model.

Figure 6.28 and Figure 6.29 show some examples of excellent and poor history matching results based on the best history matched model.

Figure 6.30 also illustrates the history matching result for the entire field. As illustrated in Figure 6.30, the history matching result for the entire field in best history matched model is better than the previous models particularly over the last months of production.

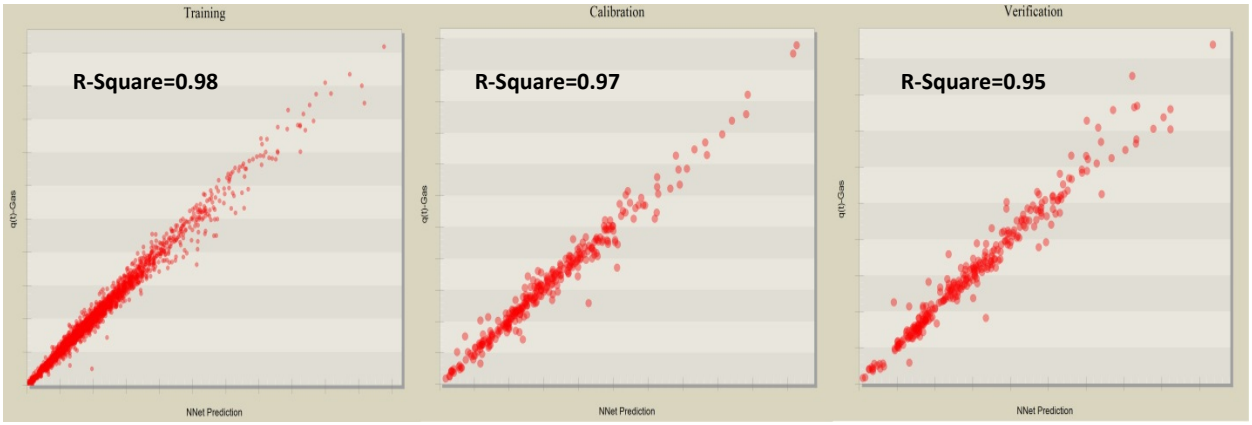

Figure 6.27: Training, Calibration and Verification Cross Plots for Best History Matched Model

Figure 6.28: History Matching of Well #10013 and Well#10074-Excellent Match- Best History Matched Model

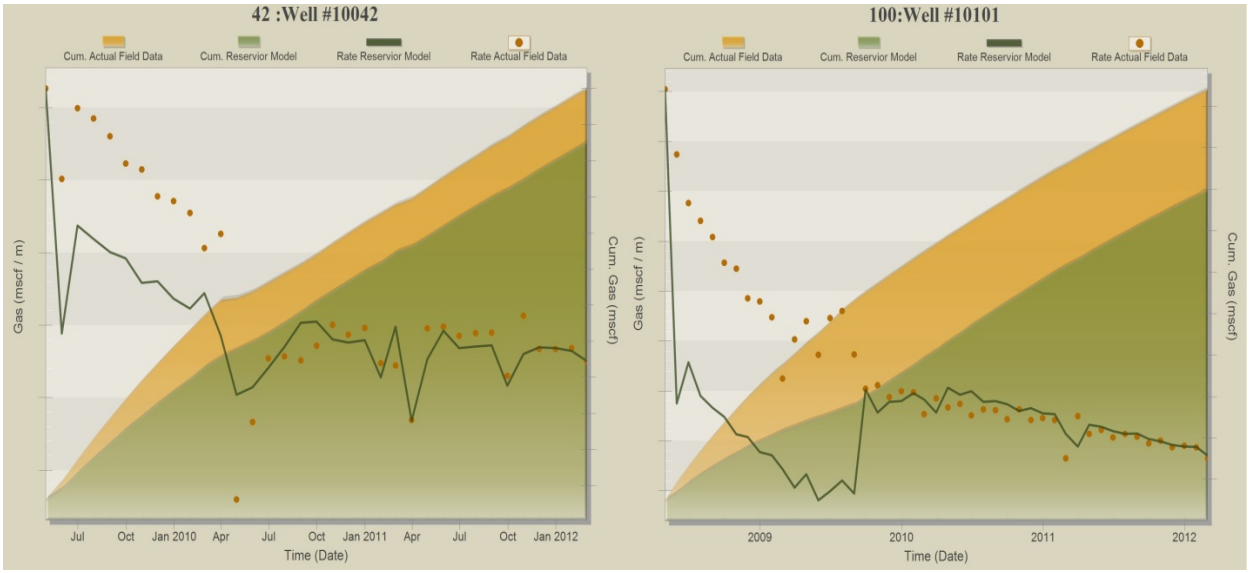

Figure 6.29: History Matching of Well #10042 and Well#10101-Poor Match- Best History Matched Model

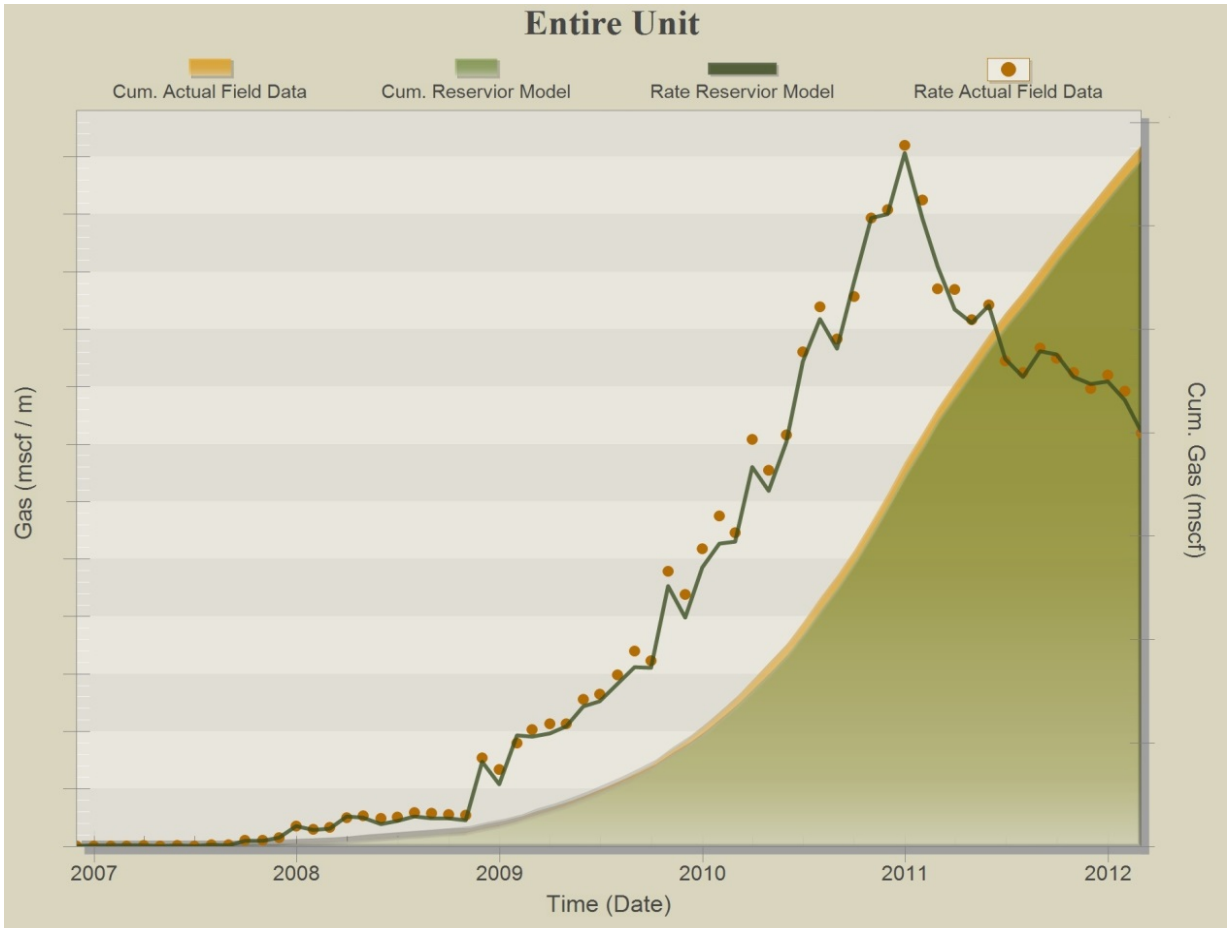

Figure 6.30: The History Matching Result for Entire Field- Best History Matched Model with Optimum Number of Inputs

Upon completion of history matching, an appropriate function (Equation 22) was used in order to estimate the error associated with each well in the best history matched model.

$$MAPE = \frac{\sum_{t=1}^{Nt(i)} \left| Y_{i,t}^{AI\ Model} - Y_{i,t}^{Actual} \right| / Y_{i,t}^{Actual}}{Nt(i)} \times 100 \ldots \ldots \ldots \ldots \ldots \ldots \ldots \ldots \ldots \ldots \ldots \ldots \ldots \ldots \ldots \ldots . (22)$$

Figure 6.31shows the histogram of errors for the best history matched model. As it has shown, more than 90% of the wells have an error less than 20%. Out of 135 wells, five wells have shown an error above 20% which were analyzed and discussed in details in next section. The error of history matching for the entire field is also around 8.8%.

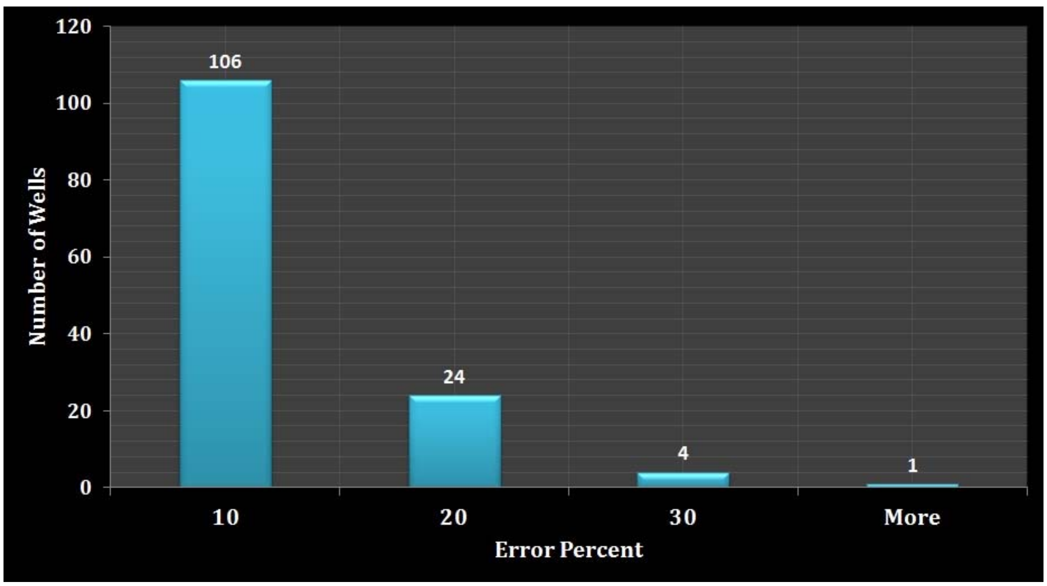

Figure 6.31: Histogram of Estimated Error for the Wells in Best History Matched Model

Table 6-1 illustrates the list of 36 parameters that were used in best history matched model. Figure 6.32 shows the key performance indicator (KPI) result of parameters in best history matched model before and after AI-based modeling.

Table 6-1: List of Parameters in Best History Matched Model

Main Well	***Group 1- Well Information***	Easting
		Northing
		Inside Distance
		Outside Distance
		Type of the Well
		Measured Depth (ft)
	Group 2- Reservoir Characteristics	Matrix Porosity
		Net Thick(ft.)
	Group 3- Geomechanical Properties	Min Horizontal Stress
	Group 4- Completion Data	Total Clusters
		Days between Completion and Production
	Group 5- Stimulation Data	Avg. Injection Rate (bbl/min)
		Clean Vol. (bbl)
		Total Injected Proppant (lb)
	Group 6- Dynamic Properties	Rich Gas @(t-1) & (t-2)
		Avg. Monthly WHP @ t & (t-1)
		No. of Days of Prod. @ t & (t-1)
		Flow Regime @ (t-1)
		No. of Month of Production @ (t-1)
Offset Well	***Group 2- Reservoir Characteristics***	Matrix Porosity
		Net Thick(ft.)
	Group 3- Geomechanical Properties	Min Horizontal Stress
	Group 4- Completion Data	Total Clusters
		Days between Completion and Production
	Group 5- Stimulation Data	Avg. Breakdown Pressure
		Avg. Injection Pressure
		Injected Clean Water Volume (bbl)
		Total Injected Proppant (lb)
	Group 6- Dynamic Properties	Rich Gas @ (t-1) & (t-2)
		Avg. Monthly WHP@ t (Psi)
		No. of Days of Prod. @ (t-1)
		No. of Mon. of Prod. @ (t-1)

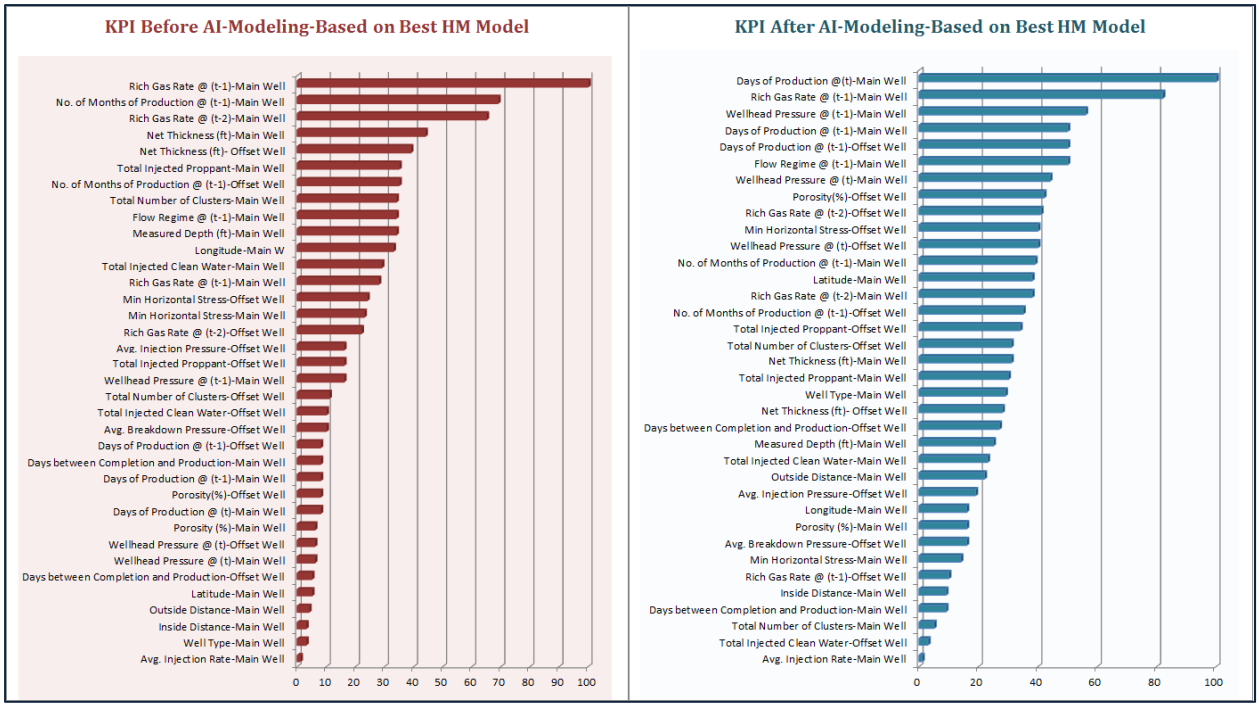

Figure 6.32: Degree of Influence for parameters (KPI) in Best History Matched Model- Before and After modeling

6.9 Detailed Analysis on Poor History Matching Results in Best History Matched Model

Out of 135 wells in this study, five wells have shown an error above 20%. A detailed evaluation was performed for each of these 5 well in order to diagnose the reasons for non-behaved prediction by the AI-based model. As the first step, all parameters involved in achieving the best history matched model were evaluated for each well and its offset well to see whether all the design and native parameters are within the defined uncertainty range for entire field or not.

In the second step, the production profile of each well and its offset well was studied in order to check the existence of any inconsistency in dynamic parameters which might cause the abnormal behavior of the AI-based model. The diagnostic results for each well are discussed as following:

Well # 10042- This well is located on a pad with four more laterals and came to production on April 2009 (Figure 6.33). All the design (such as completion and hydraulic fracturing data) and native parameters (such as reservoir characteristics) of this well are within the ranges of parameters for the entire field. Therefore this cannot be the reason for the underestimation of AI-based model.

For Well # 10042, at the beginning, the closest offset well was Well #10026 which was on production since August 2007 and it was between the first drilled horizontal well in the area. As illustrated in Figure

6.34, the behavior of Well # 10026 is very erratic and the gas rate is very low compared to the typical Marcellus Shale gas well.

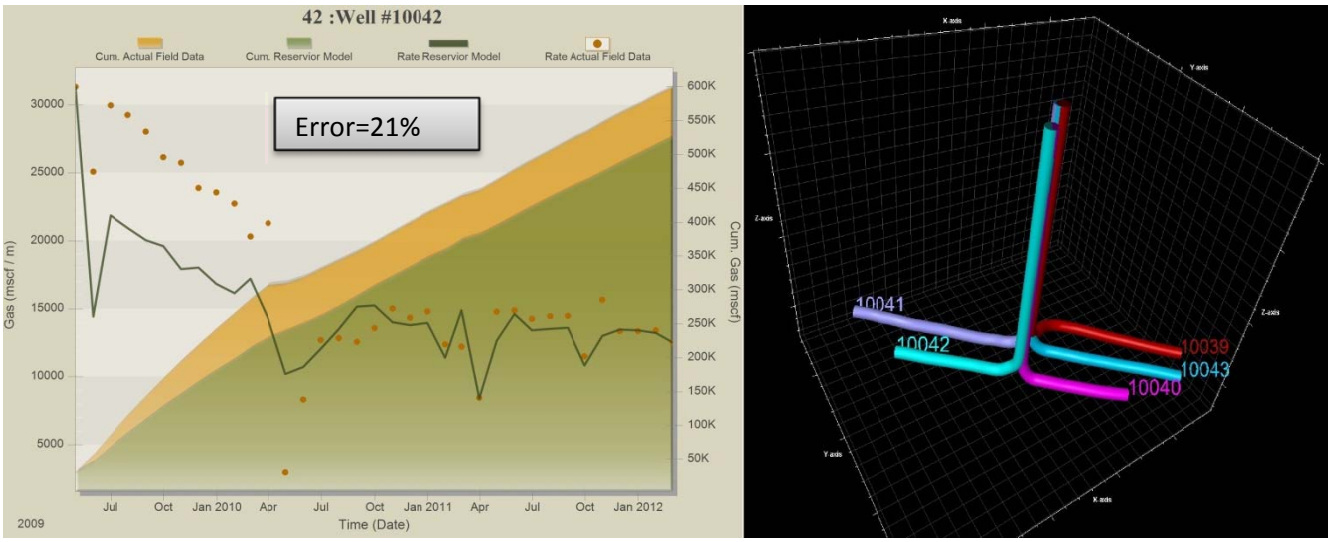

Figure 6.33: History Matching Result in Best History Matched Model and Location of the Well # 10042

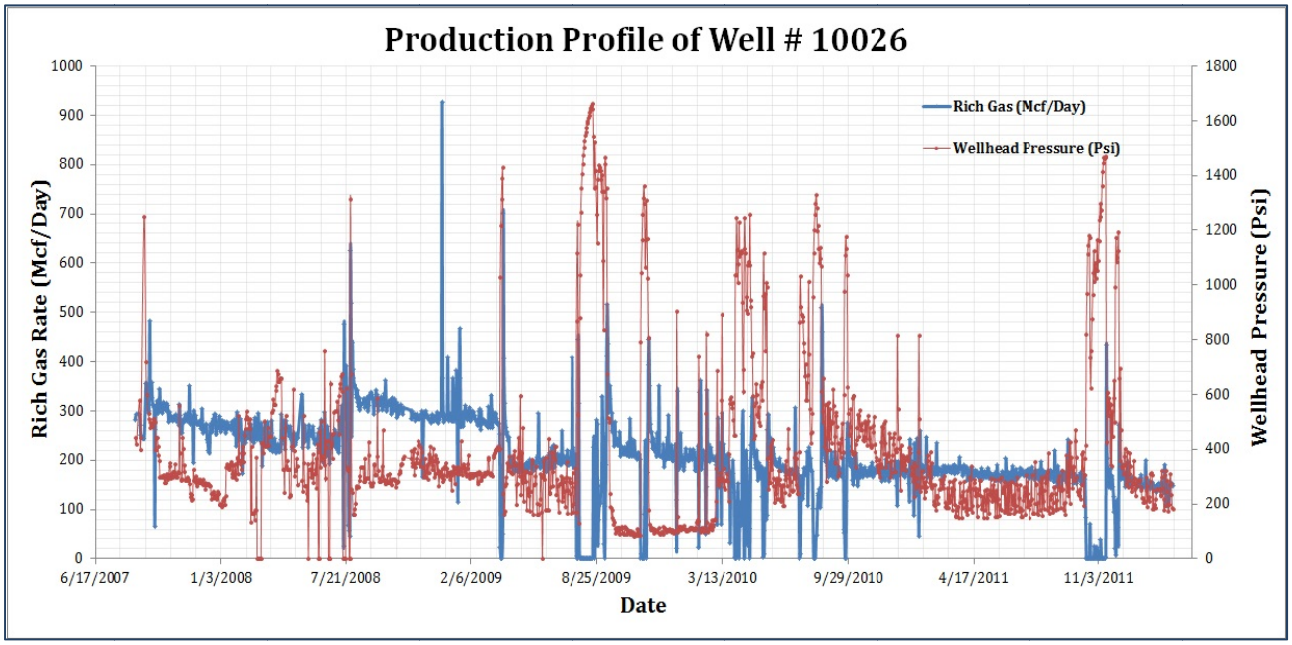

Figure 6.34: Production Profile of Well# 10026- This well came to production on August 2007 and it has very law gas rate.

As shown in Figure 6.33, the AI-based model underestimates the actual gas production from the beginning of the production up to May 2010. For this period as mentioned earlier, the offset well was Well # 10026 which produces around 10,000 Mcf/Month and this was fed to the neural network as an input. It caused the underestimation for Well # 10042 for that period of time, but after May 2010, Well #

10041 came to production and became the new offset for this well. As seen, the history matching results for Well # 10042 was improved significantly.

Well # 10053- This well is located on a two-well pad, came to production on February 2009. As shown in Figure 6.35, the AI-based model overestimates the actual rich gas with the estimated error of 28%. The well was completed in 19 clusters (5 stages) and all design and native parameters seemed to be within the range of the entire field.

At the beginning of well production, the closest offset well was Well # 10103 which came to production on January 2009 and it is located 4600 ft. away from Well #10053. By looking at the production profile of Well #10103 in Figure 6.36, it can be observed that this well is more prolific than Well # 10053(it is producing about 70,000 Mcf/Month). As an offset well in the AI-based model, it causes the overestimation for well # 10053. The AI-based Model prediction for well#10053 was improved when Well #10080 came to production on February 2010 and became the new closest offset well.

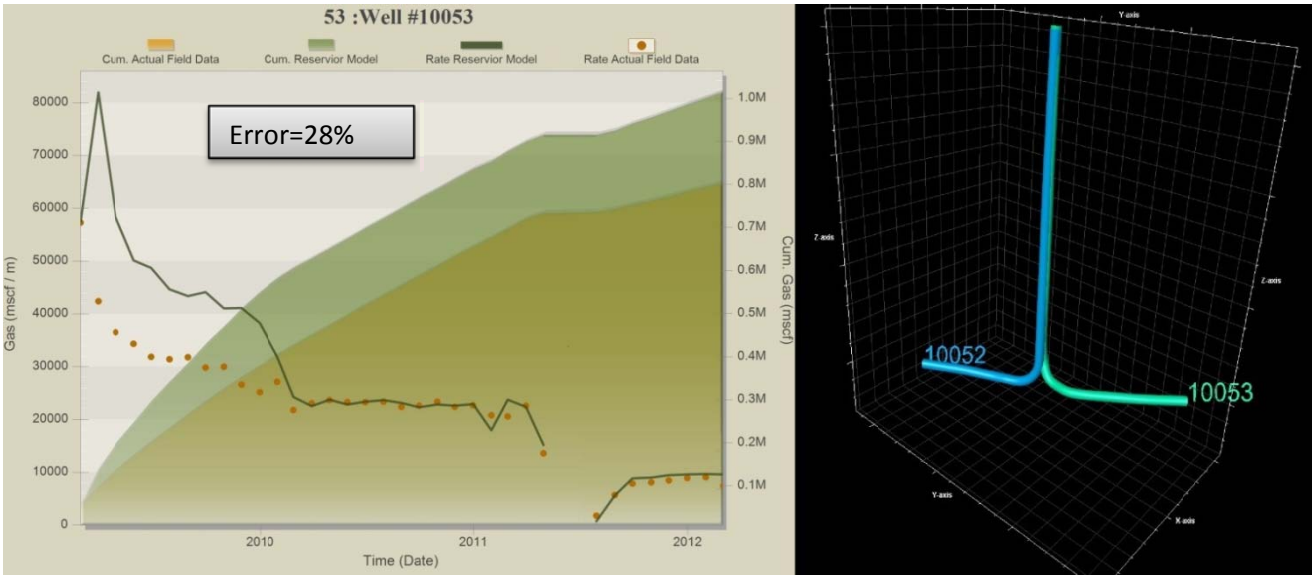

Figure 6.35: The History Matching Result in Best History Matched Model and Location of Well # 10053

Well # 10072- This well was the first horizontal well in this area which was drilled and completed in 2006 and came to production by August 2007. Due to the lack of experience in horizontal drilling in Marcellus, this well was completed in 4 stages (8 clusters), 200 ft. away and because of this large spacing, the well has not shown good performance. The completion and stimulation data was not available for this well and the AI-based model used the information of offset well. Figure 6.37, shows the location and

history matching result of this well in the best history matched model. As shown in this figure, the well has a very erratic behavior and the AI-based model could not capture it very well.

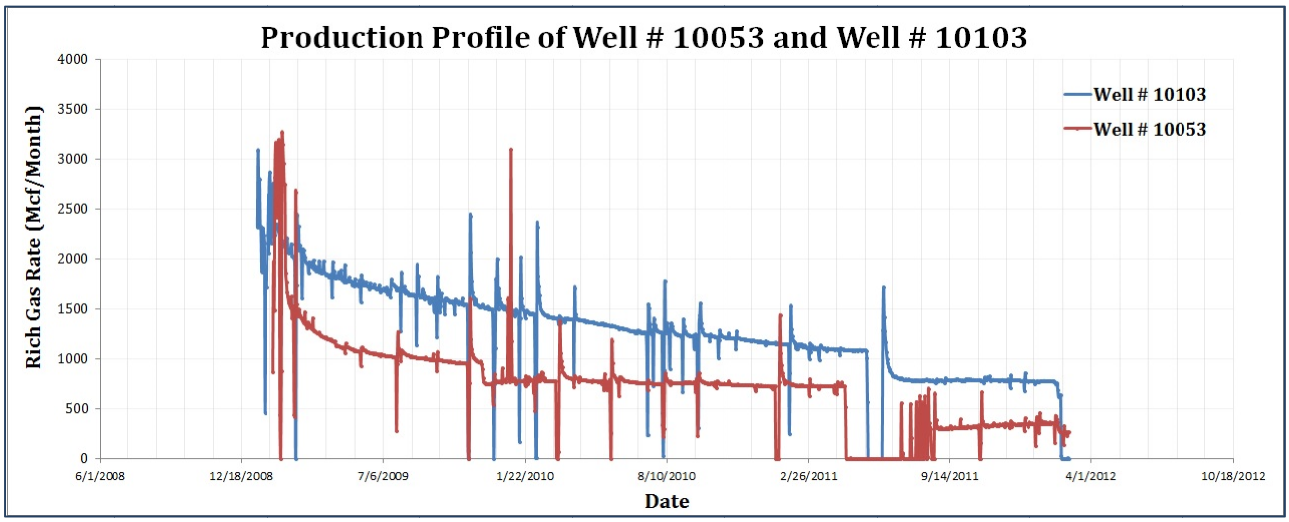

Figure 6.36: The Production Profile of Wells # 10053 and Wells # 10103- Figure shows that the performance of Well # 10103 is much better than Well # 10053 and as an offset, it caused the overestimating by AI-Based Model in history matching.

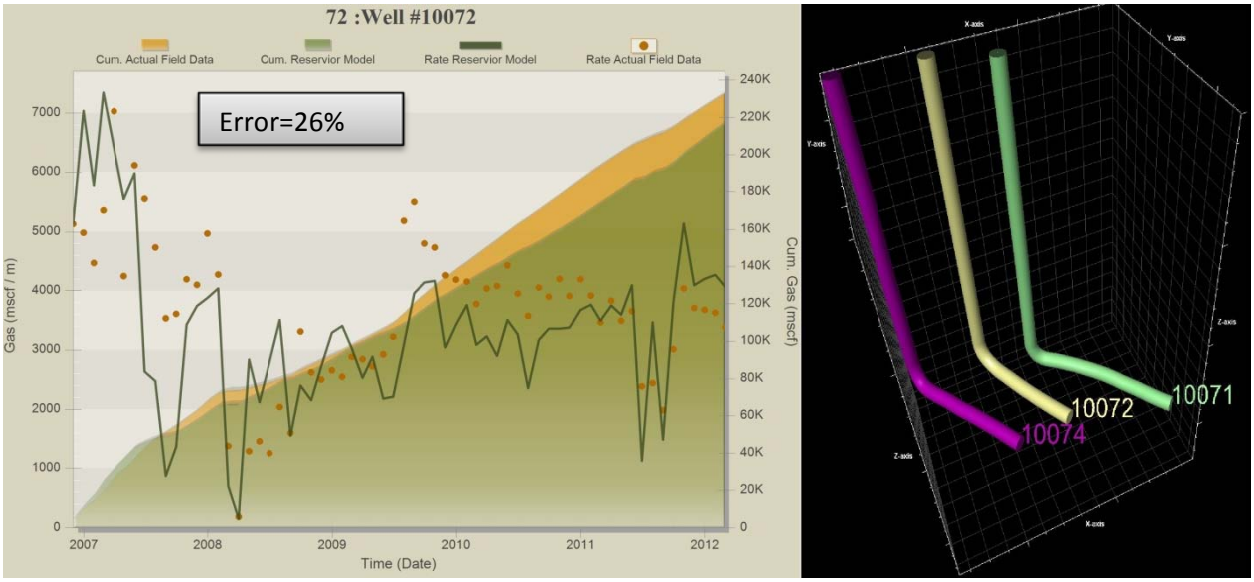

Figure 6.37: The History Matching Result in Best History Matched Model and Location of Well # 10072

Compared to the entire field, this well is amidst those wells with the minimum number of clusters. It is probably one of the reasons for having the low rates, although there are some other wells with the same number of clusters but normal gas rate. As a result, however the number of clusters could have significant contribution on low rate of this well, the other parameters also can be taken into account. Because of missing completion and stimulation information, the detailed analysis of this well was done by using the

available reservoir characteristics in order to evaluate their impact on performance of the well. Figure 6.38, shows the different reservoir properties along the horizontal section of Well # 10072 and also the placement of clusters.

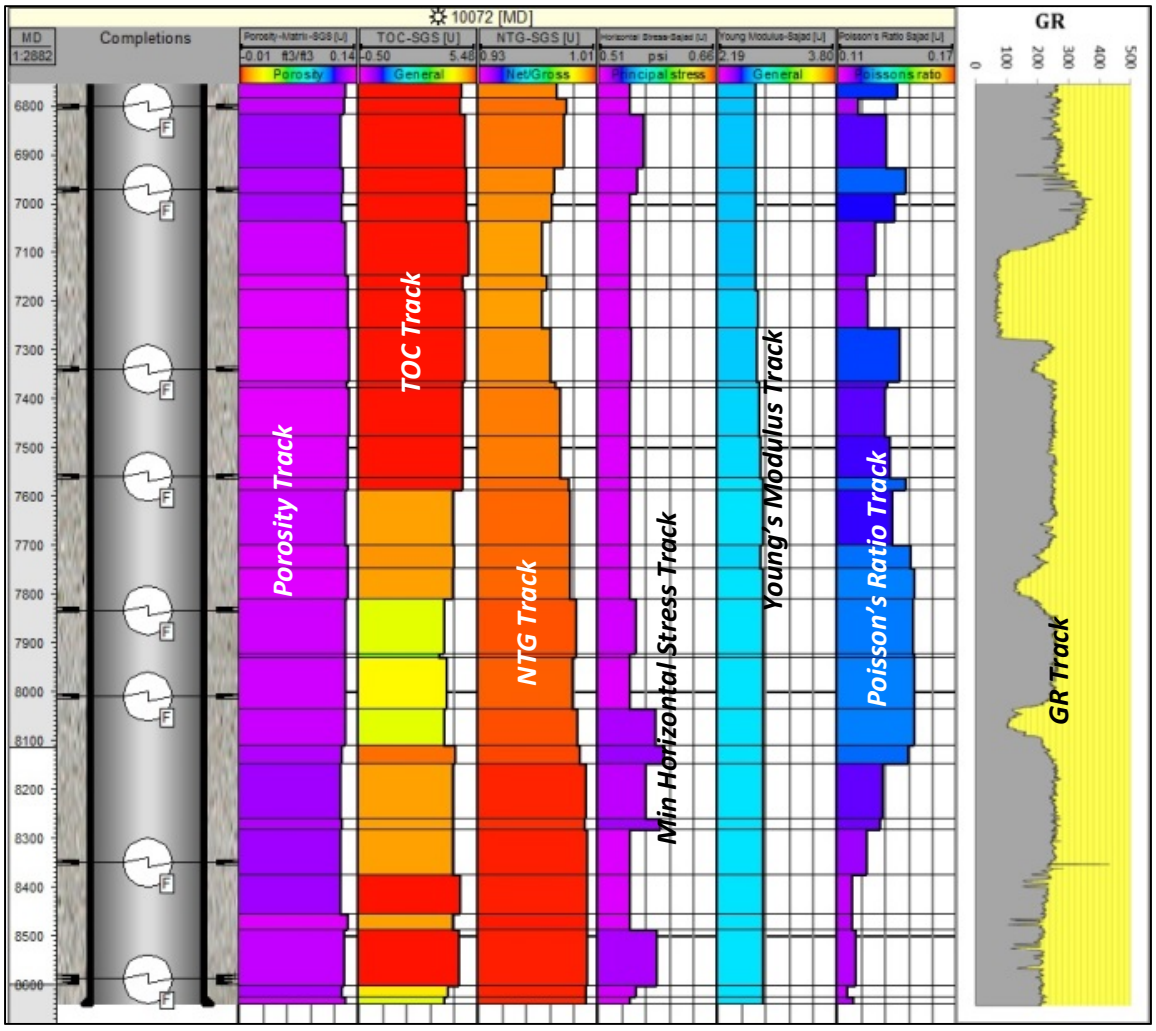

Figure 6.38: Different Reservoir Characteristics along the horizontal section of Well # 10072- In this figure the Matrix Porosity, TOC, NTG, Minimum Horizontal Stress Gradient, Young' Modulus, Poisson Ratio and GR were shown from left to the right.

In this figure, all shown parameters except GR, which was run along the horizontal lateral, were extracted from the distribution maps based on the information of vertical wells. Following the proposed algorithm by Cipola et al. (2011) for staging in horizontal wells, two different categories for properties; reservoir and completion properties; should be evaluated in selecting the perf-cluster placement. Table 6-2 shows the reservoir and completion quality criteria in Cipola's algorithm.

Table 6-2: Reservoir and Completion Quality Criteria- Cipola et al .(2011)

Reservoir Quality	Completion Quality
TOC >= 3%	Stress- Low
GIP > 100 scf/ton	Resistivity > 15 Ohm-m
Kerogen > High	Clay < 40%
Shale Porosity > 4%	YM > 2 mm Psi AND PR < 0.2
Kgas > 100nD	Neutron porosity<35% and density Porosity > 8%

As it has illustrated in Figure 6.38, the matrix porosity is about 14%, the TOC is between 3.5% and 5% and the NTG is almost 1 for this lateral, therefore the criteria for reservoir quality in location of all clusters is met. The completion properties, the minimum horizontal stress gradient, the young's modulus (YM), the Poisson ratio (PR) and GR were available that were shown as the last four tracks of Figure 6.38. Based on the given information, this well is located in the area with low stress gradient (around 0.6 Psi/ft) and the values of Young's modulus and PR are in the range of given criteria.

By definition, brittle shales are those with higher YM and lower PR and are more likely to be naturally fractured and responding favorably to hydraulic fracturing treatment. Figure 6.39 shows the Brittleness Index (BI) histogram of all the wells in the area of study which is defined as following [Waters et al., 2011]:

$$BI = \frac{\left[\frac{100(E_v - E_{v-min})}{(E_{v-max} - E_{v-min})} + \frac{100(\mu_v - \mu_{v-max})}{(\mu_{v-min} - \mu_{v-max})}\right]}{2} \quad \ldots\ldots\ldots\ldots\ldots\ldots\ldots\ldots\ldots\ldots\ldots\ldots\ldots\ldots\ldots\ldots\ldots\ldots\ldots\ldots\ldots\ldots (23)$$

Where

E_{v-min}= Minimum vertical Young's Modulus in interval of interest (psi)
E_{v-max}= Maximum vertical Young's Modulus in interval of interest (psi)
μ_{v-min}= Minimum vertical Poisson's ratio in interval of interest
μ_{v-max}= Maximum vertical Poisson's ratio in interval of interest

As it shown in Figure 6.39 the resulting value of equation 23 is an index scaled from 0 to 100 and usually the higher BI can be interpreted as better shale and consequently better performance. As it has shown in this figure the brittleness index of entire field has an average of 35 while the brittleness index of Well # 10072 is around 17 which is relatively low.

Therefore it can be concluded that less number of hydraulic fracture clusters and being placed in the more elastic zone (low brittleness factor) could be the main reasons for low productivity of this well in comparison to the other wells with the same number of clusters and reservoir quality.

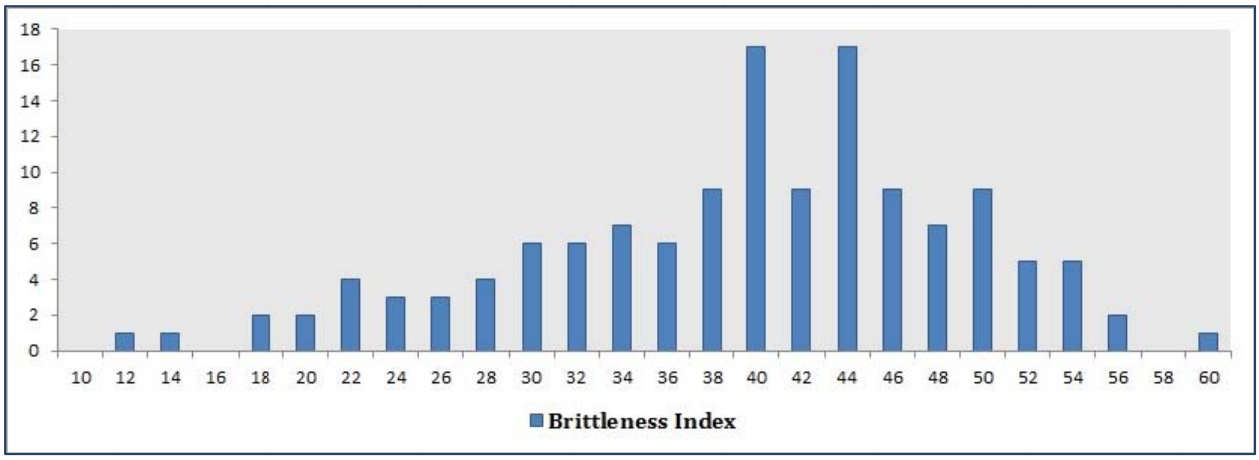

Figure 6.39: Histogram of Brittleness Index for Entire Field

Well # 10085- This well is located on a pad with five more wells, was completed on October 2007 and came to production on January 2009. As it has shown in Figure 6.40, the AI-based model overestimates the actual rich gas from the third month of production until November 2010.

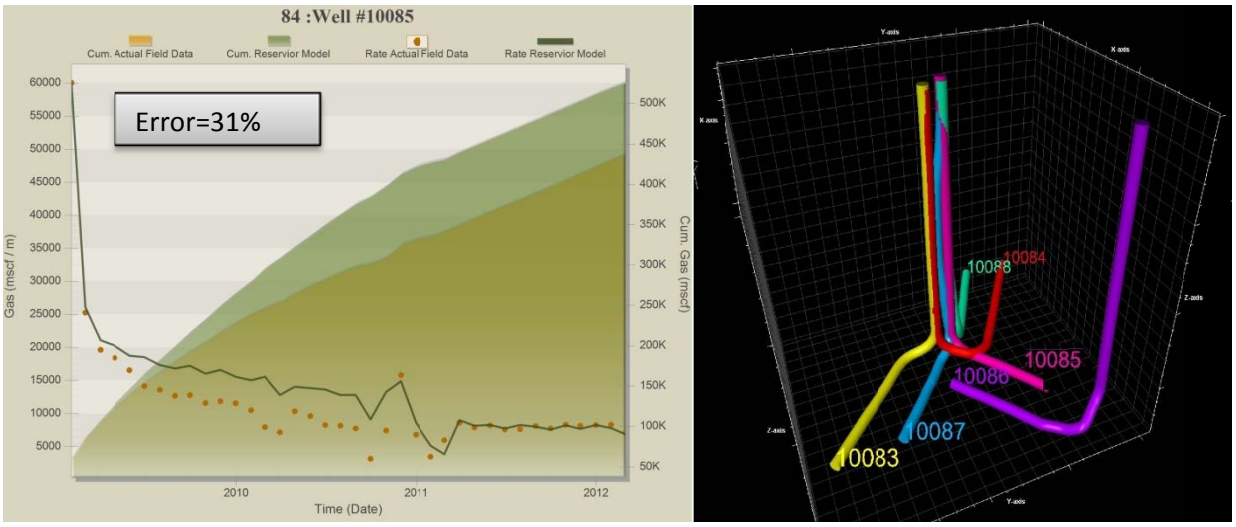

Figure 6.40: The History Matching Result in Best History Matched Model and Location of Well # 10085

Compared to the other wells in this pad (Figure 6.41), this well has the lowest performance particularly in the period of beginning 2009 to end of 2010. By looking at the completion and stimulation data it was

found that this well was completed with the lowest number of stages in pad (8 stages-8 clusters) while all the wells in pad were completed in more clusters (between 12 clusters to 36 clusters). In addition, the delay between the completion and production had a negative impact on performance of this well.

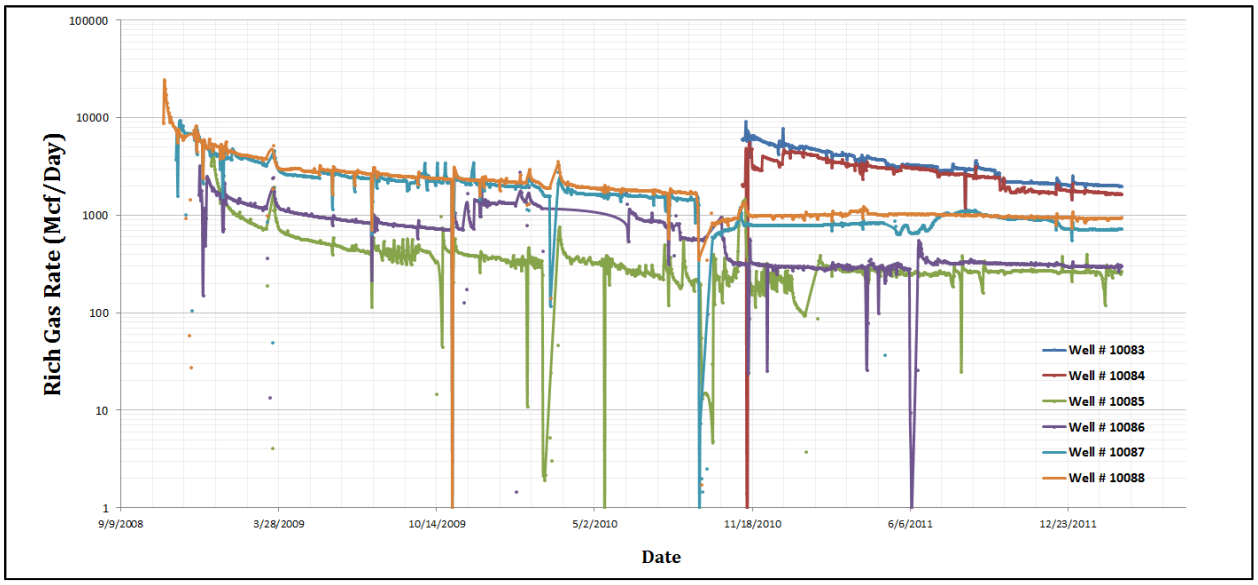

Figure 6.41: The Rich Gas Rate of all wells (Well # 10083 to Well # 10088) in same pad- Well # 10085 was identified by green curve and it has the lowest gas rate compare to the other wells

The first closest offset well was Well # 10086 which was producing since December 2008 and as illustrated in Figure 6.41, this well has the better performance than well # 10085 and as an offset; it caused the overestimated prediction by the AI-based model. At the end of 2010, both wells are producing at almost the same rate and the history matching result by AI-based model improved significantly.

Well # 10101 – This well is located on a two-well pad and immediately after completion (8 clusters) came to production on March 2008. As shown in Figure 6.42, the AI-based model is underestimating the actual rich gas from this well during the half of well life (from the beginning until September 2009).

At the beginning, Well # 10026 was the closest offset well and as its production profile was shown in Figure 6.34, this well has a very erratic and low rate. Because of the effect of offset wells, the AI-based model underestimated the production of Well # 10101 from the beginning until September 2009. At this point the closest offset well became Well # 10102 which was in production from August 2009 and it happened to have very similar behavior and as result made substantial improvements in history matching of Well # 10101.

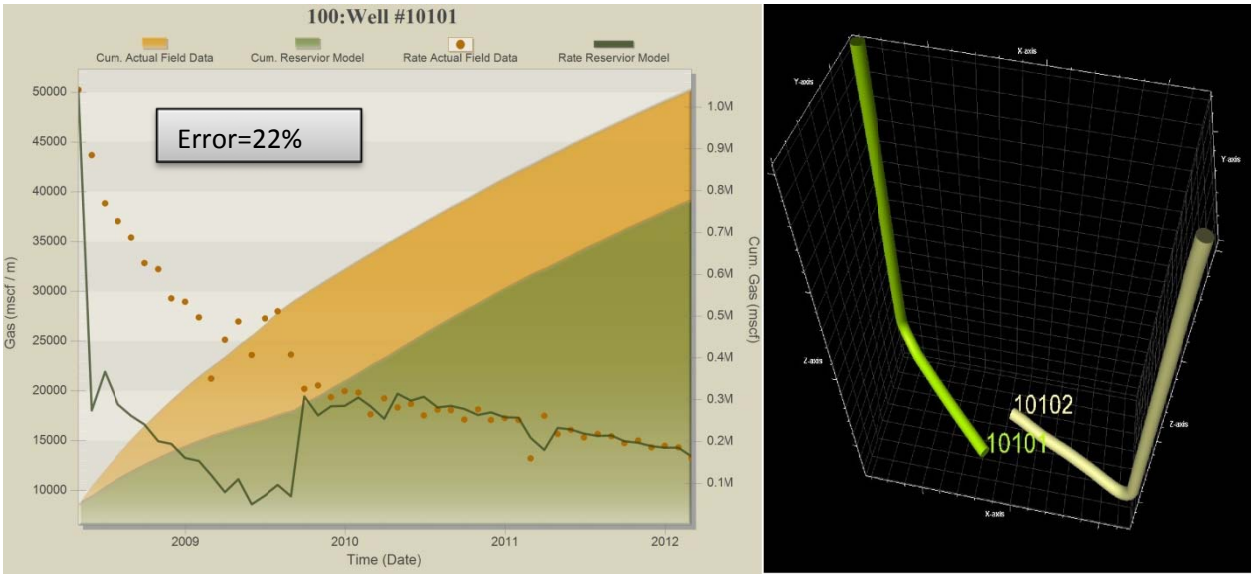

Figure 6.42: The History Matching Result in Best History Matched Model and Location of Well # 10101

7. CHAPTER VII

VALIDATION OF AI-BASED MODEL AND FORECASTING

Upon achieving the best history matched model, three scenarios were defined in order to validate the model's capability for forecasting the future reservoir performance as well as the prediction of new wells/pads behavior.

7.1 Scenario 1- Blind History Matching for Last Four Months of Production

As mentioned earlier, the production history was available for this study from August 2006 to February 2012. In this scenario the best AI-based model was trained and history matched with data from August 2006 to October 2011. Production history of the last 4 months was omitted to be used as validation of the model in the form of blind history matching. Figure 7.1 shows the history matching result of the entire field where the last 4 months of production history were removed consistently from all wells.

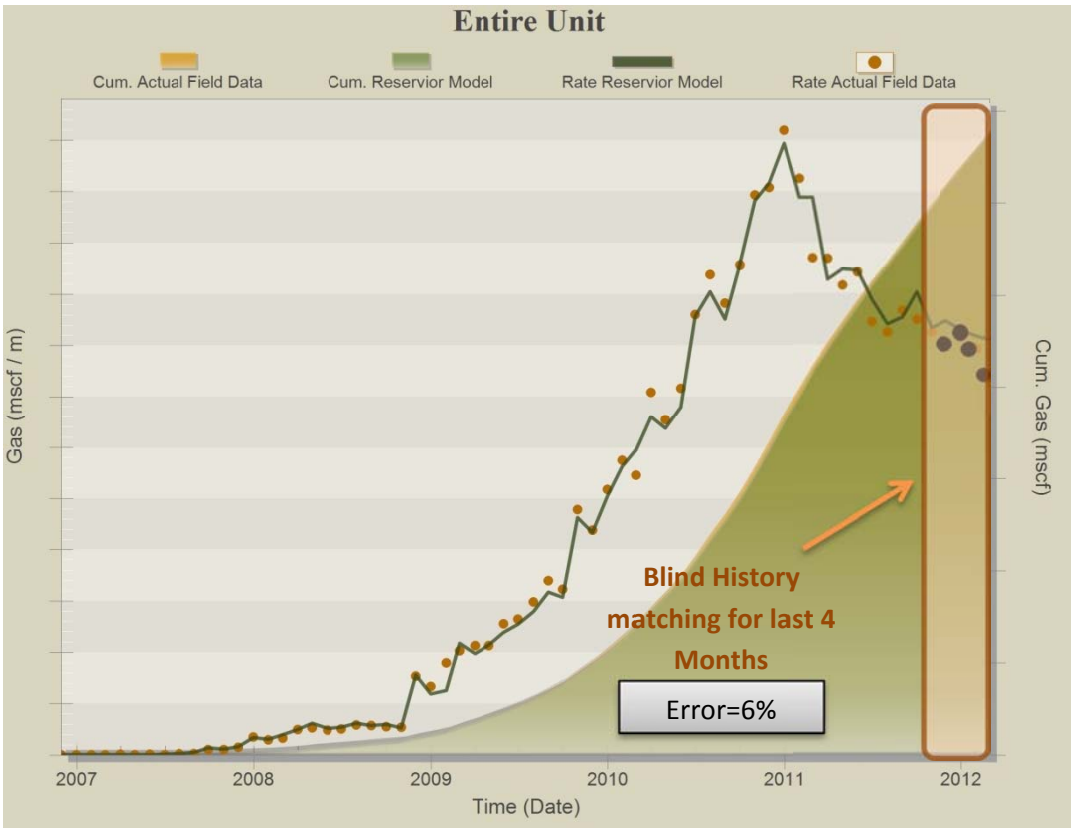

Figure 7.1: The AI-Based Prediction for the Entire Field- the Last Four Months were history matched blindly.

To demonstrate the results of the AI-based model in single wells, two examples are presented in Figure 7.2. The estimated error of 6% for the last four months of production shows the predictive capability of AI-based model.

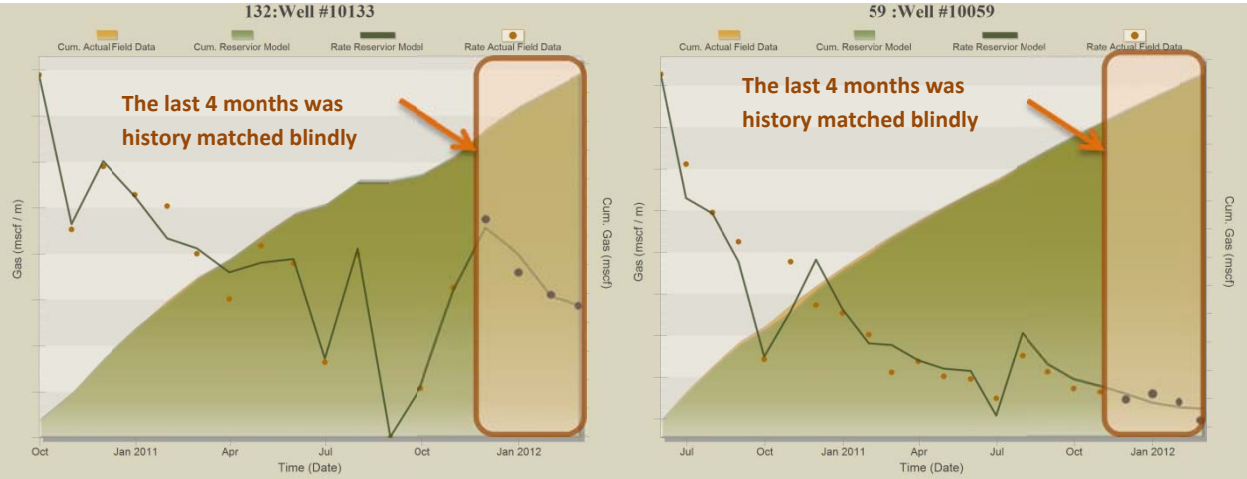

Figure 7.2: The AI-Based model prediction for Well # 10133 and Well # 10059- The last four months was blindly history matched.

7.2 Scenario 2- Forecasting the Performance of Existing Wells

Similar to any other reservoir simulation models, the trained, history matched and validated AI-based model is deployed in predictive mode in order to be used for forecasting the reservoir/well performance. In this scenario for testing the capability of model for forecasting the production performance, the operator provided the production of the wells from March 2012 to March 2013 (one year) which was used for this purpose.

In order to make a realistic case, it was assumed that the wellhead pressure and days of production for this period (from March 2012 to March 2013) were not known. Therefore, for the forecasting of well performance the last wellhead pressure was kept constant and it was expected that the wells produced for the whole month. Moreover, the flow regime was supposed to be unchanged during this year. The forecasting result of the entire field by making these assumptions is shown in Figure 7.3. In this figure, the last 12 months (from March 2012 to March 2013) were blindly forecasted by the AI-based model. Figure 7.4 illustrates the forecasting results of two wells as excellent samples. In these figures the black dots are the actual rich gas and the green line is the AI-based model prediction.

Using Equation 22 in chapter 6, the error associated with the 12 months of forecasting was estimated. Figure 7.5 presents the histogram of errors for all wells in this model.

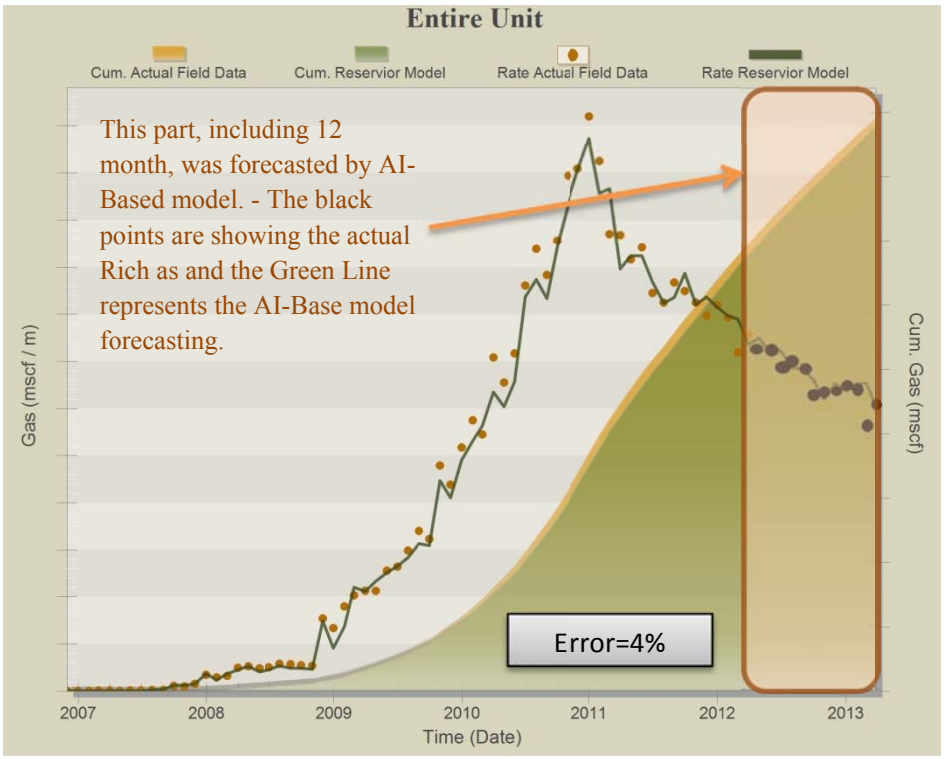

Figure 7.3: The AI-Based Model Prediction for Entire Field- The last 12 months in this figure was forecasted by the AI-Based Model

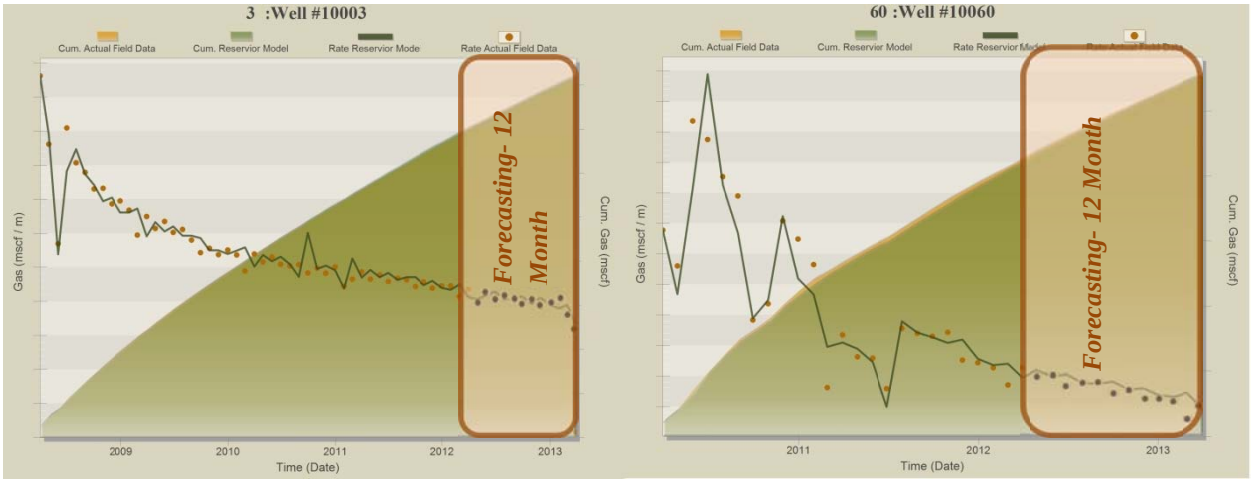

Figure 7.4: The History Matching and Forecasting by AI-Based Model for Well # 10003 and Well # 10060- Two Excellent Examples for the Forecasting Model

As it has shown in Figure 7.5, out of 135 wells, only for 14 wells, the AI-based model forecasting for the last 12 months of production has shown an error above 20 percent. The production profile of most of these wells has changed for the last 12 months of production and it has not followed the history match trend and because the operational constraint were not included for this period, thereby the AI-based model could not capture the behavior properly.

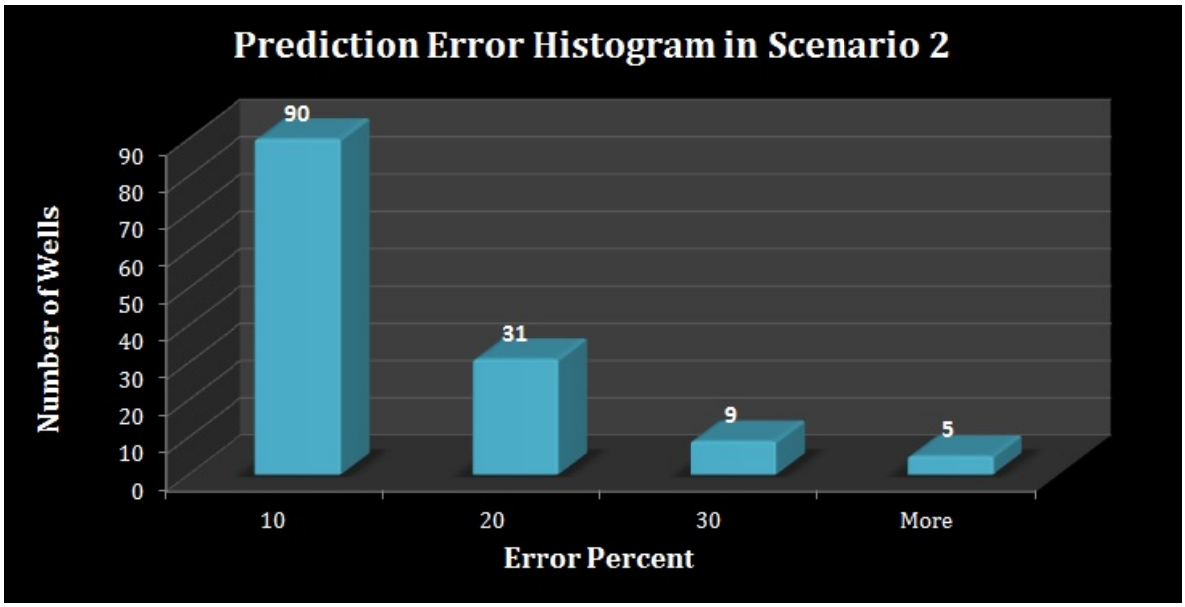

Figure 7.5: Prediction Error Histogram for the last 12 months- Scenario 2

Figure 7.6, exemplifies the AI-based model prediction for two wells that have shown an error of more than 20%. As clearly observed, the production pattern in last months for these wells has totally changed and the AI-based model cannot predict this abnormality. Figure 7.7 also shows the history matching and forecasting result for Well # 10099 with and without imposing the operational constraints. This figure shows that without having operational constraints, the AI-based model follows the production pattern from the last months and overestimates the actual production. After adding the operational constraints; the AI-based model behavior is improved.

Figure 7.6: The History Matching and Forecasting Results for Well # 10037 and Well # 10066- The production pattern in last months has changed and the AI-Based model couldn't predict this behavior.

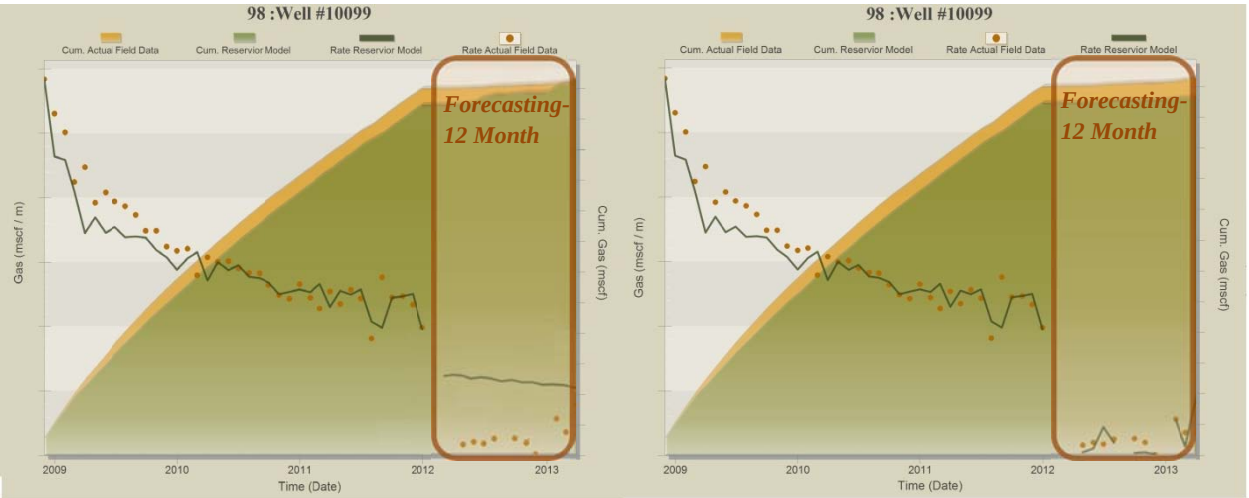

Figure 7.7: The History Matching and Forecasting Result for Well # 10099 before (Left Plot) and after imposing the operational constraints.

7.3 Scenario 3- Prediction of New Wells/Pads Performance

Taking the validation process one step further, in the third scenario, the operator provided the location of several wells/pads that came to production during 2012 (after March 2012). The best history matched model was used in order to forecast the production of these new wells by assuming the constant wellhead pressure and full days of production per each month (except the first month).

In order to determine the flow regime of each new well, an AI-based model was developed by using the information of the existing wells to predict the duration of flow regime 1. Table 7-1 shows the list of data that was used in order to develop the AI-based model for flow regime prediction.

Table 7-1: List of Parameters used for development of an AI-Base Model for predicting the duration of Flow Regime 1

Group 1- Well Information	Easting	***Group 3- Geomechanical Properties***	Shear Modulus
	Northing		Young's Modulus
	BTU Area	***Group 4- Completion Data***	Total Clusters
	Deviation Type		Days between Comp to Production
	Outside Distance	***Group 5- Stimulation Data***	Avg. Breakdown pressure
			Avg. Injection Rate
Group 2 – Reservoir Characteristics	Matrix Porosity		Total Slurry Volume
	Matrix Permeability		Max Proppant Concentration
	Initial Water Saturation		Total Injected Proppant
	Langmuir Pressure	***Group 6- Dynamic Data***	Duration of FR 1 for offset well

Figure 7.8 represents the scatter plot of training, calibration and verification for this AI-based model. In this figure, the green line is actual flow regime duration and the blue line is AI-based model prediction. During the neural network training some of the data (wells) were not included and later was used for verification purposes. These wells were randomly selected and they covered the range of flow regime duration of the entire field. Table 7-2 shows the result of the AI-based model, actual flow regime duration and associated error.

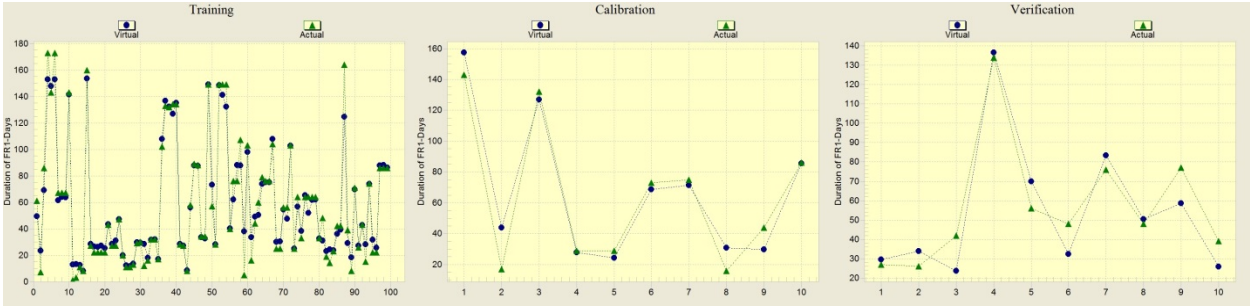

Figure 7.8: Scatter Plots for Training, Calibration and Verification for AI-Based Model of Prediction the Duration of FR 1- The R-Squares are 0.96, 0.92 and 0.85 respectively.

Table 7-2: The Actual versus AI-Based Model Prediction for Blind Wells in AI-Based model of Prediction the Duration of FR 1

Well Name	Actual Duration of Flow Regime 1	AI-Based Prediction for Duration of Flow Regime 1	Error- Percent
10023	22	27	22.7
10047	134	126	5.6
10058	89	84	5.9

After validating this model, it was used to predict the duration of flow regime 1 for the new wells. In order to check the validity of model prediction, the rate transient analysis (following the methodology explained in chapter 6) was performed in order to determine the flow regime for these new wells. The flow regime determined by rate transient analysis for the majority of the wells is within the range of those estimated by the AI-based model as shown in Figure 7.9.

As explained earlier, in order to predict the performance of the new wells/pads, the constant wellhead pressure (based on the closest offset wells) was applied to each well. It was assumed that all the wells produced for the whole month, although the days of production per first month was included in the AI-based model. Completion and stimulation data was partially available but it was not included in the AI-

based model prediction and the model used the required information from geostatsitcal distribution maps which were generated for each individual property.

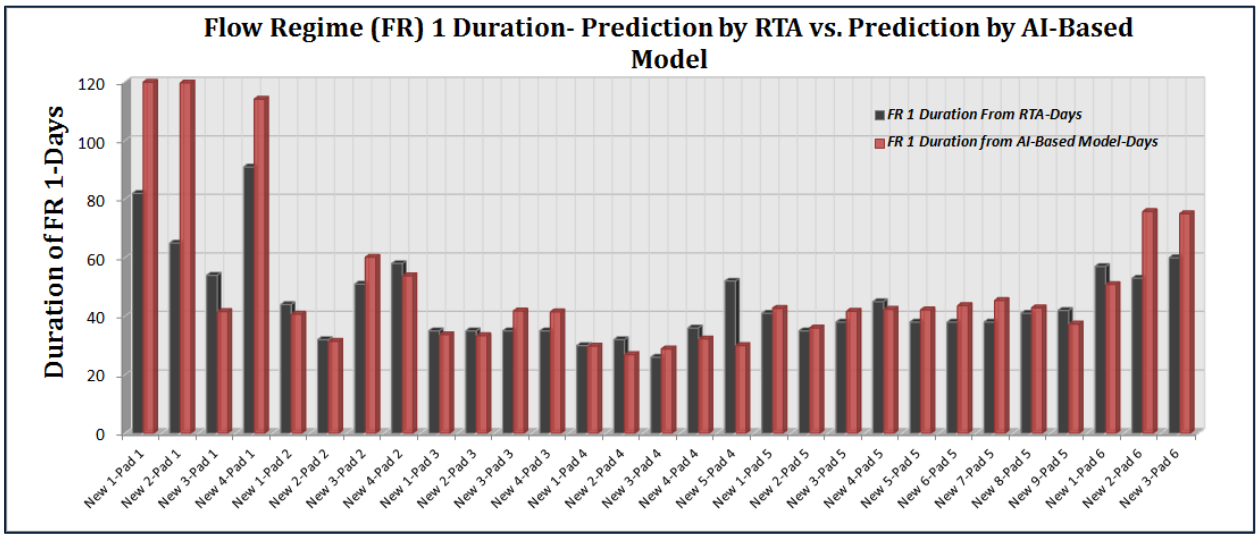

Figure 7.9: The Duration of FR 1 based on RTA and AI-Based Model for new wells

The production performance of 29 wells on 6 different pads was predicted by using the AI-based model. Figure 7.10 shows the location of new wells/pads in the area of study.

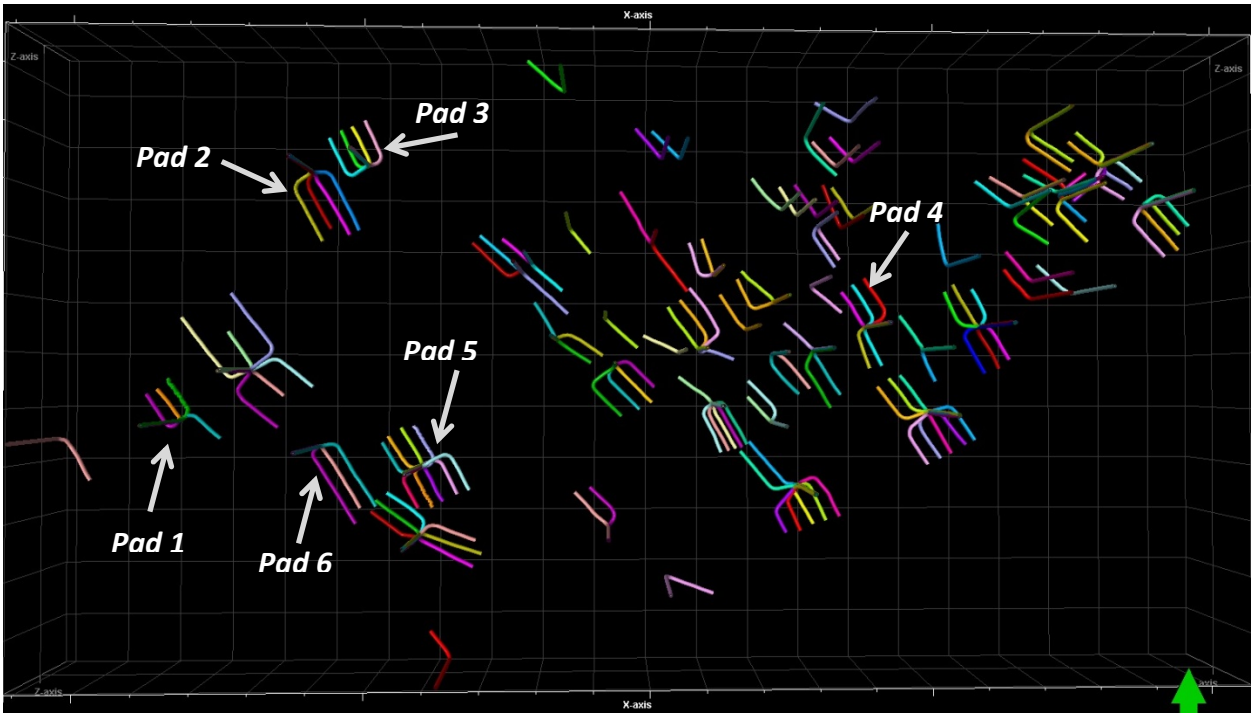

Figure 7.10: Location of New Wells/Pads in area of study- 29 new wells on 6 different pads

New Pad 1- This pad includes 4 horizontal laterals and is located on the western part of the reservoir between two existing pads. New wells 1, 2 and 3 came to production on June 2012 while new well#4 started to produce one month later. Figure 7.11 shows the result of AI-based model prediction versus actual rich gas production of two wells (with minimum and maximum error in pad), the entire pad and wells configuration.

In the top plots of this figure, green lines represent the AI-based model prediction for rate, the orange dots show the actual rich gas rate, the green shadow represents the predicted rich gas cumulative production by AI-based model and the yellow shadow shows the actual cumulative rich gas. For the entire pad plot, the blue line shows the AI-based model prediction for rich gas rate, the red dots are representing the actual rich gas rate, the blue shadow illustrates the AI-based model prediction for rich gas cumulative production, and the red shadow shows the actual cumulative rich gas.

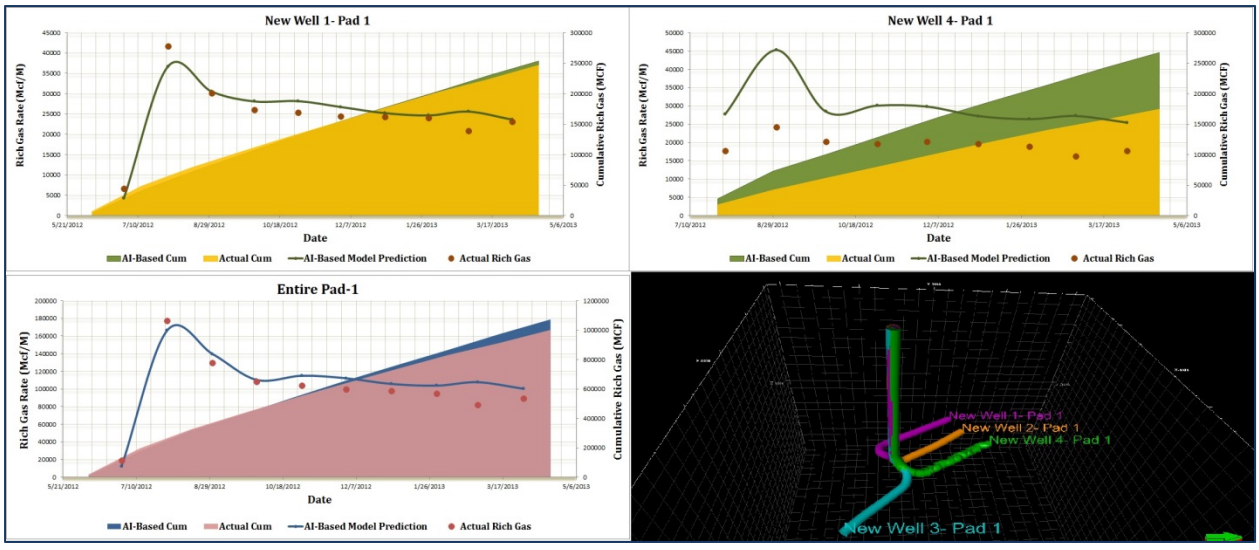

Figure 7.11: The AI-Based Model Prediction for New Pad 1- The well with minimum error (Top-Left), the well with maximum error (Top Right) and the entire pad (Bottom left)

In this pad the New Well#1 and New Well#4 has shown an error of 11 and 52 % respectively and the estimated error for the entire pad is about 13 %.

The stimulation and completion data shows that all the wells are completed with 13 hydraulic fracture stages by using almost the same amount of slurry and proppant while the production performance of New Well # 4 is less than the other three wells and because of this, the AI-based model is overestimating the production of this well.

New Pad 2- This pad includes 4 horizontal laterals and is located on the northern part of the reservoir where no pads were existed before. All the laterals came to the production by August 2012. Figure 7.12 shows the result of AI-based model prediction for two wells with minimum and maximum error as well as the entire pad result and well configuration.

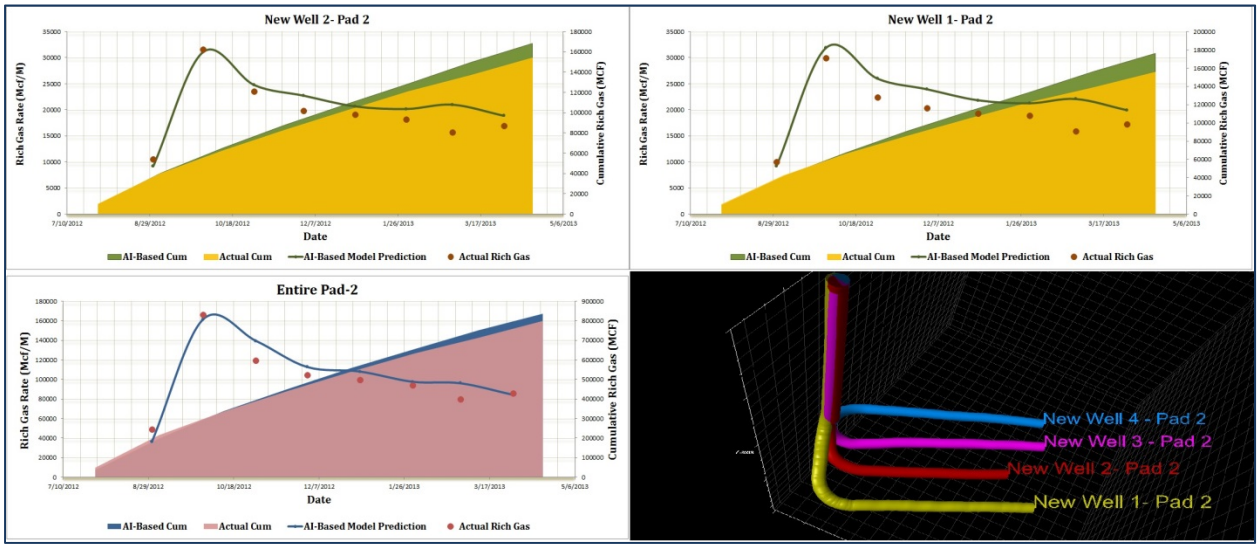

Figure 7.12: The AI-Based Model Prediction for New Pad 2- The well with minimum error (Top-Left), the well with maximum error (Top Right) and the entire pad (Bottom left)

As shown in this figure, the difference between the estimated minimum and maximum errors for two laterals are not significant (12% versus 16%) which indicates that all the wells in this pad are behaving similarly and this behavior was predicted by AI-based model with acceptable accuracy. The estimated error for the entire pad is also about 11%.

New Pad 3- Next to the ***New Pad 2*** in northern part of the reservoir, the ***New Pad 3*** with 4 horizontal laterals is located and it came to the production a month later than New Pad 2 (on September 2012). Figure 7.13 shows the AI-based model prediction for two wells with minimum and maximum errors, the entire pad production performance and the wells configuration. As it has shown in this figure, the New Well#2 with the estimated error of 5% is the best prediction result and the New Well#4 with the maximum error of 13% is the worst prediction result in this pad. In spite of same completion and stimulation information for all wells, there is some inconsistency between the predictions of AI-based model for different wells which might be due to the fact that the information of different offset well is fed to different wells in this pad. The calculated error for the entire pad is also around 10%.

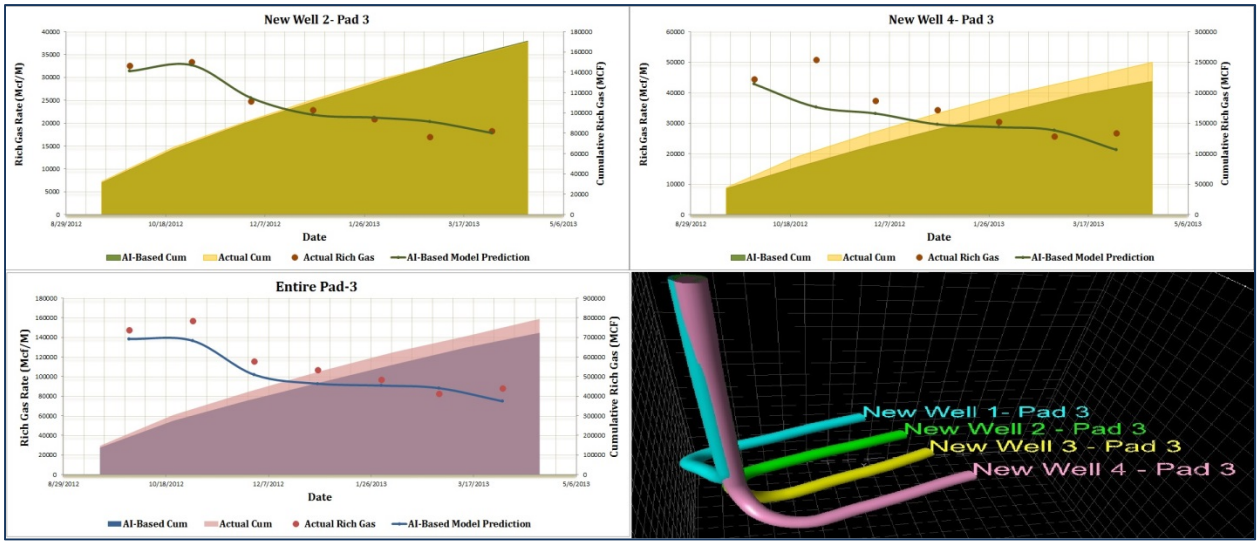

Figure 7.13: The AI-Based Model Prediction for New Pad 3- The well with minimum error (Top-Left), the well with maximum error (Top Right) and the entire pad (Bottom left)

New Pad 4- Unlike most new pads in the area of study, this pad is located in the center of the reservoir surrounded by too many existing pads. It has 5 horizontal laterals which all were completed with 9 to 11 hydraulic fracture stages and came to the production at the end of March or the beginning of April 2012. Figure 7.14 shows the predicted production performance by AI-based model for two laterals and the entire field as well as the well configuration in this pad.

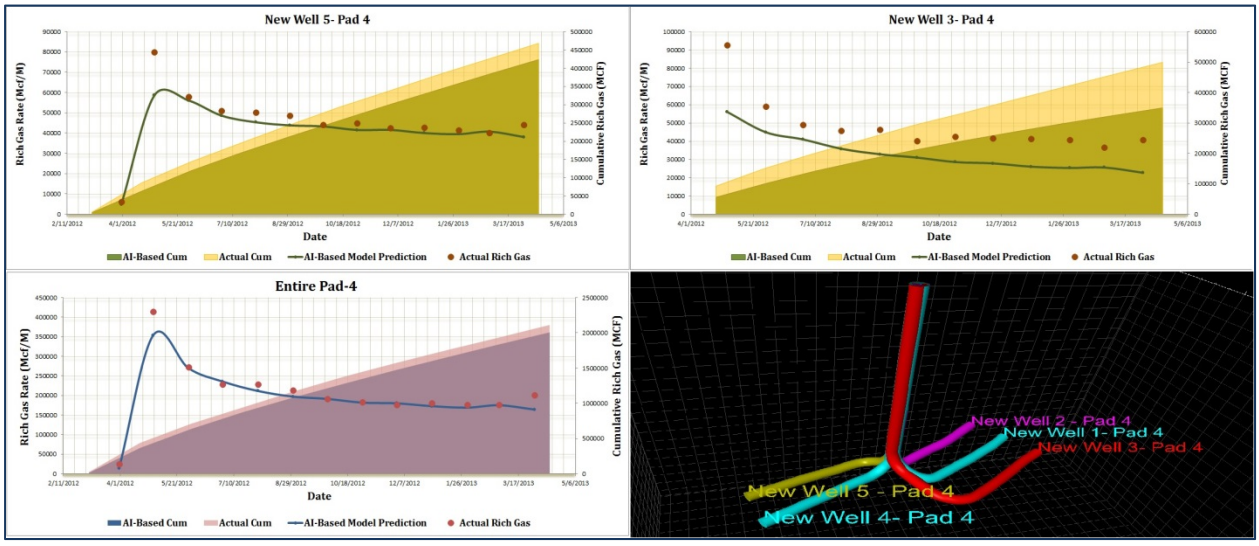

Figure 7.14: The AI-Based Model Prediction for New Pad 4- The well with minimum error (Top-Left), the well with maximum error (Top Right) and the entire pad (Bottom left)

The error for New Well#5 and New Well#3 is estimated to be around 9% and 31% respectively which are the minimum and maximum calculated errors in this pad. The calculated error for the entire pad is about 8%.

New well#3 has the maximum number of hydraulic fracture stages in this pad (11 stages) and it shows the better performance compared to the other wells. Therefore, the AI-based model underestimates the actual rich gas rate for this specific well.

New Pad 5- This pad includes 9 horizontal laterals and it is located in the south-west part of the reservoir. All these horizontal laterals simultaneously started to produce on June 2012. Figure 7.15 shows the actual production performance and AI-based model prediction for two wells and the entire field.

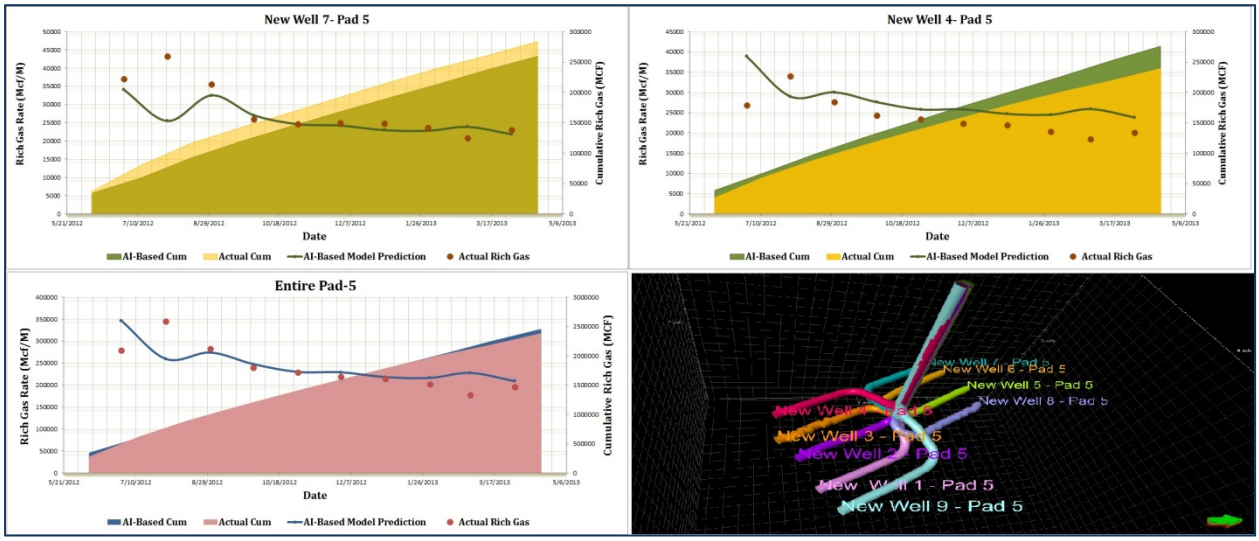

Figure 7.15: The AI-Based Model Prediction for New Pad 5- The well with minimum error (Top-Left), the well with maximum error (Top Right) and the entire pad (Bottom left)

The maximum prediction error for this pad is about 20% (New Well#4) and the minimum estimated error for the AI-based model prediction is 10% (New Well#7). The AI-based model predicted the production performance of the entire pad by the error of 10%.

For all of the wells the flow regime has changed from the second month of production and the AI-based model cannot capture this transition. Besides, the New Well # 4 has the least number of hydraulic fracture stages (8 stages). Because of this, this well's performance is not as good as the other wells in the pad, and the AI-based model overestimates its production.

New Pad 6- This pad is close to the new pad 5, located in the south-west part of the reservoir, surrounded by two other existing pads and includes 3 horizontal laterals. Figure 7.16 exemplifies the prediction of the AI-based model for the performance of two wells and the entire pad as well as the wells configuration.

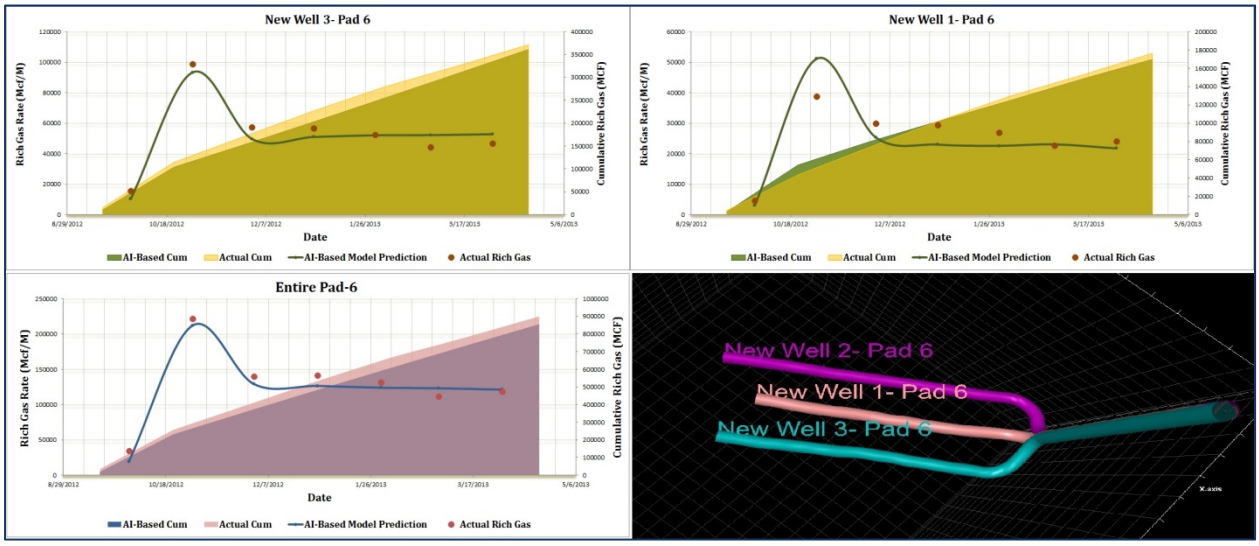

Figure 7.16: The AI-Based Model Prediction for New Pad 6- The well with minimum error (Top-Left), the well with maximum error (Top Right) and the entire pad (Bottom left)

The maximum and minimum error is estimated around 13% and 18% for New Well # 3 and New Well # 1 respectively. The estimated error for the entire pad is also around 12%. The wells in this pad were completed with a different number of stages, varying from 8 (New Well#1) to 21(New Well#2) and because of this, very different behavior is observed from these wells. For instance the monthly production of New Well#2 and New Well#3 is within the range of 50,000 MCF/Month while the average monthly production of New Well#1 is about 25,000 MCF/Month; this might lead the AI-based model to predict the performance of New Well#1 by higher error.

8. CHAPTER VIII

SENSITIVITY ANALYSIS, OPTIMIZATION AND TYPE CURVES

8.1 Sensitivity Analysis on the Impact of Different Parameters in Production from Shale

Understanding the performance of such ultra-low permeable media creates new challenges to scientists. Investigating the impact of rock properties and evaluating the effect of hydraulic fracturing processes on well performance are the primary issues that have been addressed in several studies.

Given the complex nature of hydraulic-fracture growth, the very low permeability of the matrix rock in many shale gas reservoirs, and the predominance of horizontal completions, reservoir simulation is commonly the preferred method to predict and evaluate well performance [Cipolla et al., 2010].Our limited understanding of the complex phenomena have further resulted in our limited ability to perform an accurate modeling of shale formations production which, consequently, has resulted in making significant assumptions to make our models work [Mohaghegh, 2013].

In anticipation of these major improvements in shale reservoir simulation, sensitivity analysis of production performance from shale formations based on pattern recognition technologies seems to be one of the most reasonable alternatives which are not based on any pre-determined assumptions.

The sensitivity section of this chapter consists of two main sections. The first section incorporates the sensitivity analysis based on the best history matched AI-based model by changing the different parameters involved in this model and evaluates the impact of each parameter. The second section includes the study of different parameters' impacts on the best 3 months and 24 months of production for all wells. The details of each approach will be explained in following sub-sections:

8.1.1 Sensitivity Analysis Based on the Best History Matched Model

In this section, the impact of different parameters is studied based on the best history matched AI-based model achieved in previous chapters. In order to perform such analysis, a reference model using the average value of involved properties (Table 6-1) in the best history matched AI-based model was prepared. The trained neural network was applied to achieve the production profile of each well as a reference for sensitivity analysis. Besides, this dataset, and alternatively the reference model, is a representative of the entire asset.

The range of parameters during the sensitivity analysis should be within the range of the minimum and maximum value of parameters that were used during neural network training in order to be able to do this analysis using ANN. In this study, the marginal change is obtained to be 30%; therefore, each parameter was increased by 30% to stay within the range of the neural network training boundary.

For each parameter, a separate dataset was prepared (when it was increased by 30%) and the trained neural network in best history matched AI-based model was applied on this while the other parameter in the dataset was kept constant as the values used in reference model. Table 8-1 lists the average value of each parameter that was used in order to create the reference model. The sensitivity analysis was performed based on different well types (Type 1, 2 and 3) and for each type, nine parameters were selected and the sensitivity of the trained neural network (best history matched AI-based model) was evaluated for the variation of each parameter.

Table 8-1: The average values of parameters that were used to build the reference model for sensitivity analysis

Parameter	Average Value	Parameter	Average Value
Measured Depth (ft.)	9500	Total Clusters	28
Inside Distance (ft.)	2110	Average Injection Rate (bbl/min)	75.4
Outside Distance (ft.)	4620	Average Injection Pressure (Psi)	6000
Porosity (%)	8.9	Breakdown Pressure (Psi)	6625
Net Thickness (ft.)	117	Total Proppant (lb)	4.3E6
Minimum Horizontal Stress (Psi/ft.)	0.7	Total Clean Volume (bbl)	1.2E5
		Days Between Completion to Production (days)	45

Figure 8.1and Figure 8.2 show the impact of increasing injected proppant and net thickness by 30% compared with the reference model for different well types. As illustrated in these figures, although, increasing the injected proppant and net thickness always improves the production performance; the degree of influence for different well types might be different. In both cases, the effect of these two parameters on type 1 is highest and is followed by type 2 and type 3 respectively.

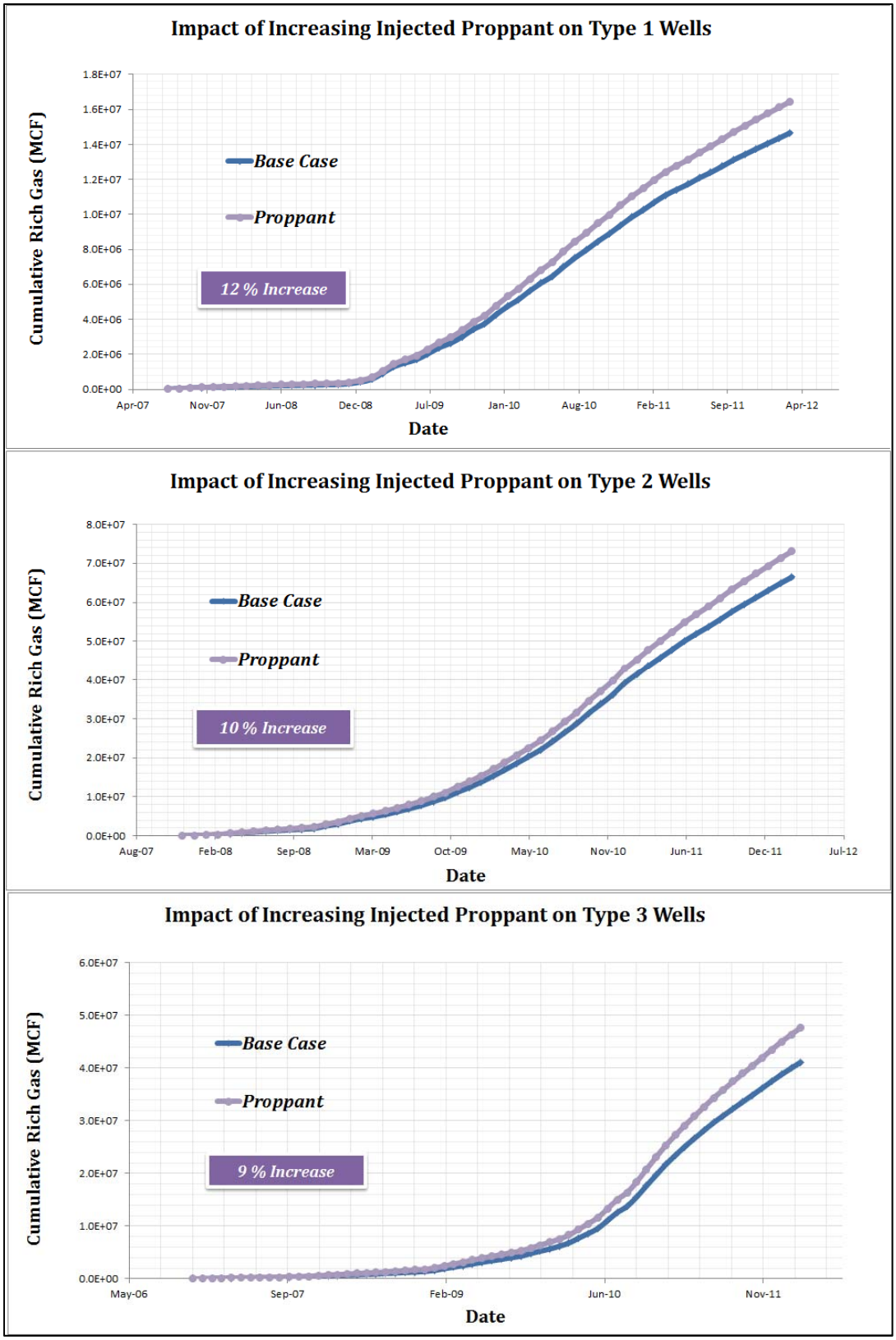

Figure 8.1: Impact of Increasing Injected Proppant on Different Type of the Wells

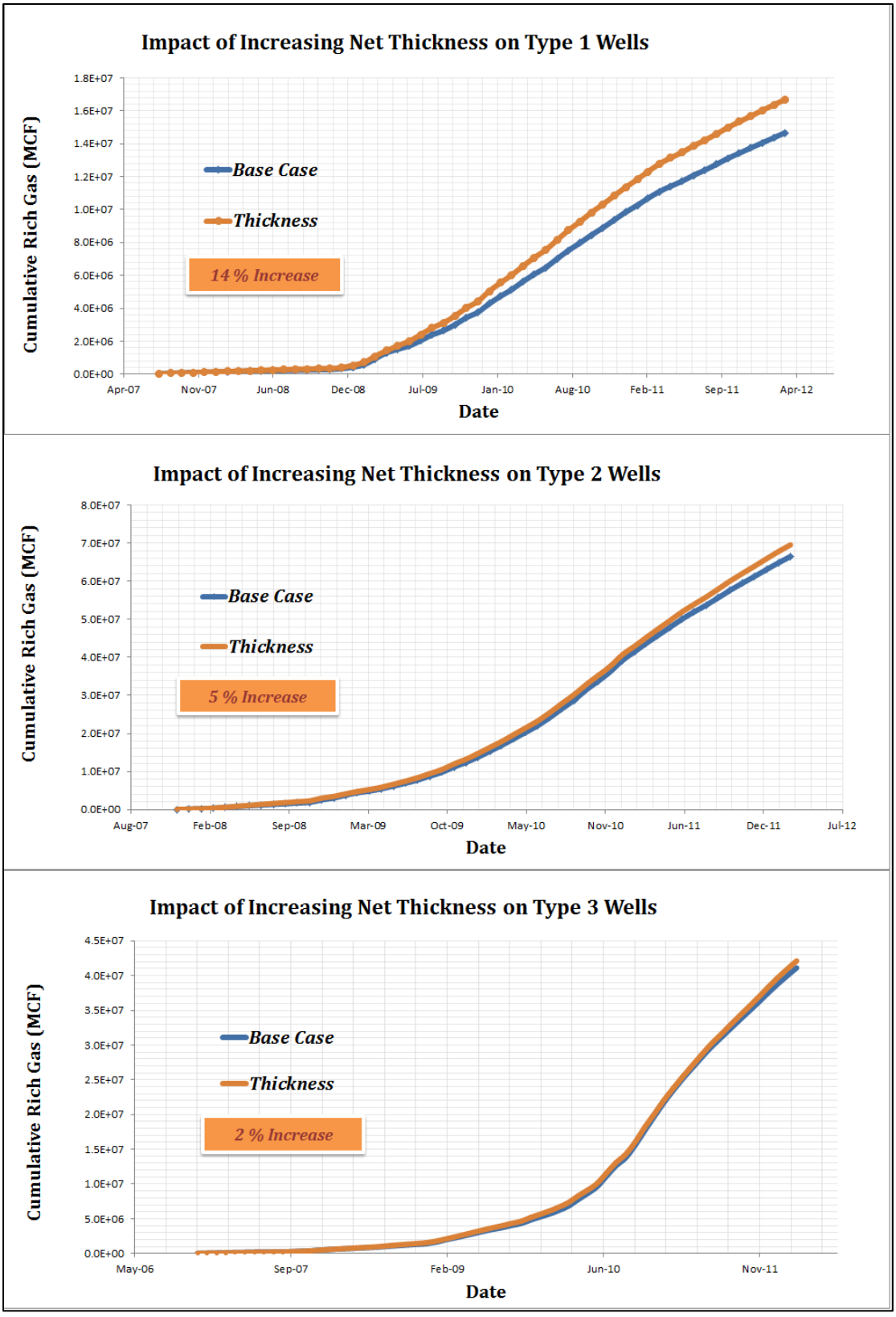

Figure 8.2: Impact of Increasing Net Thickness on Different Type of the Wells

On the other hand, because type 1 wells have either no or little interference with the other wells therefore, the effect of injected proppant is not shared with the other wells; and the higher production (achieved by increasing the amount of injected proppant mass) is expected. In the other words, during the drilling and completion of type 2 and type 3 wells, the area has already been stimulated in some degree by type 1 wells therefore; the effect of injected proppant on production performance of these two types is less than type 1 wells. Figure 8.1 clearly shows this behavior for all three well types.

For case of increasing thickness, the same analogy can be applied, the more thickness, the better performance for type 1 wells with less interference and vice versa.

A similar analysis has been performed for the rest of parameters and Figure 8.3, Figure 8.4 and Figure 8.5 shows the Pareto chart of different parameters for all well types. As it can be observed the ranking of parameters are changing from type to type as well as the degree of influence for different parameters.

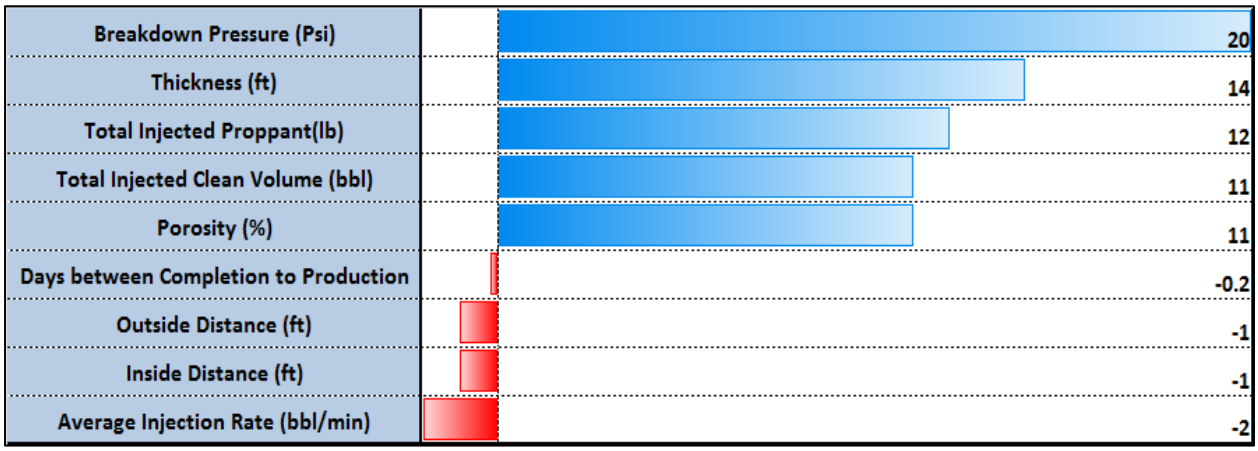

Figure 8.3: Pareto Chart for impact (in percent) of different parameters on production of type 1 wells

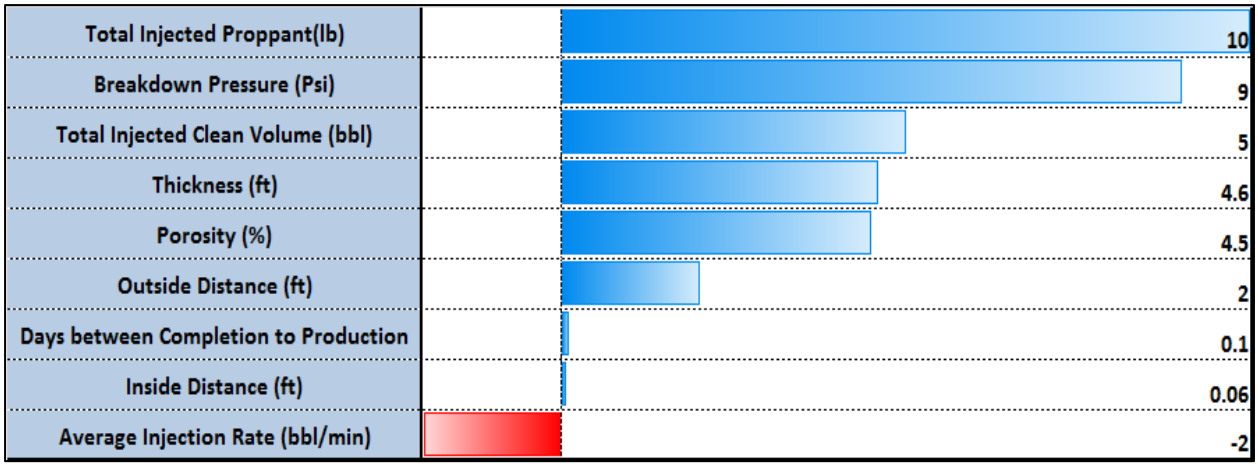

Figure 8.4: Pareto Chart for impact (in percent) of different parameters on production of type 2 wells

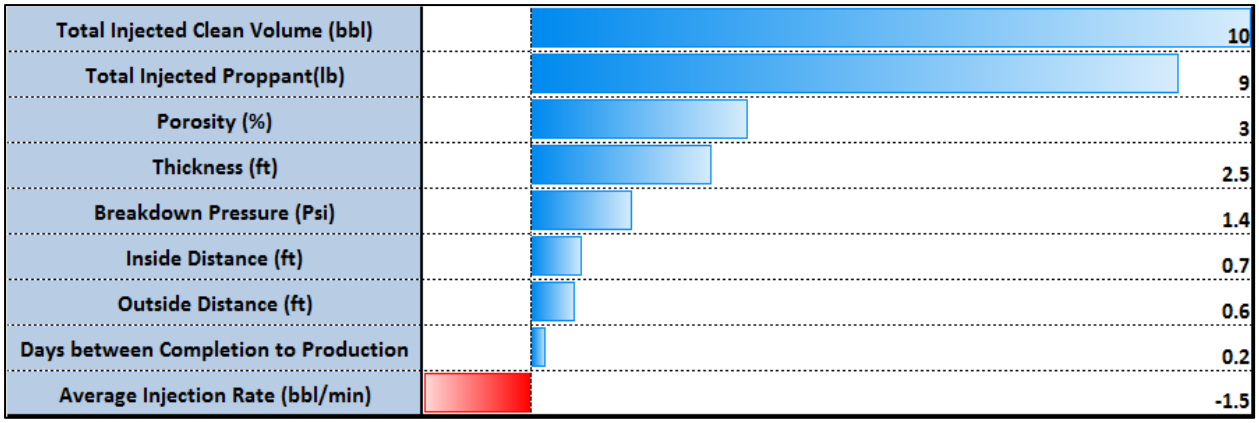

Figure 8.5: Pareto Chart for impact (in percent) of different parameters on production of type 3 wells

Breakdown Pressure- Breakdown pressure is an indication of rock brittleness. Higher breakdown pressure can be interpreted as more brittle rock which is more likely to be naturally fractured and responds favorably to hydraulic fracturing treatment. Thus, the production performance would be improved by the increase in breakdown pressure.

From Figure 8.3 to Figure 8.5 it can be observed that the degree of influence of higher breakdown pressure for type 1 wells is more than types 2 and 3. This might be due to the fact that during the completion and hydraulic fracturing of types 2 and 3 wells, the fracture network has already been developed because of the completion of offset wells (which is basically type 1) while for type 1 wells the fracture network is in its initial stage of development and therefore the impact of breakdown pressure is more apparent for type 1 wells. On the other hand if we look at the actual breakdown pressure in the database, the average value of this parameter for type 1 well is more than types 2 and 3. This means that during the neural network training the higher weight (related to breakdown pressure) was assigned to type 1 well and when the breakdown pressure is increased, its impact is more significant.

Total Injected Proppant- As it shown in Figure 8.3 to Figure 8.5, the production performance of the wells has a direct correlation with the amount of injected proppant. Regardless of its rank for each type, the degree of impact of injected proppant for type 1 wells is more than types 2 and 3 (12.2% versus 9.9% and 8.7%).

Total Injected Clean Volume- Similar to total injected proppant, it seems that better wells were treated with more clean volume than wells with lower quality as can be obviously observed from the aforementioned figures.

Matrix Porosity- Because of relatively high porosity and low TOC, the Marcellus Shale is a system dominated by matrix porosity and free gas and therefore porosity plays an important role in production. As clearly shown from Figure 8.3 to Figure 8.5, higher porosity results in better production performance in all types of wells, although the degree of response from different types of wells to increasing the porosity is variable. Type 1 wells are more affected by the porosity increase than type 2 and 3 wells.

Average Injection Rate- Figure 8.3 to Figure 8.5 show that the increasing average injection rate has a negative impact on all types of wells consistently. Increasing the injection rate while the injected volume is kept constant, yields a higher maximum fracture width (at wellbore) and fracture height but it also creates a shorter fracture. Usually it is recommended injecting the slurry with a lower rate which makes the longer fracture with more conductivity. Because of this effect, the higher injection rate is not in favor of production performance and has a negative impact. The degree of this impact in type 1 wells is more than types 2 and 3.

Inside/Outside Distance- By the given definitions in previous chapters, the inside distance is the distance between the laterals in a pad; the outside distance is the minimum distance between two laterals in different pads. Based on this definition the outside and inside distance is the same for type 1 wells in reference model and, as it can be seen from Figure 8.3, the degree of influence for these two parameters is the same and any increase in these two parameters has a negative impact on production performance.

For type 2 wells, more inside and outside distance favors production-the more distance, the better production. Figure 8.4 shows that the positive impact of increasing outside distance is more than the increasing inside distance (2 % versus 0.06%).

By contrast, Figure 8.5 shows that the degree of influence for inside distance is slightly greater than the outside distance for type 3 wells. Similar to type 2 wells, increasing both of these parameters has a positive impact on production.

Days between Completion and Production- Figure 8.3 to Figure 8.5 illustrates that the sensitivity of the AI-based model to this parameter is negligible, although it is changing for different well types. While the increase of this parameter has a negative impact on production performance of type 1 wells, it has revealed a positive influence on both types 2 and 3. The actual field data shows that for type 1 wells the lag between completion and production is much more than the other type of the wells. The majority of type 1 wells are those which came to production very early (in 2007 or 2008). Additionally,

having brought the well to the production with delay seems to have had a negative impact on their production (the neural network assigned a negative weight to this parameter for type 1 wells).

8.1.2 Sensitivity Analysis Based on the Best 3 and 24 Months of Production

Because of the effect of operational constraints in history matched AI-based model, the sensitivity of the model to some parameters may not be very clear or doesn't show any reasonable trend. Moreover some of these parameters were not involved in best history matched AI-based model. Therefore, operational constraints, including any unexpected shut downs, sudden changes in pressure, number of days of production and etc. were removed and the actual performance of the wells was taken into account by considering the best 3 months and 24 months of production. Two separate neural networks were developed in order to predict the best 3 months and 24 months cumulative rich gas production as a function of reservoir characteristics, well completion and stimulation design parameters. The sensitivity analysis was then performed using these two models to evaluate the impact of different parameters on the early and late time production from shale. It's worth mentioning that in order to conduct such analysis, a software application named IMprove^{TM} was used. Table 8-2 shows the list of parameters that have been used to develop these two models.

Table 8-2: Input Parameters used in the best 3 months and 24 months models

Group1- Well Information	Easting	***Group 4- Completion Data***	Stimulated Lateral Length(ft)
	Northing		Days Between Completion & Production
	Well Type		Total Clusters
	BTU Area		Cluster Spacing
	Minimum Distance to Offset Well (ft.)	***Group 5- Stimulation Data***	Avg. Injection Pressure(psi)
	Deviation Type (Down-Dip, Straight, Up-Dip)		Avg. Breakdown Pressure(psi)
Group 2- Reservoir Characteristics	Matrix Porosity		Avg. Injection Rate(bbl./min)
	Net Thickness (ft)		Avg. Max Rate
	Water Saturation (%)		Slurry Vol.(bbl.)
	TOC (%)		Proppant per Stage(lb.)
Group 3- Geomechanical Properties	Brittleness Index		Total Proppant Inj.(lb)
	Min Horizontal Stress		Slurry per Stage (bbl.)
			Duration of Flow Regime 1

The models were developed using 80% of the data while the remaining 20% was left for calibration and validation purposes and was not used during the model building (as blind data). Figure 8.6 and Figure 8.7 show the results of neural network prediction versus actual best 3 months and 24 months of production. The training dataset in the best 3 months model has an R-Square of 0.95 and the calibration and verification have an R-Square of 0.90 and 0.97 respectively. These parameters for the best 24 months of production are 0.94, 0.88, and 0.92 correspondingly.

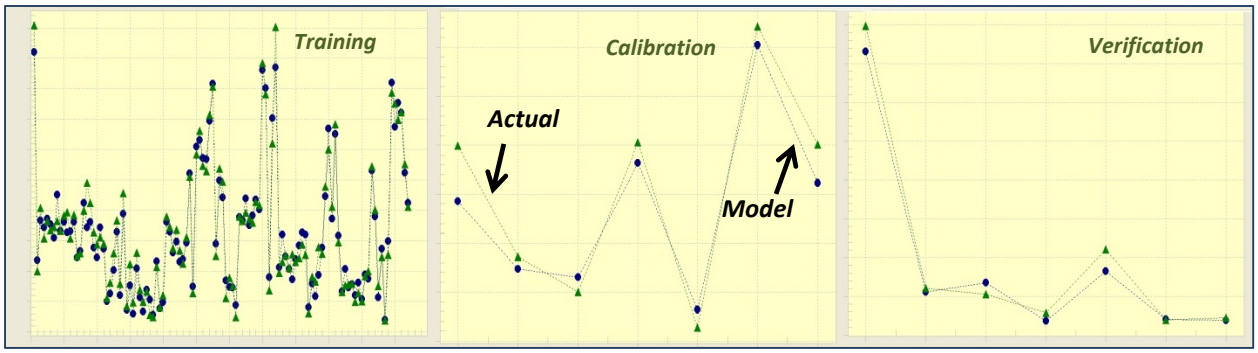

Figure 8.6: The Scatter plots of training. Calibration and verification for the best 3 months production model

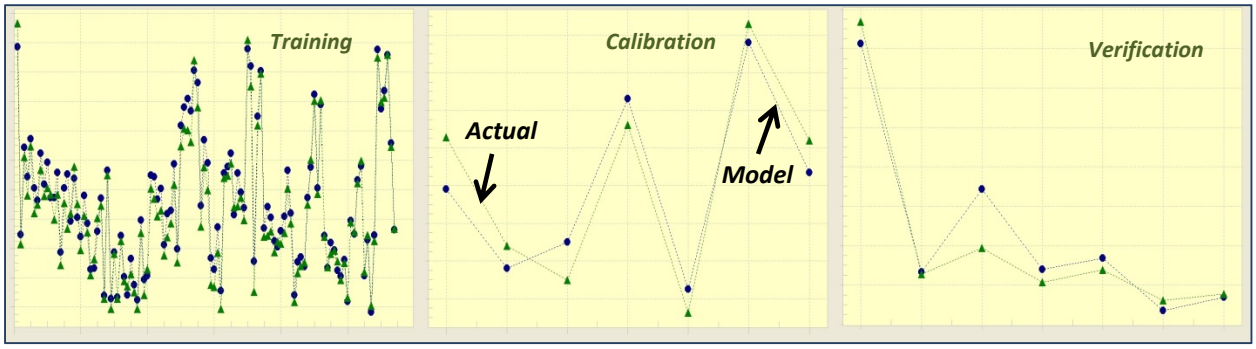

Figure 8.7: The Scatter plots of training. Calibration and verification for the best 24 months production model

Upon having the acceptable models, the sensitivity analyses can be performed on individual well which includes the analysis for each single parameter and multiple parameters. During the single parameter sensitivity analysis, parameters are selected one at a time to be studied, while all other parameters are kept constant at their original value. The value of the target parameter is varied throughout its range and the model output (the best 3 months and 24 months cumulative rich gas production) is calculated (using the trained neural network) and plotted for each variation. Figure 8.8 to Figure 8.10 show the single parameter sensitivity result for TOC, Brittleness Index, Stimulated Lateral Length and Cluster Spacing for three different types of wells (type 1, 2 and 3) resulting from both models (the best 3 months and 24 months cumulative rich gas production).

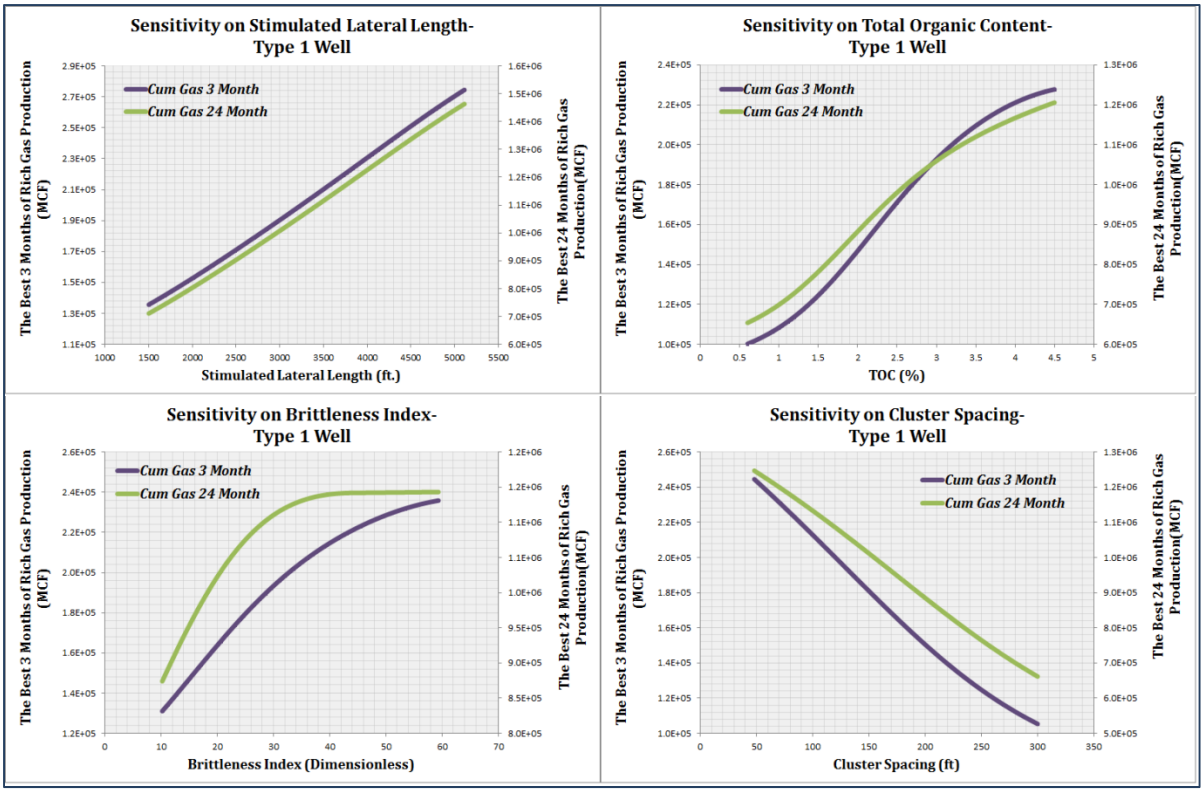

Figure 8.8: Sensitivity Result for different parameters based on the best 3 and 24 months of production for type 1 well

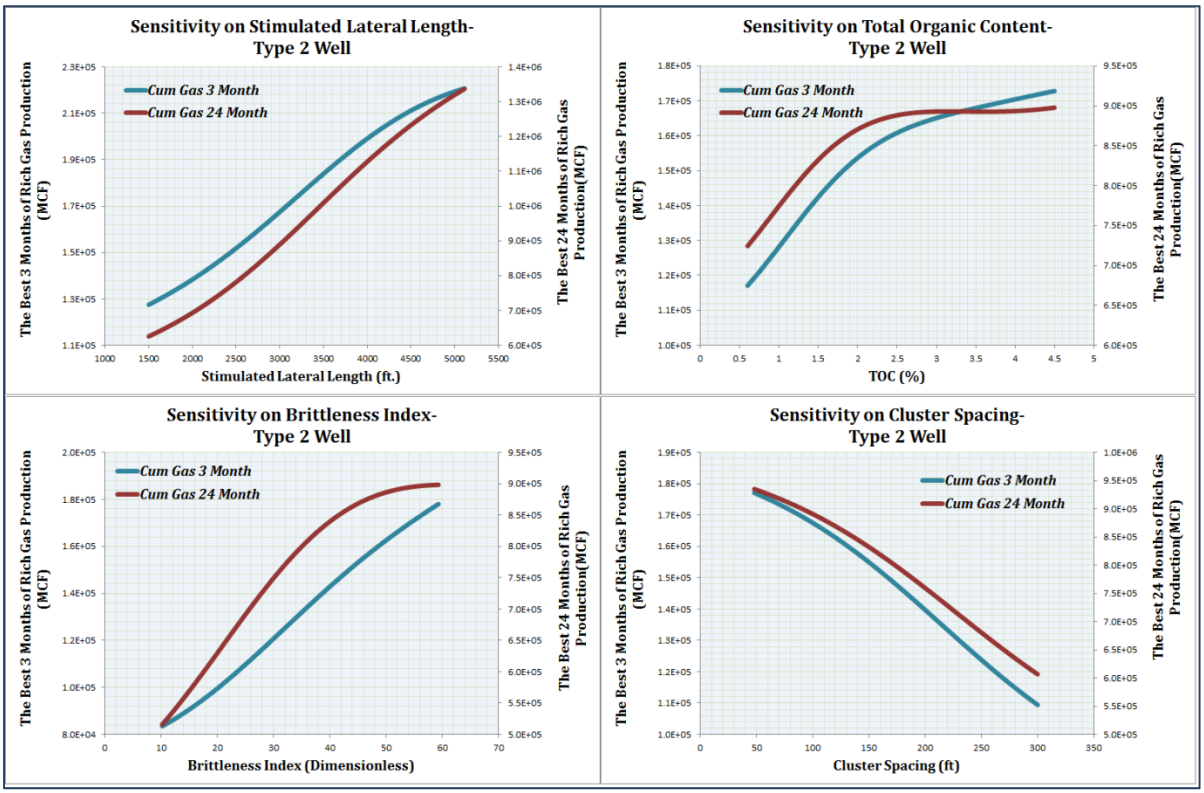

Figure 8.9: Sensitivity Result for different parameters based on the best 3 and 24 months of production for type 2 well

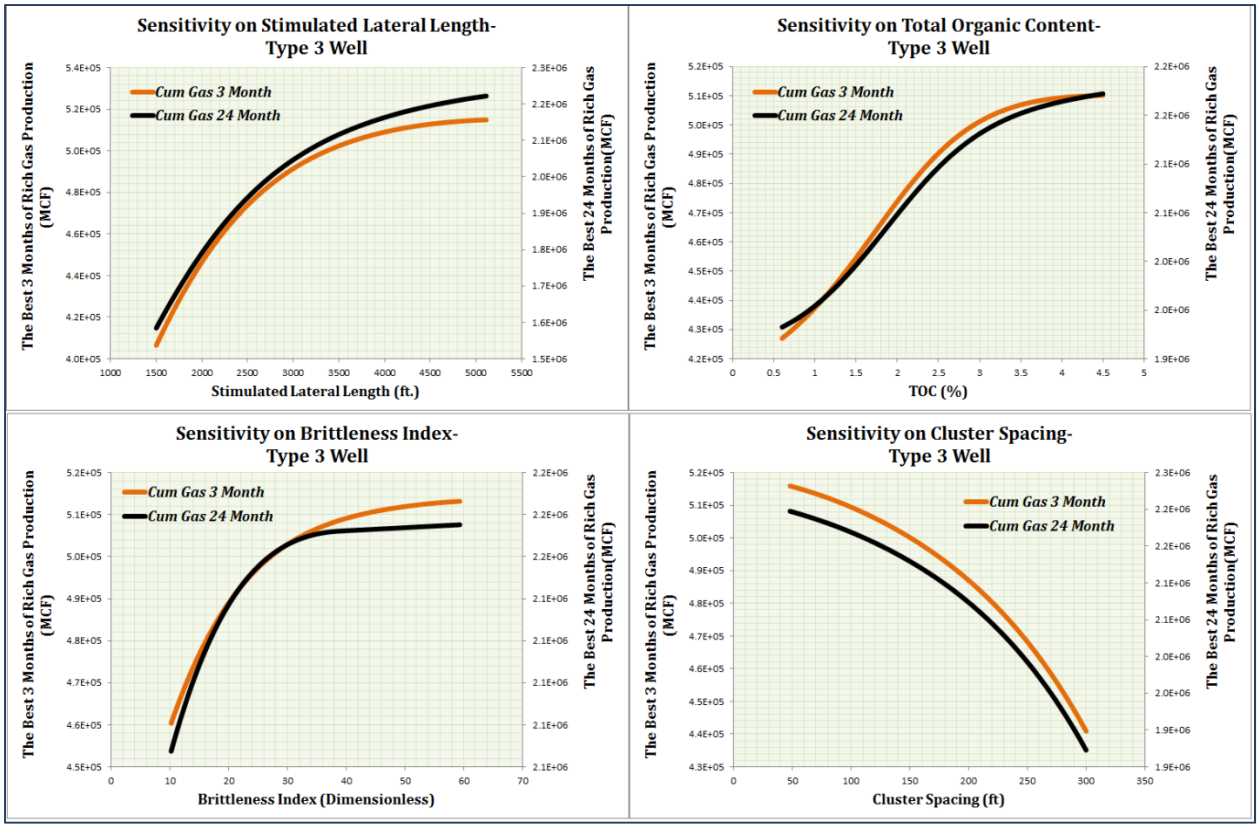

Figure 8.10: Sensitivity Result for different parameters based on the best 3 and 24 months of production for type 3 well

As explained earlier in this section, these parameters mostly didn't show such a clear trend by performing the sensitivity analysis using the best history match AI-based model while the above figures illustrate a very apparent behavior that can be achieved by doing sensitivity analysis based on the production indicators (best 3 months and best 24 months of production).

Regardless of each parameter's degree of influence, the impact of all shown parameters on production performance of different well types is qualitatively the same. In these examples, both early and late production performance of the wells increases as the stimulated lateral length increases. It is expected that similar behavior to be followed in the case of TOC and Brittleness Index and figures show this trend. For the case of cluster spacing, the example shows that for all types of the wells, by having farthest clusters, the production performance in the early time of production will be decreased as well as the performance in late time.

Just like the single parameter sensitivity analysis, combinational sensitivity analysis was performed on individual wells. If sensitivity analysis is investigated for two parameters simultaneously, the result is called a combinational sensitivity analysis and it can be displayed using a three dimensional plot as seen

in Figure 8.11 through Figure 8.13 where the best 3 months and 24 months of cumulative rich gas production were plotted against easting and net thickness.

Similar to single-parameter sensitivity analysis, during this process all the parameters except two target parameters are kept constant at their actual values. The value of these target parameters are changed throughout their ranges and the model output (the best 3 months and the best 24 months cumulative rich gas production) is estimated and plotted for each variation.

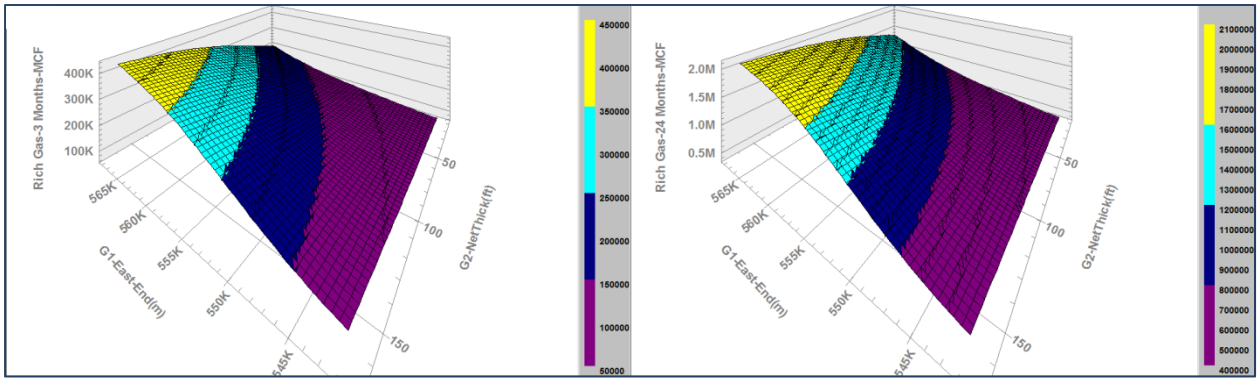

Figure 8.11: Combinational sensitivity analysis for the best 3 and 24 months models-Type 1 Well-Easting vs. Net Thickness

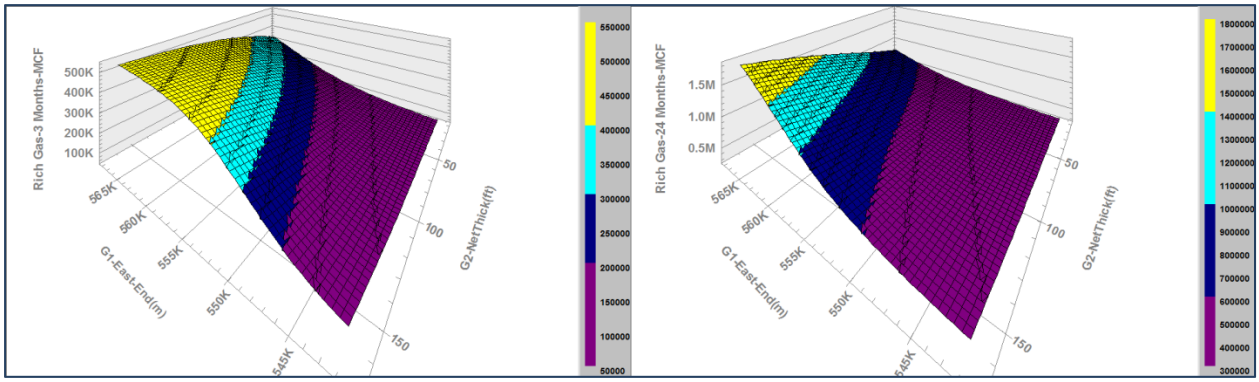

Figure 8.12: Combinational sensitivity analysis for the best 3 and 24 months models-Type 2 Well-Easting vs. Net Thickness

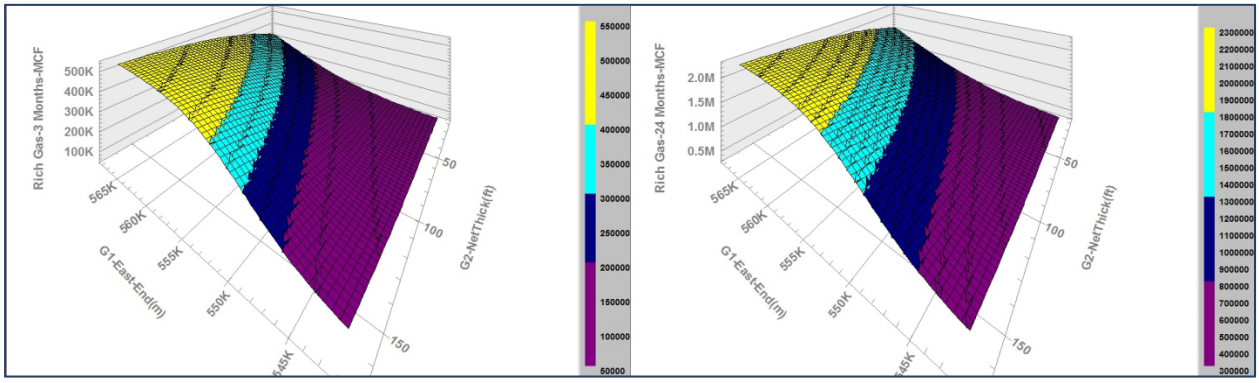

Figure 8.13: Combinational sensitivity analysis for the best 3 and 24 months models-Type 3 Well-Easting vs. Net Thickness

As illustrated in these figures in all types of the wells, by moving towards the east part of the reservoir, the net thickness is increased and alternatively the production performance of the wells improves in both early time and late time of well life.

It is worth noting that Figure 8.11 through Figure 8.13 represents the combinational sensitivity analysis results for the same wells as the single parameter sensitivity analyses were performed for.

8.2 Optimization Study

Given all the facts about the complexity of the shale reservoirs, the physics of production from these reservoirs are not fully understood. Therefore making decisions and reservoir management based on the available tools (such as analytical and numerical) could be challenging. Then data mining may be a good alternative which gives a hand to the engineers and operators to make better decision when it comes to the shale assets.

The main objective of this section is to provide insight into the operation practice of Marcellus Shale and to evaluate the role of each native and design parameters in production from shale. The outcome of this analysis is used to identify the optimum completion and stimulation design to achieve maximum productions which are the key factors in shale reservoir management.

In order to accomplish this task, three different approaches all based on the Pattern Recognition were used. When fuzzy set theory is used to determine the appropriate multidimensional space that would provide optimum separation of overlapping classes, the result is known as "Fuzzy Pattern Recognition". This analysis was also performed by using IMprove^{TM}.

When Fuzzy Pattern Recognition is applied to a limited number of well classes (Such as Poor, Average and Good wells) the process is called the "Step Analysis[2]" or "Well Quality Analysis (WQA)". When a similar analysis is performed while every single well in the dataset is treated as a potential unique well quality[3] the result is a continuous curve (rather than a discrete set of steps), called a "Fuzzy Trend Analysis (FTA)". Another application of Fuzzy Pattern Recognition is investigating the contribution (influence) of each of the parameters on any given production indicator which is known as "Key Performance Indicator". Such analyses were performed on several native and design parameters in different time intervals such as the best 3 months, 12 months, 24 months and 36 months. By definition,

[2] The name reflects the shape of the resulted graphs that are in the form of ascending or descending steps.
[3] Multiple wells with similar production indicator will be classified similarly.

the native parameters are those inherent reservoir characteristics and the design parameters refer to those manageable information that are usually measured during the operation such as injected fluid amount, injection pressure, rate etc.

The results of WQA and FTA will be shown together while the results of KPI analyses will be presented as a separate sub-section.

8.2.1 Well Quality Analysis and Fuzzy Trend Analysis

In all "Step Analysis" or "Well Quality Analyses", three different well qualities (Poor, Average and Good) were defined based on the production indicators which are the best 3 months of production, the best 12 months of production, the best 24 months of production and the best 36 months of production. Figure 8.14 to Figure 8.17 shows the fuzzy sets that were defined for each of the time intervals.

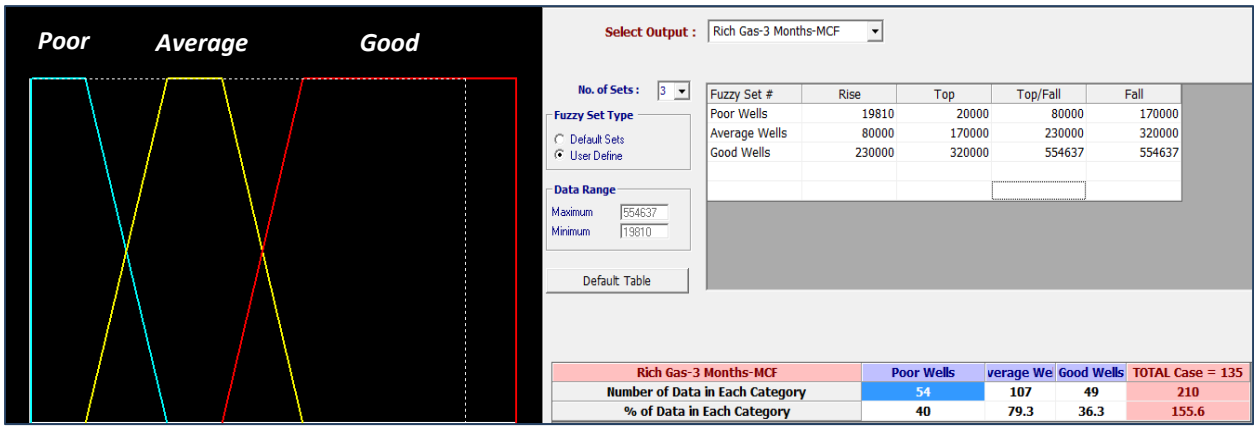

Figure 8.14: The fuzzy clusters plot and values for the best 3 months of production in WQA

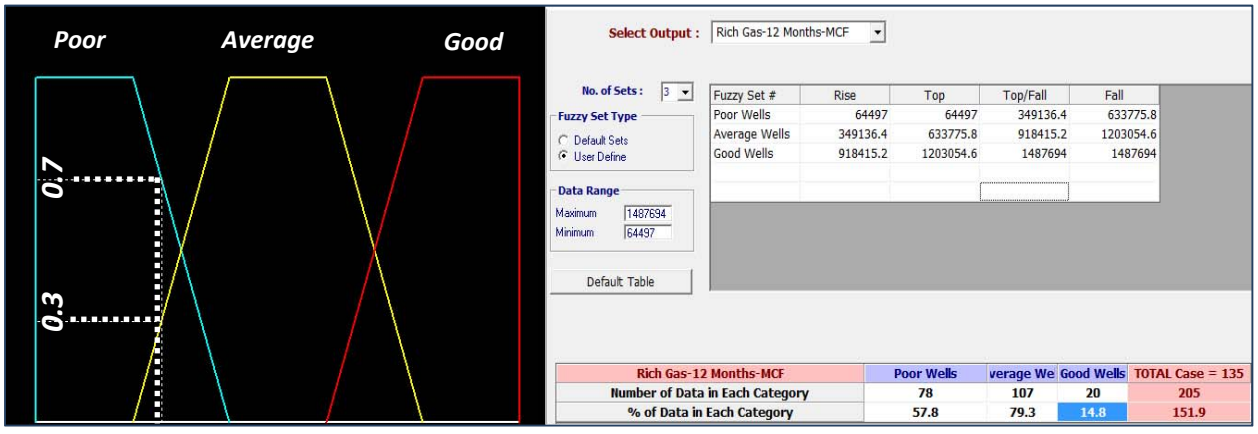

Figure 8.15: The fuzzy clusters plot and values for the best 12 months of production in WQA

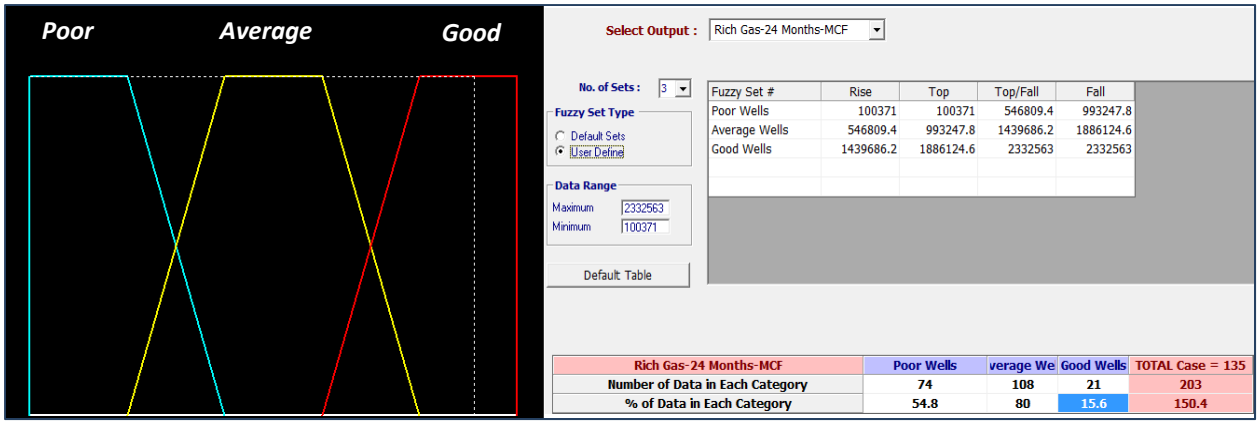

Figure 8.16: The fuzzy clusters plot and values for the best 24 months of production in WQA

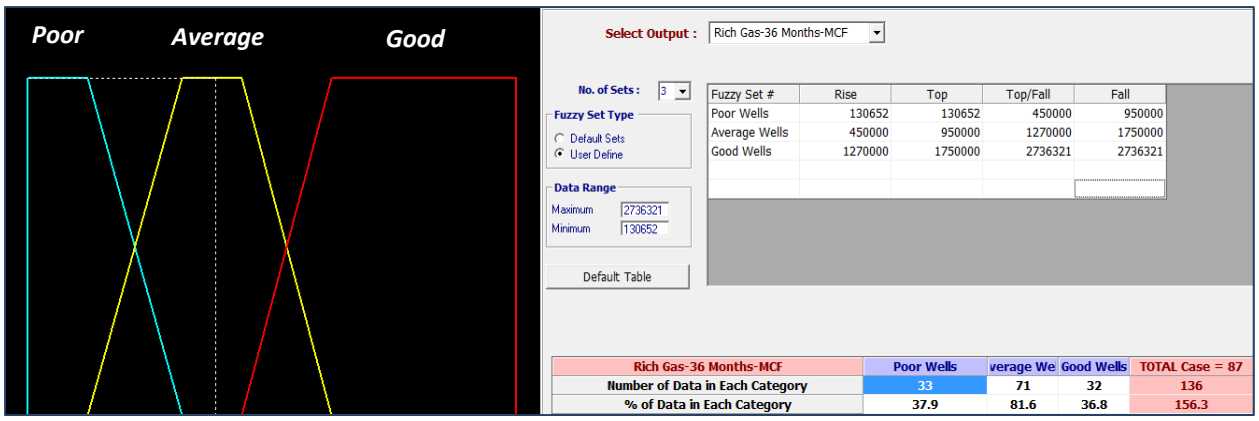

Figure 8.17: The fuzzy clusters plot and values for the best 36 months of production in WQA

A shown in these figures, there are several regions in which wells with different qualities overlap and because of this definition, some of the wells have membership in more than one class of wells. These class memberships are referred to fuzzy membership function and it is a very unique feature of this technology. For example in Figure 8.15, a well belongs to a fuzzy set of "Poor Wells" with a degree of membership equal to 0.7 and to fuzzy set of "Average Wells" with a degree of membership equal to 0.3.

In "Fuzzy Trend Analysis", on the other hand, the integrated fuzzy pattern recognition was used in order to deduce understandable trends from seemingly chaotic behavior. The result of such analysis is the continuous curves rather than a discrete set of steps.

As mentioned earlier, several native and design parameters were selected to be analyzed; Table 8-3 shows the list of these parameters. Both Well Quality Analysis and Fuzzy Trend Analysis were performed for the 4 different time intervals (3, 12, 24 and 36 Months). The detailed result for each individual parameter will be discussed as following:

Table 8-3: List of the Native and Design Parameters in FTA and WQA

Design Parameters	Native Parameters
Location Drilling	Matrix Porosity
Deviation Type	TOC
Minimum Distance to the Offset Well	Brittleness Index
Stimulated Lateral Length	Net Thickness
Total Number of Clusters	
Days between Completion & Production	
Amount of Proppant per Stage	
Cluster Spacing	

Location of Drilling- The production wells used in this study cover an area of around 190,000 acres and have been drilled very scattered, therefore it is very important to know which part of the reservoir is the better candidate for drilling. By looking at the production performance versus location of the wells (Easting) in this area (Figure 8.18 and Figure 8.19), it clearly shows a preferential trend towards gas production (in all time intervals) as we move to east.

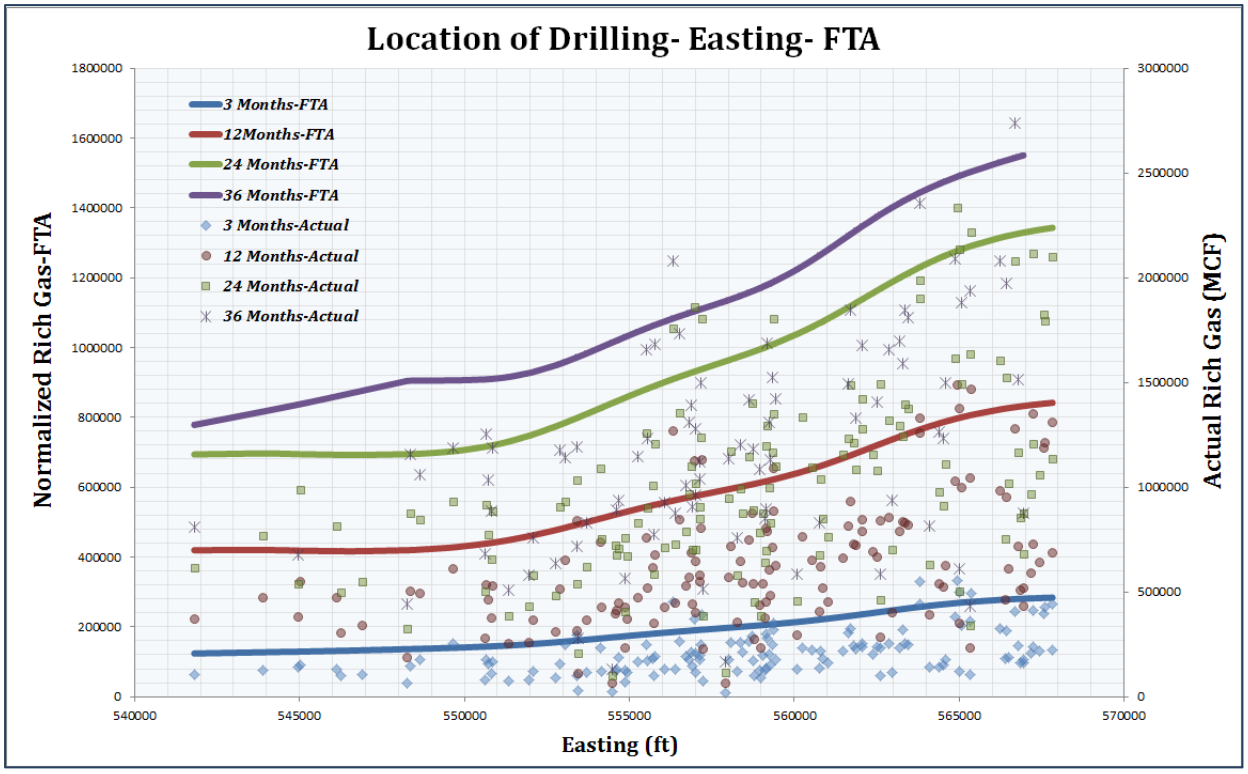

Figure 8.18: The Trend of Rich Gas Production in different time intervals versus location of the drilling- FTA Result

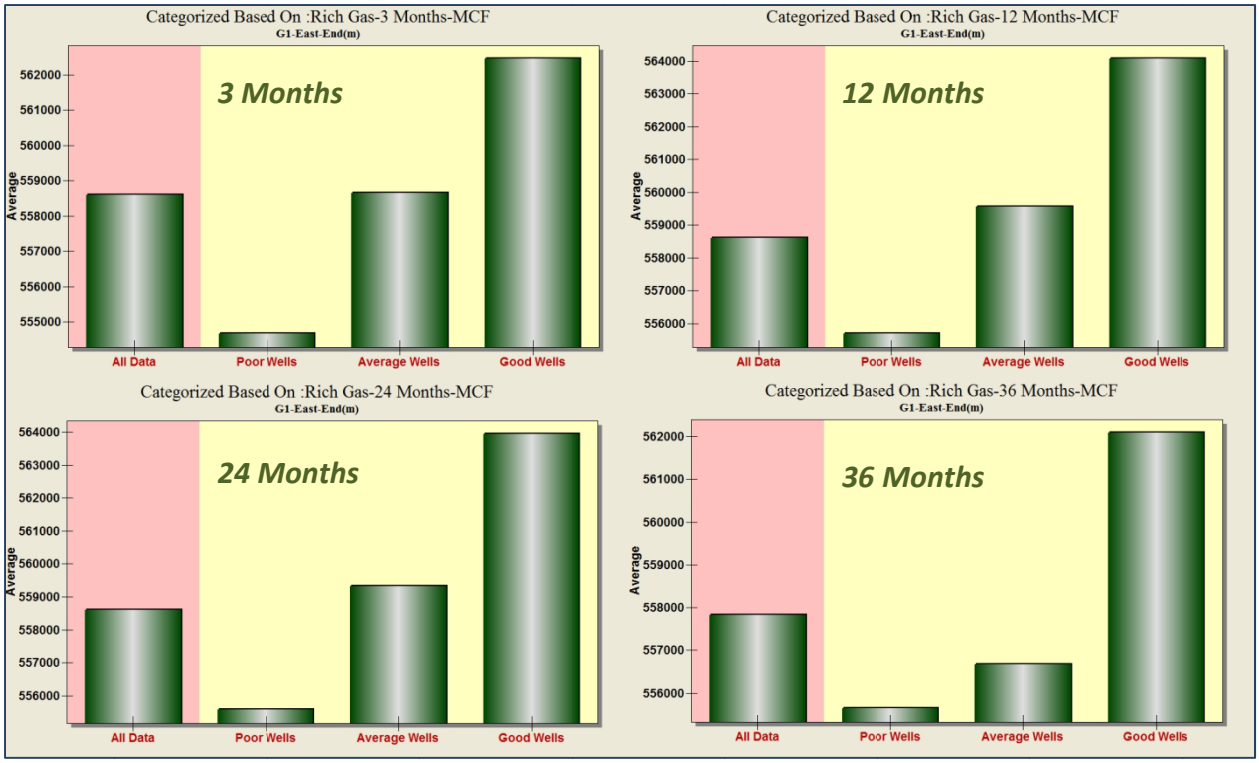

Figure 8.19: Well Quality Analysis for Easting- Different time intervals

Many factors might play role in observing such a trend for production behavior towards the east; for example, D.G.Hill (2004) in 2004 presented an isopach map for the Marcellus Shale (Figure 8.20) which shows that the reservoir becomes thicker to the east.

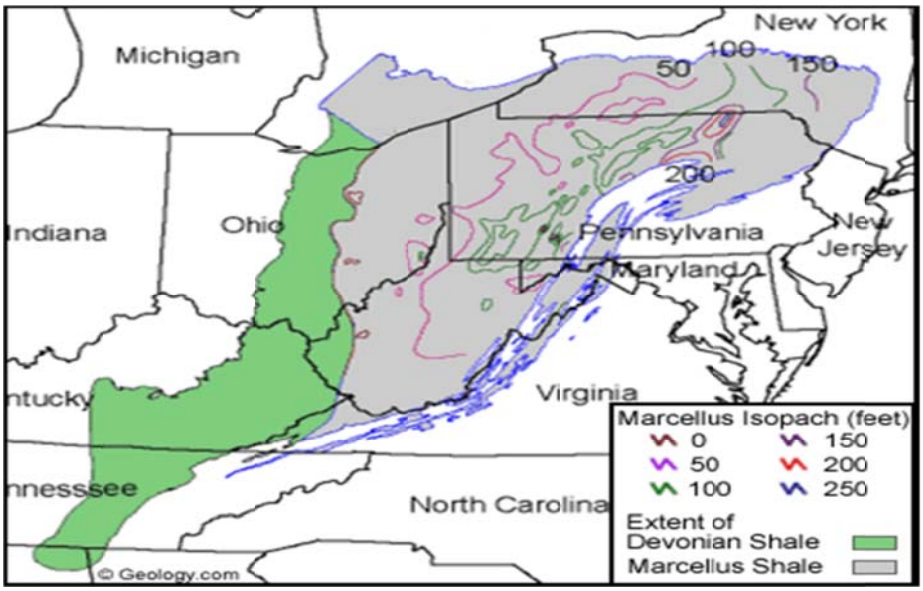

Figure 8.20: Isopach Map of Marcellus Shale- [Hill, 2004]

On the other hand, the limited available FMI logs for some vertical wells in this area show indications of open or partially open natural fractures in the center towards the east of the area (positive impact on well performance) while most of the natural fractures in the western part are healed fractures. Moreover some faults have been observed in the west part of the reservoir and seem to have a negative impact on production performance of the wells on that area.

Well Deviation Type- In this area of study, wells were drilled with different types of configuration and deviation. As discussed in chapter five, mainly three types of deviation, identified as Up-Dip, Down-Dip and No Dip can be observed.

The Well Quality Analysis (Figure 8.21) shows that in this part of Marcellus Shale, the well performance in both early and late time has been impacted by the well deviation favoring the Down-Dip wells. The Down-Dip wells are either completely or partially hydraulically fractured in Lower Marcellus which is more prolific in terms of reservoir characteristics and net thickness. Moreover those wells with downward deviation, which are hydraulically fractured in Upper and Lower Marcellus, show better performance because of more exposure to the entire pay zone.

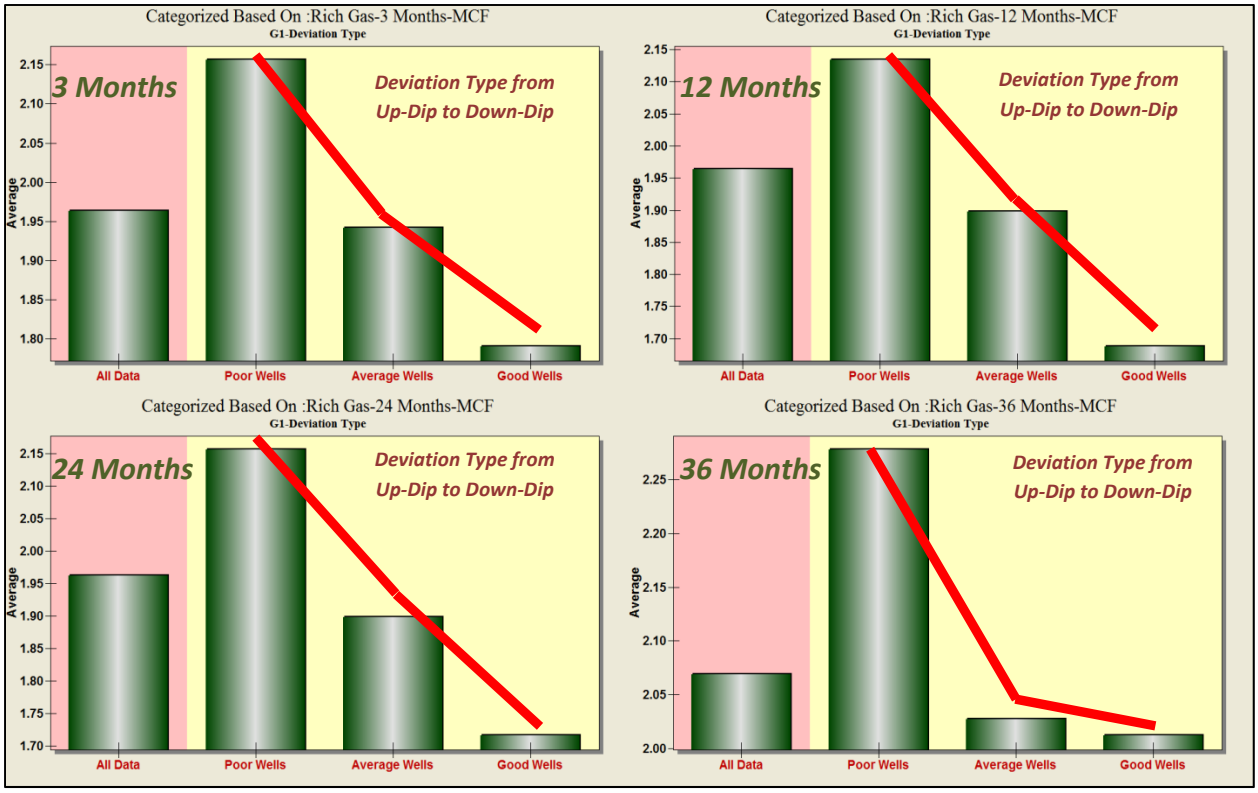

Figure 8.21: Well Quality Analysis for Deviation type- Different time intervals

Stimulated Lateral Length- Drilling the horizontal wells with a long lateral length became a successful strategy in production from shale and Marcellus Shale is not an exception. Figure 8.22 shows the trend of production behavior of the field in different time intervals as a function of stimulated lateral length.

This figure shows that the impact of stimulated lateral length at an early time (3 Months) of production is not as much as its impact at late time of production. Nevertheless the existence of an increasing trend in production performance by increasing the stimulated lateral length is quite clear from this figure.

Another important feature of this figure is that the impact of stimulated lateral length on production performance in all time intervals when it goes beyond 4000 feet is insignificant, although this might be due to the fact that the number of control point (the number of wells with more than 4000 feet stimulated lateral length) is limited in the database.

Figure 8.23 also presents that those wells with longer stimulated laterals show the better performance in either early or late times of production.

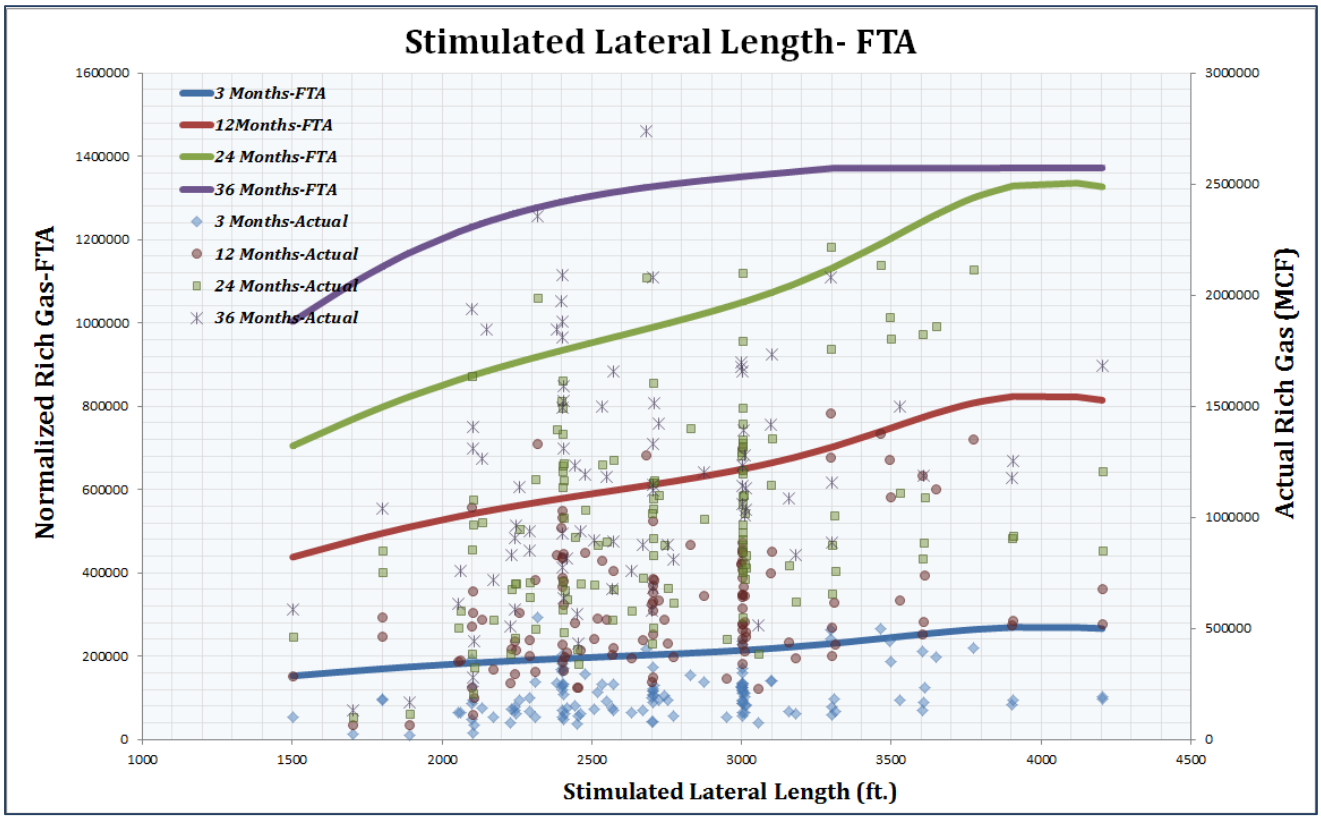

Figure 8.22: The Trend of Rich Gas Production in different time intervals versus Stimulated Lateral Length- FTA Result

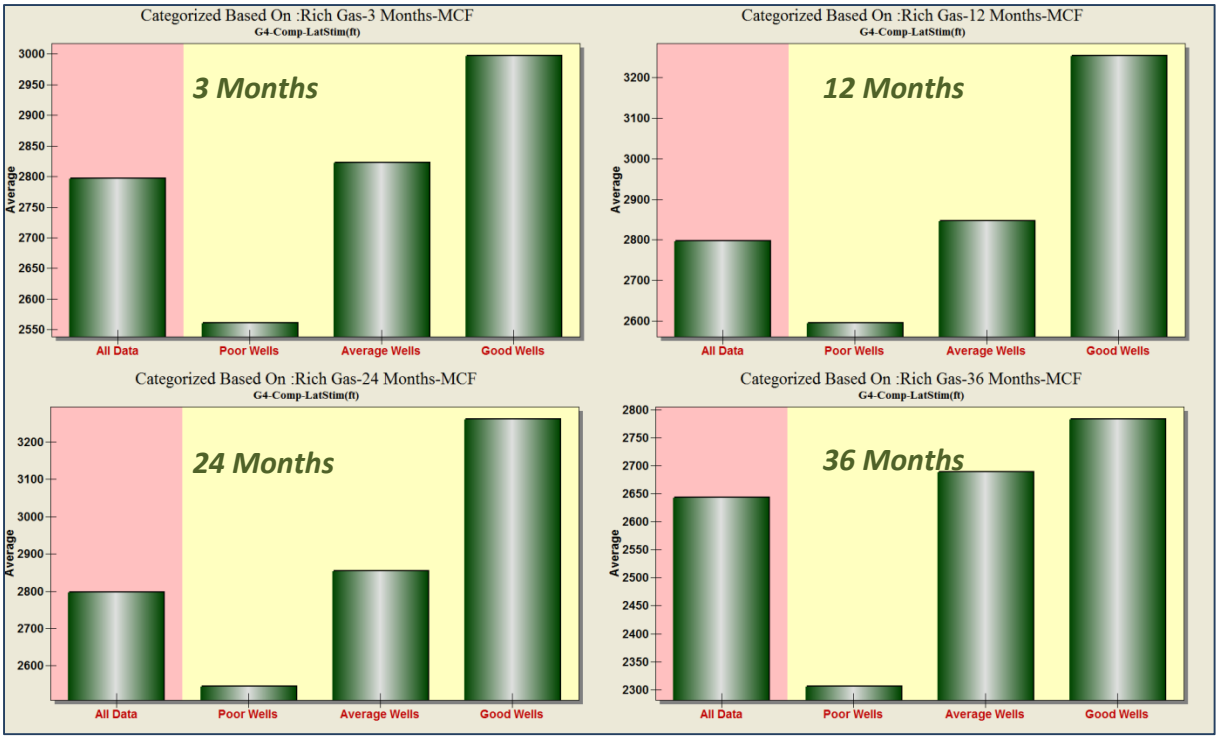

Figure 8.23: Well Quality Analysis for Stimulated Lateral Length- Different time intervals

Total Number of Clusters- the common practice in developing the Marcellus Shale is hydraulic fracturing the wells with multi stages multi clusters. The number of clusters in this dataset changes widely, some wells have experienced up to 45 clusters while other wells possess a number of clusters as low as 8.

Figure 8.24 shows the increasing trend of production (for all time intervals) as a function of total number of clusters. This behavior is also observed in Figure 8.25 in which the wells were categorized into fuzzy clusters.

Although the increasing trend of production performance is clearly observed in Figure 8.24, it also shows that as times goes on; the impact of the number of clusters in wells becomes more important. The FTA curves in this figure show a non-linearly increasing pattern in the production performance with the total number of clusters that start with the sharp slope and decreases in steepness as the number of total clusters increases beyond 24.

Minimum Distance to the Offset Well- Most of the laterals in the Marcellus Shale are spaced from 1000 ft. to 2000 ft. apart even though some operators experimented drilling with decreasing spacing.

Figure 8.26 shows the Fuzzy Trend Analysis result for the effect of minimum distance to the offset well on production behavior of the wells in different time intervals.

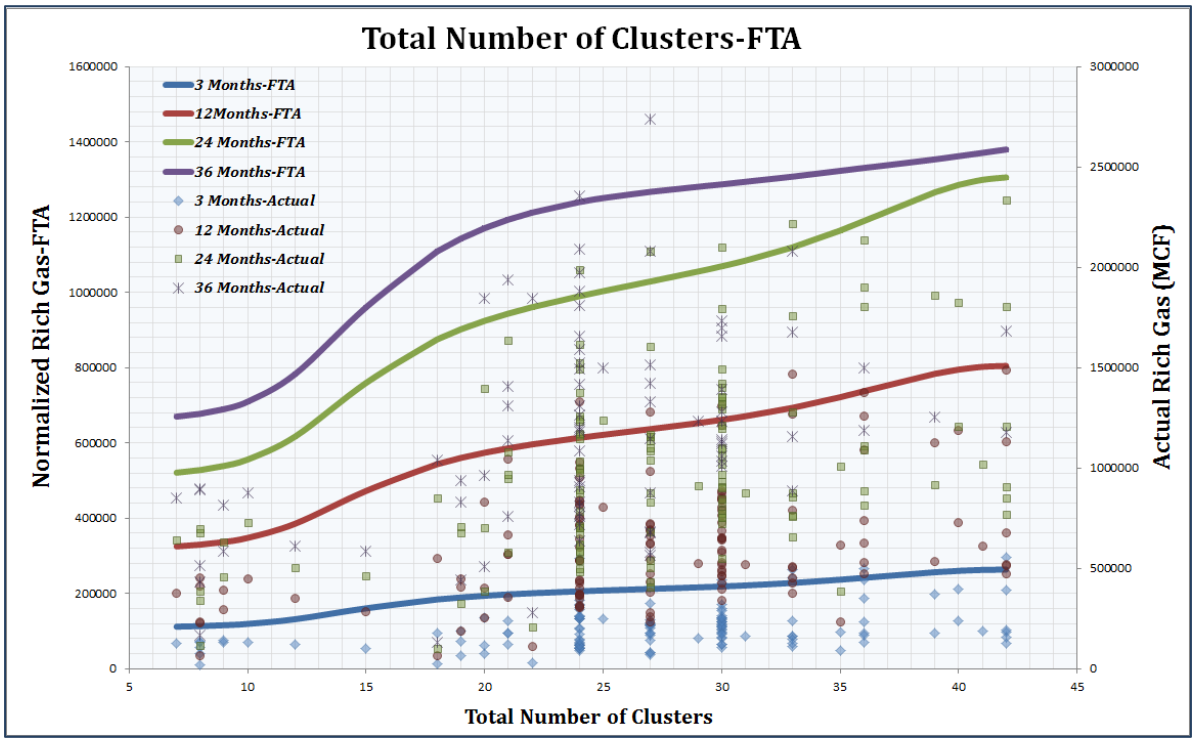

Figure 8.24: The Trend of Rich Gas Production in different time intervals versus total number of clusters- FTA Result

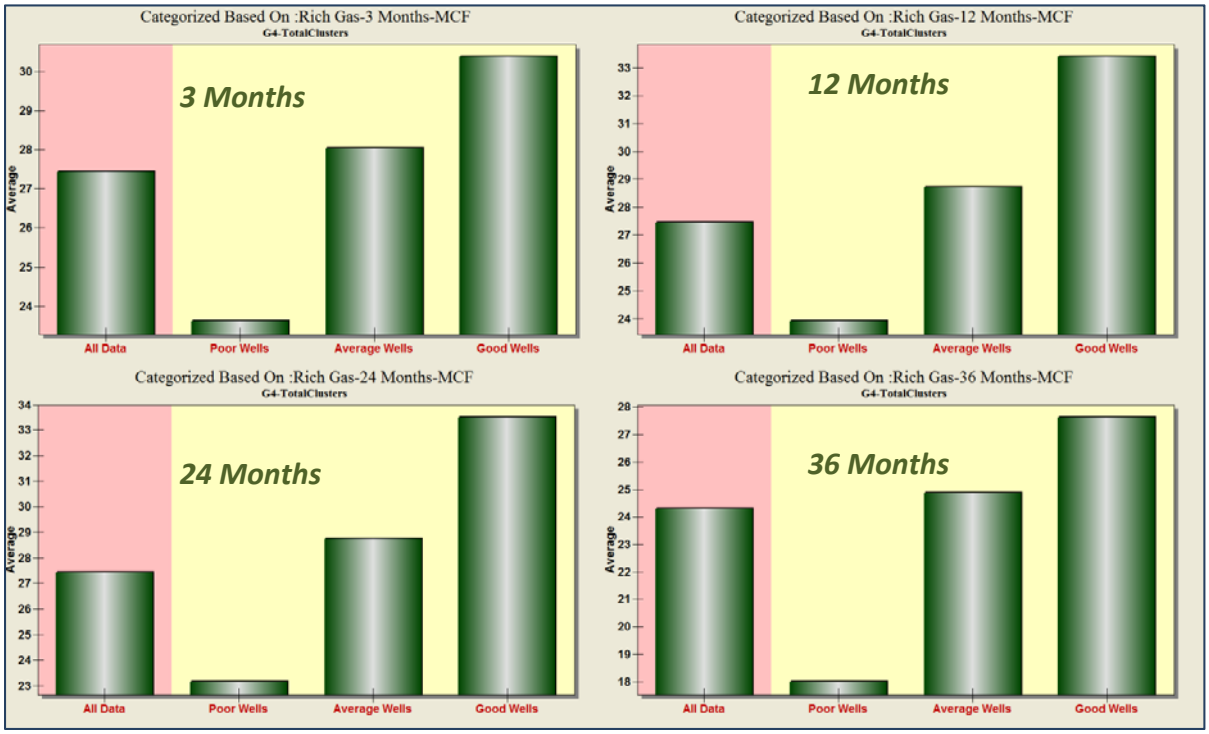

Figure 8.25: Well Quality Analysis for total number of clusters- Different time intervals

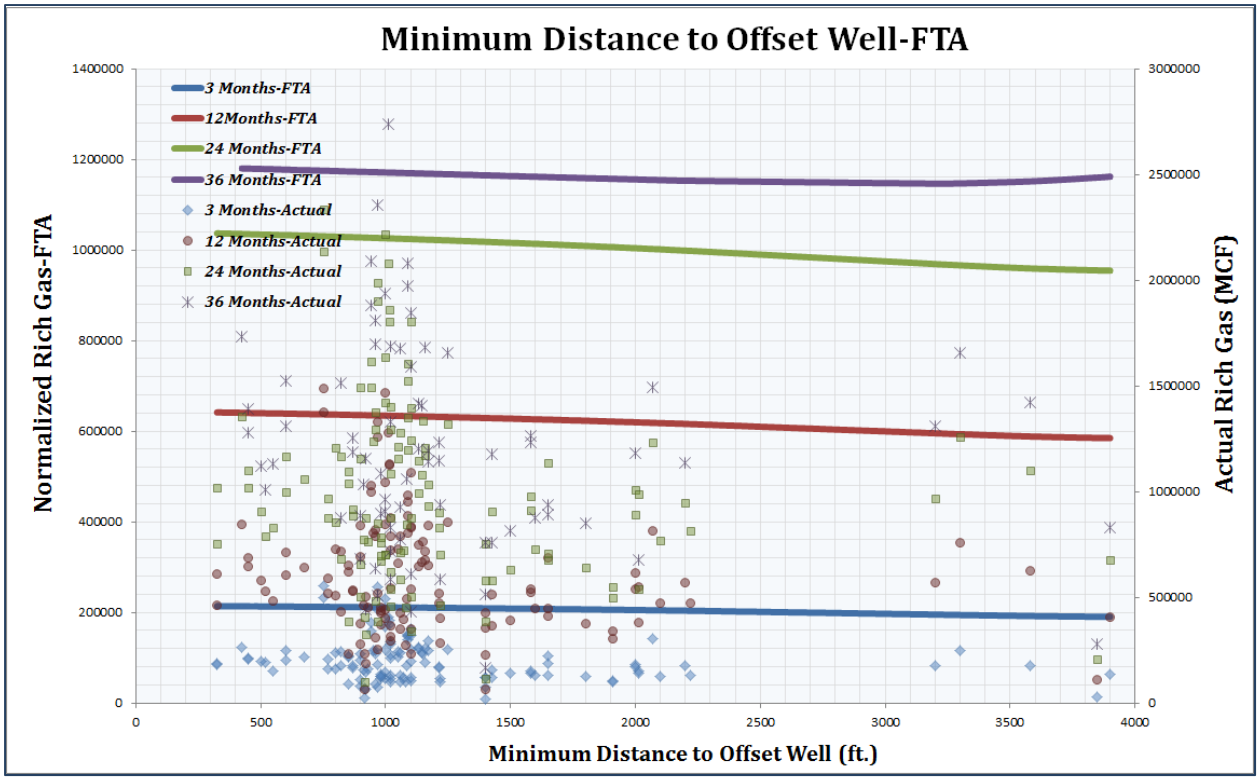

Figure 8.26: The Trend of Rich Gas Production in different time intervals versus minimum distance to the offset well- FTA Result

As illustrated in this figure, the production performance of the wells slightly decreases by increasing the minimum distance between the laterals. This descending trend is more obvious for the time interval up to two years of production where the closer distance between the laterals (it might be translated to more so-called stimulated reservoir volume because of more interaction between the hydraulic fractures and existing natural fractures) causes the higher productivity.

For the longer production indicator (36 months of production) the impact of minimum distance between the laterals becomes insignificant where the wells start to produce from the absorbed gas in matrix.

Figure 8.27 also represents the result of Well Quality Analysis for the behavior of production in different time intervals versus minimum distance between the laterals. As expected the production performance of the wells decreases as the minimum distance between the laterals increases. This trend cannot obviously be observed in the time intervals of 3 months and 12 months.

It should be noted that increasing the inside distances between laterals does not necessarily increase the well performance as the well produces more, therefore there should be an optimum distance to (1) establish enough connectivity to the matrix and (2) avoid well interference. The WQA in Figure 8.27

justifies this statement and shows that for the wells in this study, the minimum distance of around 2000 feet might be an optimum distance between the laterals.

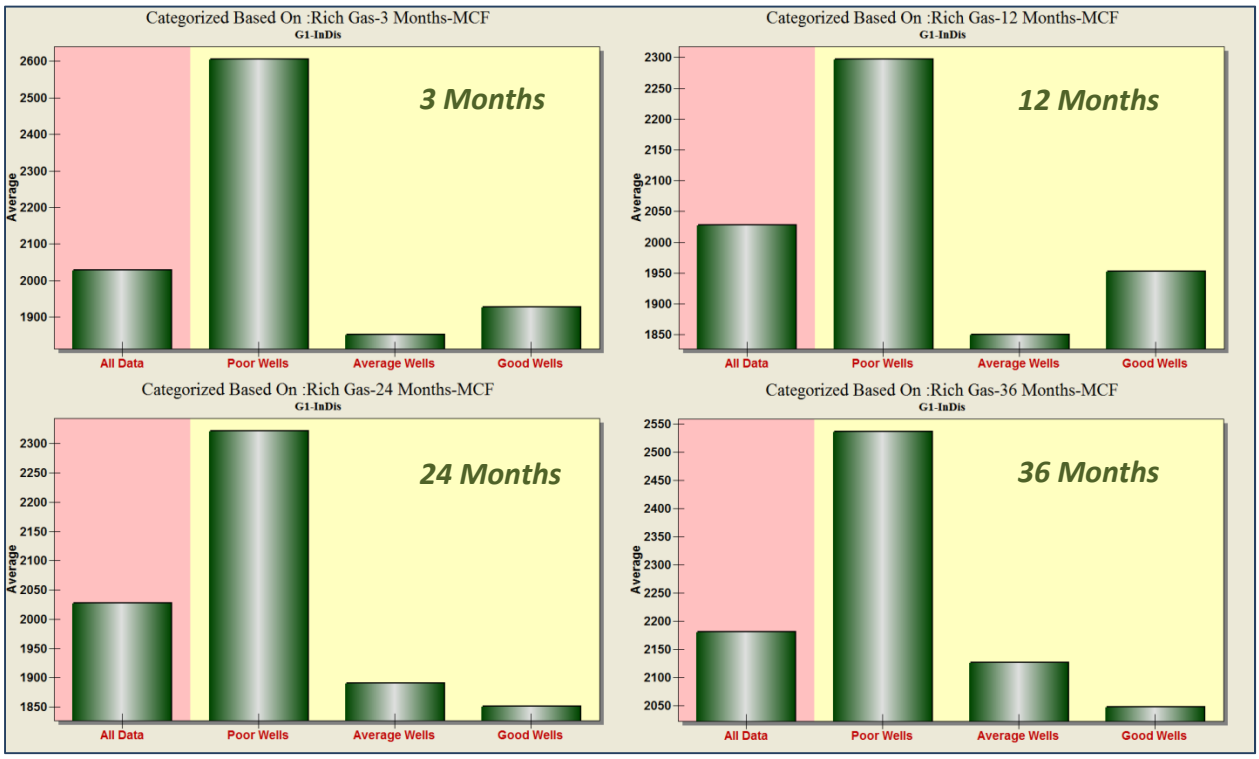

Figure 8.27: Well Quality Analysis for Minimum distance to the offset wells- Different time intervals

Injected Proppant per Stage- The unique characteristics of shale (ultra-low permeability) have led to the evolution of hydraulic fracture stimulation involving high rates, low viscosities, and large volumes of proppant. As illustrated in Figure 8.28 and Figure 8.29 the production performance of the wells has a direct correlation with the amount of proppant pumped in each stage. These figures show that better wells were treated with more proppant than wells with lower quality.

Days between Completion and Production- As explained in chapter six, the damages caused by injected water can be different in cases of having delay in bringing the well to production because in this case the injected water may reduce the formation permeability in the invaded zone because of clay swelling, scaling and fines migration [Holditch, 1979]. This process along with relative permeability and capillary pressure changes can potentially cause severely adverse impacts on long-term production. Figure 8.30, shows the production performance of the well in different time intervals as a function of days between completion and production.

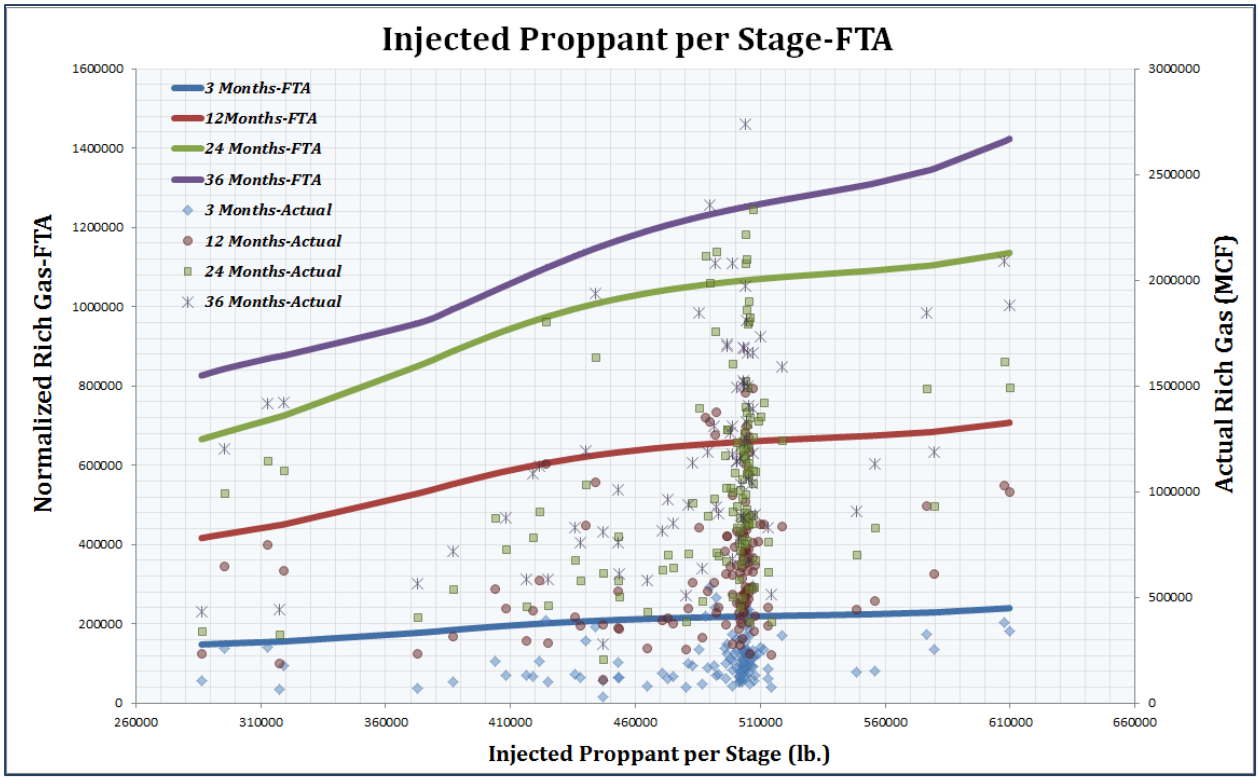

Figure 8.28: The Trend of Rich Gas Production in different time intervals versus injected proppant per stage- FTA Result

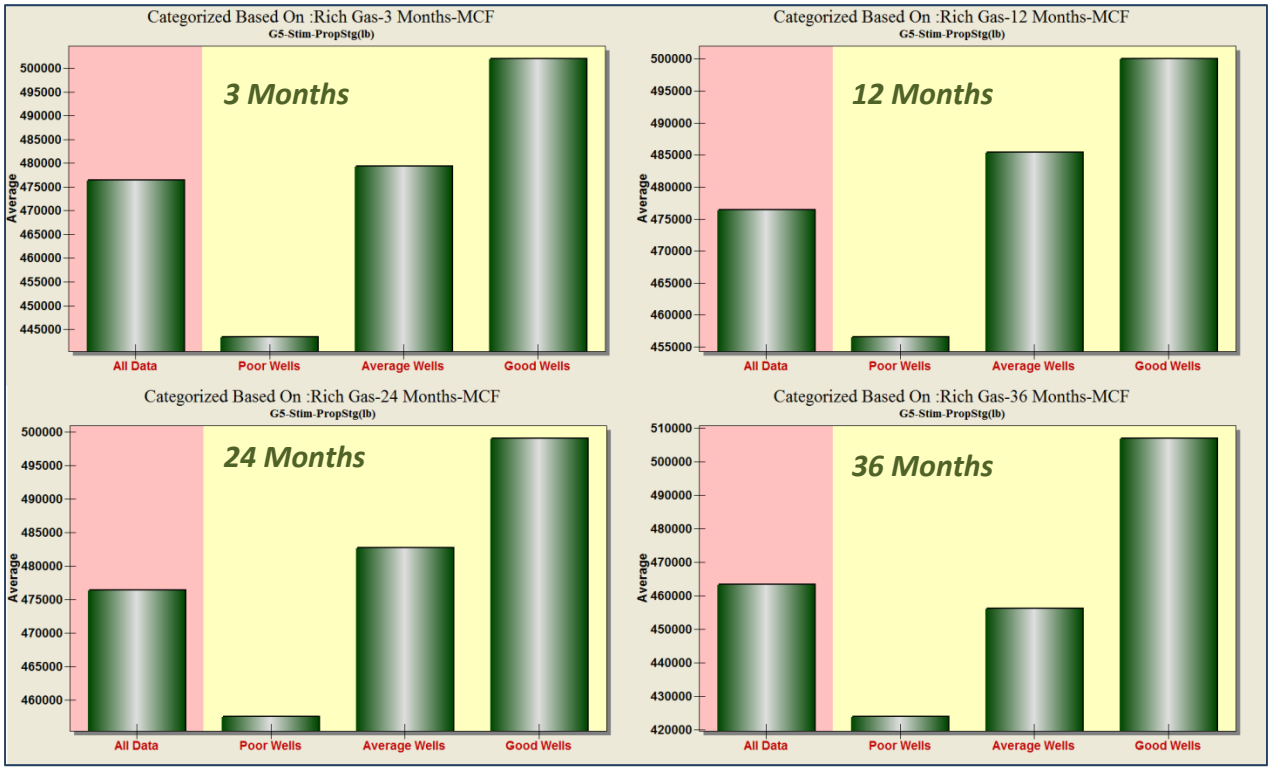

Figure 8.29: Well Quality Analysis for injected proppant per stage- Different time intervals

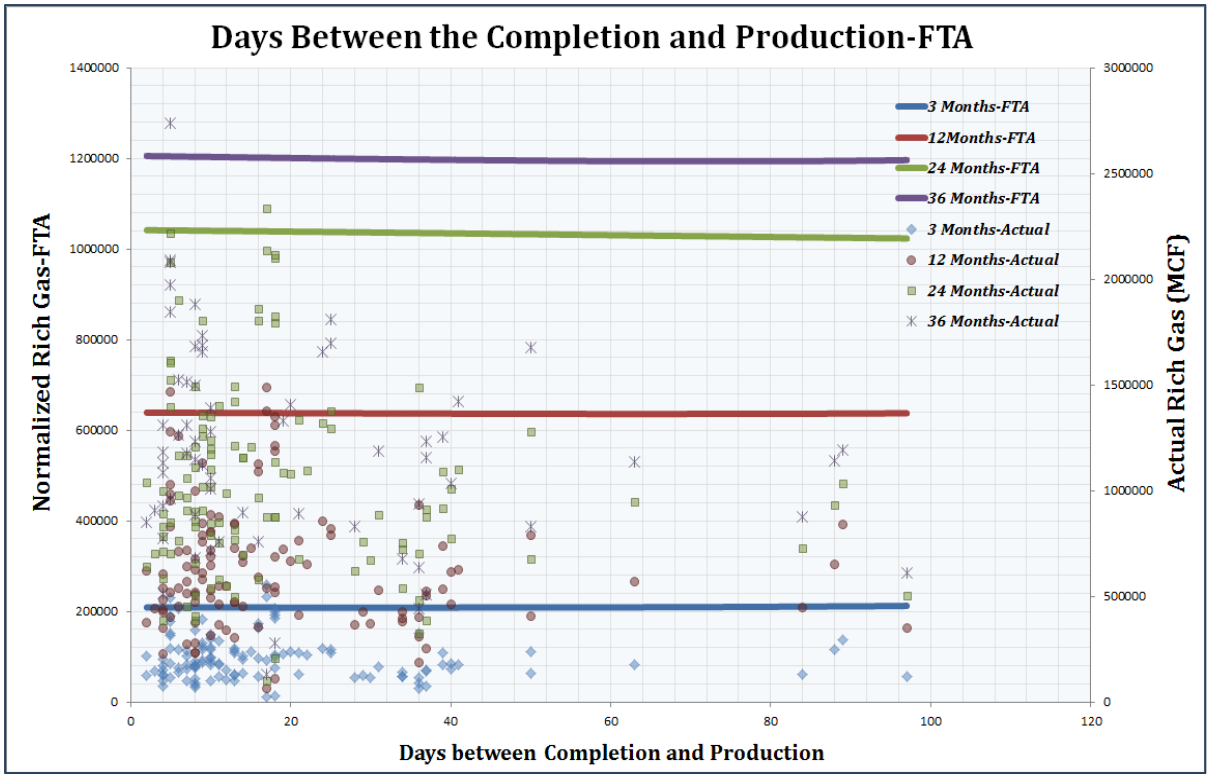

Figure 8.30: The Trend of Rich Gas Production in different time intervals versus Days between the Completion and Production- FTA Result

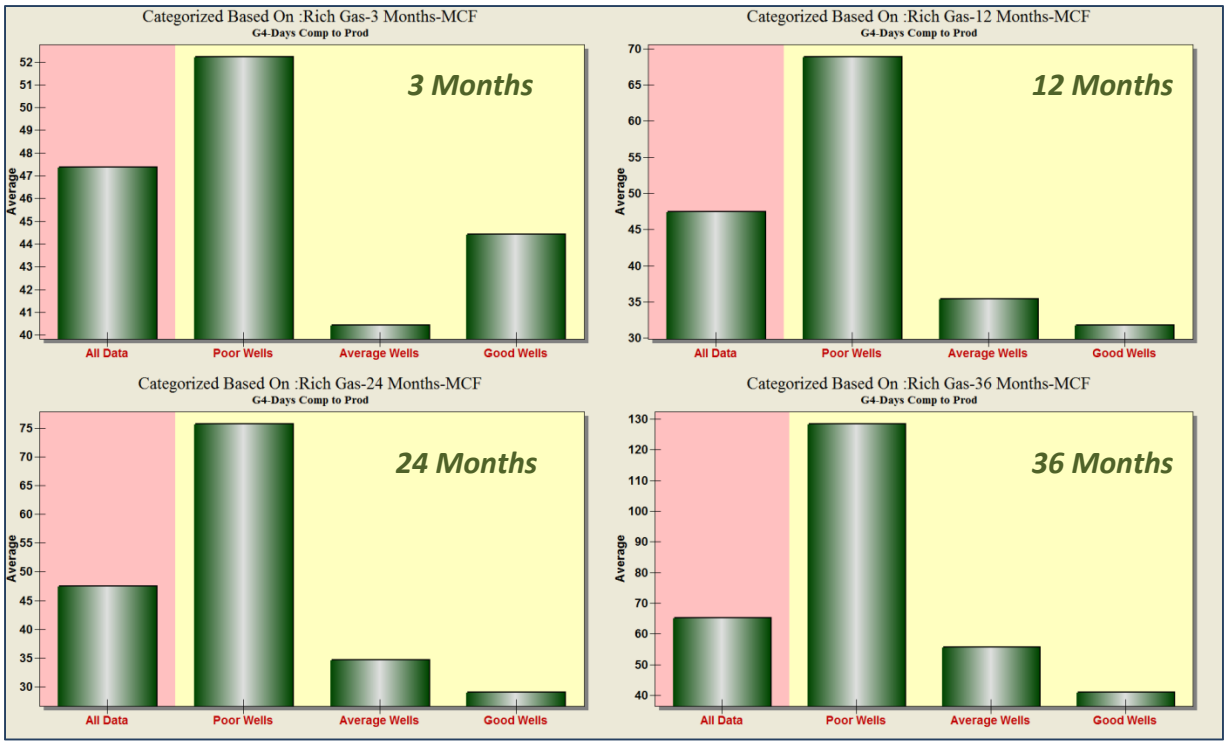

Figure 8.31: Well Quality Analysis for Days between the Completion and Production-Different time intervals

As it illustrated in Figure 8.30, the performance of the well decreases very slightly as there is more delay after completion of the well towards the production start-up date.

Similarly, the inverse effect of this delay can be observed from the Well Quality Analysis. Figure 8.31 represents such a result which shows that the good wells are those which came to production without delay or with little delay after completion. The figure also shows that the effect of this parameter cannot obviously be observed in the early time of production while as time goes on, the inverse trend of production performance becomes more apparent.

Cluster Spacing – Increasing the number of clusters and stimulated lateral length always favors more rich gas production (as it shown), but inadequate cluster spacing can actually lead to lower ultimate recovery. Cheng (2012) showed that decreasing the cluster spacing so as to increase the total number of fractures may significantly reduce gas production when the cluster spacing is reduced to an adequately small size, where the width growth of fractures is strongly inhibited because of the mechanical interaction.

Figure 8.33 and Figure 8.34 illustrate the result of FTA and WQA for cluster spacing.

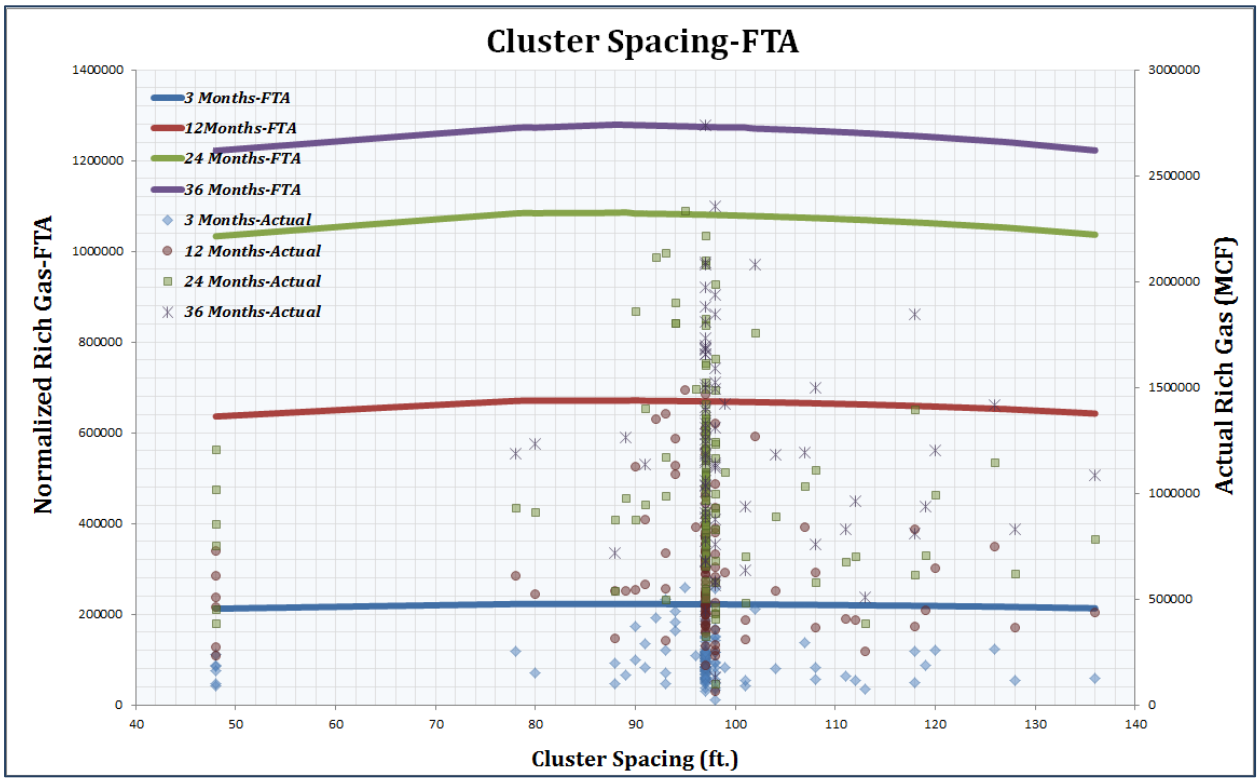

Figure 8.32: The Trend of Rich Gas Production in different time intervals versus Cluster Spacing- FTA Result

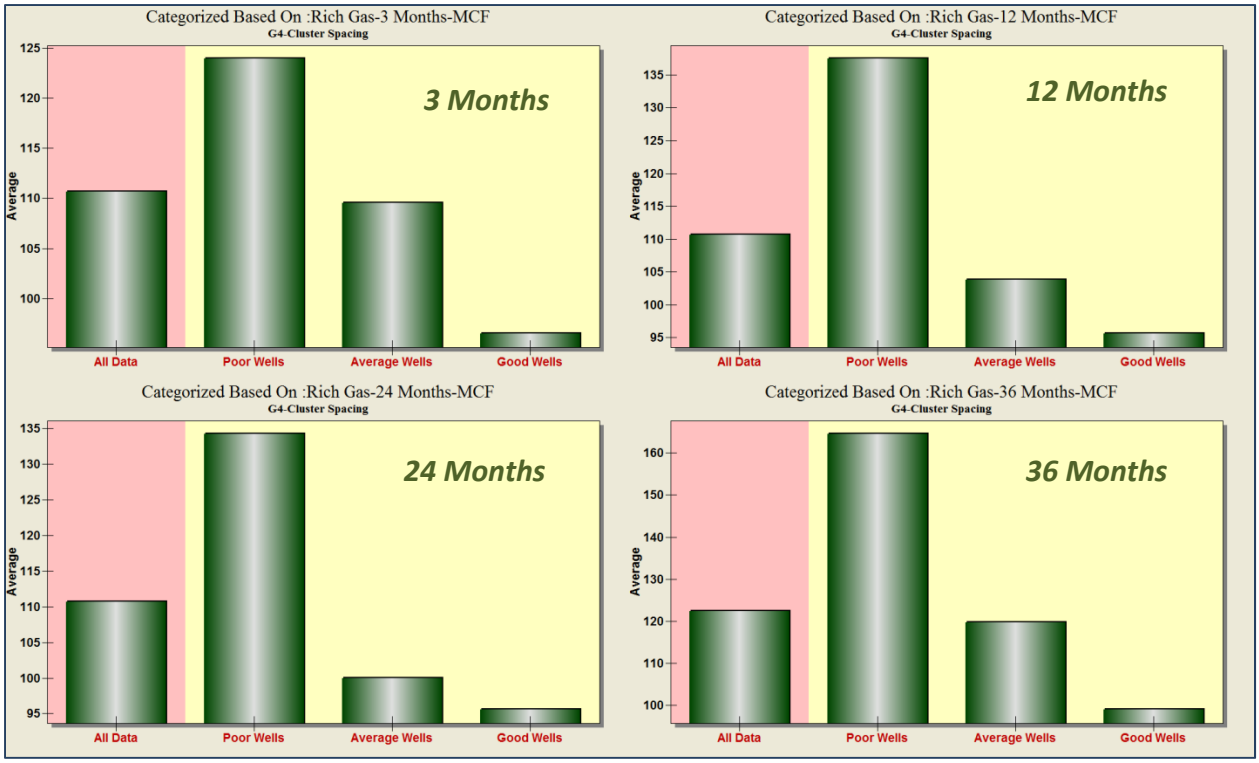

Figure 8.33: Well Quality Analysis for Cluster Spacing-Different time intervals

As shown in Figure 8.33, the production performance shows an increasing trend as cluster spacing increases from 50 feet to about 90 feet and then starts to decrease gradually.

Moreover, from Figure 8.34, it is observed that those wells with closer clusters (cluster spacing less than 100 feet) have significantly better production performance than those with higher cluster spacing. It can be concluded that the optimum cluster spacing for the wells in this area could be around 90 feet.

Matrix Porosity- As explained earlier in sensitivity analysis based on the best history matched AI-based model, the matrix porosity plays an important role in production of the Marcellus Shale.

As seen in Figure 8.34 and Figure 8.35, higher matrix porosity results in better production performance in both early and late time of well life.

Total Organic Carbon (TOC) - The amount of natural gas present in the Marcellus Shale is the product of the quantity of undecomposed organic matter trapped in the shale and it is measured as the total organic carbon (TOC) present. In comparison to some other well-known shale plays in the United States, the amount of TOC in the Marcellus Shale is fairly average to low with around 2 to 10 percent.

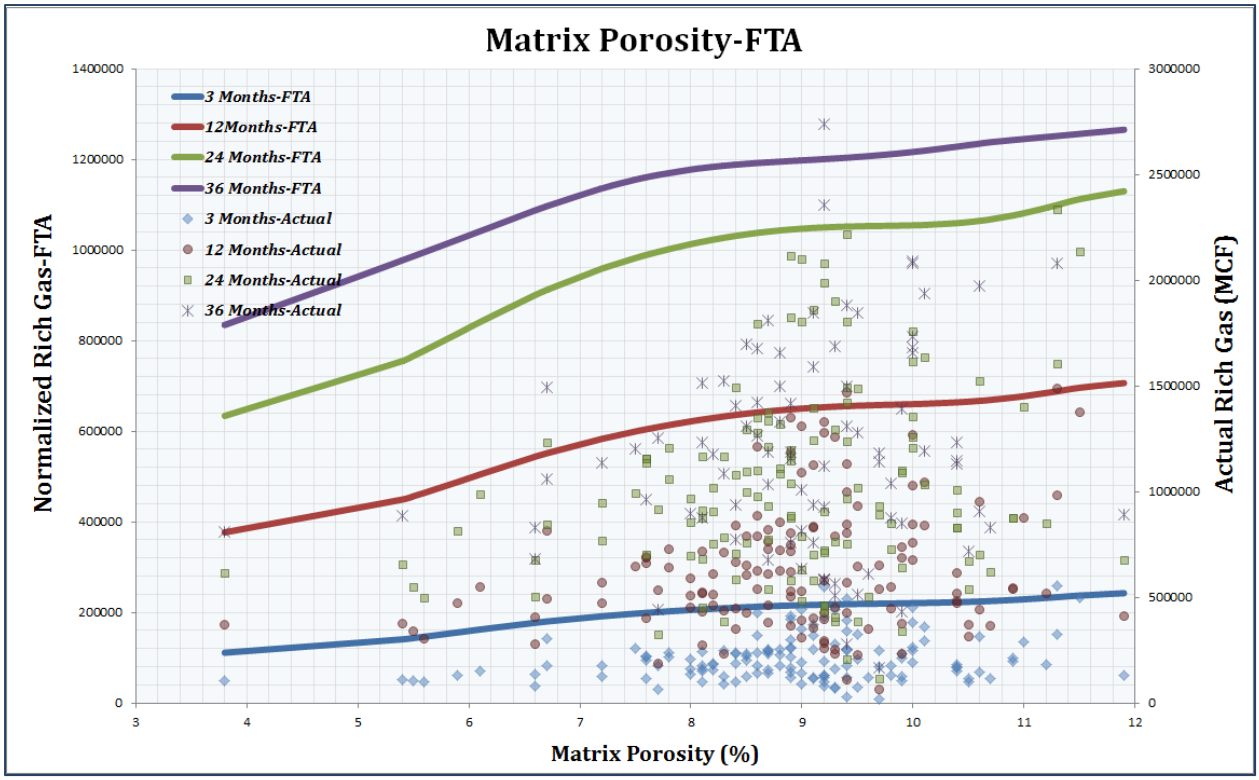

Figure 8.34: The Trend of Rich Gas Production in different time intervals versus Matrix Porosity- FTA Result

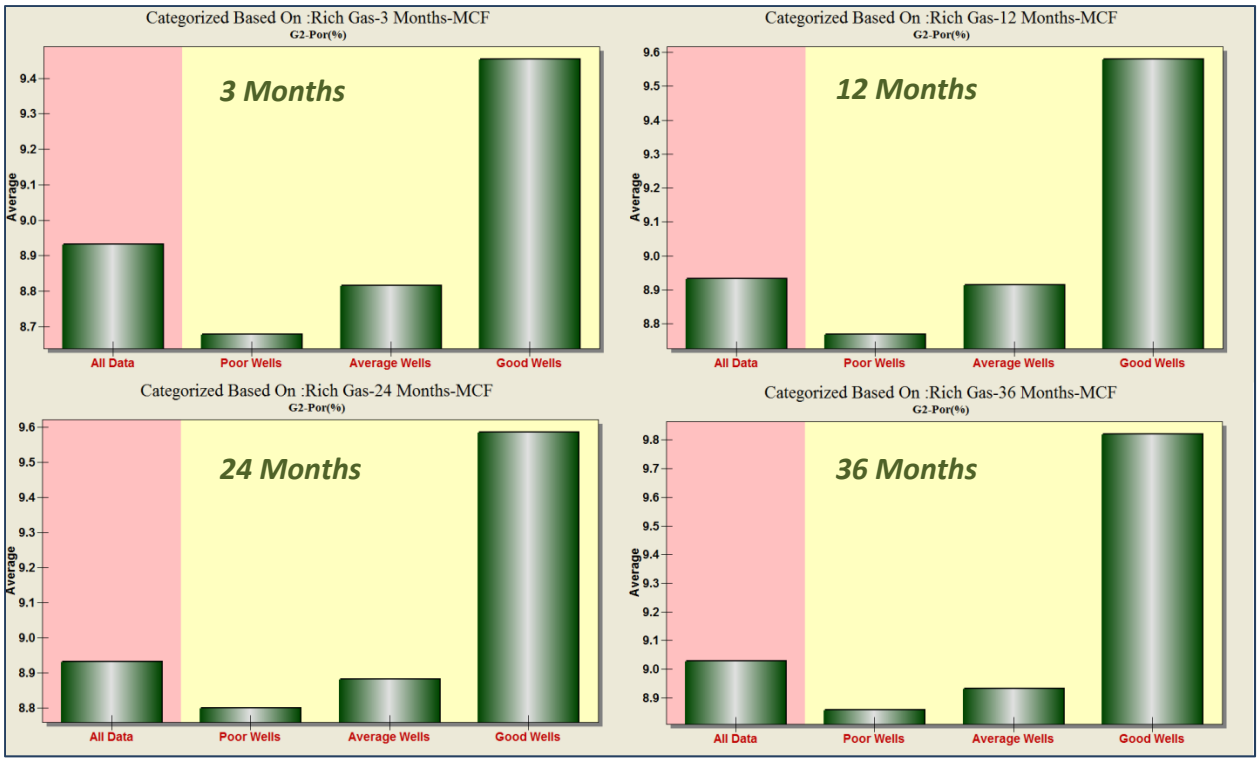

Figure 8.35: Well Quality Analysis for Matrix porosity-Different time intervals

Figure 8.36 and Figure 8.37 show the trend of improving production in all time intervals as a function of total organic carbon content.

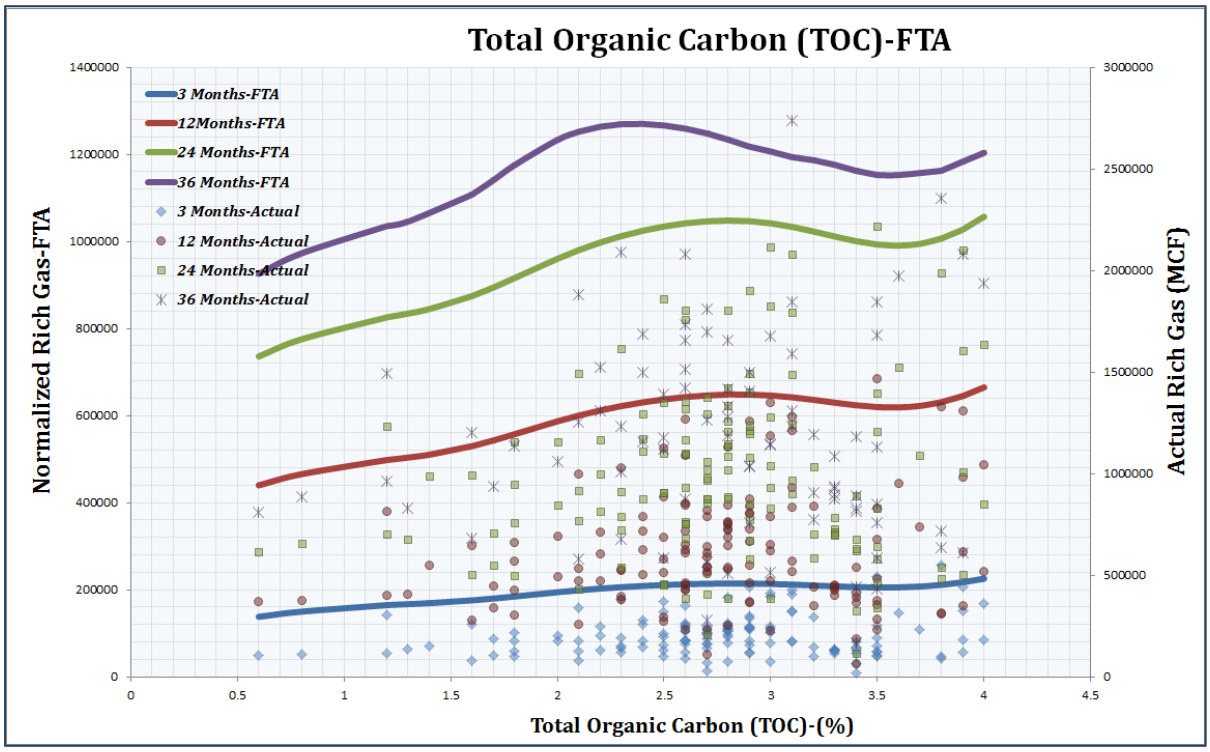

Figure 8.36: The Trend of Rich Gas Production in different time intervals versus TOC- FTA Result

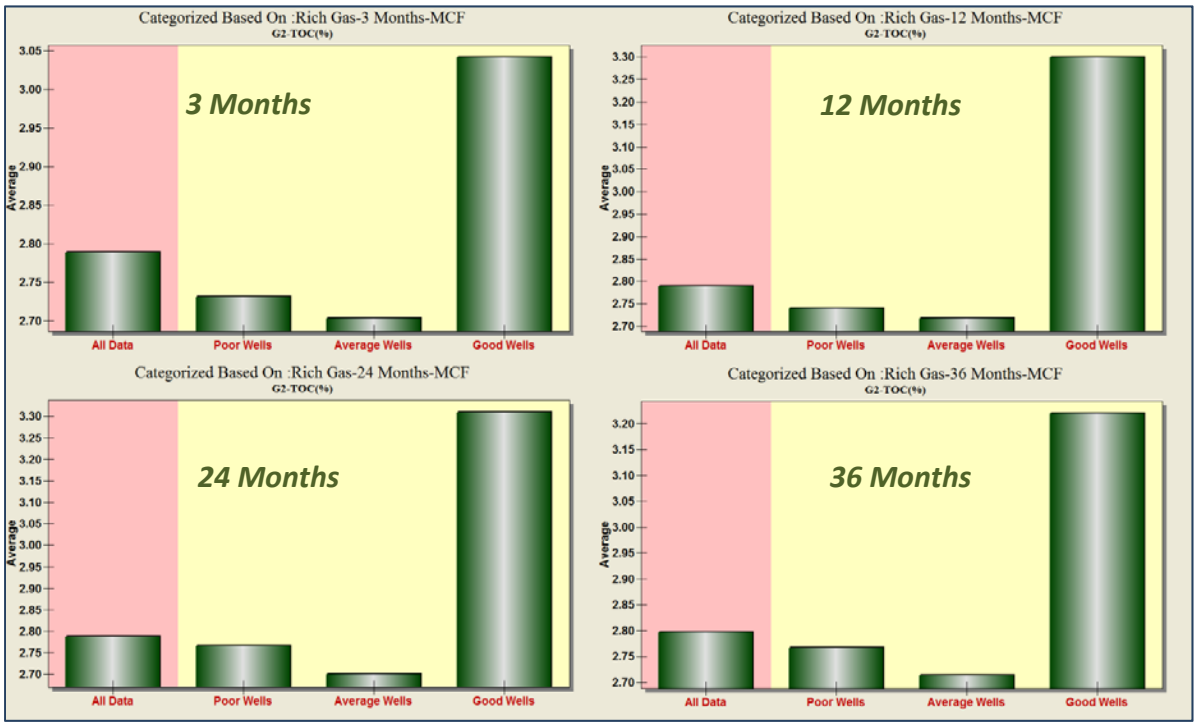

Figure 8.37: Well Quality Analysis for Total Organic Carbon-Different time intervals

The Fuzzy Trend Analysis in Figure 8.37 illustrates that those wells with TOC around 2.7 percent and less (which are categorized as poor and average wells) show the same production trend and the effect of TOC on production performance can be negligible while the good wells are those with TOC above 3 percent and the impact of this parameter on their production behavior is more apparent.

Although the TOC content is an important factor in evaluating the production potential in shale, it is not the only parameter that plays a role, the other factors such as the clay percentage and the ratio of quartz to carbonate should also be taken into account when it comes to production performance of Marcellus Shale. In the Marcellus Shale the recommended values are 40 percent for clay percentage, 3.3 for the ratio of quartz to carbonate, and 6.5 for TOC content [Wang et al. 2012].

Net Pay Thickness – The Marcellus Shale is extremely variable in thickness, ranging from a few feet to more than 250 feet, and generally becomes thicker to the east. The range of net thickness in the area of this study is 90 to 170 feet. Due to different well trajectory (deviation type), landing targets and completed stages, the pay zone is fully or partially accessible therefore this is another important factor in the production performance of the wells. Figure 8.38 shows the clear increasing trend of rich gas production for higher thickness based on FTA. The same trend can be observed in Figure 8.39 from the poor to good wells with thicker net pay.

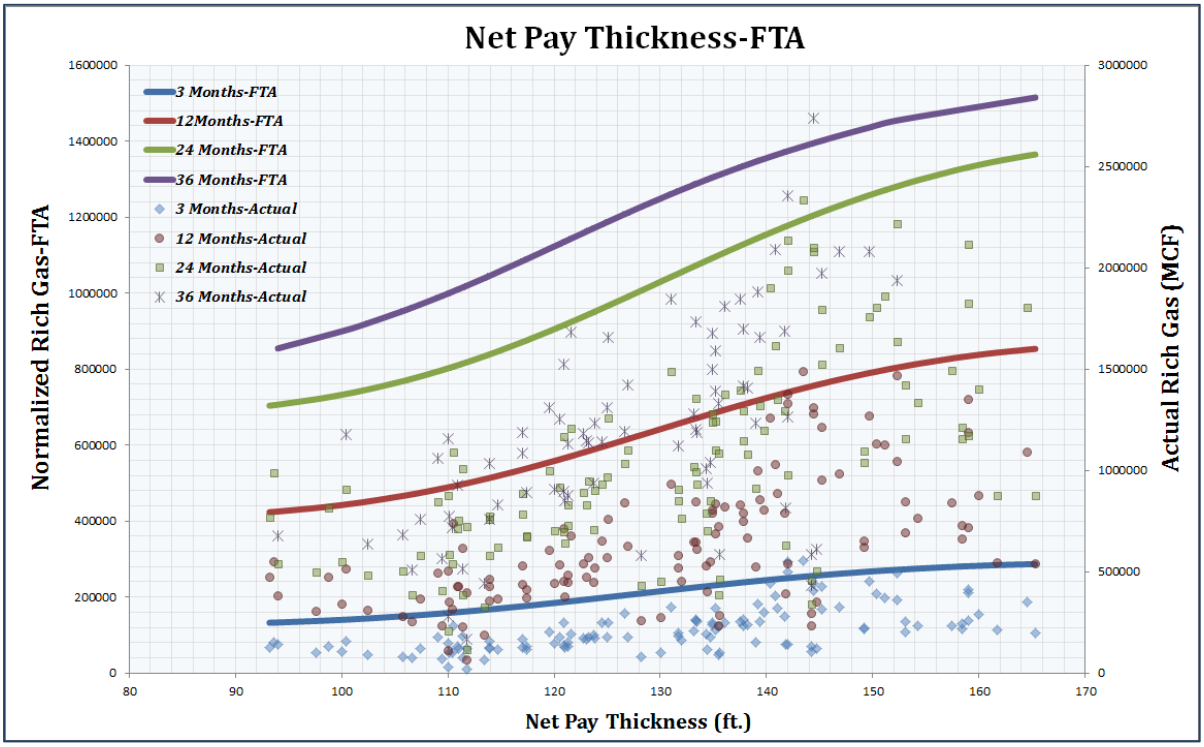

Figure 8.38: The Trend of Rich Gas Production in different time intervals versus Net Pay Thickness- FTA Result

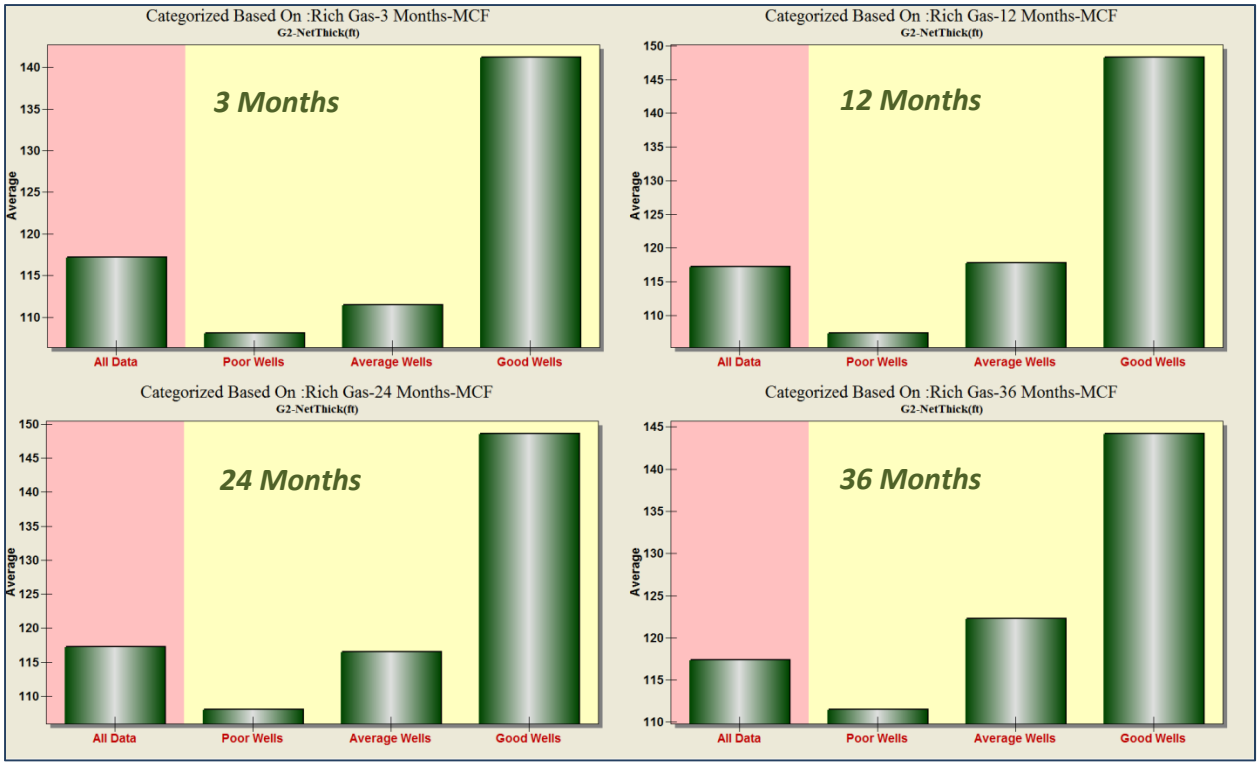

Figure 8.39: Well Quality Analysis for Net Pay Thickness-Different time intervals

Brittleness Index (BI) – As mentioned earlier in chapter 6 (section 6.9), the brittleness index was defined as a combination of Young's modulus and Poisson's ration to reflect the rock's ability to fail under stress (Poisson's ration) and maintain a fracture (Young's modulus).

By given definition, the shale with a higher brittleness factor (meaning a higher Young's modulus and lower Poisson's ration) better responds to hydraulic fracture stimulation. Alternatively those wells drilled in an area with higher brittleness index are expected to have better performance. Figure 8.40 and Figure 8.41 show the result of FTA and WQA for brittleness index.

As these figure represent, the trend of increasing production performance by increasing the brittleness index may not be very obvious and can be due to error associated with the estimation of these values. In previous chapters it was explained that out of 135 wells in the area, the geomechanical logs for 30 wells was available and by developing several data driven models, theses parameters were generated for another 50 wells which became the control points for geostatsitcal distribution maps.

The final values for each geomechanical properties (Young's Modulus, Shear Modulus, Bulk Modulus, Poisson's ration and Minimum Horizontal Stress) were extracted from the distribution map; therefore some unavoidable errors are involved with these values which might be the reason for not having such a

clear trend. Nevertheless, the better performance of "*Good Wells*" due to higher BI is quite clear compared to the "*Poor Wells*" and "*Average Wells"* in Well Quality Analysis.

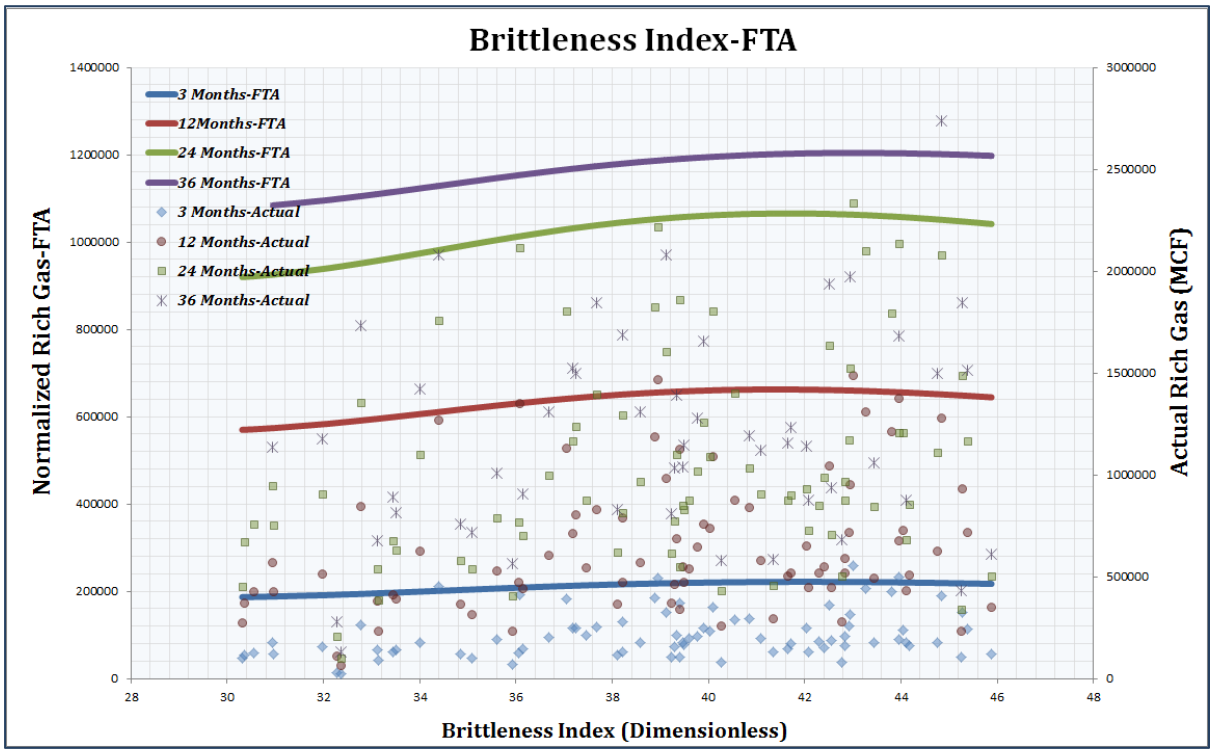

Figure 8.40: The Trend of Rich Gas Production in different time intervals versus Brittleness Index- FTA Result

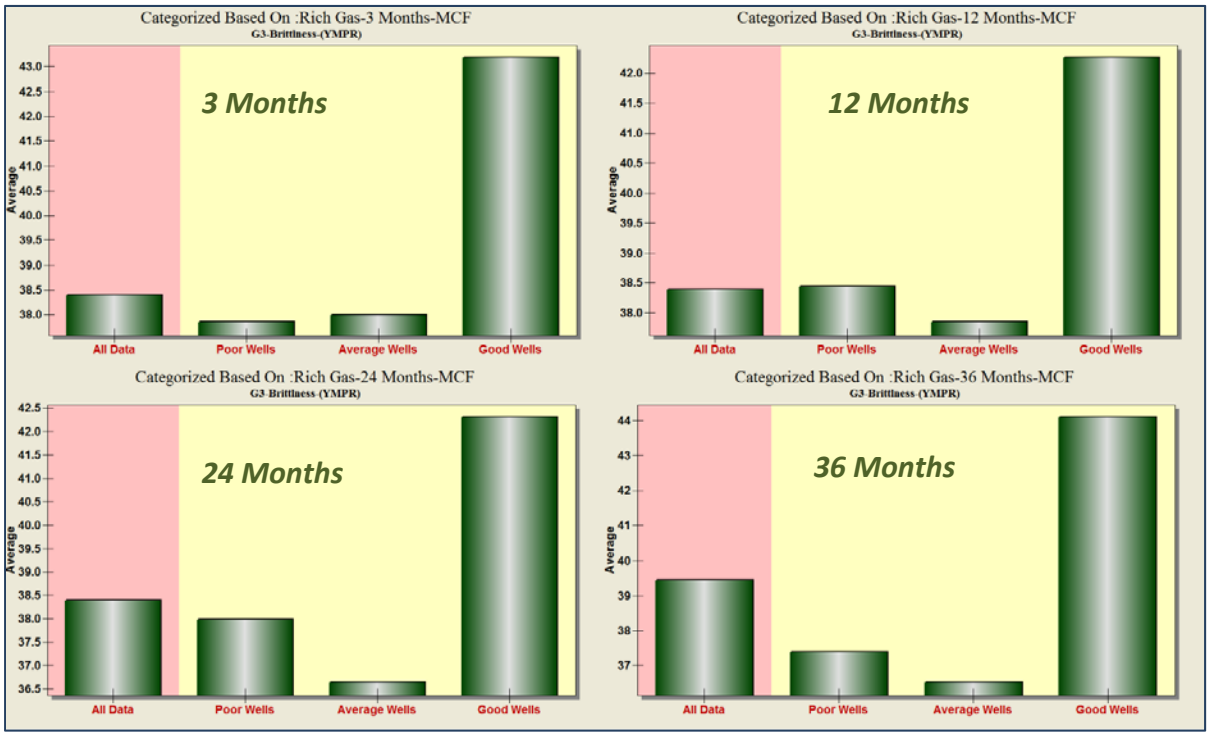

Figure 8.41: Well Quality Analysis for Brittleness Index-Different time intervals

8.2.2 Key Performance Indicator Analysis

In a similar analysis, by using the Pattern Recognition technology, the contribution (influence) of each of the parameters on any given production indicator can be calculated and compared which is known as "Key Performance Indicator (KPI)". In this study, the impact of 32 parameters (Table 8-4) including native and design (16 per each category) were analyzed against the best 3 months, 12 months, 24 months and 36 months of rich gas production.

Table 8-4: List of the Design and Native Parameters in KPI Analysis

Design Parameters	*Native Parameters*
Deviation Type	Average Lang P(psi)
Easting	Average Lang Vol.(scf/ton)
Minimum Distance (ft.)	Net Thickness(ft.)
Type	Permeability (md)
Cluster Spacing	Porosity (%)
Stimulated Lateral Length(ft.)	Water Saturation (%)
Days Comp to Prod	TOC (%)
Total Clusters	Brittleness Index
Average Max Rate	Bulk Modulus
Average Injection Pressure (Psi)	Min Horizontal Stress
Average Injection Rate (bbl./min)	Poisson's Ratio
Average ISIP	Shear Modulus
Average Max Pressure	Young's Modulus
Max Proppant Concentration (lb./gal)	Average Breakdown Pressure
Proppant per Stage (lb.)	Average Breakdown Rate
Slurry per Stage (bbl.)	Duration of Flow Regime 1 (Days)

Upon completion of KPI analyses, the score of the ranking of the parameters (representing the influence of each parameters-the higher score, the more influence) for all time intervals of rich gas production can be processed in order to analyze the overall impact of each category (native and design parameters) as a function of the production length.

In this analysis, for simplicity, the average of the scores for all native parameters and design parameters were separately calculated and plotted versus 3 months, 12 months, 24 months and 36 months of

production and Figure 8.42 illustrates the result of this analysis. As seen from this figure, the effect of native parameters at the early stage of production is much more important than the impact of design parameters. As time goes on, the design parameters effect becomes more considerable and after 2 years of production, the native and design parameters are having the same impact of production performance, and beyond that, the impact of design parameters becomes more significant than the impact of native parameters.

Figure 8.43through Figure 8.46 show the key performance indicator results for design and native parameters for each time intervals.

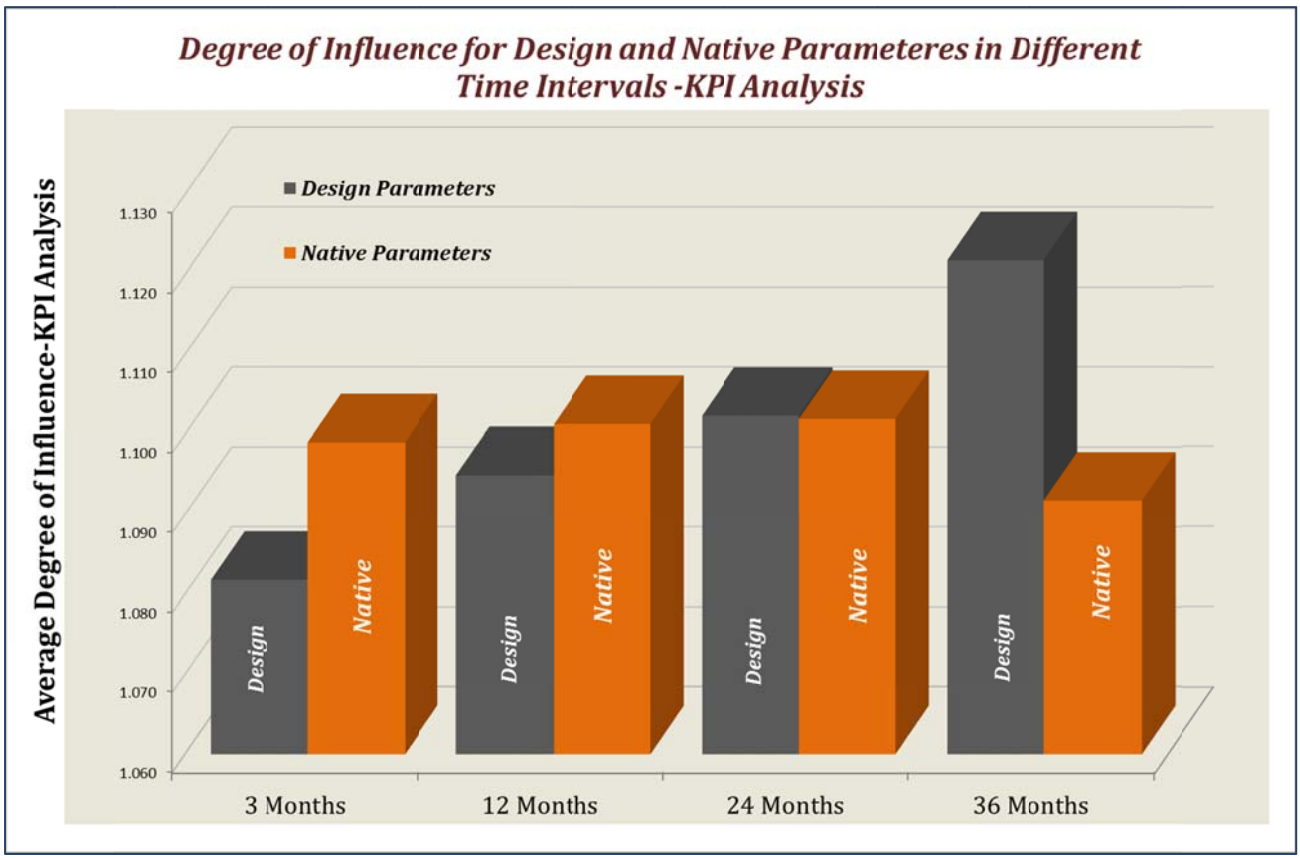

Figure 8.42: The Average Influence Degree of Native and Design Parameters on different time intervals-KPI Analysis

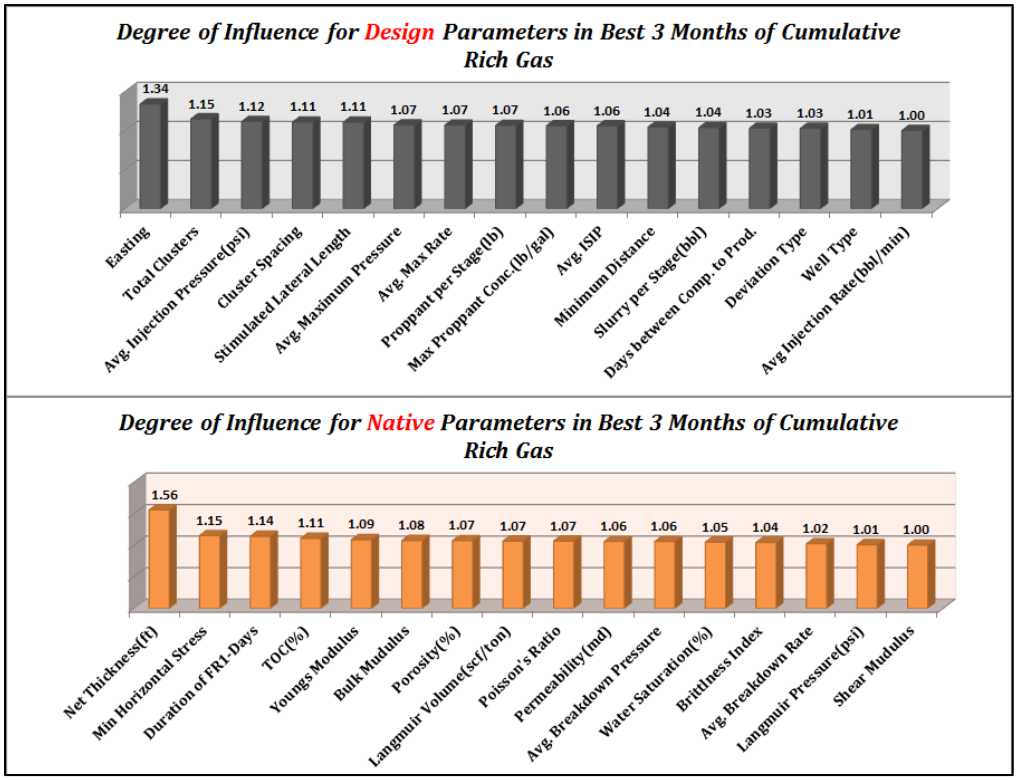

Figure 8.43: The Key Performance Indicator (KPI) Results for design and native parameters for the best 3 months of cumulative rich gas

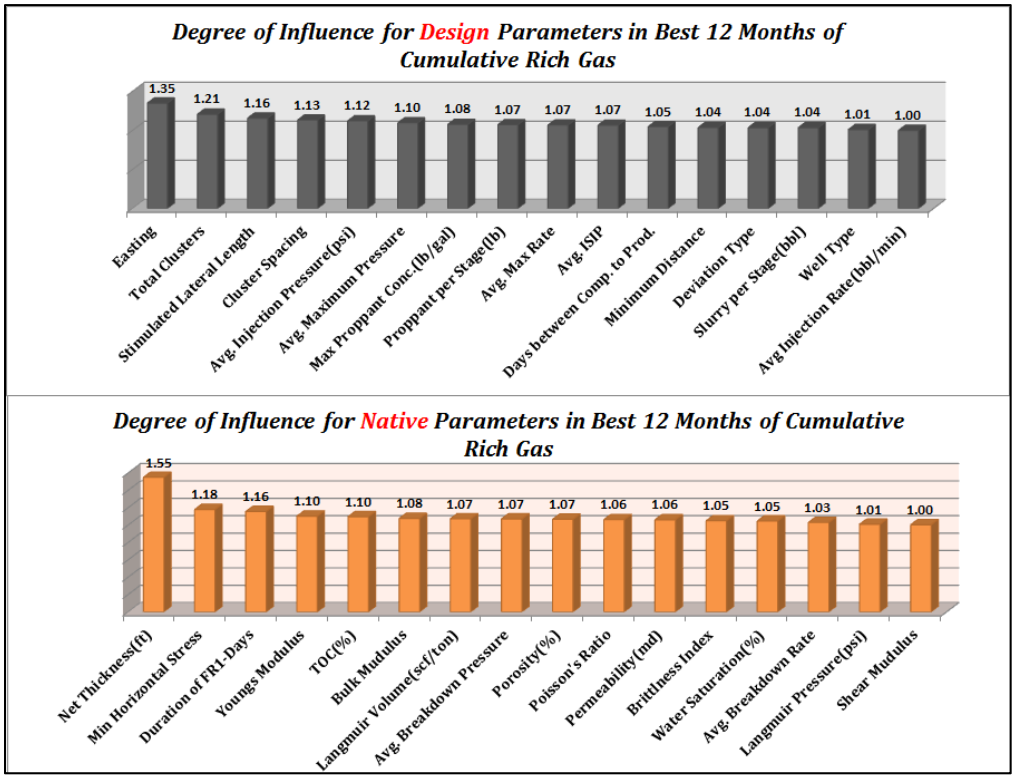

Figure 8.44: The Key Performance Indicator (KPI) Results for design and native parameters for the best 12 months of cumulative rich gas

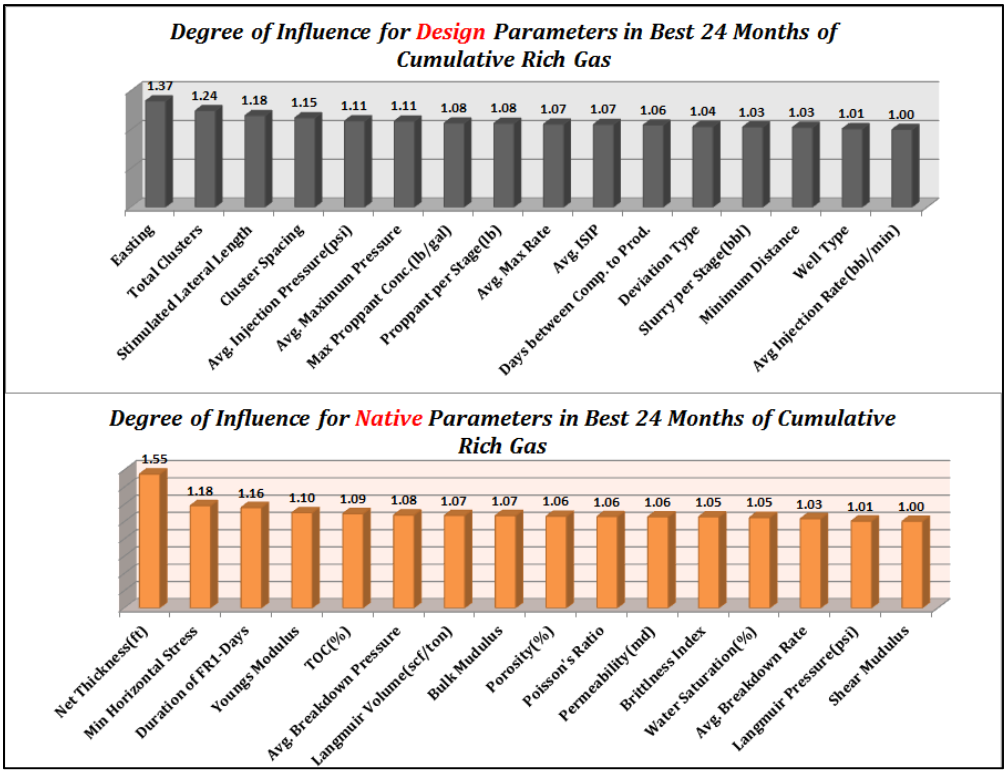

Figure 8.45: The Key Performance Indicator (KPI) Results for design and native parameters for the best 24 months of cumulative rich gas

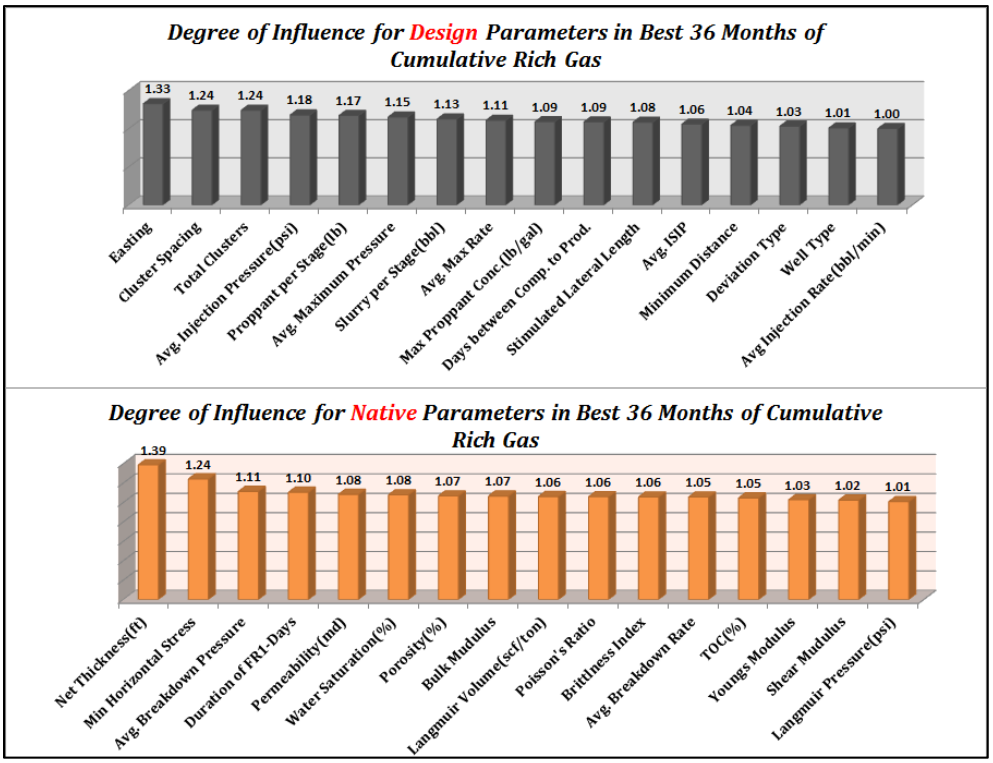

Figure 8.46: The Key Performance Indicator (KPI) Results for design and native parameters for the best 36 months of cumulative rich gas

8.2.3 Key Findings in Optimization Study

From optimization study the following conclusions can be drawn:

1- Drilling the new wells in the eastern part of the reservoir can result in better performance of the well due to better reservoir quality (thickness, more open natural fractures)
2- The wells with the deviation type of down-dip have shown more cumulative production in early and late time of production. The wells with down-dip deviation type which are partially completed in Upper and Lower Marcellus are the most productive wells.
3- The longer stimulated lateral and more clusters are always in favor of more gas production although given the same stimulated lateral length for a horizontal well, increasing the number of clusters results in reducing the cluster spacing which does not necessarily improve well performance. This study showed that the cluster spacing of about 90 feet could be a good estimation for the optimum space.
4- The minimum distance between the laterals that makes enough connectivity to the matrix and avoids well interference could be about 2000 feet. A parallel study on the economic impact of "Frac Hit" on well performance in Marcellus also showed that this process is more significant for those laterals with a distance of less than 2000 feet and causes substantial decline in gas production.
5- This study also revealed that bringing the well to the production after completion with delay is not in favor of production performance. Those wells with longer delay have shown poor performance.
6- The more injected proppant per stage and injected slurry per stage will improve well performance.
7- Drilling the wells in part of the reservoir with more matrix porosity, thicker pay zone, more TOC content and more brittleness index may result in better production in both early and late time of well life. Other factors should also be taken into account when selecting the well location such as the ratio of quartz to carbonate, the clay content, the stress of the area and etc.

8.3 Type Curves

A type curve represents the variations in pressure or rate versus time for a specific reservoir-well configuration. It is usually calculated using an analytic model and expresses in dimensionless variables. Since the discovery of shale reservoirs, the role of type curves as a handy tool for quick production

analysis has become very important. Type curves for shale reservoirs can be generated for different purposes such as evaluating the gas in place, determining flow regimes, some reservoir properties and etc.

During the past decade, so many type curves were generated by researchers; "Agarwal-Gardner", "Blasingame", "Fetkovich" and "Wattenbarger" are the most well-known existing type curves for production analysis from shale. Because of the complexity of fluid flow in shale, the generated type curves are usually based on some assumptions such as elliptical shape of fractures, the limited outer and etc. Nevertheless for a quick look shale reservoir interpretation, having type curves will make the production analysis even more convenient for practical purposes.

Upon completion of the AI-based model for different time intervals (as explained in section 8.1.2), type curves can be generated to assist operators during the decision making process: where to place the next well (or which wells should receive priority for drilling) and how to complete and stimulate that well. Type curves can be generated for individual wells, for groups of wells and for the entire field. In type curves, the y-axis is the model output (in this case, the best 3 months and 24 months cumulative rich gas production). The x-axis should be selected from one of the input parameters and curves represent a third parameter. Figure 8.47 shows two sets of type curves (3 months and 24 months) for total injected proppant (curves) as a function of stimulated lateral length (x-axis) for the entire field. Similar type curves can be developed for a group of wells as shown in Figure 8.48 and Figure 8.49.

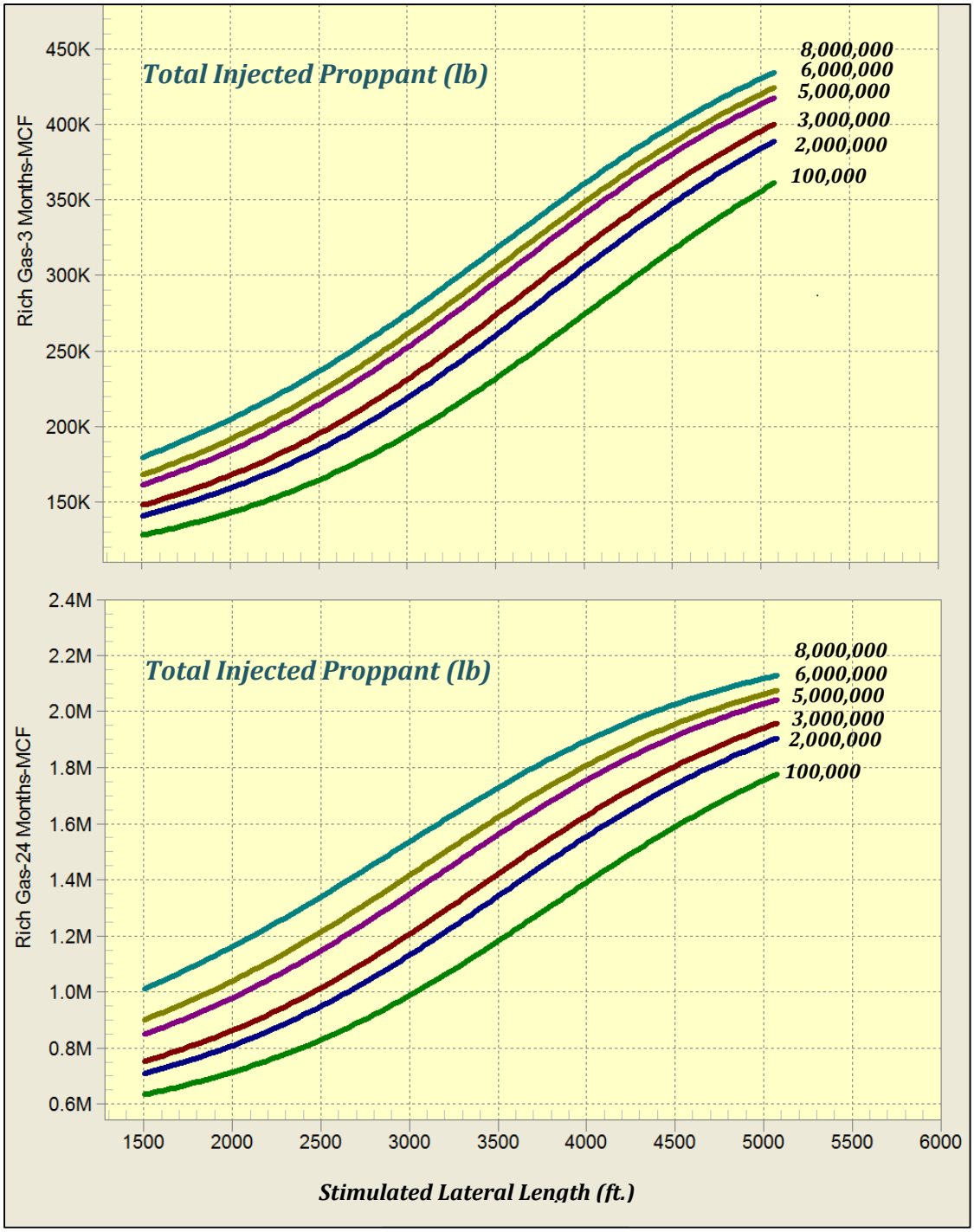

Figure 8.47: Type curves for entire field showing changes in best 3 Months and 24 Months Cum. Rich Gas as a function of stimulated lateral length and different total injected proppant

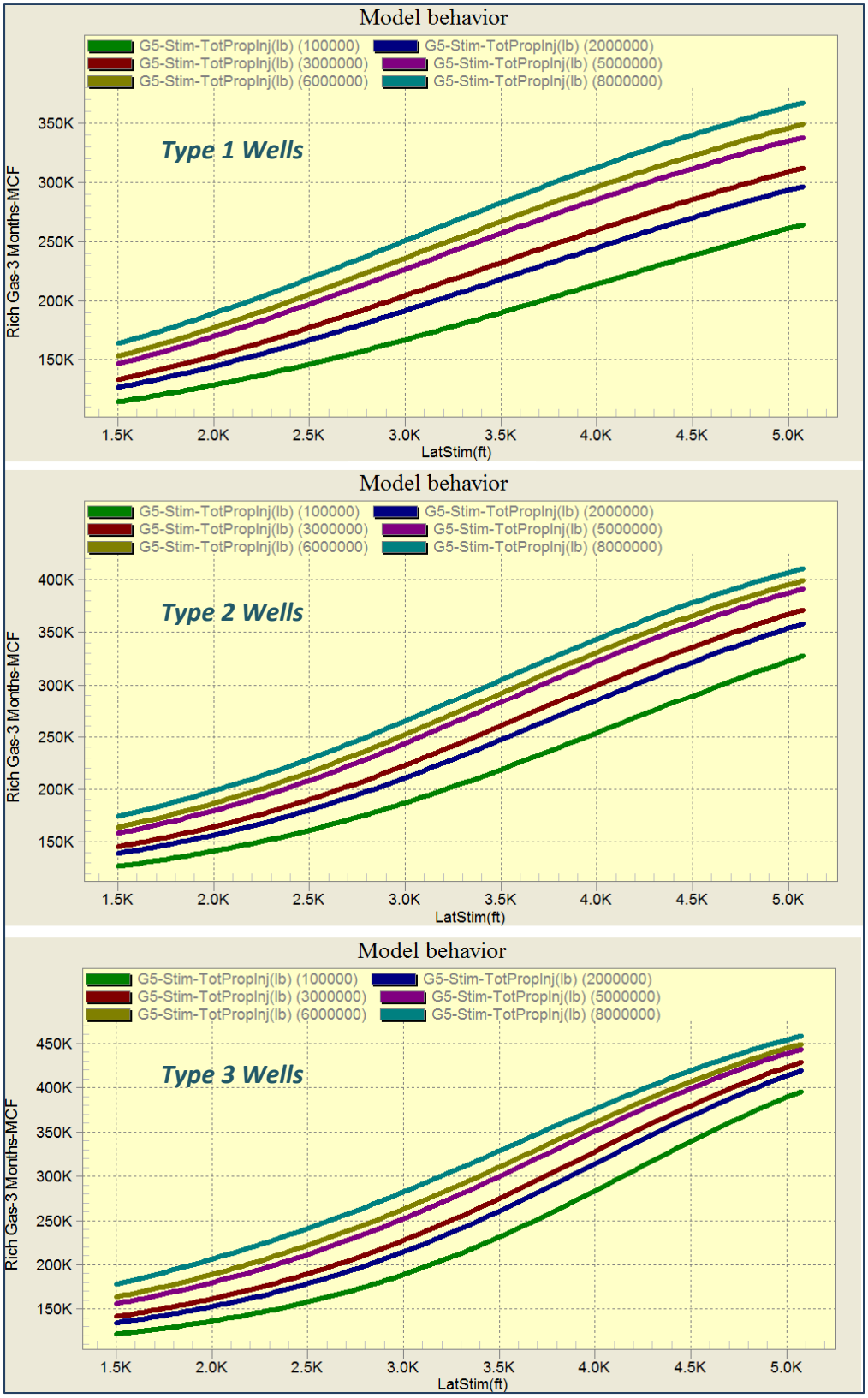

Figure 8.48: Type curves for different well types showing changes in best 3 Months Cum. Rich Gas as a function of stimulated lateral length and different total injected proppant

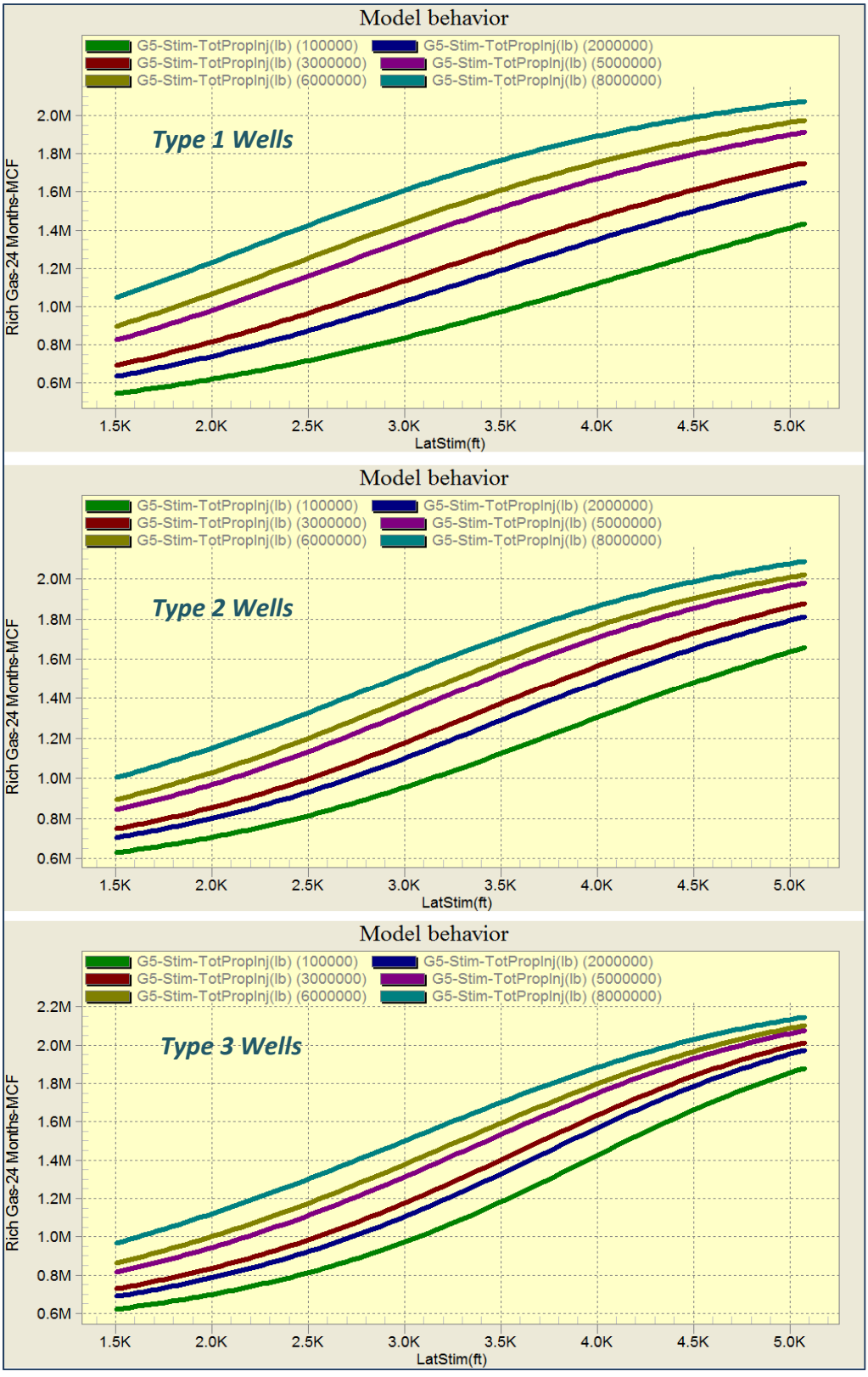

Figure 8.49: Type curves for different well types showing changes in best 24 Months Cum. Rich Gas as a function of stimulated lateral length and different total injected proppant

In order to validate the generated type curves, it was tried to predict the best 3 months production of two new wells that their production was forecasted in chapter 7 by using the type curves.

New Well 1-Pad 4- Coming into production during March 2012, this type 3 well is located in a pad with four more wells. This well was completed in 10 stages (30 clusters) and in the best 3 months of its production life it produced about 185,300 MCF rich gases. The location and some stimulation information of this well were available and used to predict its production performance for the best 3 months by using the type curves. In order to accomplish this, either the type curves of the entire field or the type curves for type 3 wells can be used, although for this specific problem the type curves of entire filed were considered.

The first type curve is the changes in the best 3 months of cumulative rich gas as a function of stimulated lateral length and total injected proppant. For this well, the stimulated lateral length is about 2700 ft. and the total injected proppant for all the stages is 3.02 million pounds. As shown in Figure 8.50, for the stimulated lateral length of 2700ft. and the total injected proppant of 3 MMlb, the best 3 months of rich gas is predicted to be 200,000 MCF which is very close to the actual production.

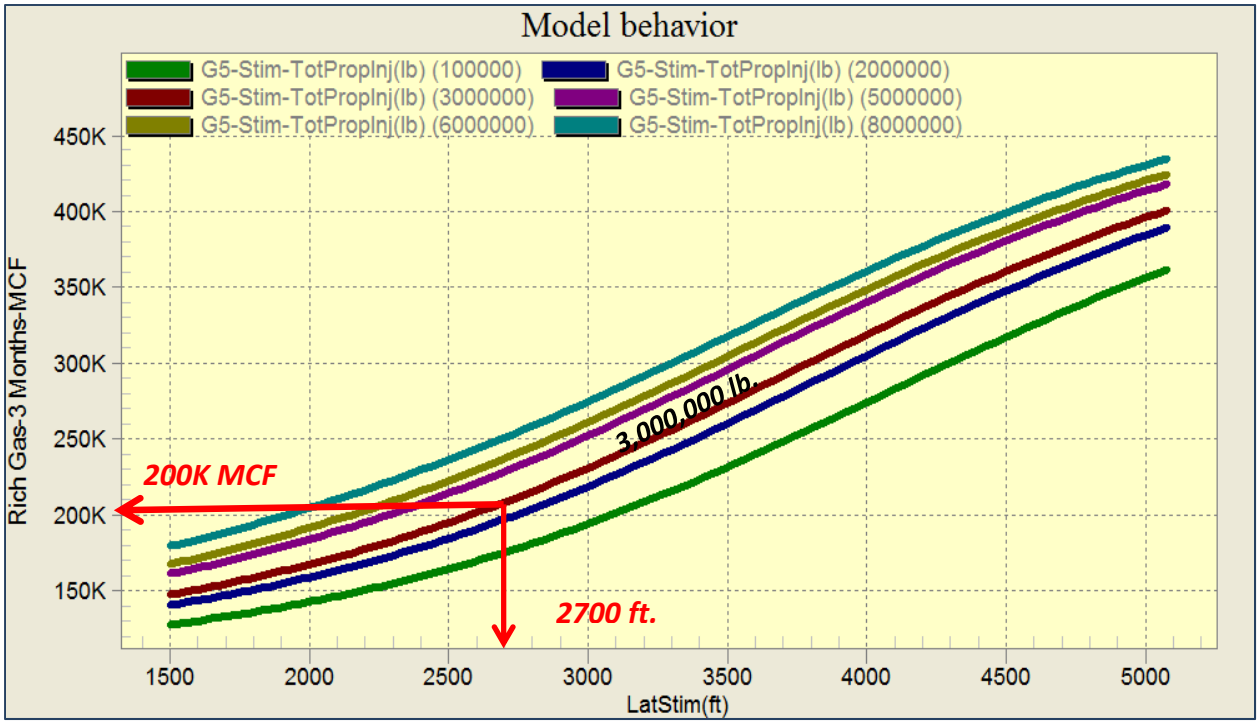

Figure 8.50: Type curve for the entire field- the Best 3 months cum. Gas as a function of stimulated lateral length and total injected proppant. For the New Well 1-Pad 4, by 2700 ft. stimulated lateral length and 3,000,000 total injected proppant, the best 3 months of rich gas is predicted about 200K MCF.

This task can be done by using the other type curves, for instance if the location of the well is known (the easting), by using one of the completion or stimulation information such as maximum injection rate, the best 3 months of cumulative rich gas can be predicted by using the type curve as illustrated is Figure 8.51.

As shown in this figure, by knowing the location of the well (easting coordinate of this well is 558166 m) and the average of maximum rate for all stages (which is around 70 bbl./min), the best 3 months of cumulative rich gas would be 205,000 MCF.

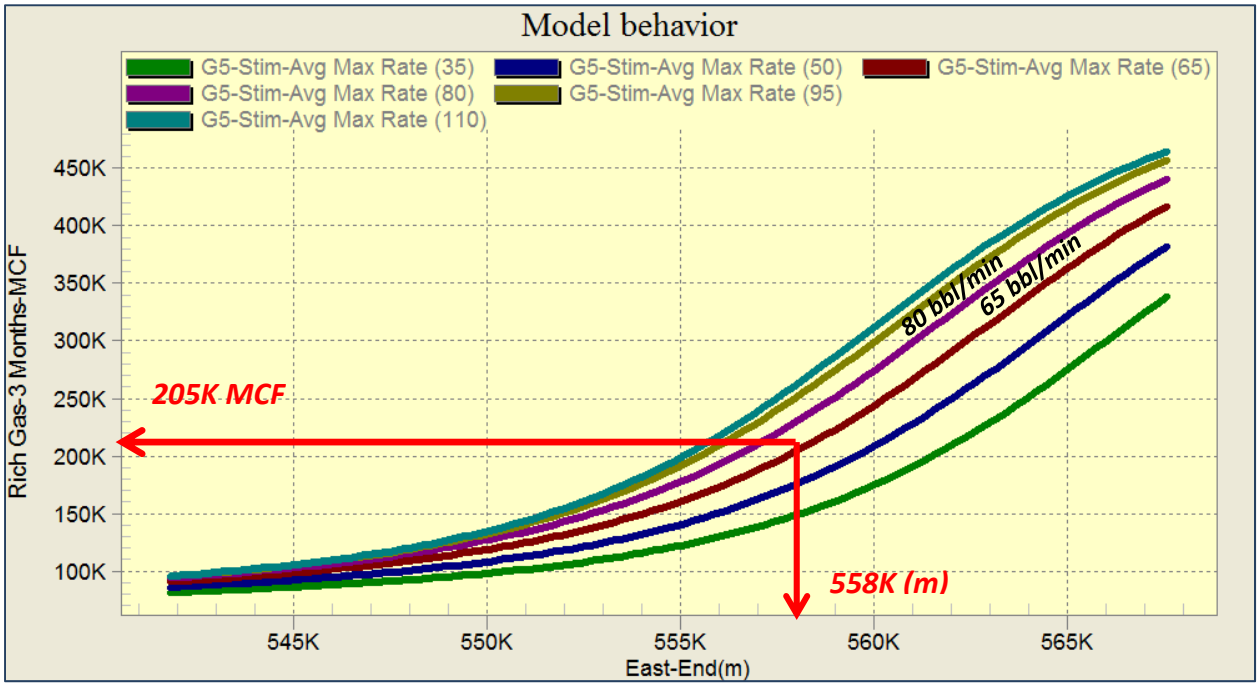

Figure 8.51: Type curve for entire field-the best 3months cum. Gas as a function of well location and average maximum injection rate. For the New Well 1-Pad 4 which is located in easting of 558K, and was completed by average maximum injection rate of 70 bbl./min, the best 3 months of rich gas is predicted to be about 205K MCF.

New Well 1-Pad 6 – This well is located on a pad with two more wells in the west part of the reservoir and it came to production on September 2012. During the best 3 months of production, 98,200 MCF rich gas was produced by this well. The well was completed by 9 hydraulic fracture stages (27 clusters) along the stimulated lateral of 2200 feet.

By using this stimulated lateral length and total injected proppant (which is about 2.7 million pounds, the total cumulative rich gas for the best 3 months of this well was predicted to be about 155,000 MCF by using the type curve (Figure 8.52).

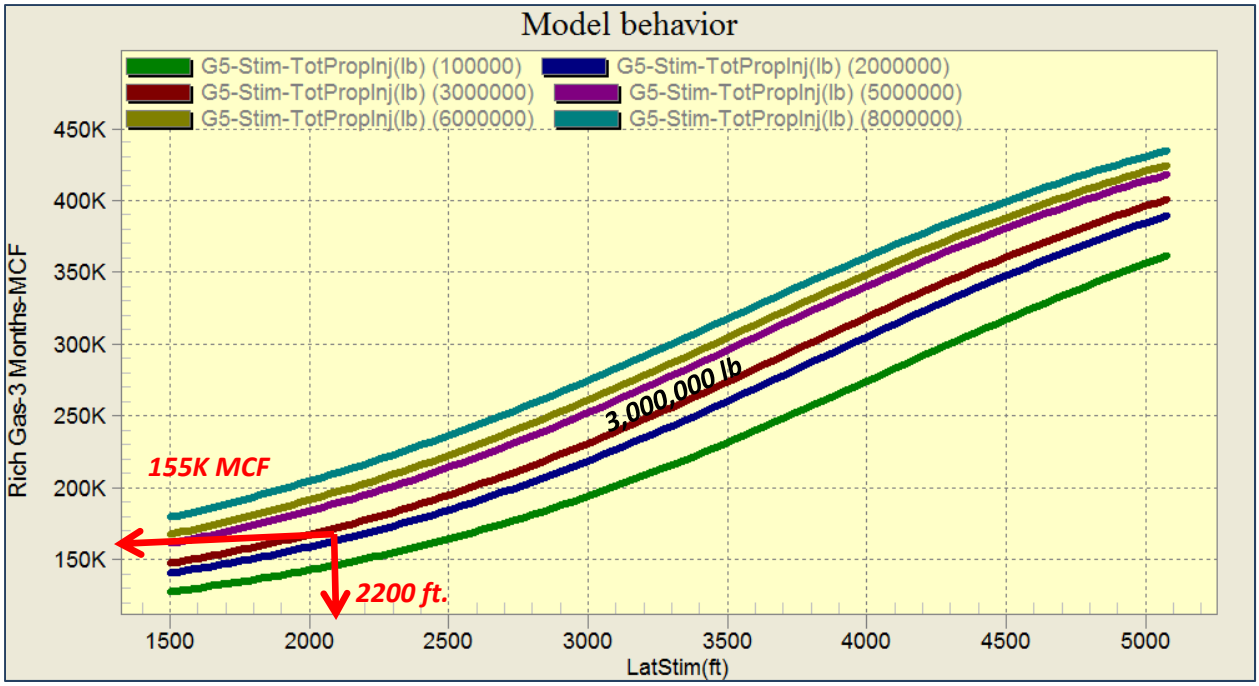

Figure 8.52: Type curve for the entire field- the Best 3 months cum. Gas as a function of stimulated lateral length and total injected proppant. For the New Well 1-Pad 6, by 2200 ft. stimulated lateral length and 2,700,000 total injected proppant, the best 3 months of rich gas is predicted about 155K MCF.

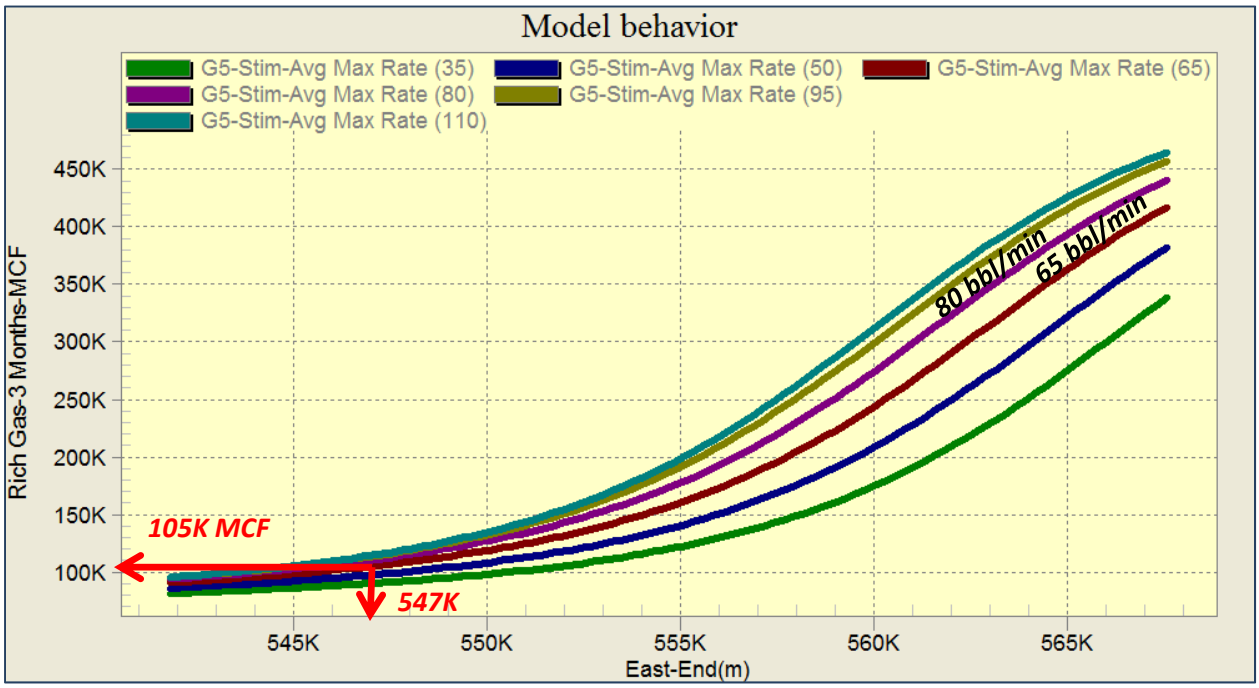

Figure 8.53: Type curve for entire field-the best 3months cum. Gas as a function of well location and average maximum injection rate. For the New Well 1-Pad 6 which is located in easting of 547K, and was completed by average maximum injection rate of 71.1 bbl./min, the best 3 months of rich gas is predicted to be about 105K MCF.

Using the location (easting) and the average of maximum injection rate (Figure 8.53), this well's best 3 months of production were estimated around 105,000 MCF which is closer to the actual production of the well.

The difference between the values from two type curves is due to the fact that during the generation of type curves as a function of one specific parameter, the other parameters are kept constant. Therefore two different values with the error of about 20% are expected to be observed.

Moreover, the west part of the reservoir has relatively less wells (possibly due to the existing of some faults) and because of this, the generated type curve as a function of easting for the values less than 555K are very close to each other (as it shown in Figure 8.53).

9. CHAPTER IX

CONCLUDING REMARKS AND RECOMMENDATIONS

9.1 Concluding Remarks

The major conclusions of this work can be summarized as follows:

1- An AI-based shale reservoir model was developed with the aim of overcoming current issues in numerical and analytical modeling of shale reservoirs. The beauty of this technology is its capability of handling and incorporating all the data and instead of imposing our vague knowledge of flow and transport mechanism in the shale system, let the data identify its functional relationship using pattern recognition approach in a non-linear and complex system.

2- The full-field history matching was performed (history matching for every single well) by using the optimum number of parameters with acceptable accuracy. The history matching result for 90% of the wells showed an error less than 15% which is a good indication of the model's accuracy.

   Out of 135 wells, five wells showed the history matching error above 20%. The detailed analysis of these five wells revealed that these are the first wells that were drilled and completed either in the field or in their own pad and therefore the existing of the offset well (which is not necessarily a closest well) has a reverse impact particularly at the beginning of the production.

   On the other hand, due to the lack of enough information from the field and the early experience of the operator in drilling and completing the horizontal wells, these wells usually produces less than the typical gas rate in Marcellus and the very erratic production behavior cannot be easily captured by the AI-based model

3- Upon completion of history matching, the AI-based model was validated by using the blind dataset. The last four months of production were consistently removed from the production history and it was tried to predict the production behavior by using the AI-based model. The estimated error of 5.7% for the prediction of these four months simply showed the capability and validity of the AI-based model.

4- Once the developing and validating of an AI-based model is completed, its utilization is similar to a conventional full field model. It was used for forecasting the well/field production performance (short term). The results showed that about 10% of the wells have a forecasting error above 20%.

These wells show a very different trend in the period of forecasting (a year after history matching period) and because of not using the corresponding operational constraints (the days of production and well head pressure), the AI-based model could not be able to forecast this abnormality. In order to confirm this, the operational constraints were updated by using the available actual values for these wells and the forecast of the AI-based model was improved significantly.

Moreover, the history matched and validated model were used to predict the production behavior of some new wells which were drilled at different locations of the reservoir. The production performance of 29 new wells on 6 different pads was predicted by the AI-based model with acceptable accuracy. The operational constraints, stimulation, completion and other reservoir characteristics of these wells were not provided to the AI-based model and the model used the information of offset well in order to predict the production performance.

5- A comprehensive sensitivity analysis was performed by both using the best history matched AI-based model and different production indicators(the best 3 months and 24 month of cumulative rich gas) in order to investigate the impact of different parameters on production behavior of the wells/field.

In the sensitivity analysis based on the best history matched AI-based model, the effect of 9 parameters, which were involved in obtaining the model, were studied. The influence of 30% increasing of these parameters (relative to the reference model) was evaluated for different types of the well (type 1, 2 and 3) and it was found that the different well types respond differently to the changes in parameters in terms of degree of influence although the general response (negative or positive) is almost the same. For example, increasing the injected clean volume has improved the production performance of all types and increasing in average injection rate has shown a negative impact on all types of wells even though the degree of influence for these two parameters in different well types is different. The 30% increasing in injected clean volume has improved the production of type 1 wells by 10.8% while it has increased the production of type 2 and type 3 wells by 5.2% and 10.3% respectively. The degree of influence for the increasing average injection rate on type 1 wells is about -2.6%, for type 2 wells is about -2.4% and for type 3 wells, is about -1.5%.

In the sensitivity analysis by using the different production indicators (the best 3 months and 24 months of cumulative rich gas) the impact of different parameters on early and late times of

production from three types of wells were studied. The objective of such analysis was investigating the behavior of the wells as a function of those parameters which didn't show the clear trend in previous sensitivity analysis and those parameters that were not involved in best history matched AI-based model such as TOC, Brittleness Index and etc. Both single-parameter and combinational parameters sensitivity analysis was performed for the three types of the wells. The result of such analysis confirmed that any variation in parameters could affect the different type of wells by different degrees, although the overall behavior (increasing or decreasing trend) is the same. For instance, both early and late production performance of all well types increases as the stimulated lateral length increases. The similar behavior is followed in the case of TOC and Brittleness Index. For the case of cluster spacing, the analysis showed that for all types of wells, by having farthest clusters, the production performance in early time of production will be decreased as well as the performance in late time.

6- Using the artificial intelligence and data mining, an optimization study with the purpose of providing a tool for operators in terms of the location of new wells, the optimum hydraulic fractures design and the best practices for completion and etc. was performed. In this analysis, different production indicators was used and by using two techniques of "Fuzzy Trend Analysis "and "Well Quality Analysis". Some recommendations for effective and integrated reservoir management have been provided.

This study shows that an increasing trend toward gas production is obviously observed as we move to the east part of the reservoir (thicker pay zone and better reservoir characteristics). Also the down-dip deviation seems to be the best deviation type for these wells as they partially completed in Upper and Lower Marcellus and have been exposed to the whole pay zone.

In terms of the reservoir characteristics, the optimization study showed that the higher matrix porosity, higher TOC, thicker pay zone and higher brittleness index are in favor of rich gas production either in early time or late time, although for determination of the drilling location, some other factors should be taken into account such as the ratio of quartz to carbonate, the clay content, the stress of the area and etc.

The optimization study also illustrated that the wells with a longer stimulated lateral and more clusters have better production performance in both early and late times of their life, although such analysis showed that the for all time intervals, the production performance does not change significantly when the length of the stimulated lateral goes above 3800 feet. Very special

attention should be paid to the number of clusters; although increasing the number of clusters/stages would improve the production performance, the closer clusters/stages (decrease in cluster spacing), on the other hand can have the reverse impact. This study shows that the cluster spacing around 90 feet is a good estimation for the optimum spacing and the production of the new wells confirms this analogy. The completion history of the new wells shows that the operator has tried to complete the new wells with more stages but closer clusters (up to 23 stages-70clusters with the spacing of 70 ft.) and the production has not been changed significantly.

This study also showed that the optimum distance between the laterals is about 2000 feet to establish enough connectivity to the matrix and to avoid well interference. A parallel study shows that the process of "Frac Hit" happens for those wells with the minimum distance of less than 200 feet and it causes a significant decrease in gas and condensate production in the long term.

During the completion of the wells, it's been noticed that some wells have a considerable delay between the completion and production; the optimization study discloses that this delay can potentially cause severely adverse impacts on long-term production.

In terms of hydraulic fracturing design, injecting more proppant per stage can always improve the production performance of the well as well as pumping more slurry for each stage.

As shown and discussed in sensitivity analysis, the increase of average injection rate has a negative impact on production performance, although it was not shown in the optimization study, it was confirmed by such analysis too. It is recommended to inject the slurry volume (after breaking the rock) with a lower rate, which makes the longer and more conductive fractures.

7- The type curves were also generated for entire field and different types of the wells in order to assist operators during the decision making process and gives them an estimation about the production performance of new and existing wells. The generated type curves were validated by the information of two new wells and the result showed an acceptable consistency between the estimation from type curves and actual production of these wells.

9.2 Recommendations for Future Work

Since they are data dependent, AI-based models are organic in nature. As more data becomes available, the model can re-trained in order to learn from the new data and to enhance its performance. The following modifications are recommended for future work in this area:

1- Incorporating the dynamic geomechanical properties in the dataset instead of static properties: The stress profile is changing during well drilling and completion. This variation may have a significant impact on production of the wells which is still unknown. By using the Artificial Intelligence, and the available geomechanical logs (which were collected in different time intervals of field development), some dynamic data-driven models can be developed which are representative of stress changes in the area during the field development.
2- The existence of natural fractures and their role in production from shale asset is one of the important issues in understanding of fluid flow in shale production. The FMI logs information can be incorporated in AI-based modeling to show the existence of natural fractures as well as their type in different locations of the field and, most importantly, their impact on production performance of the wells.
3- Advances in Microseismic application for shale reservoirs, have made it very valuable information which can be used in AI-based modeling.
4- As explained earlier, in the development of AI-based models, the decline curve analysis and type curves can be performed which the results might be useful especially in the forecasting part, although the existing type curve and decline curve functions in IMAGINE™ should be modified in order to be used for Shale reservoirs.

REFERENCES

1. Alberta Energy, 2009. http://www.energy.alberta.ca/NaturalGas/944.asp
2. Anderson, D.M., Nobakht, M., Moghadam, S. and Mattar, L., "Analysis of Production Data from Fractured Shale Gas Wells", SPE 131787, SPE Unconventional Gas Conference, Pittsburgh, Pennsylvania, February 2010.
3. Andrade, J., Civan, F., Devegowda, D., Sigal, R., "Accurate Simulation of Shale Gas Reservoirs", SPE135564, SPE Annual Technical Conference and Exhibition held in Florence, Italy, September 2010.
4. Arogundade, O. and Sohrabi, M., "A Review of Recent Developments and Challenges in Shale Gas Recovery", SPE 160869, SPE Saudi Arabia Section Technical Symposium and Exhibition, Al-Khobar, Saudi Arabia, April 2012.
5. Arps, J. J. "Analysis of Decline Curves." Transactions, May 1944:160, 228-247.
6. Arthur, J.D., Bohm, B., Layne M., "Hydraulic Fracturing Considerations for Natural Gas Wells of the Marcellus Shale", Presented at the Ground Water Protection Council, Cincinnati, Ohio, September 2008.
7. Bartuska, J.E., Pachiney, J.J. and Leonard, R.S., "Optimizing Completion Designs for Horizontal Shale Gas Wells Using Completion Diagnostics", SPE 155759, SPE Americas Unconventional Resources Conference, Pittsburgh, Pennsylvania, June 2012.
8. Basu, J. K., Bhattacharyya, D. and Kim, T., "Use of Artificial Neural Network in Pattern Recognition", International Journal of Software Engineering and Its Applications, Vol.4, No.2, April 2010.
9. Bello, R.O., "Rate Transient Analysis in Shale Gas Reservoirs with Transient Linear Behavior", PhD Dissertation, University of Texas A&M, 2009.
10. Bello,R.O. and Wattenbarger, A., "Rate Transient Analysis in Naturally Fractured Shale Gas reservoirs", SPE 114591, CIPC/SPE Gas Technology Symposium, Calgary, Alberta, 2008.
11. Bernacki, M., and Wlodarczyk, P., " Principles of Training Multi-Layer Neural Network Using Backpropagation", retrieved form : http://home.agh.edu.pl/~vlsi/AI/backp_t_en/backprop.html
12. Biswas, D., "Shale Gas Predictive Model (SGPM) – An Alternate Approach to Predict Shale Gas Production", SPE 148491, SPE Eastern Regional Meeting, Columbus, Ohio, August 2011.
13. Boulis, A.S., Ilk, D. and Blasingame, T.A., "A New Series of rate Decline Relations Based on the Diagnosis of Rate Time Data", Presented in Canadian International Petroleum Conference (CIPC), Calgary, Alberta, June 2009.

14. Can, B. and Kabir, C.S., “Probabilistic Production Forecasting for Unconventional Reservoirs with Stretched Exponential Production Decline Model”, SPE 143666, SPE Reservoir Evaluation & Engineering Journal, February 2012.
15. Carlson, E.S. and Mercer, J.C., “Devonian Shale Gas Production: Mechanisms and Simple Models”, SPE 19311, JPT, April 1991.
16. Chakraborty, RC. “Fundamentals of Neural Networks: AI Course Lecture 37-38”, June 2010.
17. Chaudhri, M.M., “Numerical Modeling of Multi-Fracture Horizontal Well for Uncertainty Analysis and history Matching: Case Studies from Oklahoma and Texas Shale Gas Wells”, SPE 153888, SPE Western Regional Meeting, Bakersfield, California, March 2012.
18. Cheng, Y., “ Impacts of the Number of Perforation Clusters and Cluster Spacing on Production Performance of Horizontal shale-Gas Wells”, SPE 138843, SPE Reservoir Evaluation & Engineering Journal, February 2012.
19. Cheng, Y., “Impact of Water Dynamics in Fractures on the Performance of Hydraulically Fractured Wells in Gas-Shale Reservoirs”, SPE 127863, Journal of Canadian Petroleum Technology, March 2012.
20. Cheng, Y., Wang, Y., McVay, D.A. and Lee, W.J., “Practical Application of a Probabilistic Approach to Estimate reserves Using Production Decline Data”, SPE 95974, SPE Economics & Management Journal, April 2010.
21. Cipolla, C., Weng, X., Onda, H., Nadaraja, T., Ganguly, U. and Malpani, R., “New Algorithm and Integrated Workflow for Tight Gas and Shale Completions”, SPE 146872, SPE Annual Technical Conference and Exhibition, Denver, Colorado, November 2011.
22. Cipolla, C.L., Fitspatrick, T., Williams, M.J. and Ganguly, U.K., “Seismic to Simulation for Unconventional Reservoir Development”, SPE 146876, SPE Reservoir Characterization and Simulation Conference and Exhibition, Abu Dhabi, UAE, October 2011.
23. Cipolla, C.L., Lolon, E.P., Erdle, J. C. and Rubin, B., “Reservoir Modeling in Shale-Gas Reservoirs”, SPE 125530, SPE Reservoir Evaluation & Engineering Journal, August 2010.
24. Cipolla, C.L., Lolon, E.P., Erdle, J. C. and Tathed, V., “Modeling Well Performance in Shale-Gas Reservoir”, SPE 125532, SPE/EAGE Reservoir Characterization and Simulation Conference, Abu Dhabi, UAE, October 2009.
25. Civan, F., Rai, C. S., and Sondergeld, C. H., “Shale Gas Permeability and Diffusivity Inferred by Improved Formulation of Relevant Retention and Transport Mechanisms”, Transport in Porous Media, Vol. 86, No. 3, 2011.

26. Clarkson, C.R., Nobakht, M., Kaviani, D. and Ertekin, T., "Production Analysis of Tight-Gas and Shale-Gas Reservoirs Using the Dynamic-Slippage Concept", SPE 144317, SPE Journal, March 2012.
27. Cramer, D., "Stimulating Unconventional Reservoirs: Lessons Learned, Successful Practices, Areas for Improvement", SPE 114172, SPE Unconventional Reservoirs Conference, Keystone, Colorado, February 2008.
28. Dehghanpour, H. and Shirdel, M., "A Triple Porosity Model for Shale Gas Reservoirs", SPE 149501, Canadian Unconventional Resources, Calgary, Canada, November 2011.
29. Du, C., Zhang, X., Melton, B., Fullilove, D., Suliman, B., Gowelly, S., Grant, D. and Calvez, J.L., "A workflow for Integrated Barnett Shale Gas Reservoir Modeling and Simulation", SPE 122934, SPE Latin American and Caribbean Petroleum Engineering Conference, Cartagena, Colombia, June 2009.
30. Eshkalak, M.O., Mohaghegh, S.D. and Esmaili, S., "Synthetic Geomechanical Logs for Marcellus Shale", SPE 163690, SPE Digital Energy Conference and Exhibition, Woodlands, Texas, March 2013.
31. FEKETE Harmony Software Packages
32. Fetkovich, M.J., "Decline Curve Analysis Using Type Curves", JPT.32 (6): 1065-1077, 1980.
33. Gershenson, C., "Artificial Neural Networks for Beginners".
34. Ghods, P., "Data Assimilation for Fractured Shale Gas Reservoirs Using Ensemble Kalman Filter", PhD Dissertation, University of Southern California, May 2012.
35. Grujic, O., Mohaghegh, S.D. and Bromhal, G., "Fast Track reservoir Modeling of Shale Formations in the Appalachian Basin. Application to Lower Huron Shale in Eastern Kentucky", SPE 139101, SPE Eastern regional Meeting, Morgantown, WV, October 2010.
36. Harikesavanallur, A., Deimbacher, F., Crick, M., Zhang, X., and Forester, P., "Volumetric Fracture Modeling Approach (VFMA): Incorporating Microseismic data in the Simulation of Shale Gas Reservoirs", SPE 134683, SPE Annual Technical Conference and Exhibition, Florence, Italy, September 2010.
37. Hill, D.G., Lombardi, T.E., and Martin, J.P., "Fractured Shale Gas Potential in New York", Northeastern Geology and Environmental Science, Vol. 26, 57-78, 2004.
38. Holditch, S.A., "Factors Affecting Water Blocking and Gas Flow From Hydraulically Fractured Gas Wells", JPT 31 (12): 1515-1524, 1979.
39. Hudson, J., Civan, F., Michel-Villazon, G., Devegowda, D. and Sigal, R., "Modeling Multiple-Porosity Transport in Gas-Bearing Shale formations", SPE 153535, SPE Latin American and Caribbean Petroleum Engineering Conference, Mexico City, Mexico, April 2012.

40. Hykin S., “Neural Networks: A comprehensive Foundation”, NY: Macmillan College Publishing Inc, 1994.
41. Ilk, D., Rushing, J.A., Perego, A.D. and Blasingame, T.A., “exponential vs. hyperbolic Decline in Tight Gas Sands-Understanding the Origin and Implications for Reserve Estimates using Arp’s Decline curves”, SPE 116731, SPE Annual Technical Conference and Exhibition, Denver, Colorado, September 2008.
42. Intelligent Solution Inc. Software Packages (IDEA, IMagine, IMprove)
43. Kalantari-Dahaghi, A. and Mohaghegh, S.D., “Economic Impact of Reservoir Properties, Horizontal Well Length and Orientation on Production from Shale formations: Application to New Albany Shale”, SPE 125893, SPE Eastern Regional Meeting, Charleston, West Virginia, September 2009.
44. Kalantari-Dahaghi, A. and Mohaghegh, S.D., “Numerical Simulation and Multiple Realizations for Sensitivity Study of Shale Gas Reservoir”, SPE 141058, SPE Production and Operations Symposium, Oklahoma City, Oklahoma, March 2011.
45. Kalantari-Dahaghi, A. and Mohaghegh, S.D., “Top-Down Intelligent Reservoir Modeling of New Albany Shale”, SPE 125859, SPE Eastern Regional Meeting, Charleston, West Virginia, September 2009.
46. Kalantari-Dahaghi, A., Mohaghegh, S.D., and Khazaeni, Y., “New Insight into Integrated Reservoir Management using Top-Down, Intelligent Reservoir Modeling Technique; Application to a Giant and complex Oil Field in the Middle East”, SPE 132621, SPE Western Regional Meeting, Anaheim, California, May 2010.
47. Khazaeni, Y., and Mohaghegh, S.D., “Intelligent Time Successive Production Modeling” ,SPE 132643, SPE western Regional Meeting, Anaheim, California, May 2010.
48. Knudsen, B. R., “Production Optimization in Shale Gas reservoirs”, Master’s Thesis, Norwegian University of Science and Technology (NTNU), Norway, 2010.
49. LaFollette, R., Holcomb, W., and Aragon, J., “ Practical Data Mining: Analysis of Barnett Shale Production Results with Emphasis on Well completion and fracture stimulation”, SPE 152531, SPE Hydraulic Fracturing technology Conference, Woodlands, Texas, February 2012.
50. LaFollette, R., Izadi, G. and Zhong, M., “ Application of Multivariate Analysis and Geographic Information Systems Pattern-Recognition Analysis to Production Results in the Bakken Light Tight Oil Play”, SPE 163852, SPE Hydraulic Fracturing technology Conference, Woodlands, Texas, February 2013.
51. Lee, J. and Sidle, R., “Gas-Reserves Estimation in Resource Plays”, SPE 130102, SPE Economics & Management Journal, Volume 2, Number 2, 2010.

52. Li, J., Du, C.M. and Zhang, X., "Critical evaluation of Shale Gas Reservoir Simulation Approaches: Single-Porosity and Dual-Porosity Modeling", SPE 141756, SPE Middle East Unconventional Gas conference and Exhibition, Muscat, Oman, February 2011.
53. Mayerhofer, M.J., Lolon, E.P., Warpinski, N.R., Cipolla, C.L. and Walser, D., "What is Stimulated Reservoir Volume (SRV)?", SPE 119890, SPE Shale Gas Production Conference, Fort Worth, Texas, November 2008.
54. Mohaghegh, S.D., "An Intelligent System's Approach for Revitalization of Brown Fields Using Only Production Rate Data", .International Journal of Engineering, Volume 22, Number 1. pp 89-106, February 2009.
55. Mohaghegh, S.D., "Data-Driven Reservoir and Production Management of Shale", White Paper, Intelligent Solutions Inc., 2013.
56. Mohaghegh, S.D., "Reservoir Modeling of Shale Formations", Journal of Natural Gas Science and Engineering 12 (2013) 22-33, January 2013.
57. Mohaghegh, S.D., "Top-Down intelligent Reservoir Modeling (TDIRM): An Alternative Reservoir Modeling Technique; Integrating Classic Reservoir Engineering With Artificial Intelligence & Data Mining Techniques", Search and Discovery Article # 40441- Presented at AAPG Annual Conventional and Exhibition, Denver, Colorado, June 2009.
58. Mohaghegh, S.D., "Top-Down, Intelligent Reservoir Model", Vol. 12.European Geological Union General Assembly. EGU2010-233, Vienna, Austria, May 2010b.
59. Mohaghegh, S.D.," Reservoir Simulation and Modeling based on Artificial Intelligence and Data Mining (AI&DM)", Journal of Natural Gas Science and Engineering, Elsevier B.V., 2011
60. Naik, G.C., "Tight Gas Reservoirs-An Unconventional Natural Energy Source for the Future", 2005.
61. Neuro AI, Artificial Intelligence Technology Webpage, retrieved from: http://www.learnartificialneuralnetworks.com/#training
62. Neuroshell. Neuroshell 2 tutorial. Ward Systems, Inc., Fredrick, Maryland. 1998
63. Nobakht M. and Clarkson, C.R., "A New Analytical method for Analyzing Linear Flow in Tight/Shale Gas Reservoirs: Constant Flowing Pressure Boundary Condition", SPE 143989, SPE Reservoir Evaluation & Engineering Journal, June 2012.
64. Nobakht M. and Clarkson, C.R., "A New Analytical method for Analyzing Linear Flow in Tight/Shale Gas Reservoirs: Constant Rate Boundary Condition", SPE 143990, SPE Reservoir Evaluation & Engineering Journal, February 2012.

65. Nobakht, M. and Mattar, L., "Analyzing Production Data from Unconventional Gas Reservoirs with Linear flow and Apparent Skin", SPE 137454, Journal of Canadian Petroleum Technology, January 2012.
66. Nobakht, M., Mattar, L., Moghadam, S. and Anderson, D.M., "Simplified Yet Rigorous Forecasting of Tight/Shale Gas Production in Linear flow", SPE 133615, SPE Western Regional Meeting, Anaheim, California, May 2010.
67. Osholake, T., Wang, J.Y., and Ertekin, T., "Factors Affecting Hydraulically Fractured Well Performances in the Marcellus Shale Gas Reservoirs", SPE 144076, SPE North American Unconventional Gas Conference and Exhibition, Woodlands, Texas, June 2011.
68. Peters, K.E., and Moldowan, J.M., "The Biomarker Guide: Interpreting Molecular Fossils in Petroleum and Ancient Sediments", Prentice Hall Publication, 1993.
69. Popa A.S., "Automatic Hydraulic Fracturing Design for Low Permeability Reservoirs Using artificial Intelligence", PhD Dissertation, West Virginia University, 2004.
70. Priddy, L. and Keller, P.E., "Artificial Neural Networks; an Introduction", the International Society for Optical Engineering Publication, 2005.
71. Robert Gordon University Lectures Notes; Retrieved from: http://www4.rgu.ac.uk/files/chapter3%20-%20bp.pdf
72. Rokosh, C.D., Pawlowicz, J.G., Berhane, H., Anderson, S.D.A and Beaton, A.P., "What is Shale Gas? An Introduction to Shale-Gas Geology in Alberta", Energy Resources Conservation Board, Alberta Geological Survey, 2008.
73. Shelley, R. F., O'Connell, K.E, Skari, D. and Baribault, R. A., " Use of Data-Driven and Engineering Modeling to Plan and Evaluate Hydraulic Fracture Stimulated horizontal Bakken completions", SPE 145792, SPE Annual Technical Conference and Exhibition, Denver, Colorado, November 2011.
74. Shelley, R.F., Dzubin, B. and Shah, K., " Evaluating the Production Potential of Hydraulically Fractured horizontal Completions using Engineering and Data-Driven Modeling Techniques", SPE 138423, SPE Tight Gas Completions Conference, San Antonio, Texas, November 2010.
75. Shelley, R.F., Saugier, l., Al-Tailji, W., Guliyev, N., Shah, K. and Godwin, J., "Data-Driven Modeling Improves the Understanding of Hydraulic Fracture Stimulated Horizontal eagle Ford Completions", SPE 152121, SPE Hydraulic Fracturing Technology Conference, Woodlands, Texas, February 2012.
76. Siripatrachai, N. and Ertekin, T., "Alternate Representations in Numerical Modeling of Multistage Hydraulically Fractured Horizontal Wells in Shale Gas Reservoirs", SPE 153813, SPE Western Regional Meeting, Bakersfield, California, March 2012.

77. Siripatrachai, N., "Alternate Representations for Numerical Modeling of Multi Stage Hydraulically Fractured horizontal Wells in Shale Gas Reservoirs", Master's Thesis, the Pennsylvania State university, 2011.
78. Solomatine, D., See, L.M. and Abrahart, R.J., "Data-Driven Modeling-Concepts, Approaches and Experiences", Springer, Computational Intelligence and Technological Developments in Water Applications, 2008.
79. Speight, J.G., "Shale Gas Production Process", Gulf Professional Publishing, 2013.
80. Strickland, R., Purvis, D. and Blasingame, T., "Practical Aspects of reserve Determination for Shale Gas", SPE 144357, SPE North American unconventional Gas Conference and Exhibition, Woodlands, Texas, June 2011.
81. U.S. Department of Energy, "Impact of the Marcellus Shale Gas Play on Current and Future CCS Activities", 2010.
82. U.S. Department of Energy, "Modern Shale Gas Development in United States", 2009.
83. U.S. Energy Information Administration (EIA), "Annual Energy Outlook Overview", 2012.
84. Valko, P.P., "Assigning Value to Stimulation in the Barnett Shale: A Simultaneous Analysis of 7000 plus Production Histories and Well Completion Records", SPE 119369, SPE Hydraulic Fracturing Technology Conference, Woodlands, Texas, January 2009.
85. Walton, I., "Shale Gas Production Analysis, Phase 1", University of Utah Publication, 2012.
86. Wang, F., "Effects of Petrophysical and Engineering Factors on Fluid Flow and Production in Gas Shales", AAPG Search and Discovery Article # 90122, Presented at APPG Hedberg Conference, Austin, Texas, December 2010.
87. Wang, G. and Carr, T.R.," Methodology of Organic-Rich Shale Lithofacies Identification and Prediction: A Case Study from Marcellus Shale in the Appalachian Basin", PhD Dissertation, West Virginia University, 2012.
88. Warren, J. E., and Root, P. J., "The Behavior of Naturally Fractured Reservoirs (SPE 426)", Society of Petroleum Engineers Journal, 3(3):245-255, 1963.
89. Waters, G.A. , Lewis, R.E. and Bentley, D.C., "The Effect of Mechanical Properties Anisotropy in the generation of Hydraulic Fractures in Organic Shales", SPE 146776, SPE Annual Technical Conference and Exhibition, Denver, Colorado, November 2011.
90. Wikipedia, Definition of Sensitivity Analysis Retrieved from : http://en.wikipedia.org/wiki/Sensitivity_analysis
91. Wikipedia, Neural Network retrieved from: http://en.wikipedia.org/wiki/Neural_network

92. Wilson, K. C. and Durlofsky, L. J., “Computational Optimization of Shale Resource Development Using Reduced-Physics Surrogate Models”, SPE 152946, SPE Western Regional Meeting, Bakersfield, California, March 2012.
93. Wilson, K.C., and Durlofsky, L.J., “Computational Optimization of Shale Resource Development using Reduced-Physics Surrogate Models”, SPE 152946, SPE Western Regional Meeting, Bakersfield, California, March 2012.